RESEARCH

Report No. UT-10.09

SHEAR CAPACITY OF IN SERVICE PRESTRESSED CONCRETE BRIDGE GIRDERS

Prepared For:

Utah Department of Transportation Research Division

Submitted By:

Utah State University
Department of Civil & Environmental Engineering

Authored By:

Paul Barr
Marv Halling
Dave Petty
Perry Osborn

May 2010

UDOT
CONNECTING COMMUNITIES
Utah Department of Transportation - Research Division
4501 South 2700 West, Box 148410 - Salt Lake City, Utah 84114-8410

DISCLAIMER:

“The authors alone are responsible for the preparation and accuracy of the information, data, analysis, discussions, recommendations, and conclusions presented herein. The contents do not necessarily reflect the views, opinions, endorsements, or policies of the Utah Department of Transportation and the US Department of Transportation. The Utah Department of Transportation makes no representation or warranty of any kind, and assumes no liability therefore.”

1. Project No.
UT-10.09

2. Government Accession No.

3. Recipient's Catalog No.

4. Title and Subtitle
SHEAR CAPACITY OF IN SERVICE PRESTRESSED CONCRETE BRIDGE GIRDERS

5. Report Date
May 17th, 2010

6. Performing Organization Code

7. Author(s)
Paul J. Barr, Marv Halling, Dave Petty and Perry Osborn

8. Performing Organization Report No.
UT-10.09

9. Performing Organization Name and Address
Utah State University
Department of Civil and Environmental Engineering
Logan, UT 84322-4110

10. Work Unit No. (TRAIS)
5241701D

11. Contract or Grant No.
79215

12. Sponsoring Agency Name and Address
Utah Department of Transportation
4501 South 2700 West
Salt Lake City, Utah 84114-8410

13. Type of Report and Period Covered
Final Report
07/07 – 07/09

14. Sponsoring Agency Code
IB05.001

15. Supplementary Notes
Prepared in cooperation with the Utah Department of Transportation or U.S. Department of Transportation, Federal Highway Administration

16. Abstract

The design of prestressed concrete bridge girders has changed significantly over the past several decades. Specifically, the design procedure to calculate the shear capacity of bridge girders that was used forty years ago is very different than those procedures that are recommended in the current AASHTO LRFD Specifications. As a result, many bridge girders that were built forty years ago do not meet current design standards, and in some cases warrant replacement due to insufficient calculated shear capacity. However despite this insufficient calculated capacity, these bridge girders have been found to function adequately in service with minimal signs of distress.

The objective of this research was to investigate the actual in service capacity of prestressed concrete girders that have been in service over an extended period of time. The actual capacity was compared with calculated values using the AASHTO LRFD Specifications.

17. Key Word
Prestressed Concrete, girders, shear, capacity

18. Distribution Statement
Public distribution

19. Security Classif. (of this report)
Unclassified

20. Security Classif. (of this page)
Unclassified

21. No. of Pages
226

22. Price
n/a

ACKNOWLEDGMENTS

The authors would like to thank the Utah department of Transportation for the funding for this research. We especially appreciate the guidance of Daniel Hsaio, Dave Eixenburger and Chris Potter for the technical guidance. We would also like to recognize and thank BASF The Chemical Company for their generous donation of the Carbon Fiber Reinforced Polymer materials and their technical expertise. Their product and advice were vital to the success of this research project.

EXECUTIVE SUMMARY

The design of prestressed concrete bridge girders has changed significantly over the past several decades. Specifically, the design procedure to calculate the shear capacity of bridge girders that was used forty years ago is very different than those procedures that are recommended in the current AASHTO LRFD Specifications. As a result, many bridge girders that were built forty years ago do not meet current design standards, and in some cases warrant replacement due to insufficient calculated shear capacity. However despite this insufficient calculated capacity, these bridge girders have been found to function adequately in service with minimal signs of distress.

When the Utah Department of Transportation decided to replace the bridge on 45th South on I215 as one of the first Accelerated Bridge Construction replacement projects in Utah, the existing bridge provided an opportunity to investigate the ultimate shear capacity of precast, prestressed bridge girders built during this era. The original bridge was built as a four span superstructure with an overall roadway width of approximately 77 feet. The bridge had a significant change in elevation which resulted in water and deicing salts running down the length of the bridge. Each span was constructed with a fixed support on one end and an expansion joint on the other which allowed water and salt to enter the expansion joint and resulted in corrosion of the ends of the prestressed concrete girders. Due to the corrosion and the insufficient calculated shear capacity, UDOT asked researchers at Utah State University to determine the ultimate capacity of the girders as well as investigate strengthening procedures.

In order to meet the objectives of the project, eight AASHTO Type 2 girders were salvaged during the demolition and shipped to the Systems, Materials and Structural Health (SMASH) Laboratory at Utah State University. Six girders were salvage from one bridge and the last two girders were salvaged from a separate bridge. Girders 1 through 6 had an in-service span length of 22-ft 3-in, and Girders 7 and 8 had an in-service span length of 34.5-ft. The girders were simply supported and loaded at a distance of 48 inches (d + 1-ft) from the supports with a single point load.

Upon investigation, the shear reinforcement was found to consist of number 4 bars at a spacing of 21 inches on center. Material tests determined that the vertical stirrups were made of 33 ksi steel and the prestressing strand was 250 ksi stress relieved strand. Baseline ultimate shear capacities were obtained by applying a vertical load at a distance d from the face of the support. Subsequently, carbon fiber reinforced polymers that were donated by The Chemical Company (BASF) were applied to the remaining girders in five different configurations. The retrofitted girders were then tested similarly as the baseline tests so that direct comparisons could be made.

The measured data from the testing girders and the subsequent analyses lead to the following conclusions and recommendations:

1. The average measured shear capacities for Girders 1 through 6 and 7 and 8 respectively were 163.56-kips and 261.50-kips.
2. The measured capacities for the two groups of girders were compared with the calculated capacities according to procedures outlined in the AASHTO LRFD Specifications (2007) and the ACI 318 guidelines (2005). In general, the measured girder capacities were larger than any of the calculated values.
3. The strut-and-tie method was determined to provide the best estimate of the shear capacity of the girders. For girders 1 through 6, the strut-and-tie produced an ultimate shear capacity of 138.56 kips which is 84.72% of the average measured value. For girders 7 and 8, the strut-and-tie method resulted in an ultimate shear capacity of 258.7 kips which was 98.93% of the average measured value.
4. The AASHTO LRFD and ACI methods for calculating shear capacity were much more conservative in comparison to the strut-and-tie methodology. The AASHTO LRFD general method predicted a shear capacity of 82.27 kips and 100.28 kips, which was 50.3% and 38.3% of the measured capacity, for girders 1 through 6 and girders 7 through 8 respectively. The ACI-318 simplified method predicted a shear capacity of 101.74 kips and 131.09 kips, which was62.2% and 50.1% of the measured capacity, for girders1 through 6 and girders 7 through 8 respectively.
5. The experimental strengthening program consisted of the load testing of five different CFRP reinforcement configurations. The CFRP reinforcement was found to increase the shear capacity of the AASHTO I-shaped prestressed girders. The magnitude of the increased shear capacity was found to be highly dependent on the CFRP reinforcement configuration and anchorage system. The application of the CFRP reinforcement resulted in larger deflections before failure. Based on the recorded strain measurements, it was concluded that the CFRP fabric was not overstressed at failure and the primary failure mode was debonding.
6. While five CFRP configurations were evaluated, the configuration on Girders 5 and 8, which consisted of vertical stirrups and a horizontal strip placed over the vertical stirrups for anchorage, was found to produce the largest consistent increase in shear capacity consistently. This configuration was also the easiest to apply and can be credited for its consistency. The four tests on Girders 5 and 8 produced an average increased shear capacity of 55.70 kips.
7. Two analytical methods were evaluated to determine the most accurate methodology in determining the increased shear capacity of prestressed concrete I girders reinforced with CFRP. The ACI method was found to be the most accurate in predicting the increased shear capacity of the AASHTO prestressed I-shaped girders tested in this research. The Hutchinson, Donald, and Rizkalla (1999) method overestimated the increased shear capacity by 12.05%.

TABLE OF CONTENTS

DISCLAIMER I

ACKNOWLEDGMENTS IV

LIST OF FIGURES XI

LIST OF TABLES XXI

EXECUTIVE SUMMARY XXII

1.0 INTRODUCTION 1

- 1.1 Context 1
- 1.2 Ultimate Shear Capacity 2
- 1.3 CFRP Reinforcement Design 3
  - 1.3.1 Theoretical Models of Shear Contribution of CFRP 3
- 1.4 Research Objectives 4
- 1.5 Organization of Report 4

2.0 LITERATURE REVIEW 6

- 2.1 Literature Review on Shear Capacity 6
  - 2.1.1 Kordina, Hegger, and Teutsch (1989) 6
  - 2.1.2 Oh and Kim (2004) 8
  - 2.1.3 Kaufman and Ramirez (1988) 9
  - 2.1.4 Elzanaty, Nilson, and Slate (1986) 10
  - 2.1.5 MacGregor, Sozen, and Siess (1965) 11
  - 2.1.6 Saqan and Frosch (2009) 12
- 2.2 Literature Review for CFRP application 13
  - 2.2.1 Carolin and Täljsten (2005) 14
  - 2.2.2 Zhang and Hsu (2005) 14

2.2.3 Deniaud and Cheng (2004) ... 15
2.2.4 Adhikary and Mutsuyoshi (2004) ... 16
2.2.5 Diagana, Gedalia, and Dlemas (2002) ... 16
2.2.6 Hutchinson, Donald, and Rizkalla (1999) ... 17
2.2.7 Khalifa et al. (1998) ... 18
3.0 EXPERIMENTAL TESTING PROGRAM AND RESULTS ... 19
3.1 Introduction ... 19
3.2 Test Setup ... 19
3.3 Determination of Effective Prestress Force ... 27
3.4 Shear Tests ... 35
3.4.1 Shear Test Results ... 41
3.5 CFRP Design ... 42
3.5.1 Configurations ... 44
3.5.2 CFRP application ... 51
3.6 Testing Analysis of CFRP Reinforced Girders ... 52
3.6.1 Test 2A ... 53
3.6.2 Test 2B ... 54
3.6.3 Test 3A ... 56
3.6.4 Test 3B ... 57
3.6.5 Test 4A ... 58
3.6.6 Test 4B ... 60
3.6.7 Test 5A ... 61
3.6.8 Test 5B ... 62
3.6.9 Test 6A ... 64
3.6.10 Test 6B ... 65

3.6.11 Test 8A 66

3.6.12 Test 8B 67

3.6.13 Comparison of measured strains 69

3.6.14 Comparison of measured deflections 72

3.6.15 Comparison of measured shear capacity 73

4.0 COMPARISON OF MEASURED AND PREDICTED RESULTS 75

4.1 Introduction to predictive Methods for predicting Shear Capacity 75

4.1.1 Predictive Method AASHTO LRFD Bridge Design Specifications........... 75

4.1.2 Predictive Method ACI 318-08.. 80

4.1.3 Predictive Method Strut-and-Tie Model 84

4.1.4 Comparison of Calculated to Measured Shear Capacities 85

4.1.5 ASHTO LRFD Predicted Prestress Losses 86

4.1.6 Comparison of Measured and Calculated Prestress Losses 89

4.2 Introduction to Predictive Methods for Shear Contribution from CFRP........ 91

4.2.1 ACI Analytical Method for Vf 92

4.2.2 Analytical Method in Hutchinson, Donald, and Rizkalla (1999) for Vf 94

4.2.3 Comparison of Analytical Models for Vf and measured Vf 97

5.0 SUMMARY AND CONCLUSIONS 101

5.1 Summary 101

5.2 Conclusions on Existing Shear Capacity 102

5.2.1 Comparison with AASHTO LRFD 102

5.2.3 Comparison with ACI318-08 103

5.2.4 Comparison with the Strut-and-Tie Model 103

5.2.5 Cracking Test 104

        5.2.6 Comparison of Prestress Losses 104
    5.3 Conclusions on CFRP Reinforcement 104
        5.3.1 Effects of CFRP Configurations on Increased Capacity 105
        5.3.2 Observations from CFRP Theoretical Models 106
        5.3.3 Observations from Deflections.. 107
        5.3.4 Observations from Strains 107
    5.4 Recommendations for Future Work on Predicting Shear Capacity............. 107
    5.5 Recommendations for Application of CFRP Shear Reinforcement 108
REFERENCES 110
APPENDICES 112
    Appendix A... 113
    Appendix B 147

LIST OF FIGURES

Figure 3.1 3-D view of reaction frame CAD model. 20

Figure 3.2 Base plate of reaction frame. 21

Figure 3.3 Beam to column connection 21

Figure 3.4 AASHTO Type II girder dimensions. 22

Figure 3.5 Plan and profile view of bridge over I-215. 23

Figure 3.6 Bridge as it was being torn down. 24

Figure 3.7 Girders before testing. 24

Figure 3.8 Stress-strain relationship for web shear steel. 25

Figure 3.9 Stress-strain relationship for prestressing strands. 27

Figure 3.10 Typical strain gauge placements for effective prestress test. 28

Figure 3.11 Strain gauges from girder 2 showing an example of the data recorded during the decompression tests. 33

Figure 3.12 Typical load vs. micro strain plot (Girder 3 shown with an 80,000-lb limit). 35

Figure 3.13 Grout pad fitted onto girders. 36

Figure 3.14 Typical shear test setup. 38

Figure 3.15 Girder 1 after undergoing a flexural shear failure. 40

Figure 3.16 Top flange of Girder 7 after web crushing failure. 40

Figure 3.17 Placement and numbering of strain gauges. 41

Figure 3.18 Strain gauge on control Girder 1B. 42

Figure 3.19 Location of web to flange connection. 43

Figure 3.20 Girder 1: No external reinforcement. 44

Figure 3.21 Girder 1: No external reinforcement. 44

Figure 3.22 Drawing of Girder 2 CFRP design. 45

Figure 3.23 Girder 2 CFRP design 45

Figure 3.24 Drawing of Girder 3 CFRP design. 46

Figure 3.25 Girder 3 CFRP design. 46

Figure 3.26 Drawing of Girder 4 CFRP design. 47

Figure 3.27 Girder 4 CFRP design. 47

Figure 3.28 Drawing of Girder 5 CFRP design. 48

Figure 3.29 Girder 4 CFRP design. 48

Figure 3.30 Drawing of Girder 6 CFRP design. 49

Figure 3.31 Girder 6 CFRP design 49

Figure 3.32 Girder 7 with no external reinforcement. 50

Figure 3.33 Girder 7 with no external reinforcement. 50

Figure 3.34 Drawing of Girder 8 CFRP design. 51

Figure 3.35 Girder 8 CFRP design. 51

Figure 3.36 Application of CFRP MBrace® system. 52

Figure 3.37 Typical graph of measured data. 53

Figure 3.38 Failure of Test 2A and strain gauge orientation. 54

Figure 3.39 Anchorage failure and concrete surface failure. 54

Figure 3.40 Anchorage failure and strain gauge orientation. 55

Figure 3.41 Failure of Test 2B. 55

Figure 3.42 Anchorage failure and strain gauge orientation of Test 3A. 56

Figure 3.43 Failure of Test 3A. 57

Figure 3.44 Anchorage failure and strain gauge orientation of Test 3B. 58

Figure 3.45 Failure of Test 3B. 58

Figure 3.46 CFRP delamination and strain gauge orientation of test 4A. 59

Figure 3.47 Failure of Test 4A. 59

Figure 3.48 CFRP delamination and strain gauge orientation of Test 4B. 60

Figure 3.49 Failure of Test 4B. 61

Figure 3.50 Anchorage failure and strain gauge orientation of Test 5A. 62

Figure 3.51 Failure of Test 5A. 62

Figure 3.52 Shear cracks and strain gauge orientation of Test 5B. 63

Figure 3.53 Failure of Test 5B. 63

Figure 3.54 Bending cracks and strain gauge orientation of Test 6A. 64

Figure 3.55 Bending failure of Test 6A. 64

Figure 3.56 Concrete shear failure and strain gauge orientation of Test 6B. 65

Figure 3.57 Failure of Test 6B. 66

Figure 3.58 Anchorage failure of Test 8A. 67

Figure 3.59 Failure of Test 8A. 67

Figure 3.60 Anchorage failure of Test 8B. 68

Figure 3.61 Failure of Test 8B. 69

Figure 3.62 Load vs strain of strain gauges 3 on control
Test 1A and CFRP reinforced Test 4A……………………………………………70

Figure 3.63 Load vs strain of strain gauges 3 on control
Test 1A and CFRP reinforced Test 3A……………………………………………70

Figure 3.64 Load vs strain of strain gauges 3, 4, 8, and 9 on Test 5A. 71

Figure 3.65 Stress vs strain graph of the CFRP fabric (CF 160). 71

Figure 3.66 Load vs deflection of control and Girder 5 configuration 72

Figure 4.1 Dimensional variables for CFRP shear reinforcement
design found in ACI 440.2R-08. 93

Figure 4.2 Dimensional variables for CFRP shear reinforcement
design found in Hutchinson, Donald, and Rizkalla (1999). 96

Figure A.1 Bridge plans page 1 of 23. 115

Figure A.2 Bridge plans page 2 of 23. 115

Figure A.3 Bridge plans page 3 of 23. 116

Figure A.4 Bridge plans page 4 of 23. 116

Figure A.5 Bridge plans page 5 of 23. 117

Figure A.6 Bridge plans page 6 of 23. 117

Figure A.7 Bridge plans page 7 of 23. 118

Figure A.8 Bridge plans page 8 of 23. 118

Figure A.9 Bridge plans page 9 of 23. 119

Figure A.10 Bridge plans page 10 of 23. 119

Figure A.11 Bridge plans page 11 of 23. 120

Figure A.12 Bridge plans page 12 of 23. 120

Figure A.13 Bridge plans page 13 of 23. 121

Figure A.14 Bridge plans page 14 of 23. 121

Figure A.15 Bridge plans page 15 of 23. 122

Figure A.16 Bridge plans page 16 of 23. 122

Figure A.17 Bridge plans page 17 of 23. 123

Figure A.18 Bridge plans page 18 of 23. 123

Figure A.19 Bridge plans page 19 of 23. 124

Figure A.20 Bridge plans page 20 of 23. 124

Figure A.21 Bridge plans page 21 of 23. 125

Figure A.22 Bridge plans page 22 of 23. 125

Figure A.23 Bridge plans page 23 of 23. 126

Figure A.24 Embedment anchorage detail 127

Figure A.25 Primer specifications page 1. 128

Figure A.26 Primer specifications page 2. 129

Figure A.27 Putty specifications. 130

Figure A.28 Saturant specifications page 1. 131

Figure A.29 Saturant specifications page 2. 132

Figure A.30 CF 160 fabric specification page 1. 133

Figure A.31 CF 160 Fabric Specifications Page 2 134

Figure A.32 Topcoat specifications page 1 135

Figure A.33 Topcoat specifications page 2 136

Figure A.34 Application instructions page 1. 137

Figure A.35 Application instructions page 2. 138

Figure A.36 Application instructions page 3. 139

Figure A.37 Application instructions page 4. 140

Figure A.38 Application instructions page 5. 141

Figure A.39 Application instructions page 6. 142

Figure B.1 Test 1A Load vs Time. 148

Figure B.2 Test 1A Strain Gauge 1 148

Figure B.3 Test 1A Strain Gauge 2 149

Figure B.4 Test 1A Strain Gauge 3 149

Figure B.5 Test 1A Strain Gauge 4 150

Figure B.6 Test 1A Strain Gauge 5 150

Figure B.7 Test 1A Strain Gauge 6 151

Figure B.8 Test 1A Strain Gauge 7 151

Figure B.9 Test 1A Strain Gauge 8 152

Figure B.10 Test 1A Strain Gauge 9 152

Figure B.11 Test 1A Strain Gauge 10. 153
Figure B.12 Test 1A Strain Gauge 11. 153
Figure B.13 Test 1A Strain Gauge 12. 154
Figure B.14 Test 1A Strain Gauge 13. 154
Figure B.15 Test 1B Load vs Time. 155
Figure B.16 Test 1B Load vs Deflection. 155
Figure B.17 Test 1B Strain Gauge 1. 156
Figure B.18 Test 1B Strain Gauge 2. 156
Figure B.19 Test 1B Strain Gauge 3. 157
Figure B.20 Test 1B Strain Gauge 4. 157
Figure B.21 Test 1B Strain Gauge 7. 158
Figure B.22 Test 1B Strain Gauge 8 158
Figure B.23 Test 1B Strain Gauge 9. 159
Figure B.24 Test 1B Strain Gauge 10. 159
Figure B.25 Test 1B Strain Gauge 11 160
Figure B.26 Test 1B Strain Gauge 12. 160
Figure B.27 Test 2A Load vs Time. 161
Figure B.28 Test 2A Load vs Deflection. 161
Figure B.29 Test 2A Strain Gauge 1 162
Figure B.30 Test 2A Strain Gauge 2. 162
Figure B.31 Test 2A Strain Gauge 3. 163
Figure B.32 Test 2A Strain Gauge 4. 163
Figure B.33 Test 2A Strain Gauge 5. 164
Figure B.34 Test 2B Load vs Time. 164

Figure B.35 Test 2B Load vs Deflection. 165

Figure B.36 Test 2B Strain Gauge 1. 165

Figure B.37 Test 2B Strain Gauge 2. 166

Figure B.38 Test 2B Strain Gauge 3. 166

Figure B.39 Test 2B Strain Gauge 4. 167

Figure B.40 Test 2B Strain Gauge 5. 167

Figure B.41 Test 3A Load vs Time. 168

Figure B.42 Test 3A Load vs Deflection. 168

Figure B.43 Test 3A Strain Gauge 1. 169

Figure B.44 Test 3A Strain Gauge 2. 169

Figure B.45 Test 3A Strain Gauge 3. 170

Figure B.46 Test 3A Strain Gauge 4. 170

Figure B.47 Test 3A Strain Gauge 5. 171

Figure B.48 Test 3A Strain Gauge 6. 171

Figure B.49 Test 3A Strain Gauge 7. 172

Figure B.50 Test 4A Load vs Time. 172

Figure B.51 Test 4A Load vs Deflection. 173

Figure B.52 Test 4A Strain Gauge 1. 173

Figure B.53 Test 4A Strain Gauge 2. 174

Figure B.54 Test 4A Strain Gauge 3. 174

Figure B.55 Test 4A Strain Gauge 4. 175

Figure B.56 Test 4A Strain Gauge 5. 175

Figure B.57 Test 4A Strain Gauge 6. 176

Figure B.58 Test 4A Strain Gauge 7. 176

Figure B.59 Test 4B Load vs Time. 177

Figure B.60 Test 4B Load vs Deflection. 177

Figure B.61 Test 4B Strain Gauge 1. 178

Figure B.62 Test 4B Strain Gauge 2. 178

Figure B.63 Test 4B Strain Gauge 3. 179

Figure B.64 Test 4B Strain Gauge 4. 179

Figure B.65 Test 4B Strain Gauge 5. 180

Figure B.66 Test 4B Strain Gauge 6. 180

Figure B.67 Test 4B Strain Gauge 7. 181

Figure B.68 Test 5A Load vs Time. 181

Figure B.69 Test 5A Load vs Deflection. 182

Figure B.70 Test 5A Strain Gauge 1 182

Figure B.71 Test 5A Strain Gauge 2. 183

Figure B.72 Test 5A Strain Gauge 3. 183

Figure B.73 Test 5A Strain Gauge 4. 184

Figure B.74 Test 5A Strain Gauge 5. 184

Figure B.75 Test 5A Strain Gauge 6. 185

Figure B.76 Test 5A Strain Gauge 7. 185

Figure B.77 Test 5A Strain Gauge 8. 186

Figure B.78 Test 5A Strain Gauge 9. 186

Figure B.79 Test 5B Load vs Time. 187

Figure B.80 Test 5B Load vs Deflection. 187

Figure B.81 Test 5B Strain Gauge 1. 188

Figure B.82 Test 5B Strain Gauge 2. 188

Figure B.83 Test 5B Strain Gauge 3. 189

Figure B.84 Test 5B Strain Gauge 4. 189

Figure B.85 Test 5B Strain Gauge 5. 190

Figure B.86 Test 5B Strain Gauge 6. 190

Figure B.87 Test 5B Strain Gauge 7. 191

Figure B.88 Test 5B Strain Gauge 8. 191

Figure B.89 Test 5B Strain Gauge 9. 192

Figure B.90 Test 6A Load vs Time. 192

Figure B.91 Test 6A Strain Gauge 1. 193

Figure B.92 Test 6A Strain Gauge 2. 193

Figure B.93 Test 6A Strain Gauge 3. 194

Figure B.94 Test 6A Strain Gauge 4. 194

Figure B.95 Test 6A Strain Gauge 5. 195

Figure B.96 Test 6A Strain Gauge 6. 195

Figure B.97 Test 6A Strain Gauge 7. 196

Figure B.98 Test 6B Load vs Time. 196

Figure B.99 Test 6B Load vs Deflection. 197

Figure B.100 Test 6B Strain Gauge 1. 197

Figure B.101 Test 6B Strain Gauge 2. 198

Figure B.102 Test 6B Strain Gauge 3. 198

Figure B.103 Test 6B Strain Gauge 4. 199

Figure B.104 Test 6B Strain Gauge 5. 199

Figure B.105 Test 6B Strain Gauge 6. 200

Figure B.106 Test 6B Strain Gauge 7. 200

Figure B.107 Test 7A Load vs Time. 201

Figure B.108 Test 7A Load vs Deflection. 201

Figure B.109 Test 7B Load vs Time. 202

Figure B.110 Test 7B Load vs Deflection. 202

Figure B.111 Test 8A Load vs Time. 203

Figure B.112 Test 8A Load vs Deflection. 203

Figure B.113 Test 8B Load vs Time. 204

Figure B.114 Test 8B Load vs Deflection. 204

LIST OF TABLES

Table 3.1 Girder decompression loads with corresponding residual prestress force……………..35

Table 3.2 Beam spans 37

Table 3.3 Ultimate shear capacity of each girder 39

Table 3.4 Comparative results of experimental program...74

Table 4.1 Calculated shear values...86

Table 4.2 Factors used with AASHTO Detailed Method for P_e 90

Table 4.3 Effective prestress force comparison...91

Table 4.4 Calculated results for ACI analytical methods for Vf 93

Table 4.5 Results for method in Hutchinson, Donald, and Rizkalla (1999) for Vf.......................96

Table 4.6 Results of actual Vf and analytical methods for Vf...100

Table A.1 Girder section properties.. 114

Table A.2 Calculation of effective prestress force.. 114

EXECUTIVE SUMMARY

The Utah Department of Transportation (UDOT) is interested in the existing shear capacity of their AASHTO prestressed concrete bridge girders and the options for shear capacity rehabilitation. Utah's bridges are exposed to deterioration from rain, snow, and the introduction of salt for ice removable. The shear capacity of prestressed concrete girders is difficult to predict accurately, especially after being in service for an extended period of time. This report presents research findings on the existing shear capacity of prestressed concrete girders. It also presents an innovative rehabilitation technique for deteriorated highway bridges using a Carbon Fiber Reinforced Polymers (CFRP) system provided by BASF.

Eight AASHTO Type II bridge girders were tested up to failure by applying external loads near the supports to determine their ultimate shear capacities. The measured results were then compared to predictive models for the existing shear capacity, prestressing force, and the additional shear capacity from the CFRP. Calculated values for the existing shear capacity were obtained using the AASHTO LRFD bridge design code, and the ACI 318-08 design code. Prestress losses were measured by means of a cracking test and then compared to values calculated according to the AASHTO prestress loss equations. The additional shear capacity from the CFRP was compared against the ACI 440.2R-8 method and a method presented in a research paper by Hutchinson, Donald, and Rizkalla (1999).

1.0 INTRODUCTION

1.1 Context

The ultimate shear capacity of prestressed concrete beams is difficult to predict accurately, especially after being in service for an extended period of time. The Utah Department of Transportation asked researchers at Utah State University to experimentally determine the existing shear capacity of 41-year-old prestressed, decommissioned concrete bridge girders and then provide recommendations on how to increase that ultimate shear capacity.

Eight AASHTO Type II bridge girders were tested up to failure by applying external loads near the supports to determine their ultimate shear capacities. The measured results were then compared to predictive models for the existing shear capacity, prestressing force, and the additional shear capacity from the CFRP. Calculated values for the existing shear capacity were obtained using the AASHTO LRFD bridge design code, and the ACI 318-08 design code. Prestress losses were measured by means of a cracking test and then compared to values calculated according to the AASHTO prestress loss equations. The additional shear capacity from the CFRP was compared against the ACI 440.2R-8 method and a method presented in a research paper by Hutchinson, Donald, and Rizkalla (1999).

This research investigates the application of rehabilitation techniques to strengthen AASTHO prestressed bridge girders for shear. Carbon Fiber Reinforced Polymers (CFRP) are becoming more prevalent as a tool in highway bridge rehabilitation. The research presents the application of CFRP fabrics on AASTHO prestressed I-girders for shear reinforcement.

The testing involved retrofitting five of the girders with various configurations of CFRP fabric. Based on the initial tests, the most effective configuration was then applied to another set of I-shaped concrete girders for verification. After the experimental testing, two analytical models developed for predicting the additional shear contribution of the CFRP reinforcement were compared with the measured results from the experimental program. After testing and comparisons, a CFRP reinforcement configuration and theoretical model was selected as a reliable and effective method for application of external shear reinforcement of AASHTO prestressed I-shaped girders.

1.2 Ultimate Shear Capacity

There are three principle methods in which a reinforced prestressed concrete beam can fail in shear. The first type of shear failure is a web crushing failure. For a web crushing failure, the concrete compressive strength is exceeded and the web crushes typically at the top flange of an I-shaped section near the applied load. For a web crushing failure, the cracking is initiated in the web and then extends out in both directions.

The second type of shear failure is called a flexural shear failure. For this type of failure, the initial cracks form due to flexure at a 90-degree angle with respect to the longitudinal axis of the beam. As the externally applied load increases, shear forces and principal tensile stresses dominate the flexural effects causing the cracks to change direction (close to a 45 degree angle from the longitudinal axis) and continue until the principal stresses produce enough dilation of the crack to cause failure.

The third type of failure occurs in the discontinuity regions of the beam where plane sections don't remain plane due to the load being applied so close to the support. Typical failure mechanisms occur due to arching action between the applied load and the support. Both the AASHTO LRFD and the ACI 318-08 design codes account for these three types of failure.

The ultimate shear capacity is a very complicated failure mechanism which is not fully understood or easy to quantify, despite significant advances over the past several years. There are several analytical methodologies which have been accepted as accurate approximations of the overall shear behavior of reinforced prestressed concrete beams. This research focused on shear behavior produced by applying load at the near support (d-region) regions of AASHTO Type II girders. The deterioration that occurred over the service life of these girders added another level of uncertainty. Laboratory tests were performed on the eight girders to determine their existing shear capacities.

1.3 CFRP Reinforcement Design

The research program consisted of the testing of a total of five different CFRP configurations. The CFRP fabric selected for this research was the MBrace® CF 160 system that was generously provided by The Chemical Company (BASF). This product was selected based on its simplicity in application and proven superior performance. A specific performance issue was acknowledged when using external CFRP fabrics for I-shaped girders in comparison to typical rectangular cross sections used in previous research. When loaded in shear, a large normal force begins to develop in the CFRP fabric on the web to flange corner which would lead to a premature delamination resulting in a small increase in capacity. Therefore, four of the five CFRP configurations had anchorage systems integrated into them.

Four of the five CFRP configurations included a U-wrap used as a stirrup anchored by one of two proposed anchorage systems. The remaining CFRP configuration did not include an anchorage system and was used as a baseline comparison to those with anchorage systems. The U-wraps were applied as either vertical or diagonal stirrups that were overlapped on the bottom of the girder. The anchorage system was applied as either a horizontal strip of CFRP fabric placed along the web and over the CFRP stirrups or a CFRP laminate that was imbedded into the girder by means of a cut at the web to flange intersection.

1.3.1 Theoretical Models of Shear Contribution of CFRP

This research also presents a comparison of two analytical design procedures to calculate the contribution of the CFRP reinforcement for shear for AASHTO prestressed girders. The design, philosophy is a natural extension to current procedures used to calculate the nominal shear capacity of a girder:

$$V_n = V_c + V_s + V_f$$

where V_c is the shear contribution from the concrete, V_s is the shear contribution from the embedded steel stirrups, and V_f is the shear contribution from the CFRP reinforcement.

The first method evaluated in this research is found in ACI 440.2R-8 entitled Guide for the “Design and Construction of Externally Bonded FRP Systems for Strengthening Concrete Structures”. The second method to evaluate V_f was a methodology presented in a research paper entitled “FRP for Shear Strengthening of AASHTO Bridge Girders” by Hutchinson, Donald, and Rizkalla (1999). Each of these methodologies is used to calculate the additional contribution of the CFRP reinforcement to the nominal shear capacity of the girder. The focus of this research is to investigate the effectiveness of the two methods for predicting the shear contribution of the CFRP reinforcement.

1.4 Research Objectives

The goal of this research was twofold: First, to obtain analytical and experimental values for the ultimate shear capacities of aged prestressed concrete bridge girders that had been subjected to corrosive conducive environments and second, to obtain analytical and experimental values for the increased shear capacity from the CFRP reinforcement. The experimentally obtained results for the existing shear capacity were compared to the calculated shear capacity obtained following the procedures outlined in the AASHTO LRFD bridge design code (2009), as well as the ACI 318-08 building code. Residual prestressing forces were experimentally obtained and compared to the values calculated using the AASHTO prestress loss equations. The experimentally obtained results for the increased shear capacity from the CFRP reinforcement were compared to the calculated shear contribution from the CFRP as outlined in the ACI 440.2R-8 as well as a method found in Hutchinson, Donald, and Rizkalla (1999).

1.5 Organization of Report

The organization of the report is as follows:

1. Chapter 2 presents a summary of past research that had been performed on the shear capacities of prestressed concrete beams and the shear contribution of CFRP fabrics on concrete girders.
2. Chapter 3 presents the full-scale experimental program for the AASHTO prestressed girders. The different stages of the experimental process are described in detail, beginning with the test setup, then discussing the effective prestress tests, the shear tests, and finally presenting the results. It also outlines the various configurations of the CFRP systems. A comparison of results between the various configurations is also presented.

3. Chapter 4 introduces the design equations to calculate the ultimate shear capacity, prestress losses, and the additional shear capacity from the CFRP. A comparison between the measured results and the predicted results is also performed.
4. Chapter 5 summarizes the report and key conclusions. Recommendations for future research on predicting ultimate shear capacity, prestress losses, and the additional shear capacity from the CFRP. Design recommendations for application of the CFRP system to AASHTO prestressed I-shaped girders are also presented.

2.0 LITERATURE REVIEW

2.1 Literature Review on Shear Capacity

As prestressed concrete beams age and deteriorate, the tendency is to reinforce them in flexure leading to a very stiff beam that is more likely to fail in shear. This trend makes it more important than ever to understand the shear behavior of prestressed concrete beams. There are many factors that influence the overall shear capacity of prestressed concrete beams, many of which are dependent on the type of concrete, aggregate used, water content, and admixtures. According to ACI 318-08, there are two methods to determine the shear capacity of prestressed concrete beams: 1) the simplified method or 2) the detailed method where V_c is the lesser of V_{ci} or V_{cw}. These equations simplify the shear capacity calculations and overlook some of the contributors to the shear strength of the member. The actual shear capacity at failure depends on a combination of shear from the concrete, longitudinal mild reinforcement, prestressing strands, and the stirrups.

One contributing factor to the ultimate shear capacity that has changed drastically over the past 20-30 years is the strength of concrete. Since high-strength concrete is now being used more frequently in the design and construction of prestressed concrete beams, the effects of this higher strength concrete need to be considered when determining the shear capacity. Much of the completed research has been to determine the adequacy of the design codes' specifications as they apply to medium and high strength concrete, because the original design codes were developed based on regular strength concrete. With these considerations in mind, this chapter reviews some of the research that has been done to better understand the total shear strength of prestressed concrete beams.

2.1.1 Kordina, Hegger, and Teutsch (1989)

This research was done to gain a better understanding of the shear capacity of prestressed concrete beams with un-bonded prestressing tendons. Most of the research done prior to this investigation focused on quantifying the shear capacity of prestressed concrete beams with bonded tendons or the flexural capacity of prestressed concrete beams with un-bonded tendons.

The goal of this research was to test prestressed concrete beams with un-bonded tendons in shear and to develop an accurate shear design methodology for this type of beam construction.

In their research, the authors conducted three series of tests. The first series utilized three monolithic beams. Each beam was simply supported and loaded at the mid-span. The beams spanned 13.12 ft (4 m). The second series of tests was carried out on two different beams. The first beam (SOV1) had a simple span of 19.69 ft (6 m), and the second beam (SOV2) was a continuous two span beam which was loaded at two points sequentially until shear failure occurred. Both of the beams used in the second series of tests were precast with joints that were carefully profiled. The third series of tests were performed on five beams simply supported over a 19.69 ft (6 m) span. These five beams, all containing stirrups, were loaded at different locations to cause up to three failure zones. All of the beams that were used in these three series of tests were I-sections with the exception of one T-shaped cross section used in the third series. Straight tendons, having a diameter of 1.04 or 1.25 in (26.5 or 32 mm), or two unbonded single-strand tendons, harped at an angle of inclination of α=3.1 degrees towards the support, were used.

Two analytical models were employed to analyze the behavior of the prestressed concrete beams, a truss analogy, and a tied-arch analogy. According to the truss analogy, the main factor governing shear was web reinforcement, whereas the tied arch analogy showed that the shear was controlled purely by the tension member. Therefore, the two main parameters looked at in this study were web reinforcement and tension reinforcement.

The initial formation of shear cracks in these test beams with unbonded tendons was similar to prestressed concrete beams with bonded tendons. The tension chords in the shear zone remained almost totally uncracked resulting in shear cracks forming independently from flexural cracks. After the initial cracking, the beams with un-bonded tendons continued to crack due to "plate-action." The shear cracking was the main observed difference between the bonded and unbonded prestressed concrete beams with regards to the shear carrying capacity.

The authors concluded that the most accurate shear model for use with prestressed concrete beams without bonded tendons is the truss analogy. The truss analogy can distinguish between tension-shear or flexural-shear failure and web-crushing failure. This analogy was found to accurately predict the load-bearing capacity and the failure mode. The tied-arch model only considered compression-arch failure which was not consistent with the test results from six of the tested beams where the obvious method of failure was yielding of the web reinforcement.

2.1.2 Oh and Kim (2004)

Several research projects have been conducted on prestressed concrete (PSC) beams with an emphasis on flexural behavior. The shear behavior, however, is much more complicated and less research has been conducted on this subject. As such, this research focused on the shear capacity of prestressed, post-tensioned concrete beams. The authors employed the use of large-scale, post-tensioned PSC girders made with medium and high-strength concrete with compressive strengths of 40 and 60 MPa respectively. Strain gages were used on the stirrups to analyze the strain behavior of the shear stirrups, and surface concrete strain gages were attached to the side surfaces on the beams to detect strain at that surface. Because of the deformation that occurs during shear failure, many grids of sensors were needed, and the average strain was used to describe the strain in the PSC beam during shear failure. With all of the data collected during this study, more advanced design and analysis procedures of PSC beam structures were proposed.

For this research two large-scale, post-tensioned PSC girders with grouted ducts were constructed using normal and high-strength concrete. Each girder was a 1200 mm deep and 10,600 mm long I-section. Girder 1 had a design compressive strength of 40 MPa, and Girder 2 was designed for a 60 MPa target compressive strength (42.8 and 62.1 MPa, respectively, at testing). The prestressing strands used were seven-wire strands with nominal diameter of 12.7 mm and nominal area of 98.71 mm^2 having a yield strength of 1620 MPa and an ultimate strength of 1890 MPa. Each girder encases three tendons consisting of six strands each. The girders each had mild steel reinforcements as stirrups (13 mm diameter) and as longitudinal steel bars (16 mm diameter), both having a yield strength of 345 MPa and ultimate strength of 540 MPa. Two different stirrup arrangements were used. The first was a 200 mm spacing on the right side and the second with a 400 mm spacing on the left side of each girder.

Girders 1 and 2 were loaded up to the ultimate load while strains in the stirrups and concrete surface were measured and compared. The cracking patterns were similar in both girders, but with some slight variation. Girder 2 exhibited more cracking, but with less dilation. This was a result of the high-strength concrete that was used in that girder. The strains on the surface of the girders remained small until diagonal shear cracks formed, and then a rapid increase was observed on the surface strains. Principal stresses along with their directions were calculated based on the strain and the deformations of the LVDTs that were attached to the sides of the girders. The principal directions were shown to rotate greatly as the load increased, and the principal directions approached 23 to 25 degrees at the ultimate load stage.

Oh and Kim concluded that: 1 - the high-strength concrete girder exhibited a more distributed cracking pattern, that is, there were more diagonal cracks with a smaller crack width, 2 - the principal directions decreased as the load increased, and 3 - the concept of average strains and the changing of principal directions according to the applied load can be used for a more realistic shear analysis of PSC girders.

2.1.3 Kaufman and Ramirez (1988)

This paper presents research on high-strength prestressed concrete beams loaded in shear and flexure. The focus of this paper was on the ultimate shear behavior of high-strength, prestressed concrete beams. The authors employed the truss model to obtain an accurate model which shows the behavior of the entire beam as opposed to the segmental approach sometimes used. In their investigation, Kaufman and Ramirez tested six full-scale AASHTO I-beams that included four Type I and two Type II. The beams were cast at a local precast plant and designed according to ACI and AASHTO bridge specifications. Each of the beams were loaded to failure and monitored for strain and centerline deflection. Three different failure modes were observed: (1) flexural, (2) web crushing, and (3) shear tension. The web crushing, flexural and shear tension failures were all very explosive and brittle, however, if conservatively detailed following either ACI or AASHTO specifications a more ductile failure was achieved.

High-strength concrete increased the capacity of the diagonal truss member which allowed for smaller inclination angles. As the angle of inclination gets smaller, the web reinforcement becomes more efficient through the mobilization of more stirrups. The effectiveness of the truss model was contingent on the detailing of the members to allow redistribution of internal forces and increased ultimate strengths. The amount of reinforcement, both longitudinal and transverse and the proper development of these reinforcements have a great affect on the shear strength of prestressed, high-strength concrete beams. Proper development must be achieved by controlling the concrete stress in the web and flexural compression zone before web crushing occurs.

In order to prevent early tension shear failure, it is important to ensure that the transfer zone of the prestressing steel is behind the support region. If shear cracks develop that cross the transfer region of the prestressing steel, the bond will be damaged leading to a shear tension failure. The authors proposed that an alternative mechanical anchorage could be used to avoid this problem. Also noted was the fact that the ACI and AASHTO provisions are conservative in properly detailed members.

2.1.4 Elzanaty, Nilson, and Slate (1986)

This research investigated the effect of high-strength concrete on the shear capacity of reinforced concrete beams. The authors tested 18 beams with different concrete compressive strengths ranging from 6,000-12,000 psi (41-83 MPa). Of the 18 beams, only three had web reinforcement. Shear strength contribution from the concrete is essentially the "shear resistance of the still uncracked compression concrete above the top of the diagonal crack, aggregate interlock along the diagonal crack, and dowel resistance provided by the longitudinal reinforcement." In high-strength concrete, the diagonal tension crack usually forms suddenly and typically has a much smoother shape than regular strength concrete leading to a decrease in aggregate interlock and subsequently reducing the shear capacity of the member.

The beams were reinforced with longitudinal ASTM Grade 60 deformed reinforcing bars with a yield strength of f_y=63 ksi (434 MPa). The stirrups were smooth round bars ¼ inch in diameter (6.4 mm) with f_y=55 ksi (379 MPa). The beams were all 7 inches (178 mm) wide by 12 inches (305 mm) deep. To identify the influence that f'_c, a/d, and ρ_w had on the shear capacity, beams without web reinforcement were tested, whereas the beams with web reinforcement had a constant a/d ratio of 4.0 while f'_c varied. The tests on all of the beams were all loaded with symmetric concentrated loads. The loading was done in 4 kip (17.8 kN) increments up to a predicted load of 70 percent of the ultimate load where the load increments were reduced to 2 kips (8.9 kN). Strains, displacements, and crack development/propagations were measured at each load step. Material samples taken from each beam were tested to determine the compressive strength and modulus of rupture after each beam test.

Once flexural cracks formed in the shear spans the behavior of the beam varied depending upon the values of f'_c, a/d, and ρ_w, and was shaped by the presence or absence of web reinforcing steel. Beams without web reinforcing and with ρ_w=0.012 failed suddenly in shear by forming a diagonal crack from the compression zone near the applied load towards the support. The beams without stirrups and with an a/d = 4 had an ultimate capacity in shear that was a little greater than the cracking load, but beams with an a/d = 2 showed significant shear capacity beyond the diagonal cracking load. Failure was observed to occur by either splitting along the flexural reinforcement or sudden propagation of the critical inclined crack into the compression zone of the beam.

The authors concluded that the shear strength of beams without any web reinforcements increased with the increase of concrete compressive strength. They also stated that the current ACI codes for predicting shear capacity of concrete beams was unconservative for beams without web reinforcement and having high f'_c and a/d, with low ρ_w. This was because the ACI code didn't fully consider the effect of ρ_w and a/d, yet overestimated the benefit of increasing compressive strength. Shear failures were more abrupt and the failure surfaces were smoother for beams with high-strength concrete.

2.1.5 MacGregor, Sozen, and Siess (1965)

In this study 104 simply supported, prestressed-concrete beams were tested in shear to determine the effects of web reinforcements on the overall shear capacity. All beams' span was 9 ft with overall cross-sectional dimensions of 6 X 12 inches. Ten of the beams had a 2 X 24 inch deck cast on top after the prestressing strand was released. Five of the beams were rectangular, 43 were I-sections with 3 inch-thick webs, and 45 had a 1.75 inch-thick web. The strands had varying levels of prestress force ranging from 60-127 ksi, but with most beams' strands prestressed to 120 ksi. Some of the beams had the prestressing tendons draped in the shear spans at an angle ranging from 1.5 to 10 degrees.

During the testing of the beams, different cracking patterns were observed for the inclined cracks. "Web-shear crack" was defined in this paper as an inclined crack which occurs in the web before flexural cracks appeared in its vicinity. In contrast, flexural cracks occurred in the shear span before stresses were high enough to cause web-shear cracks. If an inclined crack occurred it was either an extension of a flexural crack or it occurred over or beside a flexural crack. The flexural crack that caused the inclined crack was referred to as an "initiating crack."

For beams with draped tendons both web-shear and flexure-shear cracks were observed, however, the majority of the beams developed flexure-shear cracks. The test results indicate that draping the longitudinal reinforcement increases the inclined cracking load in the beams which developed web-shear cracks, and decreased the inclined cracking load for beams which developed flexure-shear cracks.

Two shear failures associated with the tied arch phenomenon were observed, namely tie rod connection failure and web distress failure. These failures were more prevalent in beams without web reinforcement therefore causing a large eccentricity of the compressive thrust. Shear compression failure also occurred where the inclined cracks reached the top of the beam under the loading point. In this type of failure the web reinforcement acts to restrain the opening of the inclined cracks and distribute the forces over a larger area.

The loads which caused flexure-cracking were found to correlate closely with the flexural cracking load near its point of origin. Web-shear cracking loads could be found by using an uncracked section analysis. These loads were increased for beams with web reinforcement and in general it was found that stirrups increased the shear capacity of prestressed concrete beams. The web reinforcement was also found to increase the overall strength and ductility of the beams.

2.1.6 Saqan and Frosch (2009)

The shear strength of concrete is dependent on many factors such as concrete shear strength, the shear contribution of the prestressing steel and mild steel reinforcement. This research focused on the contribution of the flexural reinforcement with respect to the overall shear capacity of prestressed-concrete beams. Nine beams with varying amounts of mild reinforcement were tested to determine their effect on the shear capacity. All of the tested beams had the same prestressing force with identical cross-sectional dimensions (14 x 28 in. [336 x 711 mm]) and concrete strengths.

The testing was divided into three series, each with three beams for experimentation. Every series contained one beam with only prestressing strands and the other two beams had different quantities of mild steel reinforcement, as noted in the research, in addition to the prestressing strands. The prestressing strands were ASTM416, 0.5 inch (12 mm) seven wire Grade 270 low-relaxation prestressing strands. The mild steel used was ASTM A615, Grade 60 reinforcing bars. The concrete was specified as ASTM C150, Type I with nominal design strength of 6000 psi (41 MPa). The beams were tested as simply supported with a concentrated load applied at mid-span. The load was applied in 5 kip increments up to the calculated cracking load after which 2 kip load increments were used. A load cell was used to measure the load and LVDTs were used at mid-span and at the supports to measure deflections. Strains were measured in the prestressing strands as well as in the mild reinforcement at mid-span by means of strain gauges.

The authors found that beams with mild reinforcement were much stiffer and the overall behavior of the beams was similar to that of a tied arch. All of the beams failed in shear-compression with the failure surface as the primary flexure-shear crack. For beams with only prestressing strand reinforcement the failure was more violent. It was also noted that by increasing the cross-sectional area of the prestressing steel the shear capacity also increased. Adding mild reinforcement (for larger moment capacity) increases the shear strength of the prestressed member.

2.2 Literature Review for CFRP application

All over the United States those responsible for the maintenance of our highway bridges are looking for better methods to rehabilitate them. The use of carbon fiber reinforced polymers (CFRP) for the rehabilitation of reinforced concrete members has been a rapidly growing rehabilitation option over the last few years. CFRP has been found to be useful due to its high strength, light weight, corrosion resistance, non-metallic properties, and its ease in application. The purpose of this literature review is to summarize the application of CFRP in the case of shear reinforcement for in service highway bridge girders.

There has been a large amount of research and testing on the use of CFRP for flexural strengthening but little on its application for shear strengthening. A selection of papers on the subject of CFRP for shear reinforcement is summarized in the following sections. These papers focus on the design and effectiveness of CFRP reinforcement for shear. Some of the important parameters that are needed for accurate design are the fiber thickness, fiber orientation, strip spacing, the fiber wrapping, and anchorage. In the papers, the authors present equations that can be used to calculate the additional shear capacity. Also provided are testing results that compare and verify the test and analytical results.

2.2.1 Carolin and Täljsten (2005)

This paper presents testing and research on the use of Carbon Fiber Reinforced Polymers for shear strengthening of reinforced concrete members. The paper addresses parameters of CFRP such as fatigue, anchorage, and the strain field in shear spans. There are several methods in designing of reinforcement with CFRP. These CFRP reinforcement design varies with respect to the orientation of the fibers, strip orientation, and strip thickness. The aim of the study was to address the various methods and compare them to provide insight into their application.

To provide data for the experimental study of CFRP for shear reinforcement the authors tested 23 rectangular beams. Each beam had a different configuration of the CFRP with respect to their angle of orientation, spacing, and fiber thickness. Each beam was loaded with a two point scheme to failure. Strains, stress, and shear strength were measured. Particular attention was paid to the failure mode of the reinforcement, whether it be anchorage or fiber rupture.

The study was able to provide insight into the use of CFRP in shear reinforcement. The authors found that the orientation of the fibers was a critical parameter. To maximize their performance, they must be aligned perpendicular to the shear cracks. Another aspect that was found to be of importance was the anchorage of the CFRP. Full wrapping was ideal, but in the field it may not be plausible. The author recommended further study in the field of anchorage. Measurement of the strain at specific points was found to be insufficient due to non-uniformity. Therefore, the authors suggest using strain measuring methods that cover the beam as a whole.

2.2.2 Zhang and Hsu (2005)

In this paper the authors present four objectives for their research of CFRP as shear reinforcement for concrete beams. The first is to increase the test database of shear strengthening using externally bonded composites. The second, to investigate the shear behavior and modes of failure of RC beams with shear reinforcement deficiencies with CFRP laminates. Thirdly, to study the effect of various CFRP types and shear reinforcement configurations on the shear behavior of the beam; and finally, to propose design methodologies that are based on experiments and analytical results.

Experimental data was obtained by testing 11 beams in shear with four CFRP configurations. Vertical strips, strips at a 45-degree angle from the longitudinal axis, a longitudinal strip along the middle, and a CFRP fabric placed along the whole side walls of the beam. The reinforced beams test results were compared to the test results with a control beam. Two design equations were used for calculating the shear contribution of the CFRP reinforcement. The design approaches were based on the traditional truss analogy.

Comparison of the test results led to the conclusion that CFRP provides an increase in shear capacity. CFRP strips were found to be very effective compared to CFRP fabrics. The diagonal side strips with angles of 45 and 135 degrees were found to provide the greatest increase in shear strength. The proposed design equations provided acceptable predictions for the reinforced beams shear strength.

2.2.3 Deniaud and Cheng (2004)

In this article the authors present their findings on shear design methods for concrete beams strengthened with Fiber Reinforced Polymer sheets. The two methods presented combine both the strip method and the shear friction approach. The methods describe the interaction between the concrete, the stirrups, and the FRP sheets. The equations were used and compared to 35 experimental test results.

The Strip Method is described in detail in the paper. An interface shear strength curve is needed for the use of the strip method and is explained in detail. One aspect of the method that was found was, as the width of the FRP sheets become smaller, the bond strength increases. The Shear Friction Method is also explained in detail. The continuous and discrete equations were used to support of the proposed method. Examples were also provided to demonstrate the usefulness of the two methods.

Various conclusions were obtained concerning the two methods. The first was that the design formulations can conservatively predict the experimental results. In addition, the strip method can be used and adapted in various anchorage configurations. Finally, despite the simplicity of the method, it well describes the interaction between the concrete, the stirrups, and the FRP sheets. Overall, the paper presents viable information to the formulation of design equations for FRP reinforcement.

2.2.4 Adhikary and Mutsuyoshi (2004)

The authors of this research tested and analyzed the effectiveness of using Carbon Fiber Sheets (CFS) as shear reinforcement of RC beams. CFS can be oriented in many ways with respect to fiber orientation, CFS thickness, and sheet depth. The authors address various methods of design in the experimental program to evaluate the contribution of CFS reinforcement.

Eight beams were used with different CFS reinforcement configurations. Different configurations were varied with respect to vertical and horizontal fiber reinforcement, U wrap or just side beam wraps only, thickness, and height of reinforcement on the side of the beam. The beams were loaded and failed in shear as expected. During the test strains, vertical deflection, and applied load was monitored and recorded. There were two prediction models evaluated that were developed to calculate the contribution of the CFS in shear.

The CFS was found to provide up to 109% increase in the shear capacity for the RC beams. This was based on the results of the configuration consisting of vertical U-wrapped beams. The researchers compared the two equations to the test data and found that both provided satisfactory results in predicting the added shear strength from the CFS. In conclusion, the authors provided sufficient analysis of the equations and test data to provide a confirmation on the usefulness of CFS in shear reinforcement.

2.2.5 Diagana, Gedalia, and Dlemas (2002)

In this research the authors studied the shear behavior of RC beams reinforced with CFRP. CFRP have been shown to be an effective option for the retrofitting of concrete beams for flexure and shear. The paper focuses on the reinforcement of shear because it is important to insure flexural failure of beams instead of shear. A total of ten beams were tested in this research. Two were used as control specimens, while the other eight were reinforced with CFRP's in various configurations. An equation was also used to calculate the increased shear strength of beams retrofitted with CFRP.

The two control beams were constructed with longitudinal steel for flexure and with steel stirrups for shear. An important part of this study was that the beams are already provided with steel stirrups, which is typically of in-service beam conditions. Four beams were given U-shaped CFF strips at 90- and 45-degree orientations at different spacing. The other four were given full-wrap CFF strips at 90- and 45-degree orientations at different spacing's. The beams were then loaded with a single point load to failure. An equation used in many design codes was used to calculate the increase shear capacity and was then compared with the test results.

Each configuration was found to have its pros and cons. However, all configurations were found to increase the shear capacity. Vertical full-wraps were found to produce the largest increase in shear strength but in field operations full-wraps are not always plausible. Diagonal U strips were found to provide the next highest increase in shear strength, which is a more plausible method in the field. An important aspect of failure of U strips is that they fail due to debonding which is addressed in the predictive equation. The equation used in design was found to provide accuracy up to 14% for most of the beams. The authors concluded that the equation is acceptable for CFRP design.

2.2.6 Hutchinson, Donald, and Rizkalla (1999)

This research paper presents the results of scale-model testing of AASHTO girders that had been strengthened in shear by applying external carbon fiber reinforced polymer (CFRP). The authors tested ten different configurations of CFRP wraps. The AASHTO I-girders present special needs when anchoring the CFRP wraps to the web to flange connection, which the authors addressed in the paper.

The experimental program consisted of seven scale-model pretensioned concrete girders. The girders were divided into two types consisting of two different internal stirrup configurations that are typically found in practice. The CFRP wraps configurations consisted of vertical wraps, diagonal wraps, and full wraps. The CFRP wraps were anchored by either clamping or a horizontal strip along the web. The beams were then loaded to their ultimate shear capacity. The capacity of the CFRP was then analytically calculated and compared to the actual found capacity.

The authors found that externally bonded CFRP wraps increased the shear capacity. The configurations that yielded the highest capacities were the diagonal and horizontal wraps anchored by a horizontal strip. They yielded a 36% and 35% increase, respectively.

2.2.7 Khalifa et al. (1998)

The authors of this research paper present their findings on the contribution of externally bonded FRP to shear capacity of RC beams. They reviewed research on shear reinforcement and testing of RC beams. The aim of the paper was to use the previous research to propose simple design algorithms for computing the contribution of FRP to shear strength of RC members.

The experimental results from 48 test specimens were used to validate the proposed design algorithms. The 48 specimens were collected from eight different research studies previously published. Two different design approaches were used; one based on Effective FRP Stress, and one based on Bond Mechanism. The paper presents all aspects of the approaches that need to be defined for design. These aspects include fiber orientation, fiber thickness, spacing, bond lengths, etc. Examples were provided for the use of each method. This provided the reader with a thorough explanation of each design approach.

Each design approach was found to be consistent with the ACI 318 protocol and was able to be easily applied for FRP reinforcement on RC beams. The first approach is based on effective FRP stress. This method was found to be valid for CFRP continuous sheets or strips with any orientation angle. The key aspect of that method is that the failure is controlled by sheet rupture. The second approach based on bond mechanism was also found to be valid for CFRP continuous sheets or strips. The key to this method is the effective width of the FRP sheet at delamination. This is because the method is controlled by the sheet delaminating. Both methods were found to conservatively underestimate the actual shear strength of the beams. The authors concluded that the design approaches can be used in calculating the contribution of CFRP's as shear reinforcement of RC beams.

3.0 EXPERIMENTAL TESTING PROGRAM AND RESULTS

3.1 Introduction

Eight precast, prestressed concrete girders were experimentally tested for this research. Two different tests were performed on the salvaged girders. The first test was to determine the effective prestress force that remained in the girder after more than 40 years of service, and subsequently the second test was performed to determine the ultimate shear capacity at the end of the girder. Details about these two tests are presented in this chapter. Section 3.2 describes the test setup and all of the preparatory work completed prior to the experimental testing. Section 3.3 summarizes the determination of the effective prestress force. Section 3.4 details the existing shear capacity tests. Section 3.5 presents the shear test results.

3.2 Test Setup

In order to apply the necessary external loads to the AASHTO girders, a steel reaction frame was designed and constructed. The completion of a new structural testing facility at Utah State University (USU) was finalized just prior to the commencement of this research. The Systems Materials and Structural Health Lab (SMASH Lab) at USU contains a strong floor which provided the means to anchor the reaction frame and develop the required external loads. A steel reaction frame was designed to be used in conjunction with this strong floor. The reaction frame was designed to maximize the width of the strong floor and had a capacity of 1,000,000 lbs with a live load factoring of 1.6L according to American Institute of Steel Construction (AISC) manual (AISC, 2007).

The reaction frame consists of two I-shaped columns attached to stiffened base plates that can be anchored to the floor. The columns support a stiffened I-beam that can be bolted to the flanges of the columns as shown in Figure 3.1. The cross beam was designed so that a hydraulic ram could be attached to the bottom flange of the beam and easily positioned anywhere along the length of the beam according to the test requirements. Once the reaction frame was designed and fabricated, it was delivered to the USU SMASH Lab and installed on the strong floor by means of eight 2.5 inch diameter threaded rods which held the base plates of the columns to the strong floor. Figure 3.2 shows a close-up of the base plate and Figure 3.3 shows the connection of the beam to the column.

Eight American Association of State Highway and Transportation Officials (AASHTO) Type II girders were procured for this testing. The first six were shorter in length and the last two girders were longer and from a different bridge. All girders had the same cross-sectional dimensions as shown in Figure 3.4. A portion of the bridge deck was left over the top flange of each girder and the resultant structural properties are listed in Table A.1.

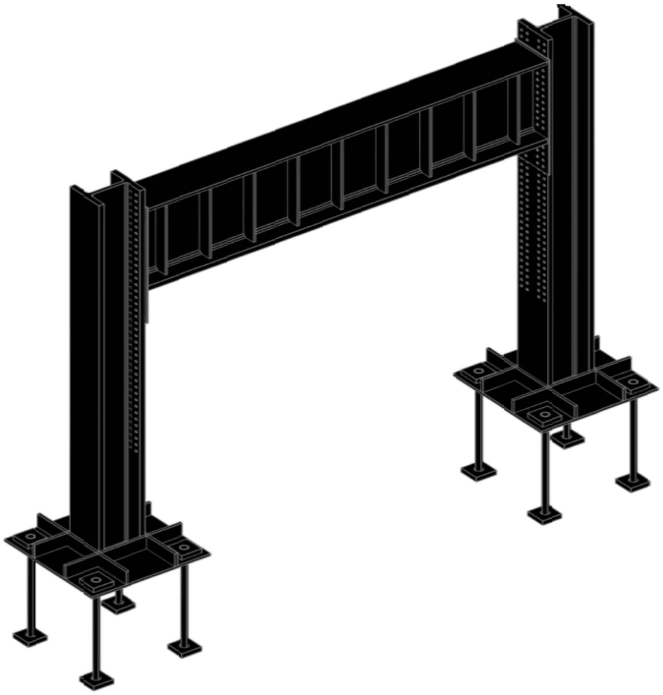

Figure 3.1 3-D view of reaction frame CAD model.

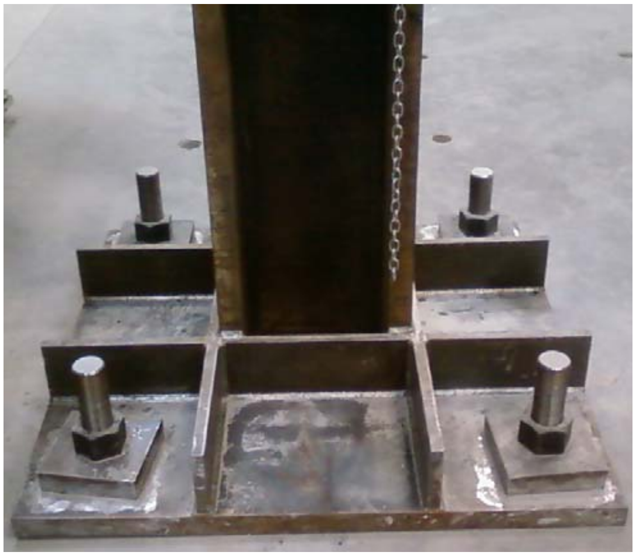

Figure 3.2 Base plate of reaction frame.

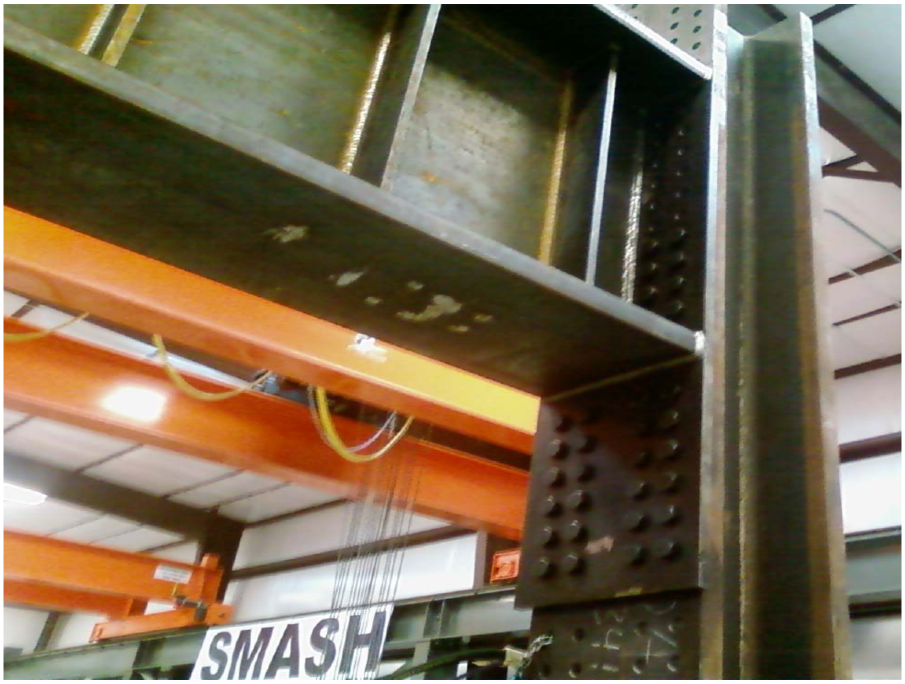

Figure 3.3 Beam to column connection

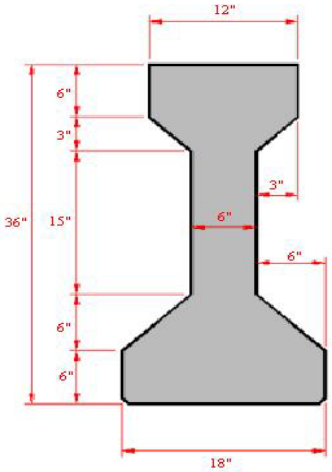

Figure 3.4 AASHTO Type II girder dimensions.

Girders 1 through 6 were salvaged from Interstate 215 (I-215) in Salt Lake City, Utah at 45th South. The bridge was built in 1968 as a four span bridge with span lengths of 23-ft, 74.5-ft, 74.5-ft, and 67-ft shown in Figure 3.5. Figure 3.6 shows a picture of the bridge as it was being torn down showing the bridge's in-service state. Figure 3.5 also shows that the bridge had a change of elevation of about 43 feet from one end to the other (for detailed bridge plans see Appendix A Figures A.3 through A.25). This slope caused the majority of the water and snow to run down into the expansion joint on the downward slope of the bridge causing degradation of the prestressed concrete girders due to corrosion of the steel reinforcements. It was the concern of UDOT that the deterioration that had occurred had reduced the shear capacity of the girders. Because they had several other bridges in similar states, UDOT was interested in evaluating the capacity of the girders. Each girder used in this testing was from Span 1 of this bridge where the most degradation had occurred. The center-to-center of bearing span length of these six girders was 22 feet 3 inches with an outside to outside dimension of 23 feet 7 inches. The girders were spaced at 9 feet on the bridge. The girders were made composite with an 8-in reinforced concrete cast-in-place deck. When the girders were delivered to USU, a portion of that deck was still intact. To prepare the girders for testing, the decking was squared up to provide a more uniform specimen (Figure 3.7).

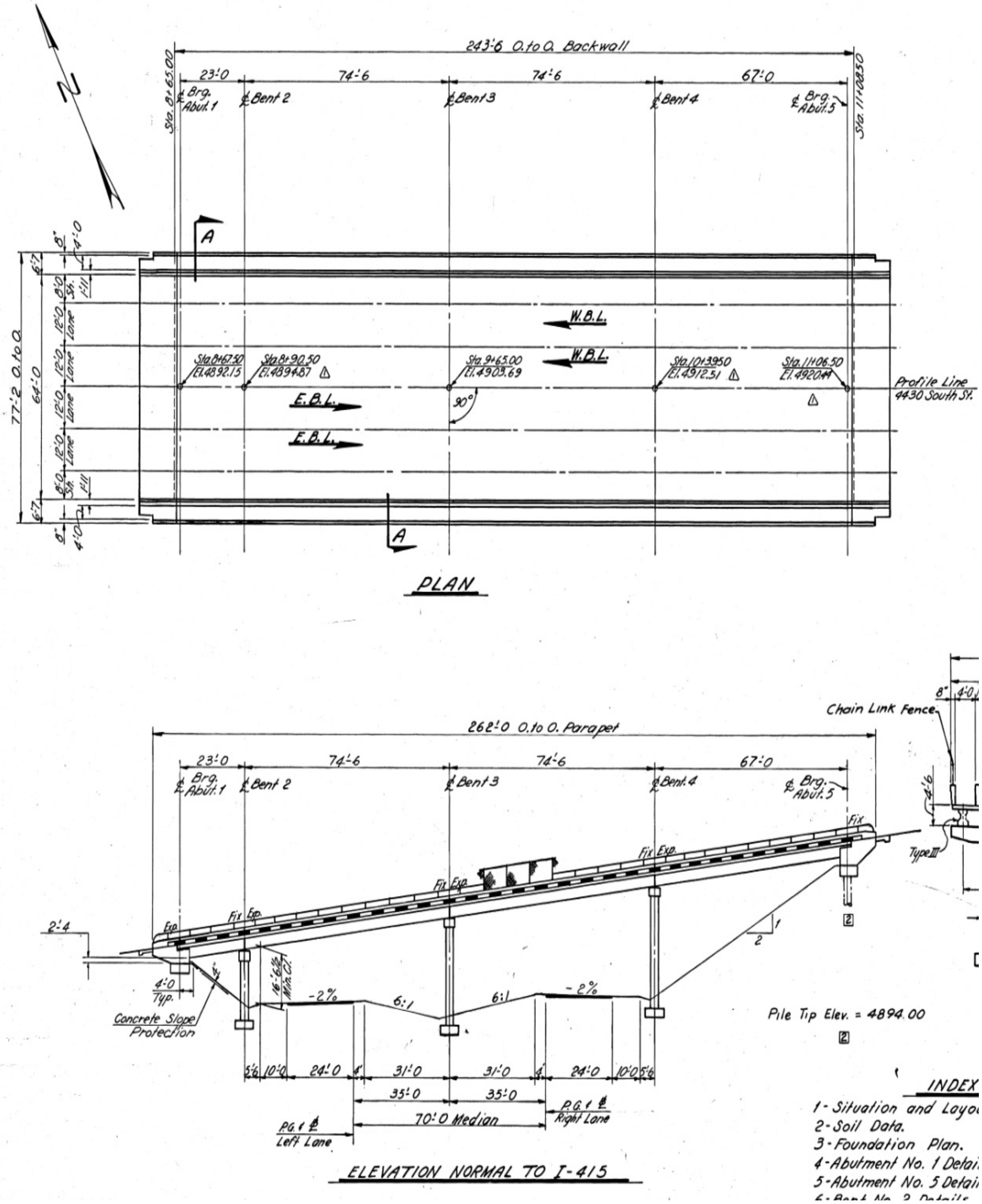
243'-6 O. to O. Backwall
23'-0
74'-6
74'-6
67'-0
Sta. 8+65.00
℄ Brg. Abut. 1
℄ Bent 2
℄ Bent 3
℄ Bent 4
℄ Brg. Abut. 5
Sta. 11+08.50
A
A
8"
4'-0
6'-7
8'-0 Sh.
1'-11
12'-0 Lane
12'-0 Lane
12'-0 Lane
12'-0 Lane
8'-0 Sh.
1'-11
6'-7
8"
4'-0
77'-2 O. to O.
64'-0
W.B.L.
W.B.L.
E.B.L.
E.B.L.
Sta. 8+67.50 El. 4892.15
Sta. 8+90.50 El. 4894.87
Sta. 9+65.00 El. 4903.69
Sta. 10+39.50 El. 4912.51
Sta. 11+06.50 El. 4920.44
90°
Profile Line 4430 South St.
PLAN
262'-0 O. to O. Parapet
23'-0
74'-6
74'-6
67'-0
℄ Brg. Abut. 1
℄ Bent 2
℄ Bent 3
℄ Bent. 4
℄ Brg. Abut. 5
Chain Link Fence
8"
4'-0
4'-6
Type III
Fix
Fix Exp.
Fix Exp.
Fix Exp.
Exp.
2'-4
4'-0 Typ.
4'
Concrete Slope Protection
16'-6½ Min. Cl.
-2%
6:1
6:1
-2%
1
2
Pile Tip Elev. = 4894.00
2
5'-6
10'-0
24'-0
4'
31'-0
31'-0
4'
24'-0
10'-0
5'-6
35'-0
35'-0
70'-0 Median
P.G. & ℄ Left Lane
P.G. & ℄ Right Lane
ELEVATION NORMAL TO I-415
INDEX
1- Situation and Layo
2- Soil Data.
3- Foundation Plan.
4- Abutment No. 1 Detai
5- Abutment No. 5 Detai

Figure 3.5 Plan and profile view of bridge over I-215.

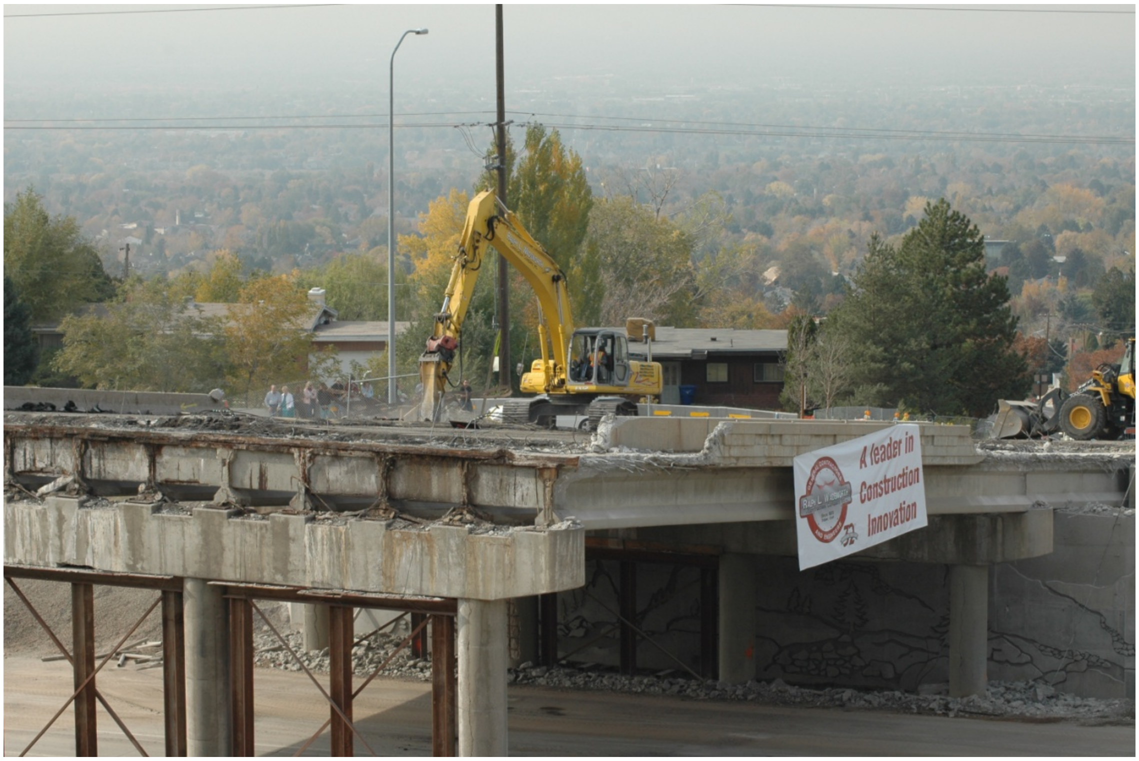
A leader in Construction Innovation

Figure 3.6 Bridge as it was being torn down.

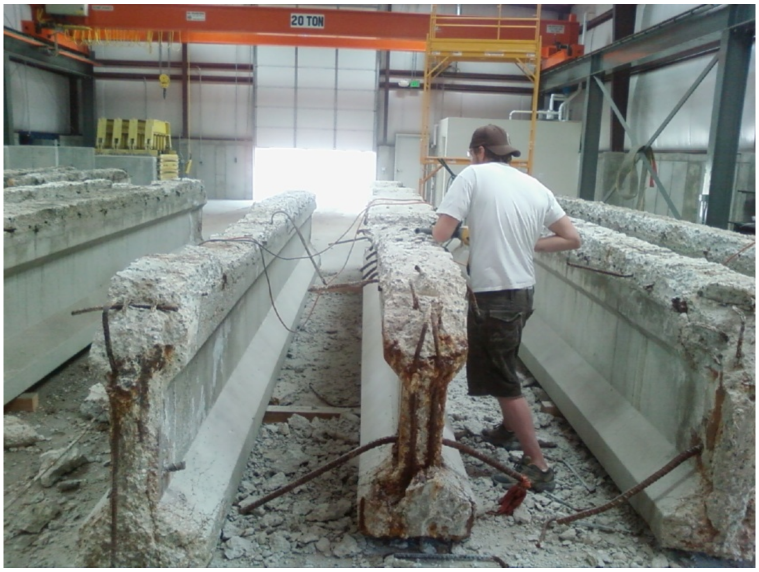

Figure 3.7 Girders before testing.

Each of the girders was reinforced for shear with No. 4 bars used as stirrups. The first stirrup was placed 7.5 inches from the center of the bearing and then 23 inches on center afterwards. The bridge plans specified that "all reinforcing steel shall be intermediate grade billet steel conforming with AASHO designation M-31. Deformations shall conform with AASHO designation M-137" (Utah State Department of Highways Structural Division, 1967). Intermediate grade billet steel was specified as 33-ksi according to the state of practice up to the 1970s. A sample of shear reinforcing steel was removed from the girder and tested using a Tinius Olsen universal testing machine and the yield strength of the web steel was verified as being 33.4-ksi. Figure 3.8 shows the stress-strain curve for the web steel that was tested.

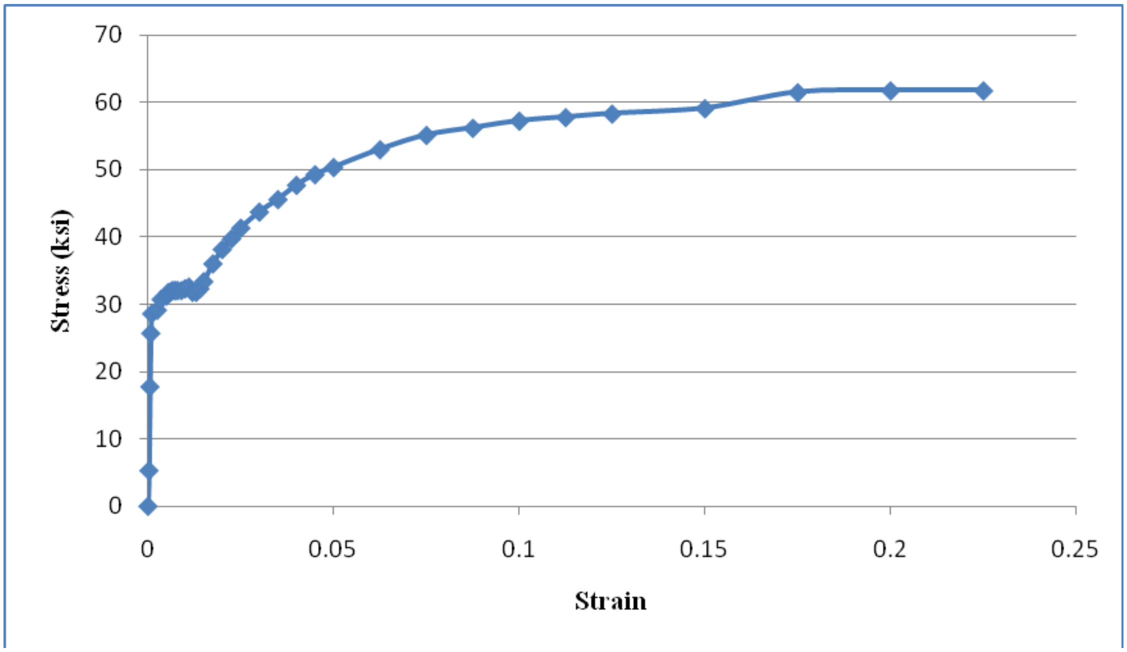

Figure 3.8 Stress-strain relationship for web shear steel.

The prestressing force after losses, according to the bridge plans, was specified as 176 kips at an eccentricity of 9 inches as measured from the bottom of the girder. The concrete compressive strength of the girder at transfer (f'_{ci}) was specified as 4,000-psi. Two concrete samples were removed from the control girder and tested in compression to determine the actual compressive strength according to ASTM standards. These tests yielded an average concrete compressive strength (f'_c) of 7,100-psi. A split-cylinder test was also conducted following

ASTM C496-86 guidelines to determine that the concrete tensile strength (f_t) was 590-psi for these girders. This relationship resulted in the tensile capacity being equal to 7.0 $f'_c{}^{0.5}$ which is close to the 7.5 $f'_c{}^{0.5}$ reported in most codes.

The prestressing strands that were used in the girders were 7/16 inch diameter, 7-wire strands. These strands were tested in the lab to establish their ultimate stress, which was measured as 258.7-ksi. Figure 3.9 shows the stress vs. strain diagram for the prestressing strands. From these results and talking with UDOT officials it was assumed that the specified grade for the strands used in these girders was 250-ksi stress relieved strands. The plans did not give any exact criteria with respect to the grade and type of prestressing strands, but 250-ksi stress relieved strands were common during this time period. The first row of four tendons was located at 2 inches from the bottom, a second row of four tendons was located at 3.5 inches from the bottom, a third row of two tendons was located at 27 inches from the bottom, and a fourth row of two tendons was located at 28 inches from the bottom. This resulted in an eccentricity of 11 inches as measured from the bottom of the girder, which disagrees with the bridge plan specifications calling for a 9 inch eccentricity for the prestressing strands (Utah State Department of Highways Structural Division, 1967).

The two longer girders were also AASHTO Type II girders. Both were 34.5 feet in length. These girders were salvaged from a highway bridge in southern Utah that had been in service for about 40 years. These two girders were also used in UDOT project No. 81F15404, Determining Residual Tendon Stress in Pre-Stressed Girders.

The girders were stressed with fourteen 7/16-inch diameter, 7-wire prestressing strands which imparted a total prestressing force of 264,600 lbs onto the beams at an eccentricity of 9.46 inches as measured from the bottom of the beam. The ultimate capacity, f_{pu}, of the strands was 250 ksi for these two girders. Two rows of four strands were placed 6 inches from the bottom of the girder followed by three rows of two strands. All strands were placed on a 2 inch center-to-center spacing. The residual prestress force in these longer girders was determined previously by means of a cracking test as 120,000-lbs. The compressive strength of these girders was specified as 5,000-psi, but was experimentally determined to be 9,300-psi. No information was available

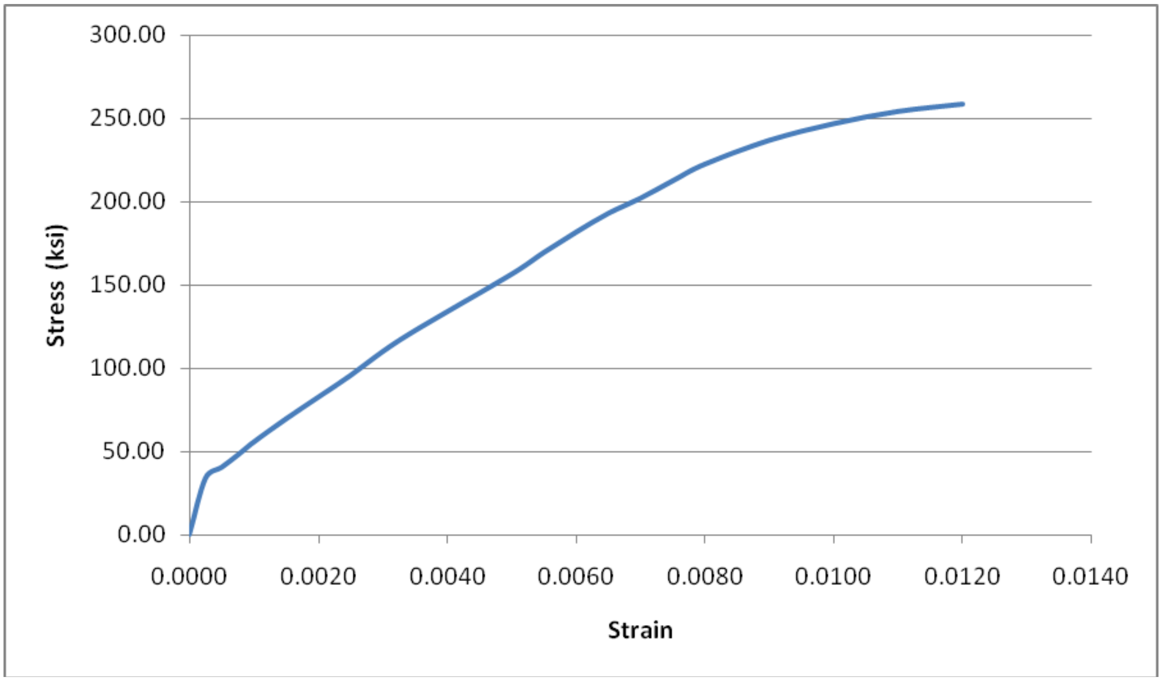

Figure 3.9 Stress-strain relationship for prestressing strands.

on the shear steel properties, but since these girders were fabricated approximately at the same time as the other six girders and detailed by the same organization (UDOT), it was assumed that the web steel was also intermediate grade steel with a yield stress of 33-ksi. In the two longer girders, the stirrups began at six inches from the center of the support and were then spaced at 17 inches throughout the length of the beam.

3.3 Determination of Effective Prestress Force

Even though the strands were horizontal and had no vertical component to contribute to shear, it was still of interest to determine the residual prestress force. Since the girders had been exposed to corrosive conditions during a large portion of their service lives as well as other deterioration, the prestress force was not likely to be easily predicted. To this end, a simple test was performed to quantify the remaining prestress force after all losses had occurred during the 40 plus years of being in service.

Each beam was simply supported under the reaction frame so that a concentrated load could be applied directly at the mid-span of the girder. The external load was incrementally increased until there was a visibly clear crack across the bottom flange of the prestressed girder. Once this crack was identified, the load was held constant until the crack could be traced with a permanent marker to provide easy identification once the load was removed and the prestress force closed the crack.

After each girder had undergone this initial cracking, strain gauges were applied to each girder in three different locations with respect to the crack as shown in Figure 3.10. One 3.5 inch long foil strain gauge was placed across the crack, and two 2 inch long gauges were placed on either side of the crack. This strain gauge configuration was used to try to quantify the load that resulted in zero stress at the extreme tension fiber of the concrete. The value of the external load which resulted in the stress being equal to zero could be determined, and this value was used to calculate the effective prestress force.

Each of the girders had slightly different cross-sectional properties due to the deck portion that remained on top of the girders. Consequently, detailed section properties needed to be determined in order to accurately calculate the residual prestress force in the girders. For detailed information on each girder's structural properties see Appendix A, Table A.1.

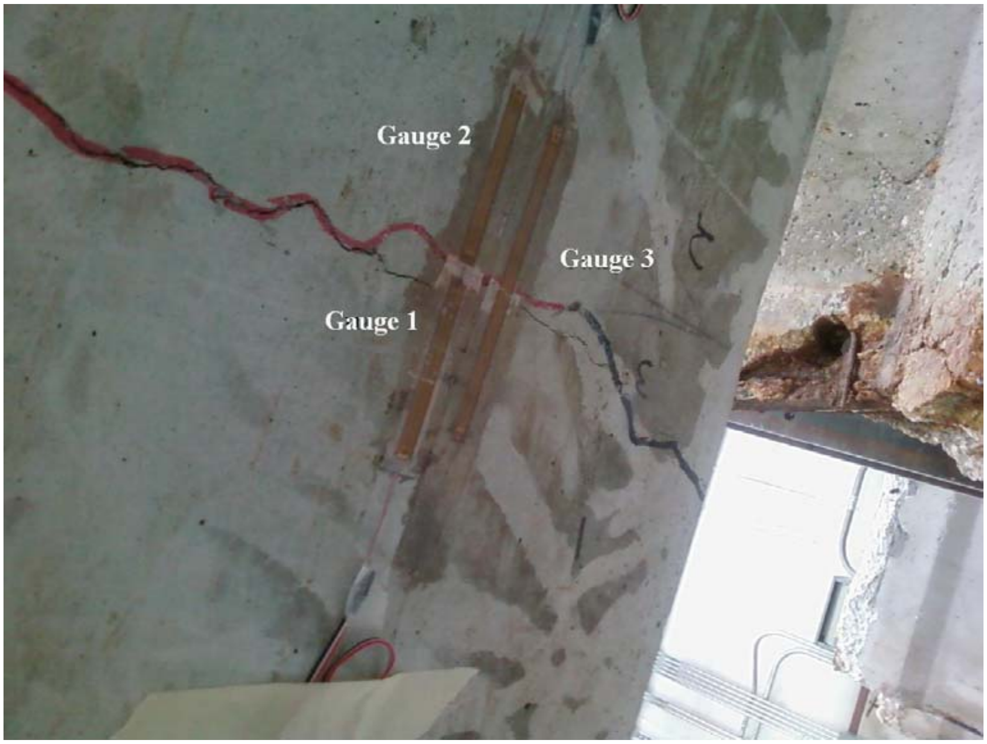

Figure 3.10 Typical strain gauge placements for effective prestress test.

Once the strain gauges were applied and allowed to cure, section properties were determined, and the cracking tests were conducted. The applied load (decompression load) was recorded throughout the duration of the test. From the decompression load the prestressing force could then be calculated by means of Equation 3.1 and Equation 3.2 with careful attention given to the sign of each term.

$$\sigma = \frac{P_e}{A_g} + \frac{P_e e y_g}{I_g} - \frac{M_{sw} y_g}{I_g} - \frac{M_{max} y_c}{I_c} \qquad (3.1)$$

Equation 3.1 can be rewritten as Equation 3.2 to find the effective prestress force.

$$P_e = \frac{\frac{M_{sw} y_g}{I_g} + \frac{M y_c}{I_c}}{\frac{1}{A_g} + \frac{e y_g}{I_g}} \qquad (3.2)$$

where:

σ = stress at the crack location (ksi)

P_e = the effective prestress force in the beam (kips)

I_g = moment of inertial of the girder at the crack location (in^4)

I_c = moment of inertial of the composite section at the crack location (in^4)

A_g = cross-sectional area at the crack location (in^2)

e = eccentricity of the prestressing force at the crack location (in.)

y_g = neutral axis location of the girder measured from the bottom of the beam at crack location (in.)

y_c = neutral axis location of the composite section measured from the bottom of the beam at crack location (in.)

M= the total moment at the crack location (kip-in.)

$$M = \frac{M_{max} x}{\frac{L}{2}} + M_{sw} \qquad (3.3)$$

x= distance from the crack to the nearest support (in.)

L= distance between supports (in.)

M_{sw}= moment at crack location due to self weight of the girder assuming a unit weight of .155 kip/ft^3 (kip-in.)

$$M_{sw} = \frac{.155}{1728} A x^2 \qquad (3.4)$$

M_{max}= maximum moment in the beam due to externally applied load (kip-in.)

$$M_{max} = \frac{P_a L}{4} \qquad (3.5)$$

P_a= externally applied load (kips)

A Vishay system 5000 data acquisition system was used to record the externally applied load measured with a Goekon strain gauge based load cell. Deflections were also measured using an LVDT placed on the top of the beam adjacent to the load cell. Three channels of strains were recorded from the strain gauges that were applied to each tested girder as described above. Measurements were recorded at a sampling rate of 10 hertz throughout each test. Tests were performed up to two different load steps. The first load was 70,000-lbs and the second was 80,000-lbs. This was done to ensure that the crack had sufficient dilation yet not enough dilation to destroy the strain gauges.

Once the test for each girder had concluded, the data was plotted as load vs. micro strain from the three strain gauges as well as plots of load vs. deflection. After analyzing the data, it was determined that the gauges that were placed directly over the crack showed the clearest point at which nonlinear behavior began. This determination came from examining others' research findings, and also observing that the collected data was most consistent from the gauges that were placed over the crack. The strain gauges placed to either side of the crack were expected to produce a bilinear response when plotted versus load, but no such response was observed. The load vs. deflection theoretically would have produced a similar bilinear response as the crack opened to that of load vs. strain, but the LVDT that was available at the time of testing did not read with the precision needed to determine the magnitude of load at which the crack opened, and therefore that data was not used in determining the decompression load. Typical plots of load vs. micro strain are shown in Figure 3.11 for each of the three gauge positions. The plots for the other girders are shown in Appendix B. The graphs produced from the gauges located to the right and left of the crack were more difficult to identify the exact load at which the crack opened up, and therefore the gauges over the crack were consistently used to determine the decompression load.

The experimentally determined decompression load was obtained by fitting a straight line to the initially "straight" portion of the load vs. strain plot produced from the strain gauges placed directly over the crack. The decompression load was defined as the load at which the strain enters the nonlinear portion and deviates from this initially straight line. As illustrated in Figure 3.12 the decompression load was 30,500-lbs for Girder 3. This definition comes from the reasoning that as soon as the externally applied load reaches a magnitude large enough to overcome the prestressing force, the section would crack and assume a different moment of inertia. With this changing moment of inertia the load vs. strain relationship would become nonlinear as the externally applied load was increased. Once the section was fully cracked, the load vs. strain continues on a "straight" line, but with a different slope having a fully cracked moment of inertia. The portion of the plot between the two "straight" lines is where there is still aggregate interlock and the section properties (moment of inertia) were changing with external load. For these reasons, the decompression load was taken as the point where the load vs. strain behavior initially changes.

The experimentally determined decompression load was obtained by fitting a straight line to the initially "straight" portion of the load vs. strain plot produced from the strain gauges placed directly over the crack. The decompression load was defined as the load at which the strain enters the nonlinear portion and deviates from this initially straight line. As illustrated in Figure 3.12 the decompression load was 30,500-lbs for Girder 3. This definition comes from the reasoning that as soon as the externally applied load reaches a magnitude large enough to overcome the prestressing force, the section would crack and assume a different moment of

inertia. With this changing moment of inertia the load vs. strain relationship would become nonlinear as the externally applied load was increased. Once the section was fully cracked, the load vs. strain continues on a “straight” line, but with a different slope having a fully cracked

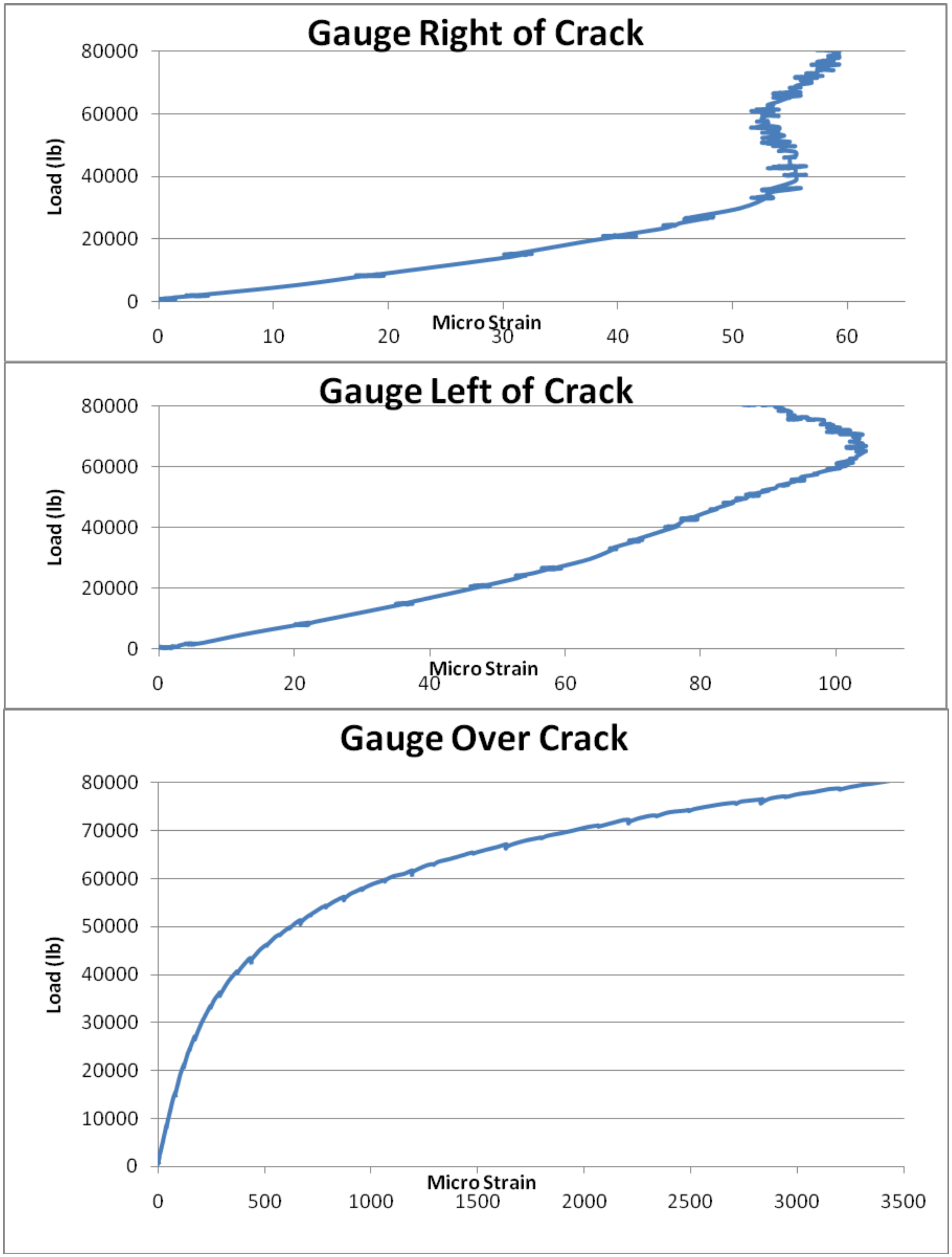

Figure 3.11 Strain gauges from girder 2 showing an example of the data recorded during the decompression tests.

moment of inertia. The portion of the plot between the two "straight" lines is where there is still aggregate interlock and the section properties (moment of inertia) were changing with external load. For these reasons, the decompression load was taken as the point where the load vs. strain behavior initially changes.

Table 3.1 lists each of the six girders' externally applied loads with their corresponding calculated decompression load as determined using Equation 3.2. Table A.2 shows all of the calculations used to determine the effective prestress force in the girders. The first load listed comes from the initial test in which an externally applied load of 70,000-lbs was reached before the test was concluded, and the second load listed comes from the test in which an externally applied load of 80,000-lbs was reached before the test was concluded. The average calculated residual prestress force shown in the fourth column is the force which was considered as the residual prestressing force in the girders. The bridge plans specified a prestress force after all losses of 176-kips.

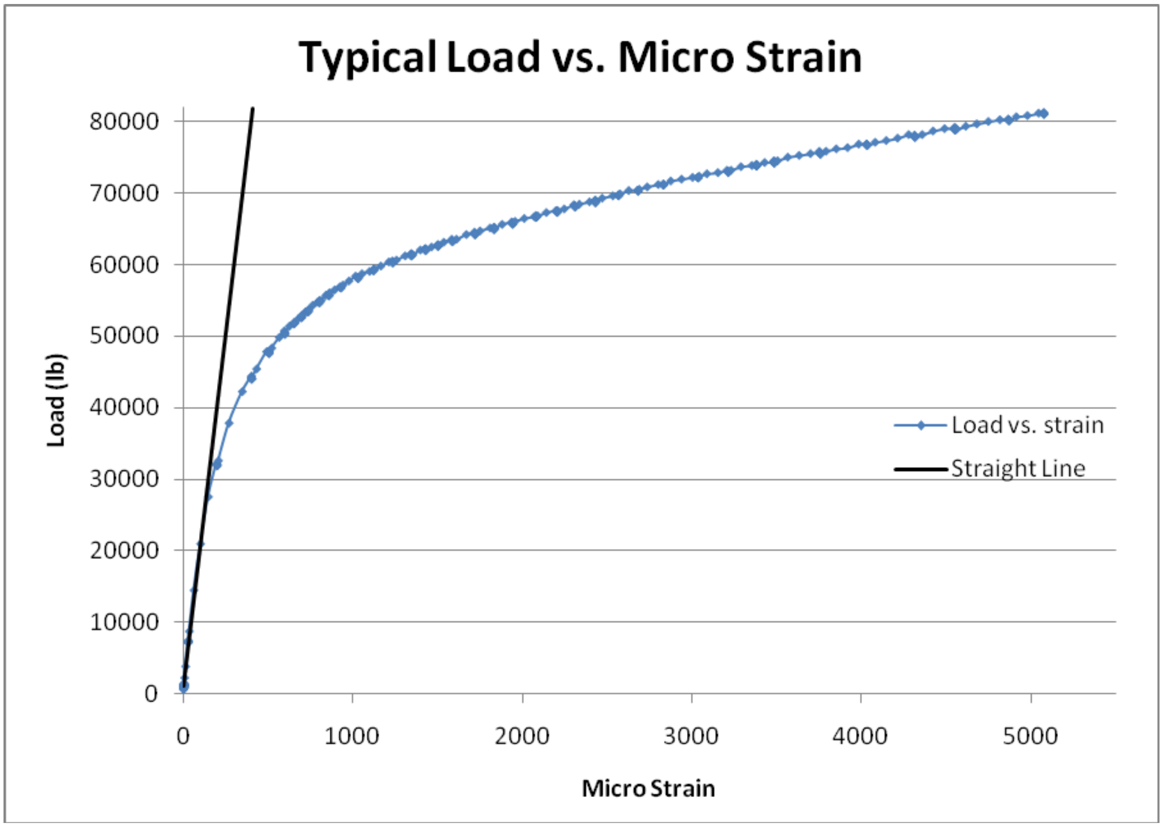

Figure 3.12 Typical load vs. micro strain plot (Girder 3 shown with an 80,000-lb limit).

Table 3.1 Girder decompression loads with corresponding residual prestress force

Beam	Decomp. Load (kips)	Residual Prestressing Force (kips)	Average Risidual Prestressing Force (kips)
1	38.5	175.2	172.3
1	37.0	169.4	
2	35.5	161.2	158.3
2	34.0	155.3	
3	30.5	138.6	145.3
3	34.0	151.9	
4	36.5	178.3	176.1
4	35.5	174.0	
5	37.5	170.0	172.9
5	39.0	175.9	
6	35.0	159.1	165.0
6	38.0	170.9	

3.4 Shear Tests

After the conclusion of the cracking test to determine the effective prestress force, shear tests were performed on each end of the eight girders. This section will focus on the shear behavior of the girders with an emphasis on the ultimate shear capacities. Of the eight girders tested, two were tested in an unaltered condition for a total of four shear tests. The other six girders were retrofitted with carbon fiber reinforced polymer at the ends. These beams were tested in shear with the goal of quantifying the additional shear capacity that the carbon fiber wraps imparted to the girders.

Prior to testing, each girder was fitted with a high strength grout pad on the top of the deck at a distance equal to the depth of the beam (not including the deck) plus one foot (d+1-ft). This was done to provide a flat surface for the hydraulic ram to react against as illustrated in Figure 3.13. The grout pad was not considered to provide any structural integrity and was not taken into account while determining the section properties of the girders (Table A.1).

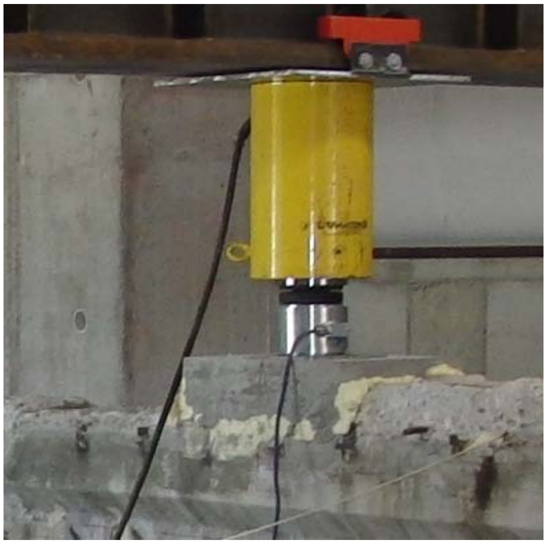

Figure 3.13 Grout pad fitted onto girders.

During testing, all girders were simply supported with varying span lengths as listed in Table 3.2. The spans varied due to the fact that both ends were tested independently. Once one end had been tested through failure, it became necessary to place the support under a portion of the beam where the cross-section was still intact. The shear spans were kept close to a constant distance of 48 inches on the ends with the exception of Girder 6. Girder six was initially tested with a 48-inch shear span, but cracking occurred in the middle of the girder rather than at the end. This failure behavior was produced by the carbon fiber reinforcement providing an increase in shear strength on the end, which was more than the shear strength in the middle of the beam where the shear force was lower. In order to ensure that failure occurred at the desired location, the shear span was decreased slightly, and the expected failure was observed. Girders 7 and 8 had varying shear spans due to space limitations in the lab, however, the desired shear failures were still observed. In Table 3.2 the A or B denotes which end was tested according to the markings on the beams. Top or Bottom denotes the orientation of the beam when it was in service (e.g. top refers to the up-slope end of the girder).

The externally applied load was measured during the shear tests in two ways. The first was by means of a pressure transducer in line with the hydraulic ram, and the second was with a

Geokon strain gauge based load cell. To calculate the load from the pressure transducer, the pressure (psi) was multiplied by the bore area of the ram (in^2) to get the load in pounds.

Table 3.2 Beam spans

Beam	Span Length (inches)	Shear Span (inches)
1A (Bottom)	268.25	48.00
1B (Top)	208.25	48.00
2A (Bottom)	206.00	48.00
2B (Top)	268.00	48.00
3A (Top)	210.00	48.00
3B (Bottom)	269.00	48.00
4A (Bottom)	215.50	48.00
4B (Top)	268.50	48.00

Beam	Span Length (inches)	Shear Span (inches)
5A (Top)	180.50	48.00
5B (Bottom)	270.00	48.00
6A(Top)	210.00	42.00
6B(Bottom)	268.00	42.00
7L A	199.50	51.50
7L B	163.00	48.00
8L A	150.5	48.5
8L B	196.00	49.00

Because the failure load was the most important criterion considered in this testing, the redundancy was desirable to verify results. Deflections were also measured with a LVDT placed on top of the girder next to the load cell. Strains were also measured in various locations on the girder. The strain gauges were placed strategically so that strains could be measured in line with the fibers of the carbon fiber wraps. Figure 3.14 shows a typical shear test setup.

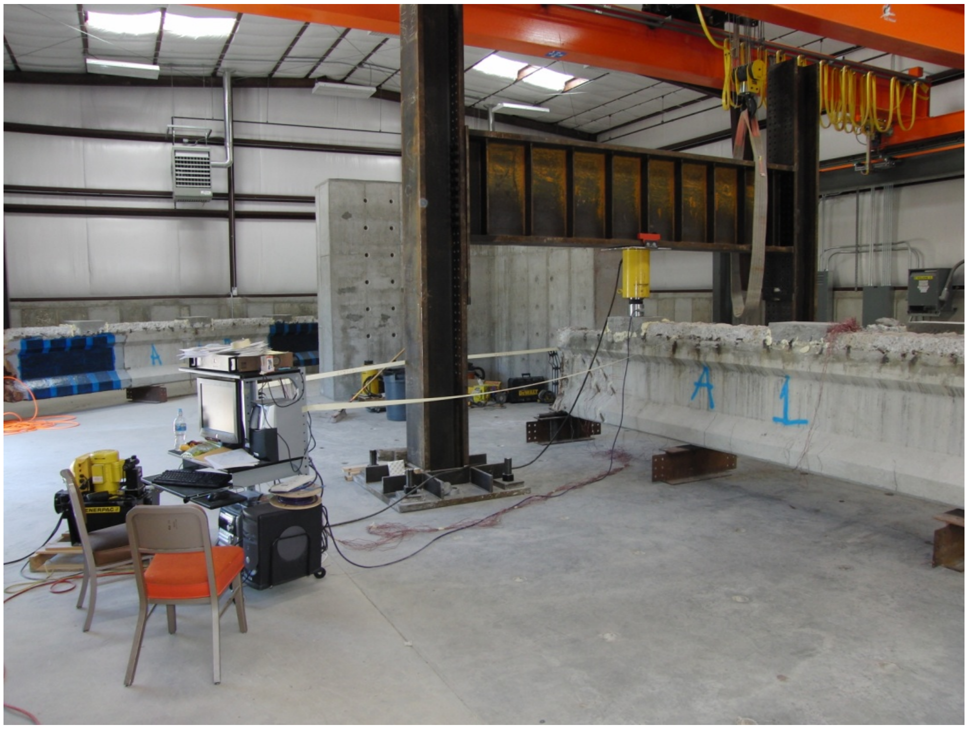
Figure 3.14 Typical shear test setup.

Once the setup was completed and the span lengths were recorded, the load tests were performed. A hydraulic ram was used to gradually apply the increasing load up to and through failure. The applied load was continuously monitored and recorded during the test by means of an online display in the Vishay software which was used in conjunction with the System 5000 data acquisition system. Once the applied maximum load had dropped off significantly, the test was terminated by completely removing the load, after which the girder and data were examined. Table 3.3 shows the ultimate shear capacities from each test.

The ultimate shear capacity was determined using simple statics. The ultimate load was determined as the maximum recorded load from the data. This load was used along with Equation 3.6 to calculate the ultimate shear force. For the completed tests, the base line shear was determined as 163.6-kips for Girders 1 through 6 and 261.5-kips for Girders 7 and 8 from the average shear of the two tests on the control girder (Girders 1 and 7). The ultimate shear capacities from Girders 2 through 6 are compared with a baseline ultimate shear capacity of

163.6-kips and Girder 8 was compared to a baseline ultimate shear of 261.5-kips to determine the increase in shear capacity that resulted from the application of the carbon fiber wraps.

Table 3.3 Ultimate shear capacity of each girder

Beam	Shear (kips)
1A(Bottom)	150.25
1B(Top)	176.86
2A(Bottom)	178.71
2B(Top)	162.70
3A (Top)	197.02
3B (Bottom)	209.50
4A (Bottom)	179.61
4B (Top)	174.80

Beam	Shear (kips)
5A (Top)	225.07
5B (Bottom)	244.94
6A(Top)	261.48
6B(Bottom)	151.79
7L A	263.36
7L B	259.63
8L A	311.96
8L B	307.97

$$V_u = \frac{P_u(L-L')}{L} \tag{3.6}$$

where:

V_u = ultimate shear force at failure (kips)

P_u= maximum applied load (ultimate load) (kips)

L = span length (in.)

L’ = shear span (in.)

For Girder 1, the failure mechanism was flexural shear where the cracks first developed at an angle of 90-degrees from the longitudinal axis. The cracks changed direction as the shear forces dominated the flexural effects, and the cracks’ directions changed to approximately 42-degrees. The cracks then dilated until there was not enough aggregate interlock or friction to hold the girder together at which point the girder experienced a significant failure as shown in Figure 3.15.

Girder 7 underwent a web crushing failure as it was loaded through its ultimate load. The cracks started in the web and extended toward the flanges as the load increased. Once the compressive strength of the concrete was reached, the top web of the top flange crushed causing the girder to fail. Figure 3.16 shows a close-up of the top flange after it had crushed.

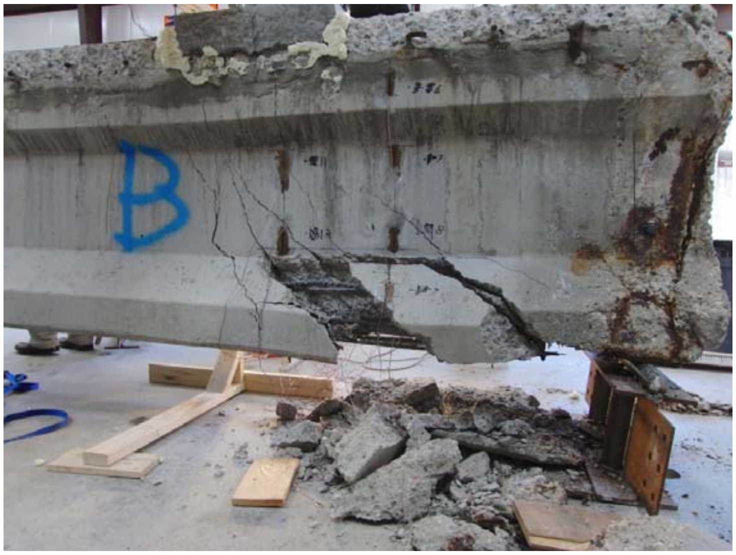

Figure 3.15 Girder 1 after undergoing a flexural shear failure.

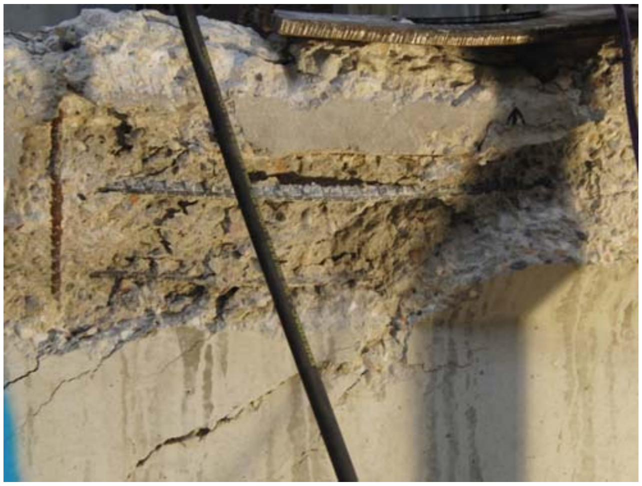

Figure 3.16 Top flange of Girder 7 after web crushing failure.

3.4.1 Shear Test Results

The experimental results will be presented in two formats. The first will be the load vs. deflection charts, and the second will be the load vs. (micro) strain charts. Due to some equipment failures, the load vs. deflection was not recorded on all beams. Load vs. deflection was of less interest in this study and consequently was not used in the determination of the results, but nevertheless will be shown herein for comparison purposes only. The load vs. strain charts are numbered in Appendix B according to the location of the corresponding strain gauge on the control girder. Figure 3.17 shows the control beam ends with their respective strain gauge locations and numbers.

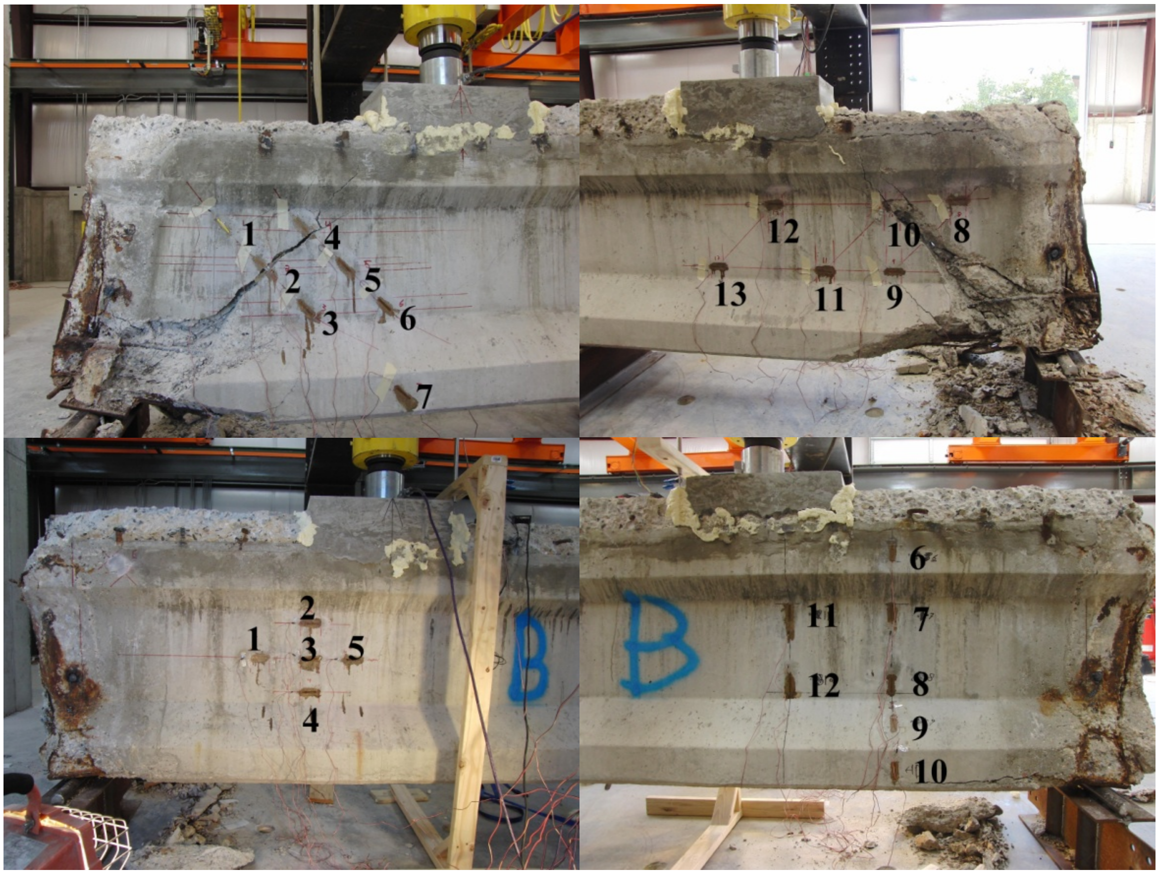

Figure 3.17 Placement and numbering of strain gauges.

Each beam failed in a repeatable manner with a primary shear crack forming at an average of 42 degrees. This shear crack began at the support and moved diagonally up the girder towards the point of the applied load. The primary shear crack was accompanied by other shear cracks, but smaller in size. The accompanying cracks were generally parallel to the primary shear crack. The behavior of the beams with the carbon fiber failed in a slightly different way, but in general the failure mode was the same.

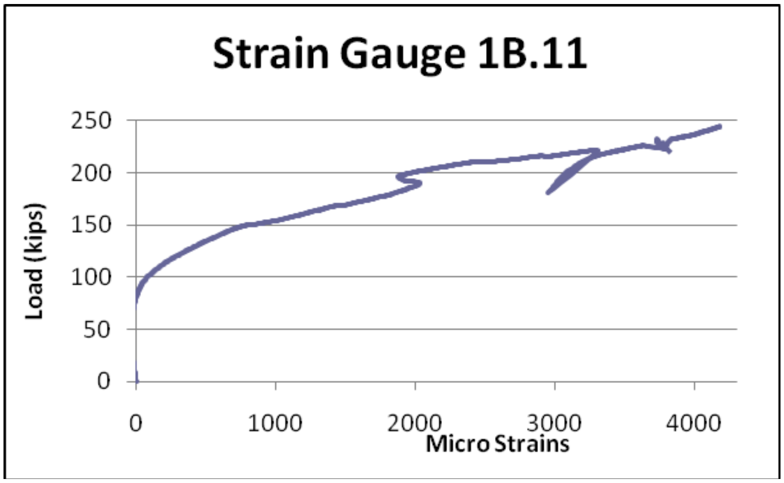

Figure 3.18 Strain gauge on control Girder 1B.

The strain was measured at the concrete surface. By measuring the strain in the concrete, compatibility can be used to assume that the strain in the steel was the same as in the concrete. As was shown in Figure 3.8 the yield stress of the shear steel was 33-ksi. This stress occurred at a strain of 0.003, yet the strain in the concrete was 0.004, showing that the stress in the concrete at failure was at, or a little above, the yield stress of the steel and therefore verifying that the girder failed as the steel yielded.

3.5 CFRP Design

Over the years CFRP fabrics have been found to be useful in providing external reinforcement of structural members. While most of the research has focused on the testing of new members, little amounts of testing and research have been done on retrofitting aged, full-scale girders, with CFRP fabrics. The CFRP fabric system chosen for this testing project was the

MBrace® CF 160 system that was generously provided by The Chemical Company (BASF). This product was chosen because of its simplicity in application and proven superior performance.

There were five different CFRP configurations tested for this research. Each configuration was tested twice by applying it on six 40-year-old AASHTO girders. After the testing of the first set of 6 girders (12 tests), the most efficient configuration was selected and then tested two more times on the second set of differently reinforced AASHTO girders to allow for further comparison. A specific issue had to be addressed when using external CFRP fabrics for I-shaped girders. When loaded in shear a large normal force begins to develop on the web to flange connection (see Figure 3.19). During loading this would cause the CFRP strips to delaminate prematurely resulting in a small increase in capacity. This delamination of the carbon fiber was one of the main criteria used in developing the CFRP application schemes.

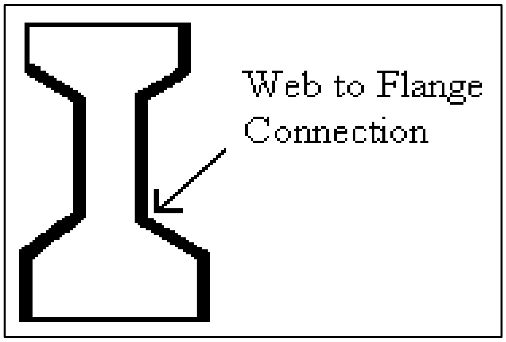

Figure 3.19 Location of web to flange connection.

3.5.1 Configurations

The first girder tested was used as the control. There was no external reinforcement put on either of the ends. Figure 3.20 is a drawing of the beams configuration while Figure 3.21 is an actual picture of one of the ends of the control girder before testing.

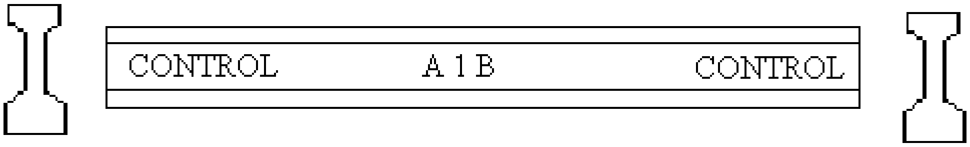

Figure 3.20 Girder 1: No external reinforcement.

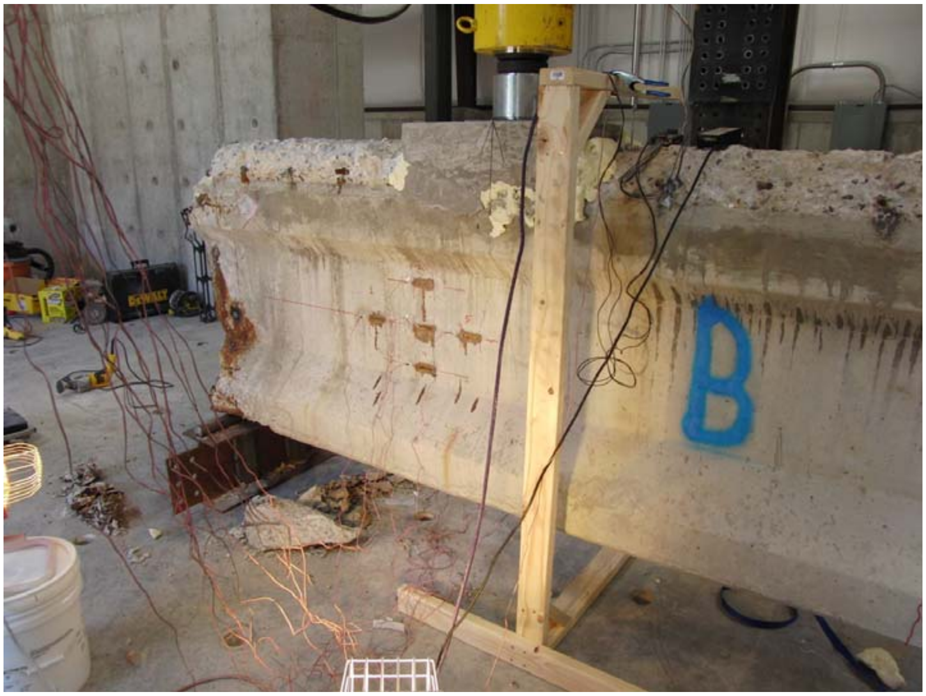

Figure 3.21 Girder 1: No external reinforcement.

The second girder tested was the first one that was reinforced with CFRP. Each side consisted of three vertical U-shaped strips that were 20 inches wide placed right next to each other (see Figures 3.22 and 3.23). The strips were anchored with an embedded CFRP laminate along the web to flange connection (see Figure A.24 in Appendix A for detail). This configuration was provided by engineers from The Chemical Company (BASF). It was selected because it addressed the anchorage of the CFRP to the web to flange connection.

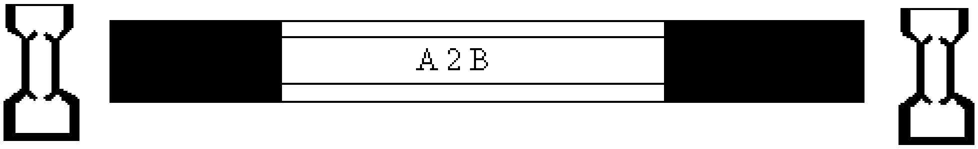

Figure 3.22 Drawing of Girder 2 CFRP design.

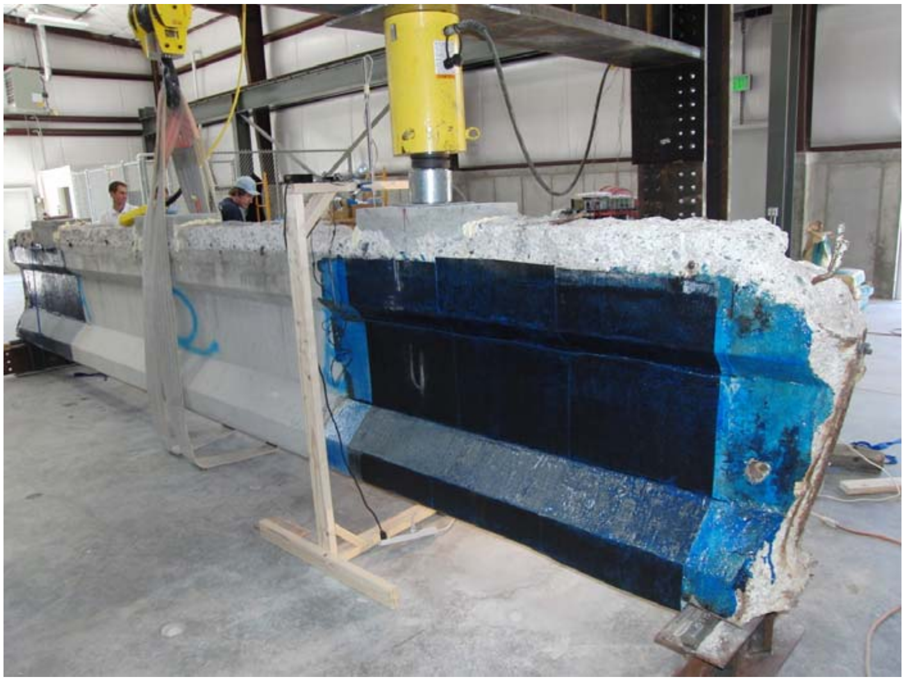

Figure 3.23 Girder 2 CFRP design

The third girder had CFRP strips oriented at a different angle. Each side consisted of six diagonal (45 degrees) strips 10 inches wide spaced at 4.5 inches and two horizontal strips with a height of 15 inches and 70 inches in length applied over the diagonal strips along the web (see Figures 3.24 and 3.25). Since the diagonal strips could not be continuous, the strips were overlapped on the bottom flange to simulate continuity. This configuration was selected from previous research entitled "FRP for Shear Strengthening of AASHTO Bridge Girders" by Hutchinson, Donald, and Rizkalla (1999). The authors found this configuration to be one of the most effective in increasing shear capacity of AASHTO prestressed girders.

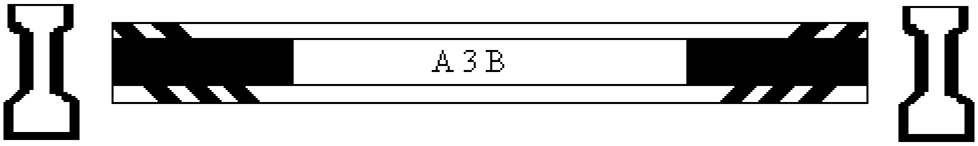

Figure 3.24 Drawing of Girder 3 CFRP design.

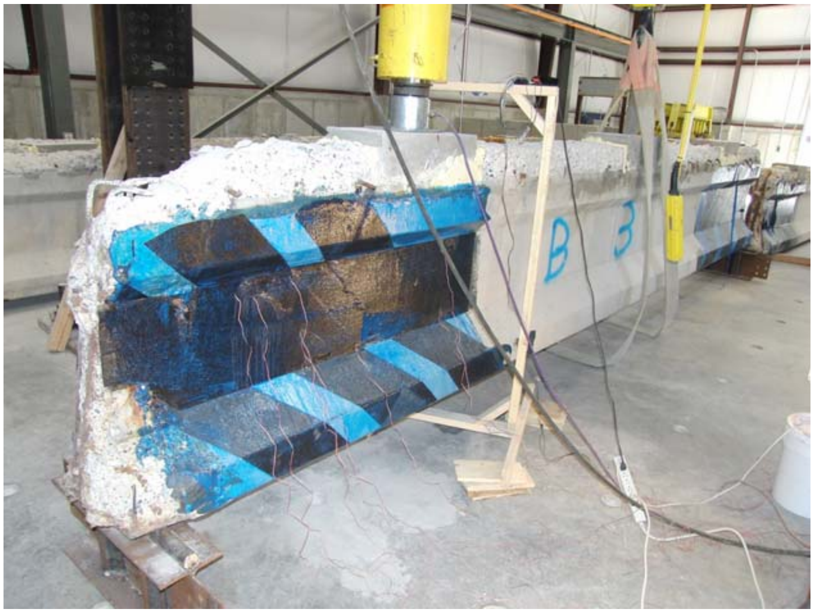

Figure 3.25 Girder 3 CFRP design.

The fourth reinforced girder was similar to the third except that the web was not reinforced with a horizontal strip of CFRP. Specifically each side consisted of six diagonal (45 degrees) strips 10 inches wide spaced at 4.5 inches (see Figures 3.26 and 3.27). Since the diagonal strips could not be continuous, the strips were overlapped on the bottom flange to simulate continuity. This configuration was selected for comparison with Girder 3 results. The configuration did not have an anchorage system which provided for comparative results with the anchored configurations. This allowed us to see how the horizontal anchorage system was performing and adding to the shear capacity.

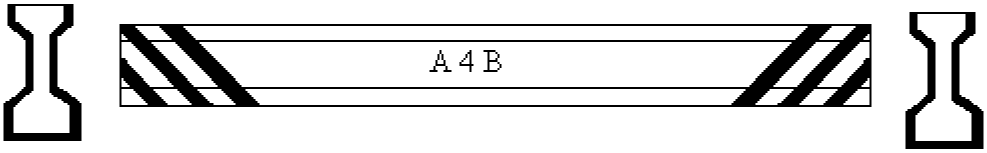

Figure 3.26 Drawing of Girder 4 CFRP design.

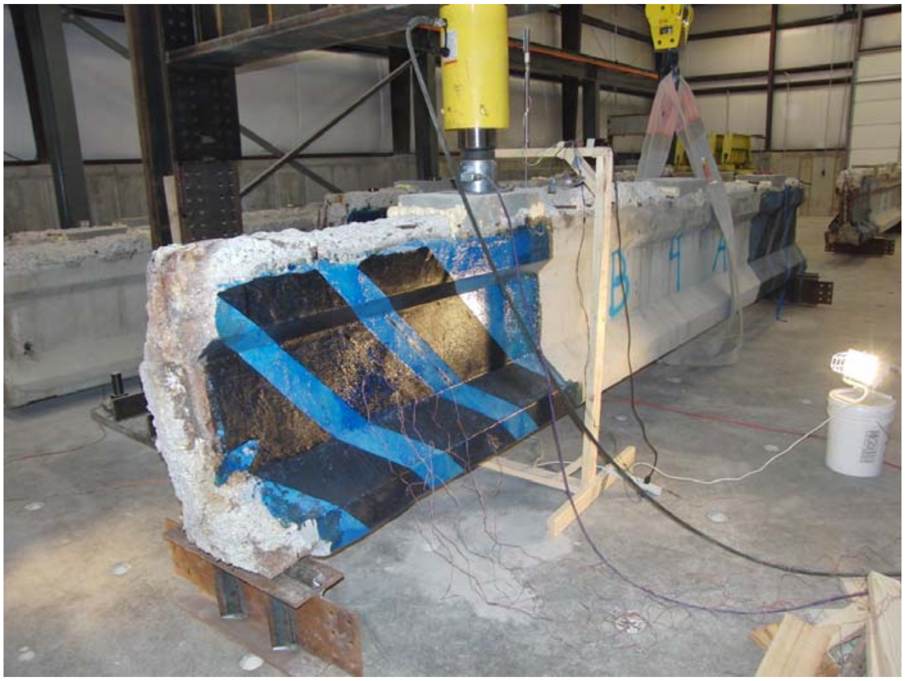

Figure 3.27 Girder 4 CFRP design

The fifth girder was instrumented with individual vertical strips of CFRP as well as the horizontal middle strip. Each side consisted of four vertical U-shaped strips with a width of 10 inches spaced at 4.5 inches and two horizontal strips with a height of 15 inches and 63 inches in length were applied over the vertical strips for anchorage along the web (see Figures 3.28 and 3.29). This configuration was selected from previous research entitled "FRP for Shear Strengthening of AASHTO Bridge Girders" by Hutchinson, Donald, and Rizkalla (1999). The authors found this configuration to be one of the most effective in increasing shear capacity of AASHTO prestressed girders.

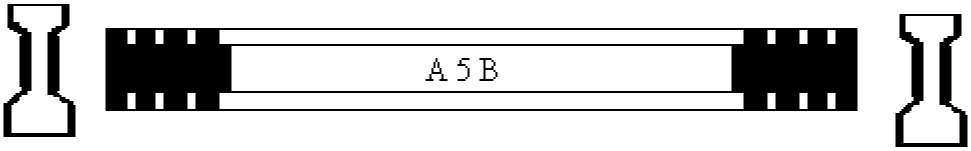

Figure 3.28 Drawing of Girder 5 CFRP design.

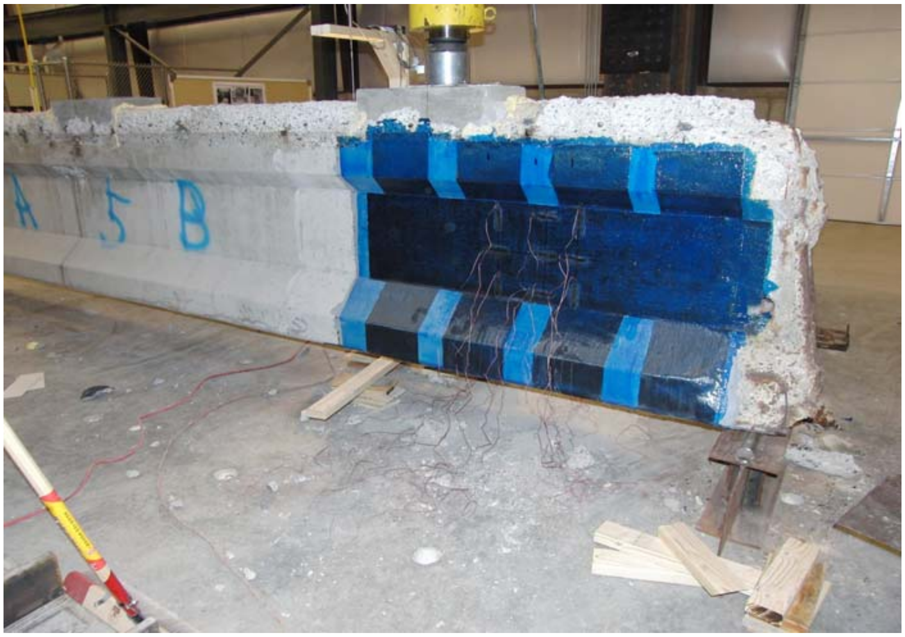

Figure 3.29 Girder 4 CFRP design.

The last reinforced girder of the group of six had a combination of reinforcing schemes. Each reinforced side consisted of six diagonal (45 degrees) strips 10 inches wide spaced at 4.5 inches (see Figures 3.30 and 3.31). The strips were anchored using an embedded CFRP laminate along the web to flange connection (see Figure A.24 in Appendix A for detail). Since the diagonal strips could not be continuous, the strips were overlapped on the bottom flange to simulate continuity. This configuration was selected to see how the embedded anchorage system would perform with diagonal strips.

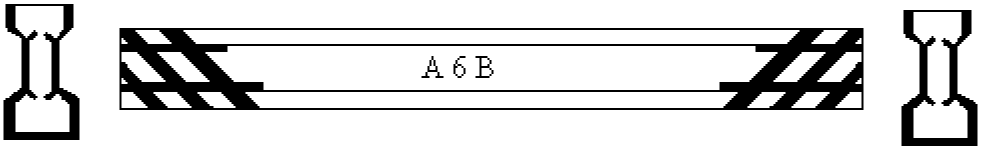

Figure 3.30 Drawing of Girder 6 CFRP design.

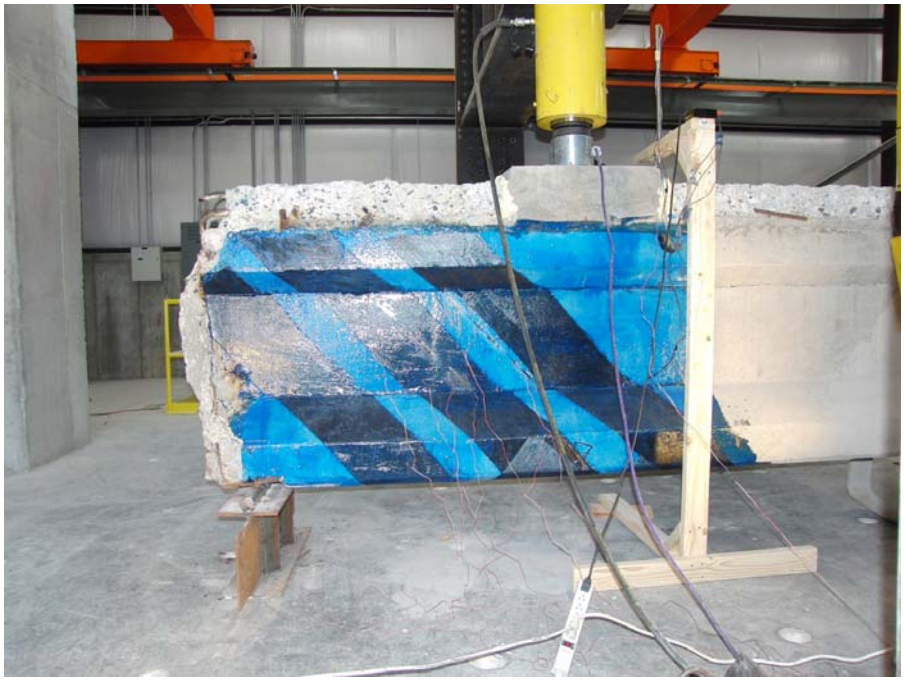

Figure 3.31 Girder 6 CFRP design

In addition to the previously mentioned six girders, two additional girders were tested. These last two girders had similar prestressing strand configurations but had smaller stirrup spacing. By testing these two girders it was believed that the CFRP reinforcement on other girders could be evaluated. Figures 3.32 and 3.33 show a drawing and picture of the seventh girder tested, the control girder from the second set of two girders.

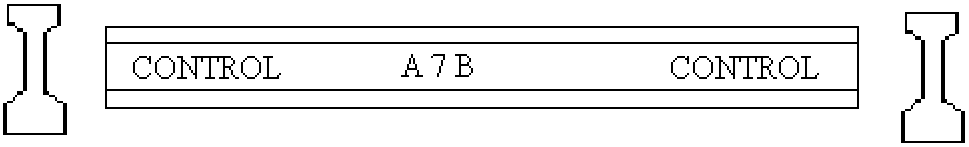

Figure 3.32 Girder 7 with no external reinforcement.

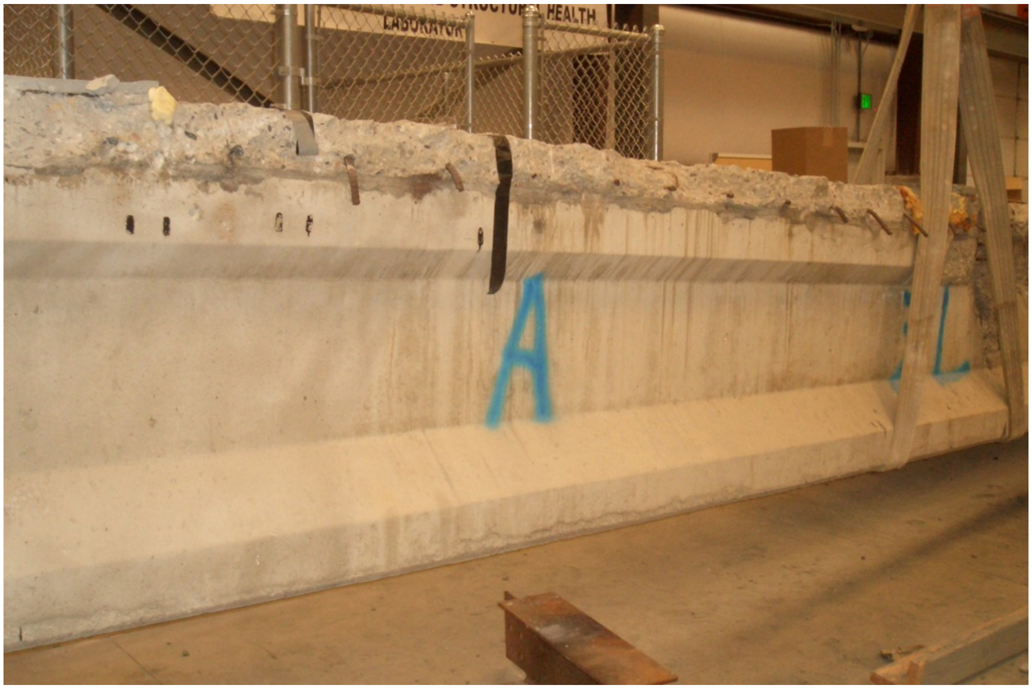

Figure 3.33 Girder 7 with no external reinforcement.

The eighth girder tested was the same girder as Girder 7 but was reinforced with the same configuration as girder 5. Each side consisted of: Four vertical U-shaped strips with a width of 10 inches spaced at 4.5 inches and two horizontal strips with a height of 15 inches and 63 inches length were applied over the vertical strips for anchorage along the web (see Figures 3.34 and 3.35). This configuration was selected because it yielded a high increase in shear capacity and its ease in application.

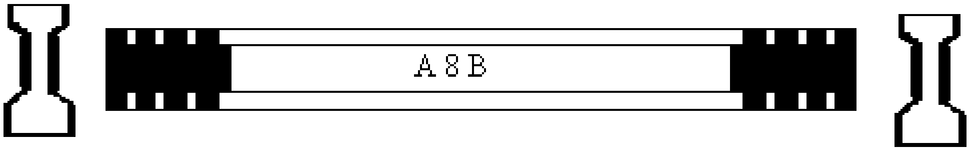

Figure 3.34 Drawing of Girder 8 CFRP design.

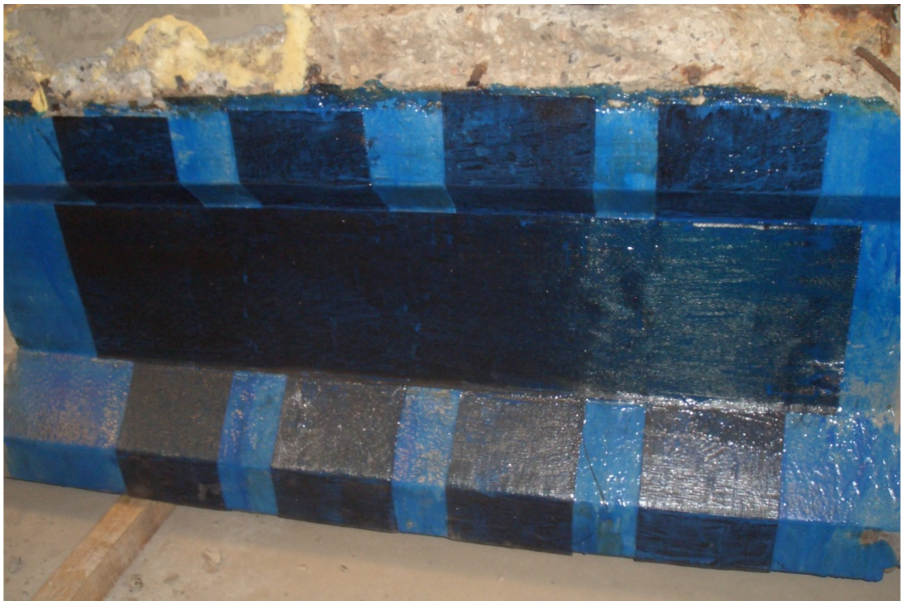

Figure 3.35 Girder 8 CFRP design.

3.5.2 CFRP application

The Chemical Company (BASF) provided detail instruction on how to apply the CF 160 System to the prestressed concrete girders. The installation required preparing the concrete surface for the application of the MBrace® materials. The concrete preparation required crack repair, sand blasting to at least an ICRI CSP 3 profile, and removal of all dust, laitenance, and bond inhibiting compounds. After the surface preparation was completed the MBrace materials were applied in the following order; the MBrace® Primer, the MBrace® Putty, the MBrace® Saturant, then the MBrace® CF 160 fabric (see Appendix A Figures A.25-A.33 for material detail). For testing, the MBrace® Topcoat was not applied for the last step because the topcoat is for a cosmetic appeal. In practice, the MBrace® Topcoat would be applied as the last step (for detailed instruction on the application see Figures A.34-A.39 in Appendix A). After application of all products the girders were given a seven day curing period.

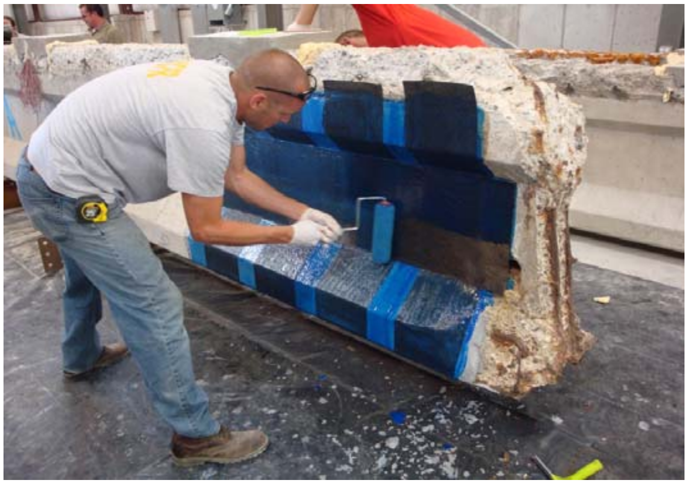

Figure 3.36 Application of CFRP MBrace® system.

3.6 Testing Analysis of CFRP Reinforced Girders

Each load test consisted of placing a hydraulic jack at a distance D (depth of the girder) plus one foot from the end support. The girder was then monotonically loaded until complete failure was achieved. Before each test the support and loading locations were measured and used to calculate the ultimate shear capacity. During each test the load, strain, and deflection (next to applied load) were monitored and recorded. Figure 3.37 is typical graph of the different types of measured data. Graphs of the measured data can be found in Appendix B.

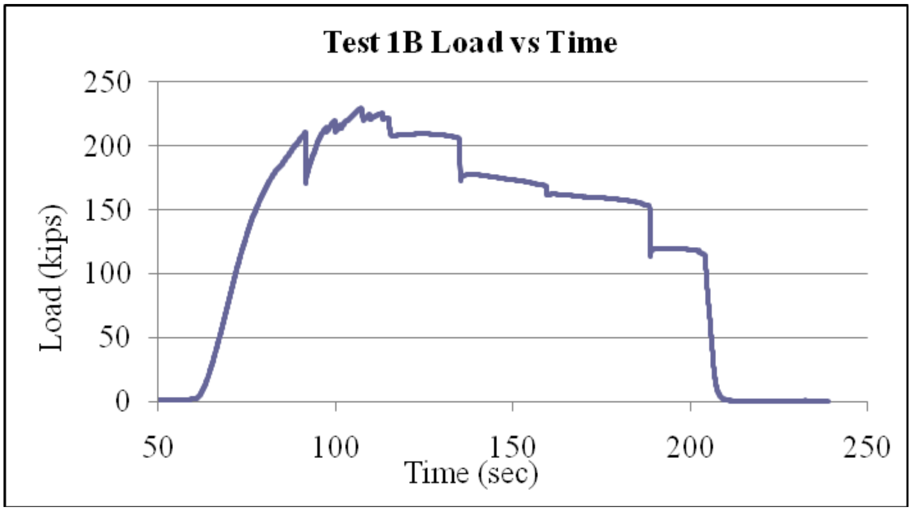

Figure 3.37 Typical graph of measured data.

3.6.1 Test 2A

For this test, the hydraulic jack applied load at a distance of 48 inches from the end support with a beam span of 208 inches. The beam failed in shear at an applied load of 333.36 kips. The CFRP system failed due the CFRP laminate anchorage failing, which led to a large normal force at the flange to web connection. After the anchorage failure, the concrete surface attached to the CFRP fabrics was ripped off causing the reinforcement to fail (see Figure 3.39 for detail). Under the CFRP reinforcement there were multiple cracks that were roughly 45-degrees from the load to support (see Figure 3.38 for failure crack orientation). The failure cracks were pushed closer to the support and towards the top of half of the girder. The test yielded an ultimate shear force of 255.68 kips which is an increase of 92.12 kips or a 36.03% increase in shear capacity compared to the average control capacity of 163.56 kips. The data recorded for load, strain, and deflection are found in Appendix B figures B.27 to B.33. The strain gauge orientation can be found on Figure 3.38 and compared to the strain gauges on control test 1B.

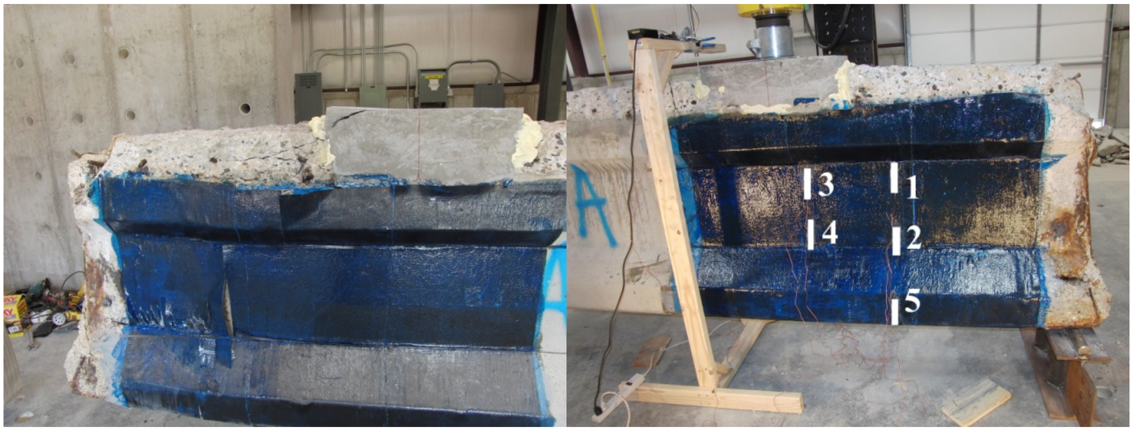

Figure 3.38 Failure of Test 2A and strain gauge orientation.

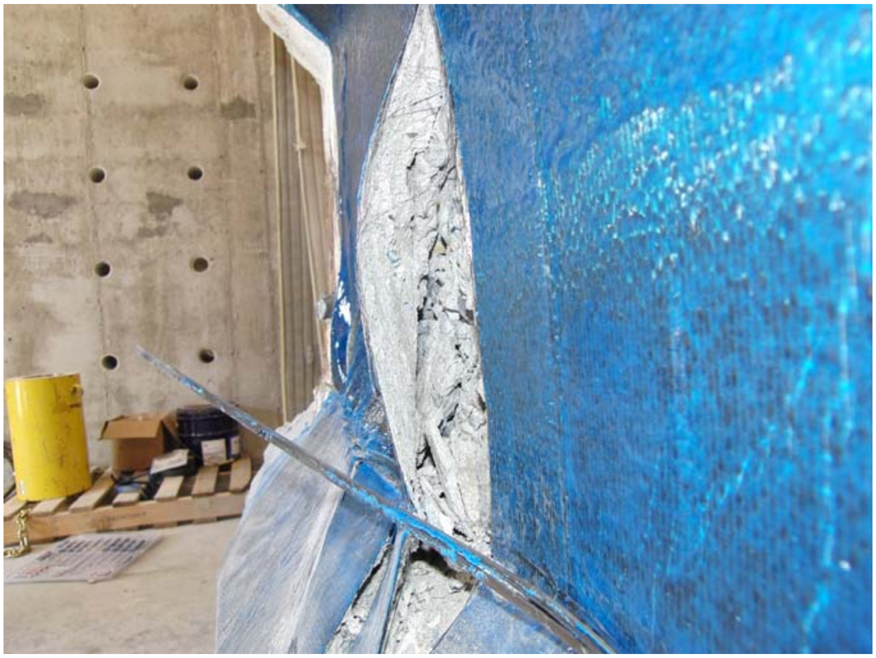

Figure 3.39 Anchorage failure and concrete surface failure.

3.6.2 Test 2B

For the second test on this beam, the hydraulic jack applied load a distance of 48 inches from the end support with a beam span of 268 inches. The beam failed in shear at an applied load of 198.2 kips. The CFRP system failed due the CFRP laminate anchorage failing, which led to a large normal force at the flange to web connection. After the anchorage failure the concrete surface attached to the CFRP fabrics was ripped off causing the reinforcement to fail (see

Figures 3.40 and 3.41 for detail). Under the CFRP reinforcement there were multiple cracks that were roughly 45-degrees from the load to support. The failure cracks were pushed farther from the support and towards the bottom half of the girder (see Figure 3.41 for failure crack orientation). The test yielded an ultimate shear force of 162.70 kips which is a decrease of 0.86 kips or a 0.53% decrease in shear capacity compared to the average control capacity of 163.56 kips. The two tests of this CFRP configuration yield large differences in increased shear capacity. The inconsistent results are assumed to be from the cuts made into the girder for the anchorage system. Further inconsistencies were found in tests 6A and 6B which had the same anchorage system. The data recorded for load, strain, and deflection are found in Appendix B Figures B.34 to B.40. The strain gauge orientation can be found on Figure 3.40 and compared to the strain gauges on control test 1B.

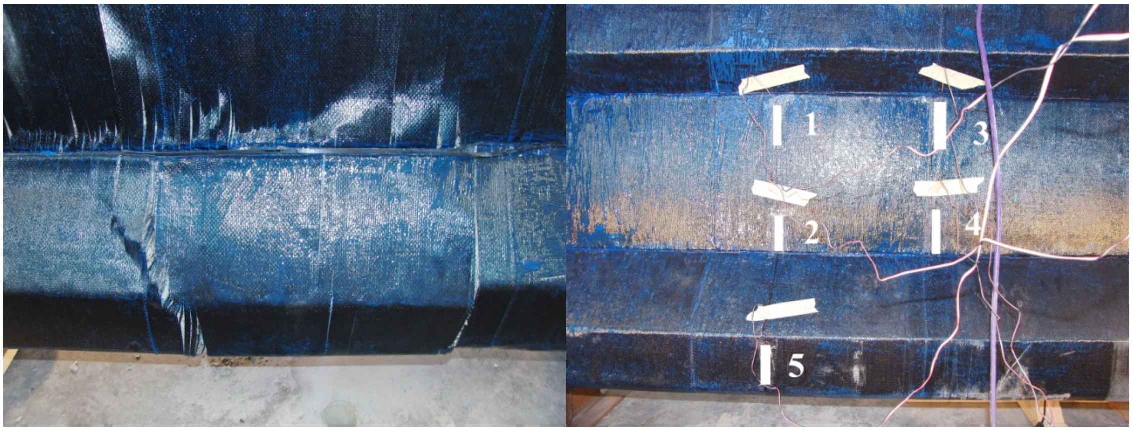

Figure 3.40 Anchorage failure and strain gauge orientation.

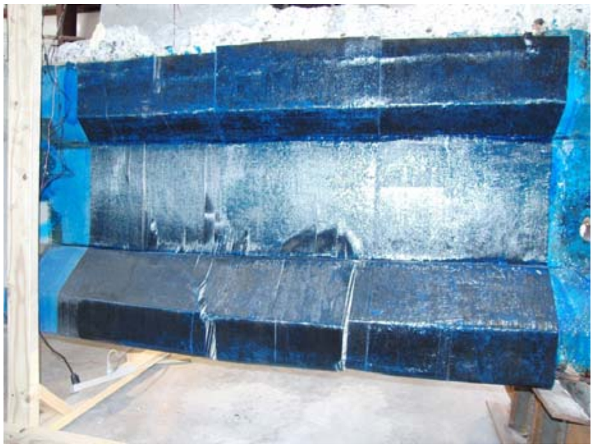

Figure 3.41 Failure of Test 2B.

3.6.3 Test 3A

For this beam, the hydraulic jack applied the load at a distance of 48 inches from the end support with a beam span of 210 inches. The beam failed in shear at an applied load of 255.4 kips. The CFRP system failed due to the horizontal strip of CFRP fabric ripping the top layer of concrete off, which led to a large normal force at the flange to web connection. After the anchorage failure the CFRP diagonal strips ripped off the top layer of concrete leading to delamination causing the reinforcement to fail (See Figures 3.42 and 3.43 for detail). Under the CFRP reinforcement there were multiple cracks that were roughly 45-degrees from the load to support. The failure cracks were similar to the controls crack orientation (see Figure 3.43 for failure crack orientation). The test yielded an ultimate shear force of 197.02 kips which is an increase of 33.46 kips or a 16.98% increase in shear capacity compared to the average control capacity of 163.56 kips. The data recorded for load, strain, and deflection are found in Appendix B Figures B.41 to B.49. The strain gauge orientation can be found on Figure 3.42 and compared to the strain gauges on control test 1A.

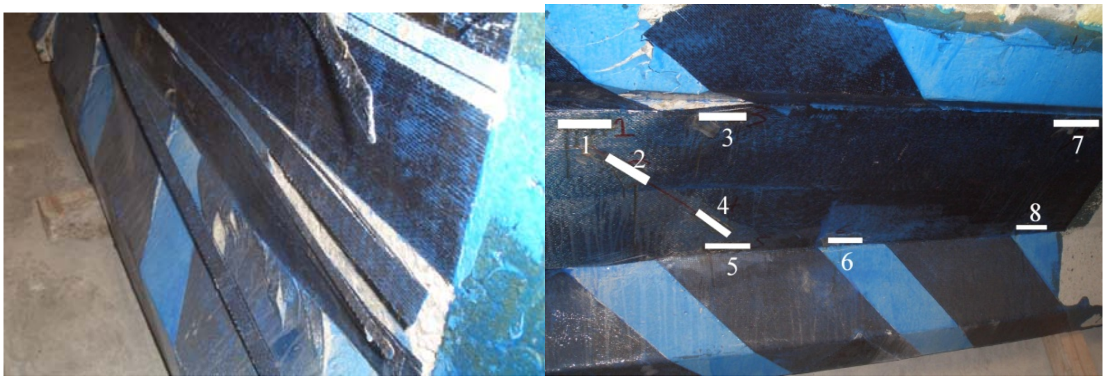

Figure 3.42 Anchorage failure and strain gauge orientation of Test 3A.

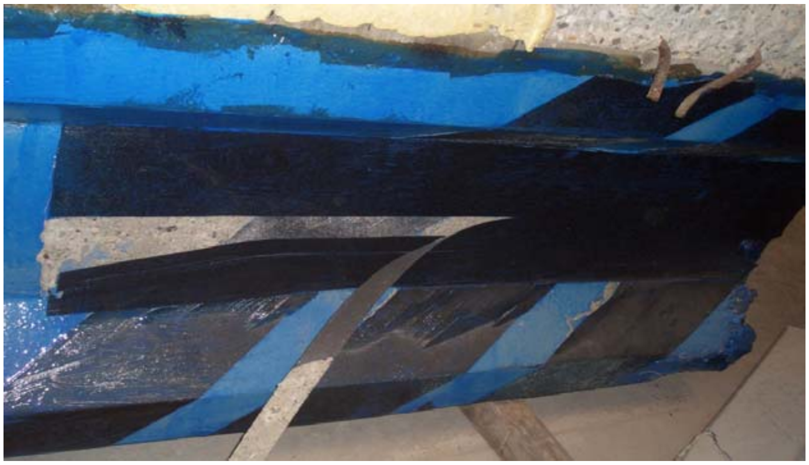

Figure 3.43 Failure of Test 3A.

3.6.4 Test 3B

For the second test on this beam, the hydraulic jack applied the load at a distance of 48 inches from the end support with a beam span of 269 inches. The beam failed in shear at an applied load of 255 kips. The CFRP system failed due the horizontal strip of CFRP fabric ripping the top layer of concrete off, which led to a large normal force at the flange to web connection. After the anchorage failure the CFRP diagonal strips ripped off the top layer of concrete leading to delamination causing the reinforcement to fail (see Figures 3.44 and 3.45 for detail). Under the CFRP reinforcement, there were multiple cracks that were roughly 45-degrees from the load to support. The failure cracks were similar to test 3A's crack orientation but were pushed up towards the top half of the girder (see Figure 3.45 for failure crack orientation). The test yielded an ultimate shear force of 209.5 kips which is an increase of 45.94 kips or a 21.93% increase in shear capacity compared to the average control capacity of 163.56 kips. The data was not recorded for load, strain, and deflection but the maximum applied load was recorded.

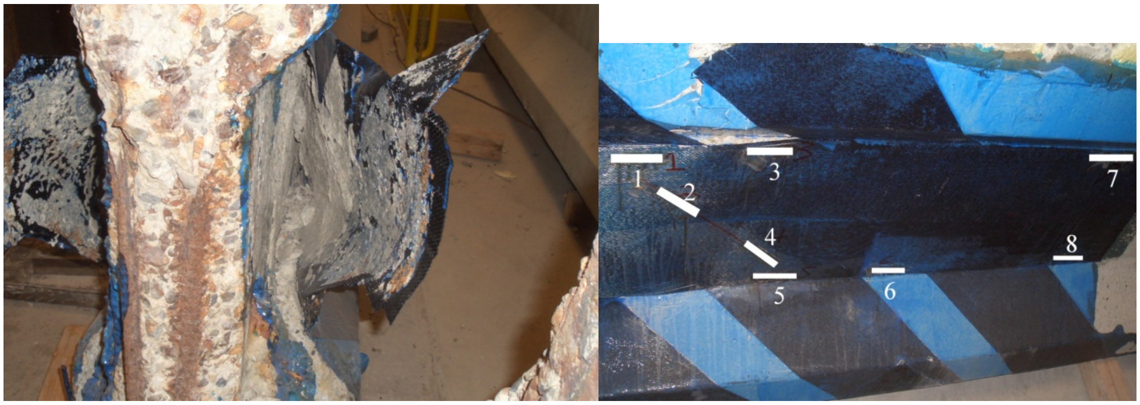

Figure 3.44 Anchorage failure and strain gauge orientation of Test 3B.

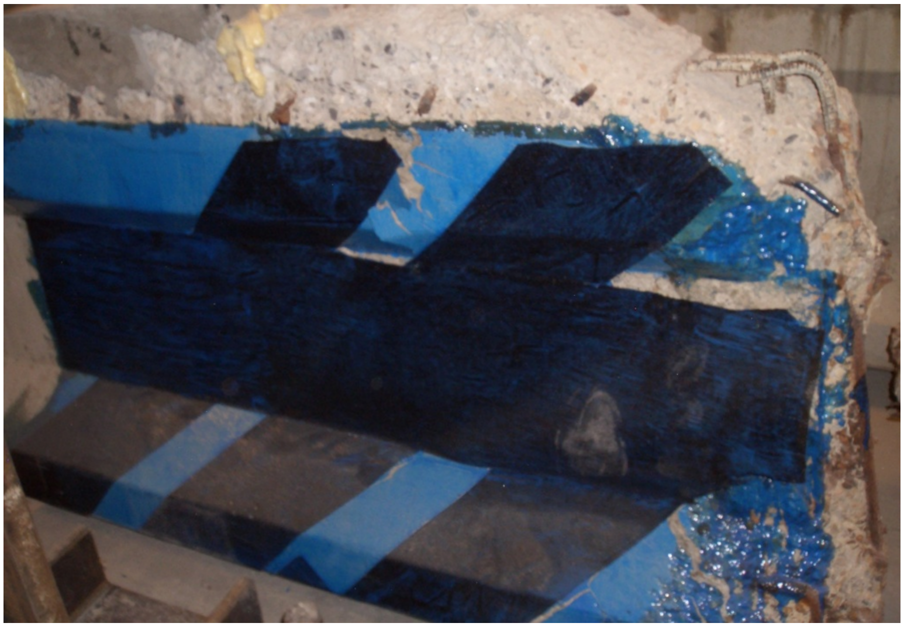

Figure 3.45 Failure of Test 3B.

3.6.5 Test 4A

For this girder, the hydraulic jack applied the load at a distance of 48 inches from the end support with a beam span of 215.5 inches. The beam failed in shear at an applied load of 231.08 kips. The CFRP system failed due to the large normal force generated at the web to flange connection. Since there was no anchorage system the CFRP fabric began to prematurely delaminate. There were still small amounts of the CFRP fabric ripping the concrete off the girder instead of delamination but the failure was primarily delamination (see Figures 3.46 and 3.47 for detail). Under the CFRP reinforcement there were multiple cracks that were roughly 45-degrees from the load to support. The failure cracks were similar to the controls crack orientation (see Figure 3.47 for failure crack orientation). The test yielded an ultimate shear force of 179.61 kips which is an increase of 16.05 kips or a 8.94% increase in shear capacity compared the average control capacity of 163.56 kips. The data recorded for load, strain, and deflection are found in Appendix B Figures B.50 to B.58. The strain gauge orientation can be found on Figure 3.46 and compared to the strain gauges on control Test 1A.

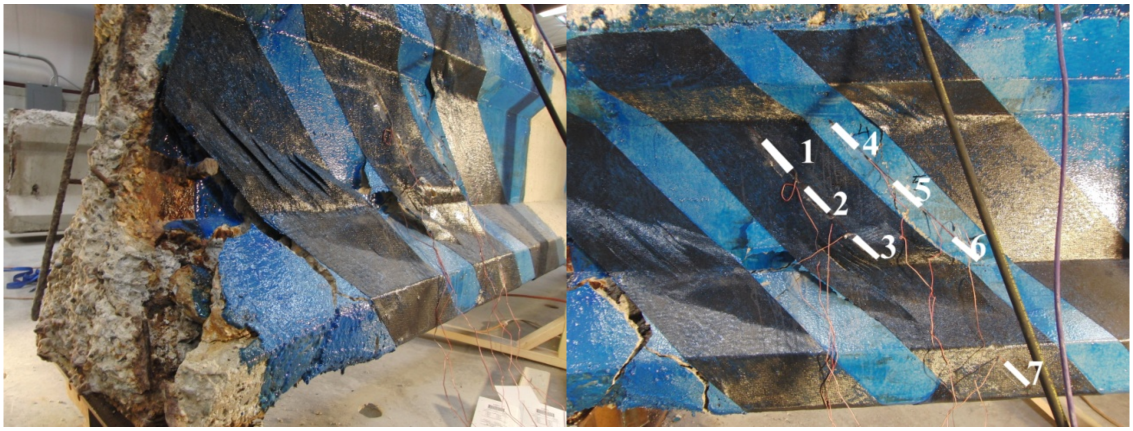

Figure 3.46 CFRP delamination and strain gauge orientation of test 4A.

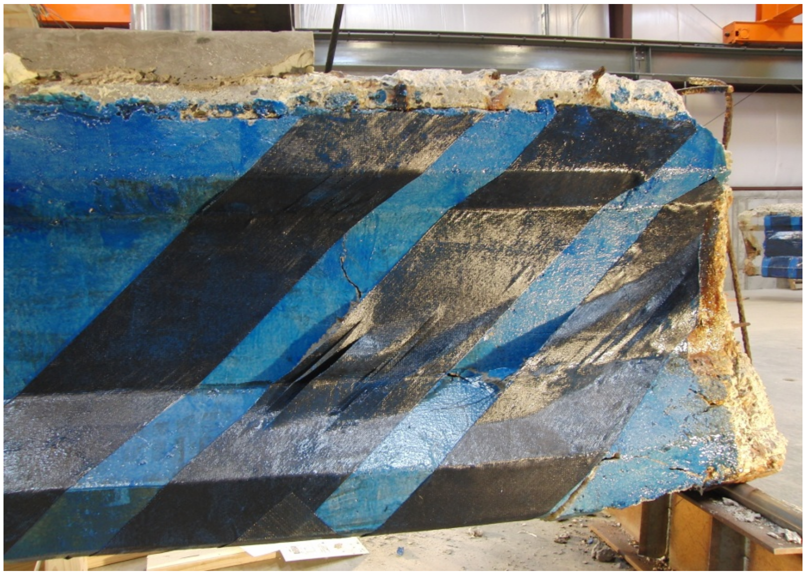

Figure 3.47 Failure of Test 4A.

3.6.6 Test 4B

For the second test of this girder, the hydraulic jack applied a load at a distance of 48 inches from the end support with a beam span of 268.5 inches. The beam failed in shear at an applied load of 212.85 kips. The CFRP system failed due to the large normal force generated at the web to flange connection. Since there was no anchorage system the CFRP fabric began to prematurely delaminate. There were still small amounts of the CFRP fabric ripping the concrete off the girder instead of delamination but the failure was primarily delamination (see Figures 3.48 and 3.49 for detail). Under the CFRP reinforcement there were multiple cracks that were roughly 45-degrees from the load to support. The failure cracks were similar to test 4A's cracks orientation (see Figure 3.49 for the failure crack orientation). The test yielded an ultimate shear force of 174.8 kips which is an increase of 11.24 kips or a 6.43% increase in shear capacity compared to the average control capacity of 163.56 kips. The data recorded for load, strain, and deflection are found in Appendix B Figures B.59 to B.67. The strain gauge orientation can be found on Figure 3.48 and compared to the strain gauges on control Test 1A.

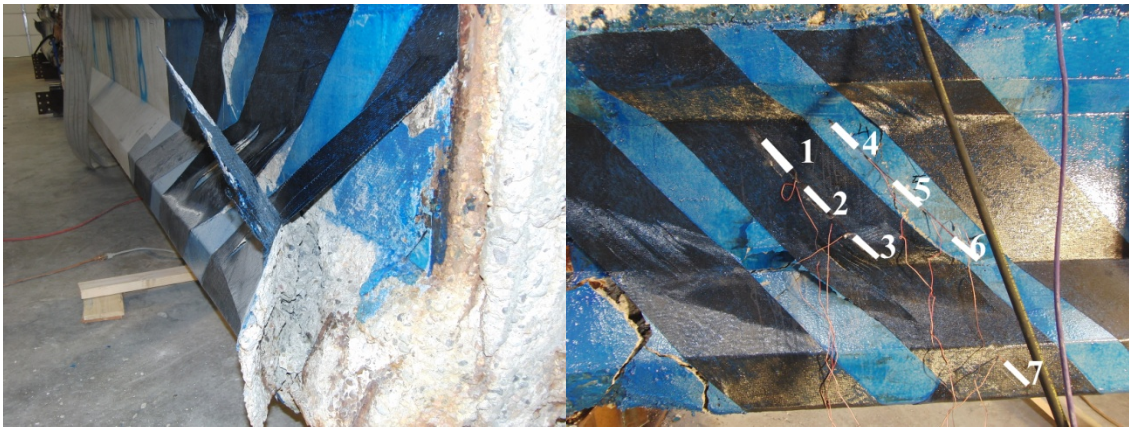

Figure 3.48 CFRP delamination and strain gauge orientation of Test 4B.

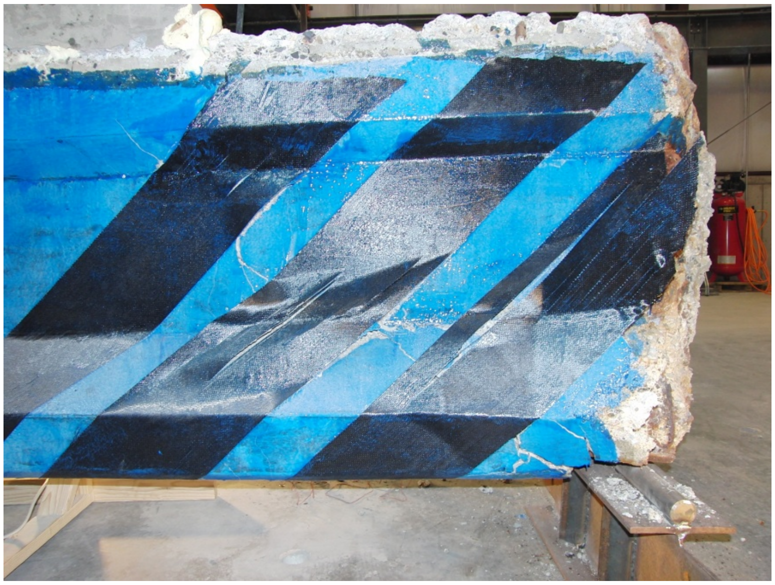

Figure 3.49 Failure of Test 4B.

3.6.7 Test 5A

For the fifth girder, the hydraulic jack applied the load at a distance of 48 inches from the end support with a beam span of 180.5 inches. The beam failed in shear at an applied load of 306.6 kips. The CFRP system failed due the horizontal strip of CFRP fabric ripping the top layer of concrete off, which led to a large normal force at the flange to web connection. After the anchorage failure, the CFRP vertical strips ripped off the top layer of concrete leading to delamination causing the reinforcement to fail (See Figures 3.50 and 3.51 for detail). Under the CFRP reinforcement there were multiple cracks that were roughly 45-degrees from the load to support. The failure cracks were similar to the controls crack orientation except for there were no vertical cracks under the applied load (see Figure 3.51 for the failure crack orientation). The test yielded an ultimate shear force of 225.07 kips which is an increase of 61.51kips or a 27.33% increase in shear capacity compared to the average control capacity of 163.56 kips. The data recorded for load, strain, and deflection are found in Appendix B Figures B.68 to B.78. The strain gauge orientation can be found on Figure 3.50 and compared to the strain gauges on control test 1B.

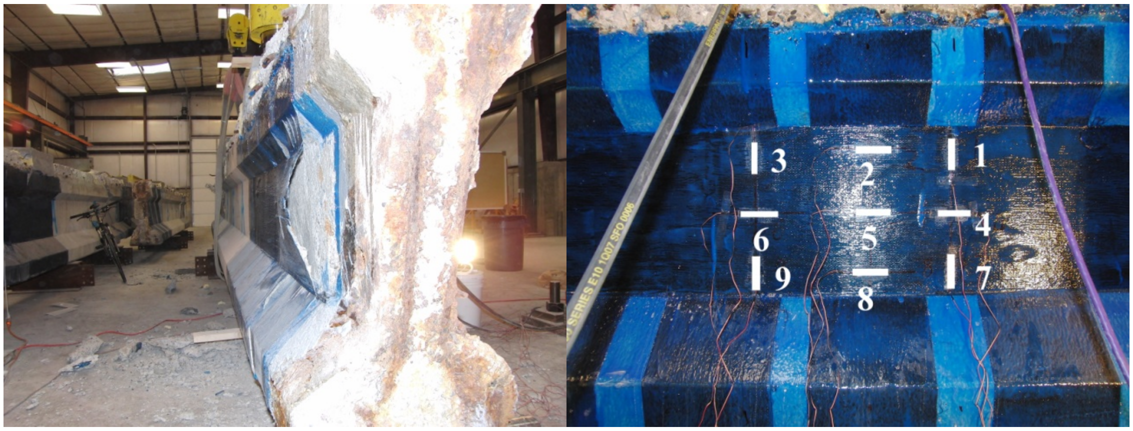

Figure 3.50 Anchorage failure and strain gauge orientation of Test 5A.

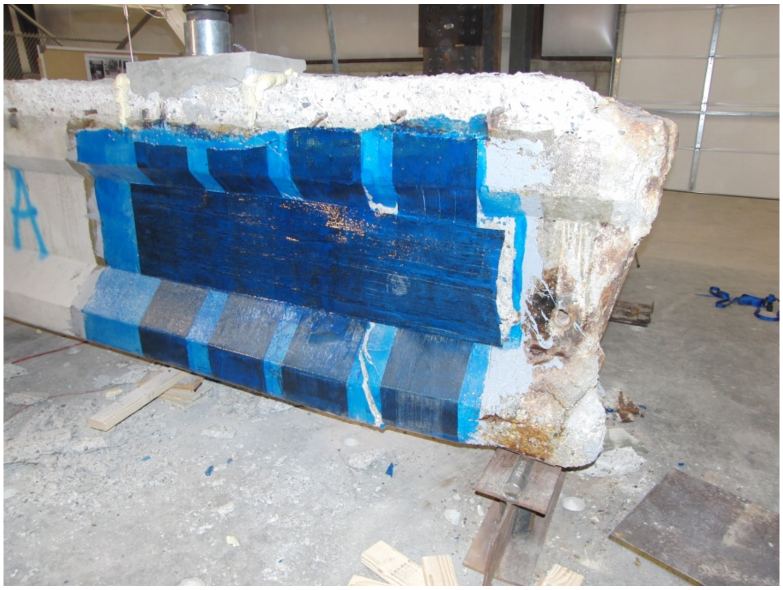

Figure 3.51 Failure of Test 5A.

3.6.8 Test 5B

For the second test on this girder, the hydraulic jack applied the load at a distance of 48 inches from the end support with a beam span of 270 inches. The beam failed in bending at an applied load of 273.58 kips. The CFRP system did not fail in shear. Right under the applied load some concrete under the CFRP system broke off but the girders reinforced shear capacity was greater than the girders moment capacity. This led to the concrete in the top flange crushing and having more of a bending failure than a shear failure (see Figure 3.53 for detail). Some shear cracks did form in the girder (see Figure 3.52 for failure crack orientation). Since the girder failed in bending the ultimate shear capacity was not obtained but the test yielded a shear force of at least 224.94 kips which is an increase of 61.37 kips or a 27.29% increase in shear capacity compared to the average control capacity of 163.56 kips. The data recorded for load and strain are found in Appendix B Figures B.79 to B.89. The strain gauge orientation can be found on Figure 3.52 and compared to the strain gauges on control test 1B.

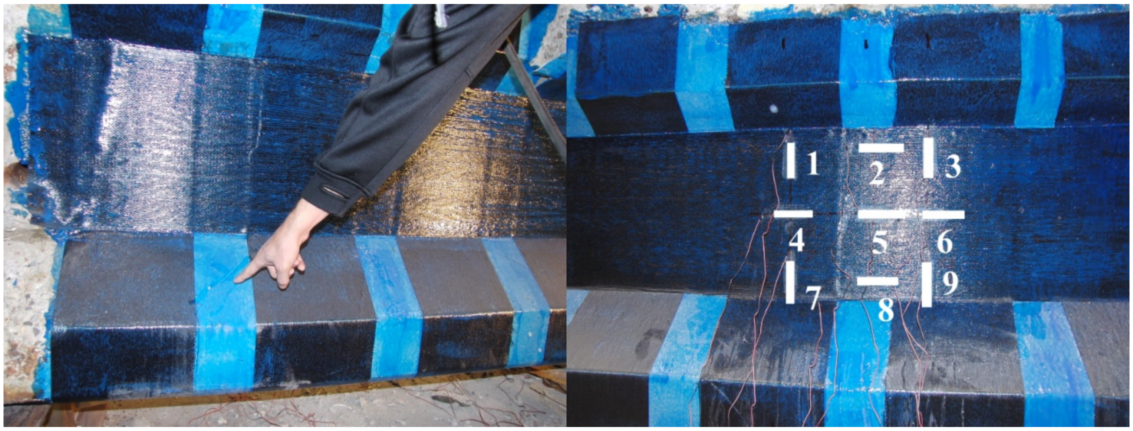

Figure 3.52 Shear cracks and strain gauge orientation of Test 5B.

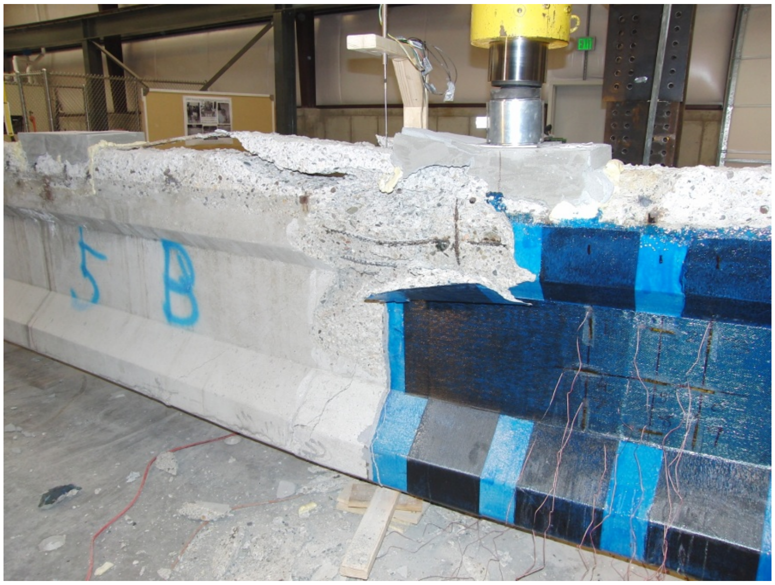

Figure 3.53 Failure of Test 5B.

3.6.9 Test 6A

For this test, the hydraulic jack applied the load at a distance of 42 inches from the end support with a beam span of 210 inches. The beam failed in moment at an applied load of 310.07 kips. The CFRP system did not fail in shear. The girders reinforced shear capacity was greater than the girders moment capacity. This led to the concrete in the top flange crushing and failing in bending (see Figures 3.54 and 3.55 for detail). Since the girder failed in bending we were unable to find the ultimate shear capacity but the test yielded a shear force of at least 248.06 kips which is an increase of 84.5 kips or a 34.06% increase in shear capacity compared to the average control capacity of 163.56 kips. The data recorded for load, strain, and deflection are found in Appendix B Figures B.90 to B.97. The strain gauge orientation can be found on Figure 3.54 and compared to the strain gauges on control test 1A.

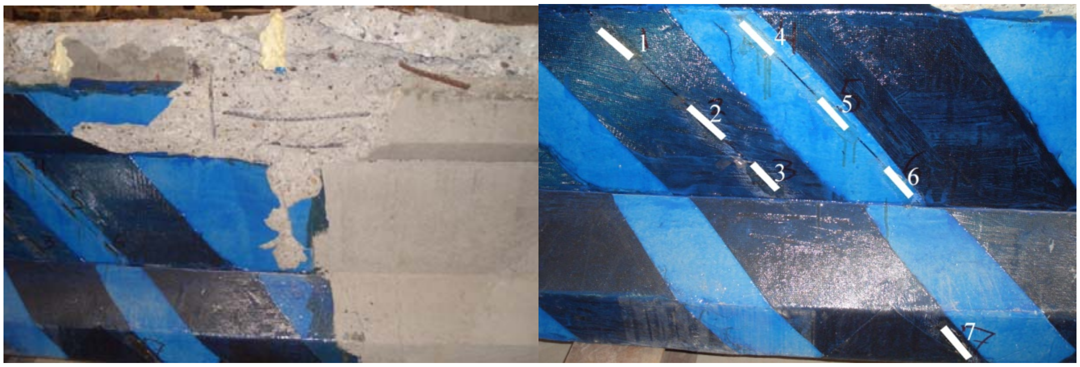

Figure 3.54 Bending cracks and strain gauge orientation of Test 6A.

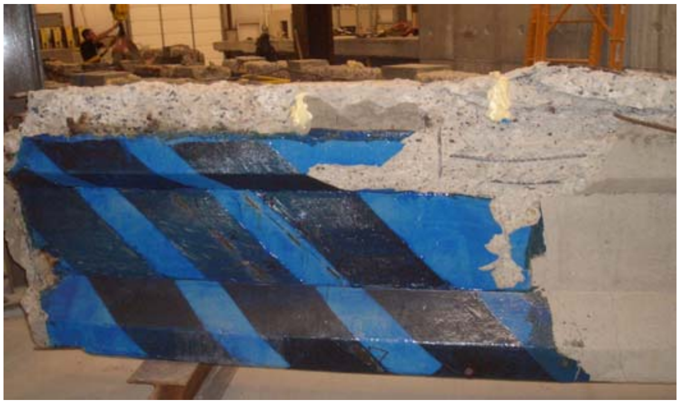

Figure 3.55 Bending failure of Test 6A.

3.6.10 Test 6B

For the second test on this beam, the hydraulic jack applied the load at a distance of 42 inches from the end support with a beam span of 268 inches. The beam failed in shear at an applied load of 180 kips. The concrete in the beam failed in shear before allowing the load to be transferred to the CFRP system. This led to some of the CFRP fabrics to delaminate without the anchorage system failing (see Figures 3.56 and 3.57 for detail). The premature failure in the girders with this type of anchorage system is assumed to be caused by the grooves cut into the girder. Under the CFRP reinforcement there were multiple cracks that were roughly 45-degrees from the load to support. The failure cracks were similar to the control (see Figure 3.57 for failure crack orientation). The test yielded an ultimate shear force of 151.79 kips which is a decrease of 11.77 kips or a 7.75% decrease in shear capacity compared to the average control capacity of 163.56 kips. The data recorded for load, strain, and deflection are found in Appendix B Figures B.98 to B.106. The strain gauge orientation can be found on Figure 3.56 and compared to the strain gauges on control Test 1A.

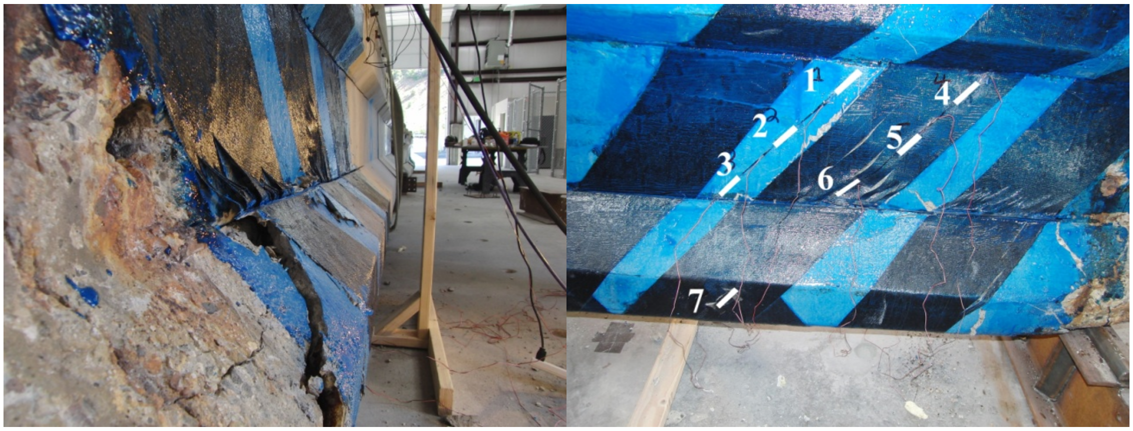

Figure 3.56 Concrete shear failure and strain gauge orientation of Test 6B.

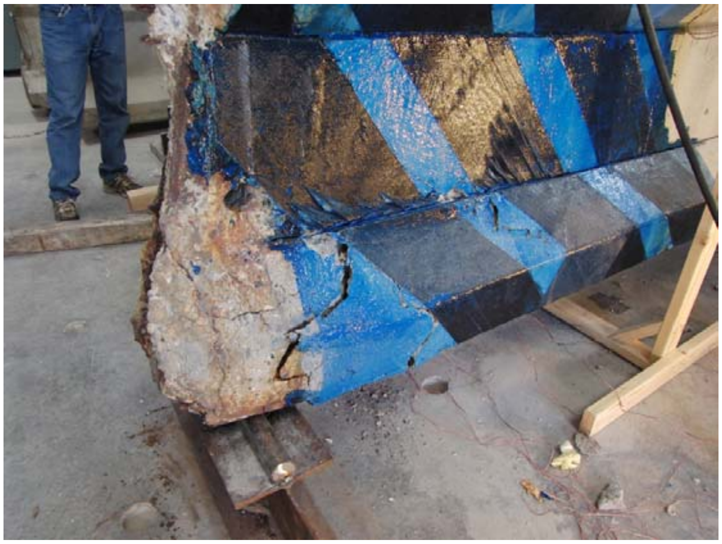

Figure 3.57 Failure of Test 6B.

3.6.11 Test 8A

For the eighth girder, the hydraulic jack applied the load at a distance of 48.5 inches from the end support with a beam span of 150.5 inches. The CFRP system failed due the horizontal strip of CFRP fabric ripping the top layer of concrete off, which led to a large normal force at the flange to web connection. After the anchorage failure, the CFRP vertical strips ripped off the top layer of concrete leading to delamination causing the reinforcement to fail (see Figures 3.58 for detail). Under the CFRP reinforcement there were multiple cracks that were roughly 45-degrees from the load to support. The failure cracks were similar to the controls crack orientation except for there were no vertical cracks under the applied load (see Figure 3.59 for the failure crack orientation). The test yielded an ultimate shear force of 311.96 kips which is an increase of 50.44 kips compared to the average control capacity of 280.44 kips. The data recorded for load and deflection are found in Appendix B Figures B.111 and B.112. There were no strains measured for this test.

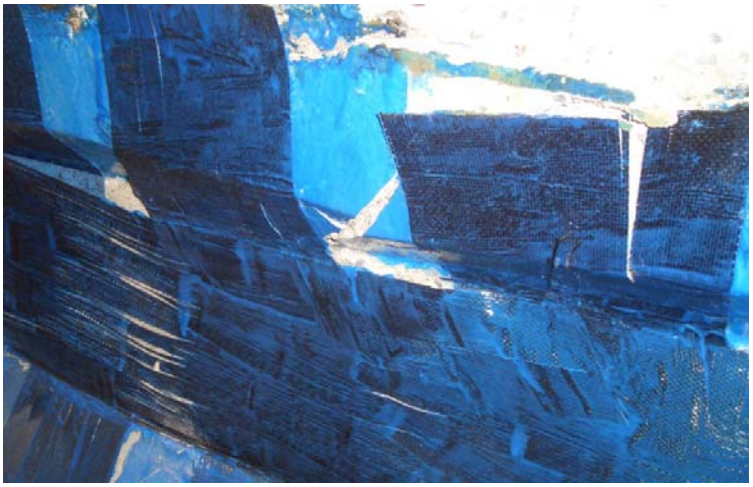

Figure 3.58 Anchorage failure of Test 8A.

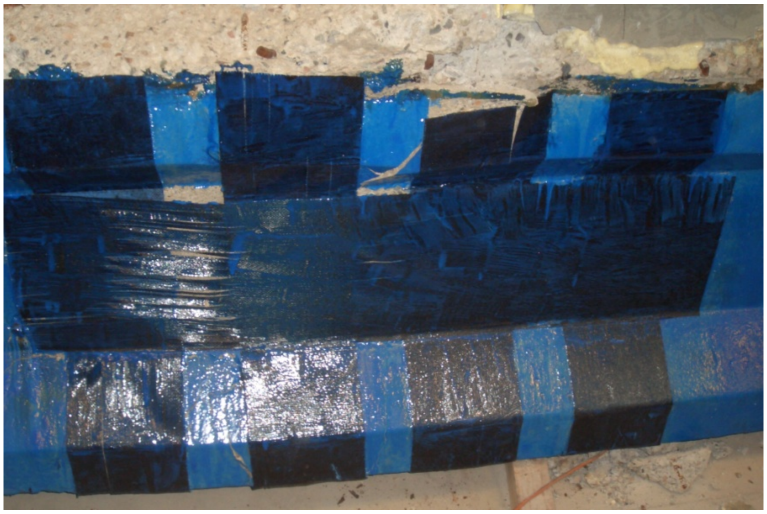

Figure 3.59 Failure of Test 8A.

3.6.12 Test 8B

For the second test of the eighth girder, the hydraulic jack applied the load at a distance of 49 inches from the end support with a beam span of 196 inches. The beam failed in shear at an applied load of 410.63 kips. The CFRP system failed due the horizontal strip of CFRP fabric ripping the top layer of concrete off, which led to a large normal force at the flange to web connection. After the anchorage failure, the CFRP vertical strips ripped off the top layer of concrete leading to delamination causing the reinforcement to fail (see Figures 3.60for detail).

Under the CFRP reinforcement there were multiple cracks that were roughly 45-degrees from the load to support. The failure cracks were similar to the controls crack orientation except for there were no vertical cracks under the applied load (see Figure 3.61 for the failure crack orientation). The test yielded an ultimate shear force of 307.97 kips which is an increase of 46.48 kips compared to the average control capacity of 261.5 kips. The data recorded for load and deflection are found in Appendix B Figures B.113 and B.114. There were no strains measured for this test.

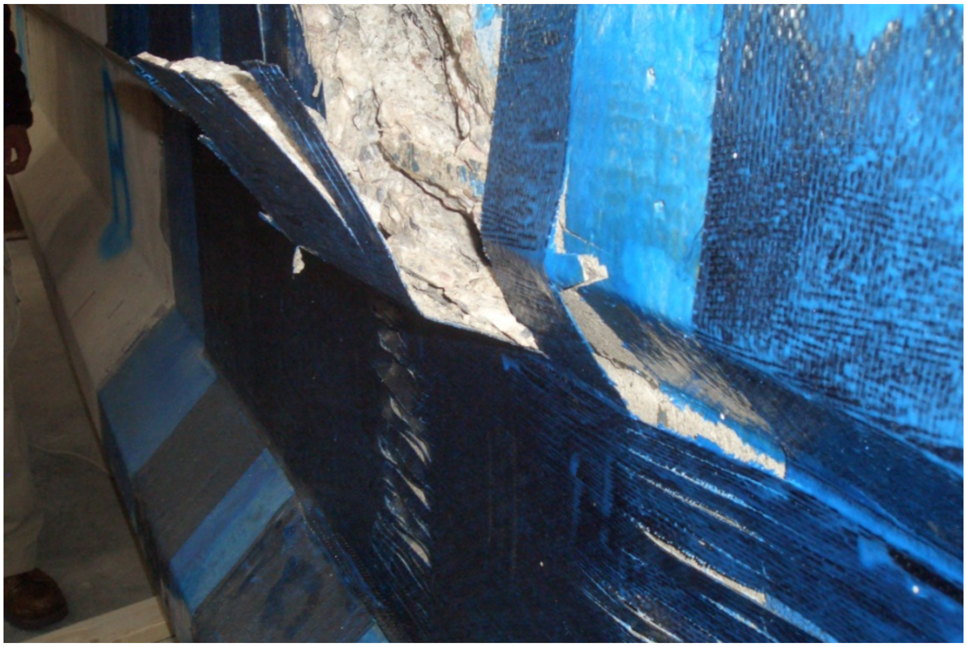

Figure 3.60 Anchorage failure of Test 8B.

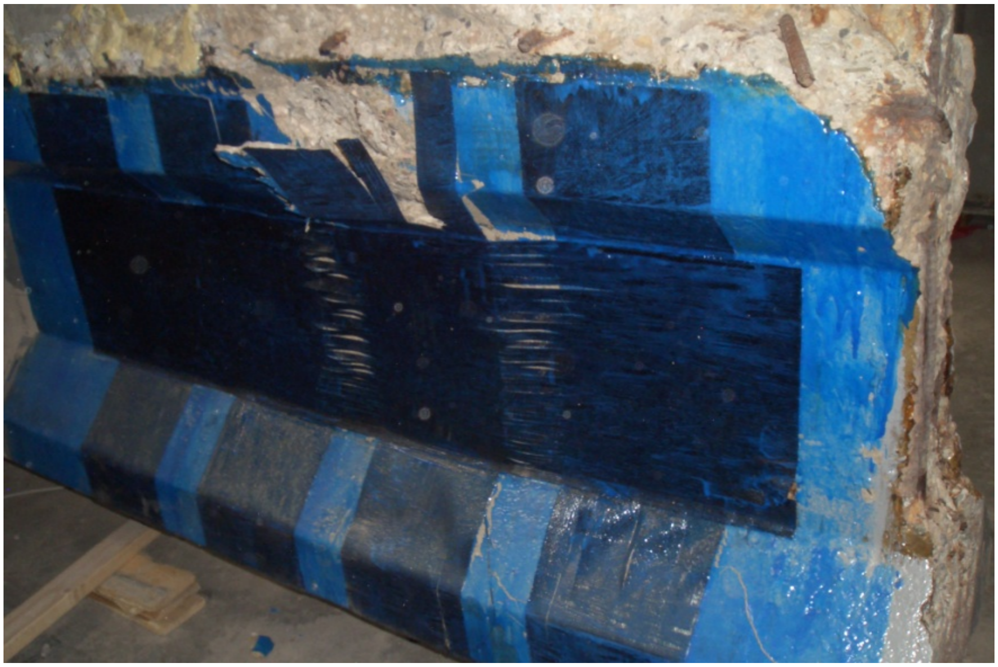

Figure 3.61 Failure of Test 8B.

3.6.13 Comparison of measured strains

During testing strain gauges were placed on the CFRP system parallel to the direction of fibers. Measuring the strain along the fibers would allow for conclusive evidence that while the girder was loaded, the shear was being transferred to the CFRP reinforcement. Figure 3.62 shows a graph of Load vs Strain for a strain gauge on the control and a strain gauge on a reinforced girder. It can be seen on the graph that as the externally applied load increases the control girders concrete begins to yield at that spot and the strain begins to increase. It can be seen also that the strain of the CFRP reinforcement begins to increase around the same external load at the same point. This is seen as evidence that the shear resistance of the girder is being transferred to the CFRP shear reinforcement. Figure 3.63 is another example of Load vs Strain comparisons of a non reinforced girder and a reinforced girder. These two graphs of Load vs Strain are evidence that the CFRP shear reinforcement is resisting the shear force applied to the girder.

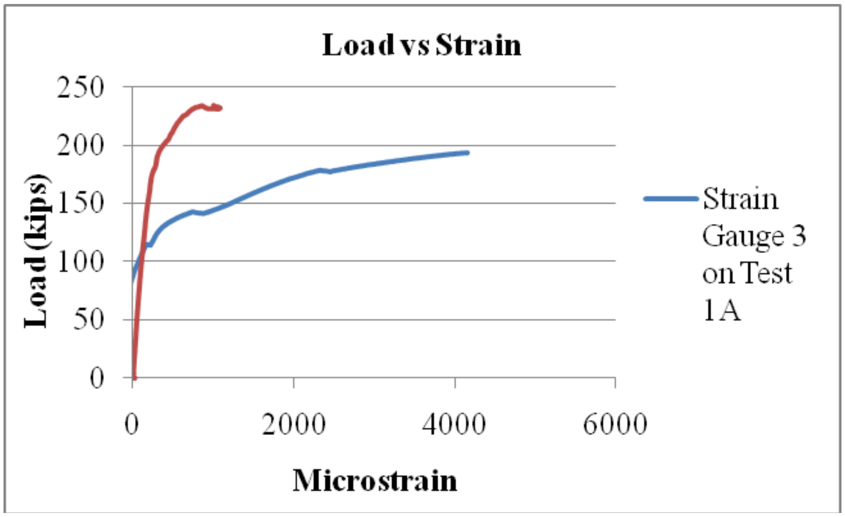

Figure 3.62 Load vs strain of strain gauges 3 on control Test 1A and CFRP reinforced Test 4A.

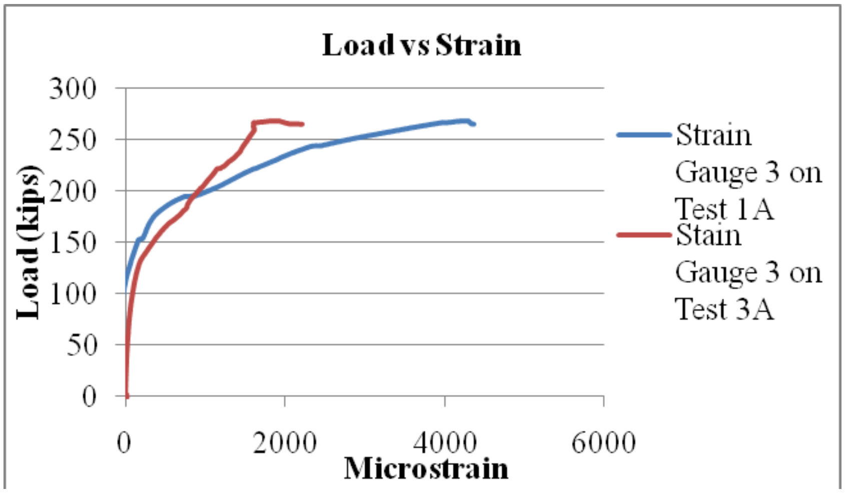

Figure 3.63 Load vs strain of strain gauges 3 on control Test 1A and CFRP reinforced Test 3A.

There is another observation made from the measurement of strain that is vital to understanding the how the CFRP reinforcement is reacting. Gauges 4 and 8 are horizontal located on the horizontal strip used for anchorage, while gauges 3 and 9 are vertical located on one of the vertical strips (see Figure 3.50 for exact of locations). It can be seen that in Figure 3.64 that the max strain measured for gauges 3,4,8, and 9 are .001, .006, .009, and .001, respectively. Plotting the max measured strains on Figure 3.65 shows us that the max stress (ksi) in the fibers are 33, 198, 297, and 33 for their respective locations. This shows that the max stress of 297 ksi is well below the rupture stress of 550 ksi. It can also be noted that there were large stresses in the horizontal strip which provides evidence that the anchorage system was successful in increasing the capacity.

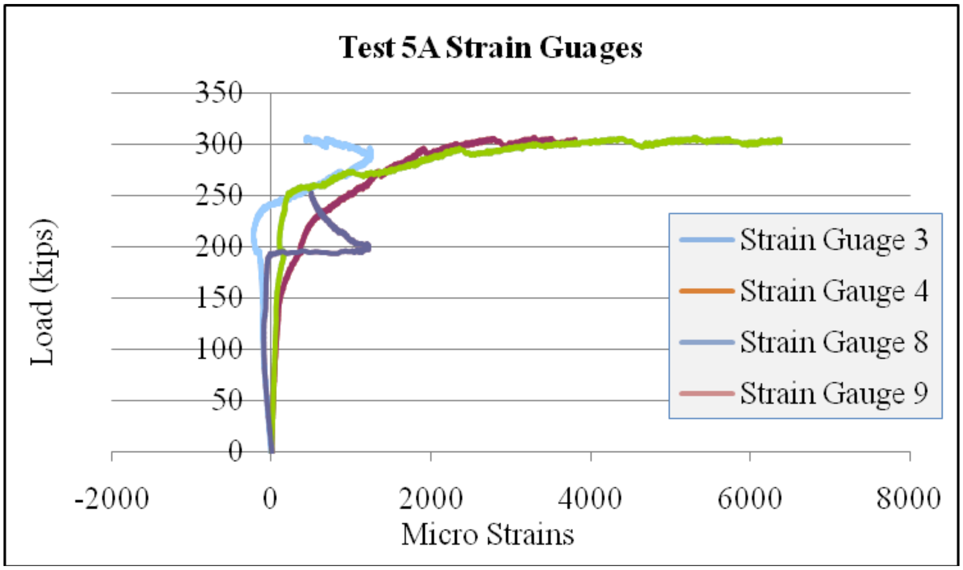

Figure 3.64 Load vs strain of strain gauges 3, 4, 8, and 9 on Test 5A.

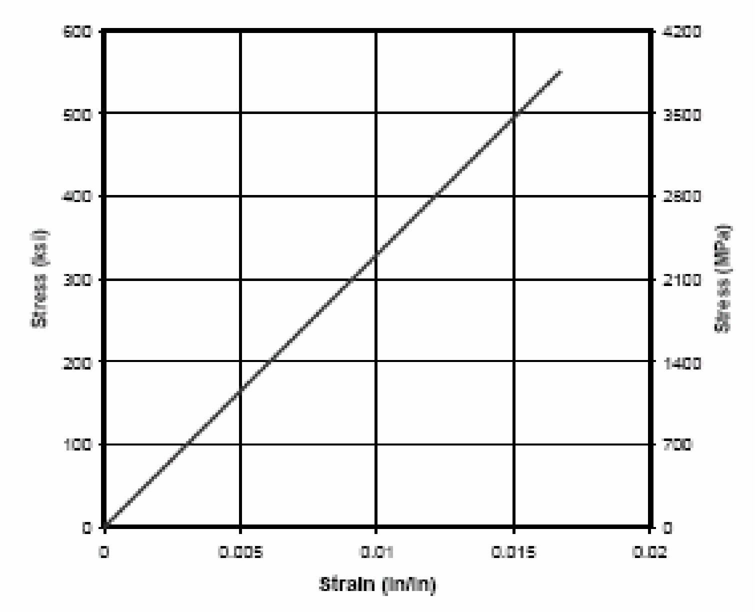

Figure 3.65 Stress vs strain graph of the CFRP fabric (CF 160).

3.6.14 Comparison of measured deflections

During each test the vertical deflection was measure at the applied load. Taking this measurement and plotting it as the load increased allowed for observations on the changes in deflection of the girder due to the CFRP reinforcement throughout reading. In Figure 3.66 it can be seen that as the load is increased the deflection is linear until yielding began, at which point the deflection began to increase more rapidly with less applied load. It can be seen that from Figure 3.66 that the girder with CFRP reinforcement was stronger and was able to produce a larger deflection than the girder without reinforcement. We can conclude that the CFRP reinforcement does provide the system with increased deflections as the girder and CFRP reinforcement act compositely.

Another observation found in Figure 3.66 is that during the loading stage where the concrete is remaining linear, the stiffness of the girder remains the same with either no reinforcement or if there is reinforcement.

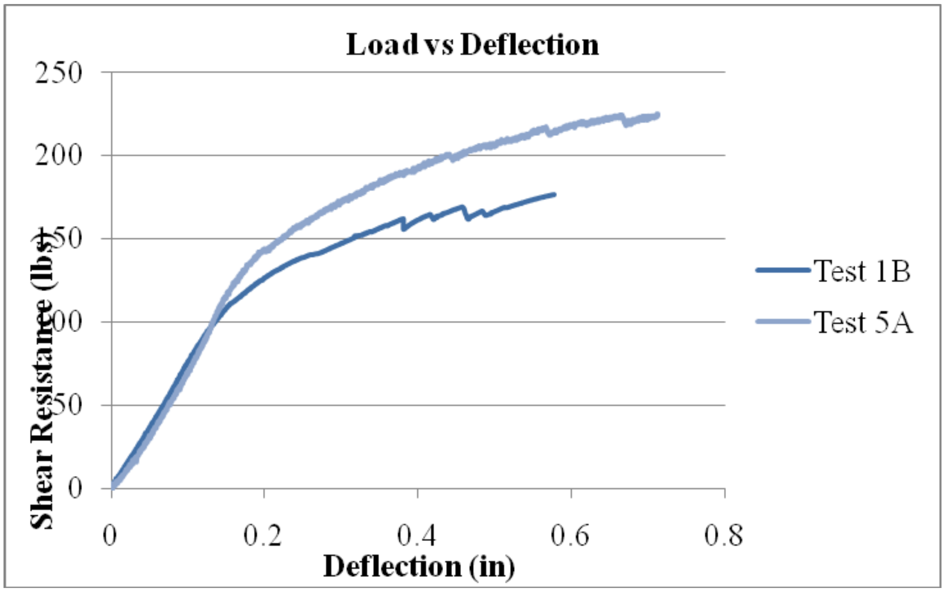

Figure 3.66 Load vs deflection of control and Girder 5 configuration

3.6.15 Comparison of measured shear capacity

During testing the externally applied load was measured using a load cell and pressure gauge. The beam distance from support to support was called the beam span and the distance from the applied external load to the nearest support (shear span). With these measurements, ultimate shear force using elemental beam theory was calculated. Table 3.4 shows the measured results recorded for each test. The unreinforced baseline shear force was obtained from the two control tests. The 163.56 kip shear force was obtained based on an average of the two tests which were 150.25 kips and 176.86 kips. After each experimental test with the CFRP reinforcement the total shear force was obtained and by subtracting the baseline shear force the magnitude of shear that was contributed by the CFRP reinforcement was obtained.

The experimental program was successful in providing evidence that CFRP reinforcement on I-shaped prestressed AASHTO girders does provide additional shear strength. Not all CFRP reinforcement configurations were as successful as others. The configurations on Girders 2 and 6 had very inconstant results of roughly -8 % to 34% changes in shear capacity, which was assumed to be due to the cuts in the girders needed for the anchorage system. The CFRP reinforcement configurations on girders 3 and 5 were found to be the most effective, ranging from an increase of 17% to 33%. The configuration on Girder 4 was similar to Girders 3 and 5 except the configuration did not have the horizontal anchorage system. This configuration was roughly 8-20% less effective than the other two. That decrease in capacity is evidence that the horizontal anchorage system was effective in anchoring the CFRP sheets and giving an overall increase in shear capacity.

From the first set of six girders we were able to conclude that the fourth CFRP reinforcement configuration (vertical strips with a horizontal anchorage strip) was the most effective in increasing the shear capacity. That configuration was then tested on the second set of two girders. On Girder 8 the same CFRP reinforcement was found to increase the shear capacity of the girder. The increase of shear capacity of was an average of 30 kips. This increase was less than that found on Girder 5 which had the same configurations; this can be due to the larger existing shear strength in the girder.

Table 3.4 Comparative results of experimental program

Test	Shear Span (inches)	Beam Span (inches)	Applied Load (kips)	Existing Shear Force (kips)	CFRP Shear Force (kips)	Total Shear Force (kips)	Percent Increase
1A	48	268.25	183.00	150.25	0.00	150.25	0.00%
1B	48	208.25	229.84	176.86	0.00	176.86	0.00%
2A	48	206	333.36	163.56	92.12	255.68	36.03%
2B	48	268	198.20	163.56	-0.86	162.70	-0.53%
3A	48	210	255.40	163.56	33.46	197.02	16.98%
3B	48	269	255.00	163.56	45.94	209.50	21.93%
4A	48	215.5	231.08	163.56	16.05	179.61	8.94%
4B	48	268.5	212.85	163.56	11.24	174.80	6.43%
5A	48	180.5	306.60	163.56	61.51	225.07	27.33%
5B	48	270	273.58	163.56	61.38	224.94	27.29%
6A	42	210	310.07	163.56	84.50	248.06	34.06%
6B	42	268	180.00	163.56	-11.77	151.79	-7.75%
7A	51.5	199.5	355.00	263.36	0.00	263.36	0.00%
7B	48	163	368.00	259.63	0.00	259.63	0.00%
8A	48.5	150.5	460.30	261.50	50.47	311.96	16.18%
8B	49	196	410.63	261.50	46.48	307.97	15.09%

4.0 COMPARISON OF MEASURED AND PREDICTED RESULTS

4.1 Introduction to predictive Methods for predicting Shear Capacity

For this research two different predictive methods were used to compare code practices with the measured results which were provided in Chapter 3. The first methodology was the current AASHTO LRFD Bridge Design Specifications (AASHTO, 2009). This is the preferred method for most state DOTs and for the Federal Highway Administration when designing bridges. Chapter 5 of this code, which describes the shear and torsion behavior of concrete beams, was the main section utilized in this research to determine the calculated capacity.

The second predictive method was from the American Concrete Institute's (ACI) concrete building code ACI-318-08 (ACI, 2008). This design code is for structural concrete both in buildings and otherwise. Chapter 11 of the ACI code was the main portion utilized for this research. This chapter describes the shear strength design codes as they apply to prestressed concrete girders.

4.1.1 Predictive Method AASHTO LRFD Bridge Design Specifications

The AASHTO LRFD Bridge Design Specifications (AASHTO, 2009) provides two different methodologies for the determination of the design shear of a reinforced prestressed concrete girder. This code summarizes the components of shear from three different factors including the tensile strength of the concrete (V_c), the shear resistance provided by the transverse reinforcement (V_s), and the vertical component of the prestressing force (V_p). The nominal or total shear capacity of the girder is taken as the lesser of the two values calculated using AASHTO Equations 5.8.3.3-1 and 5.8.3.3-2 which are provided in this research as Equations 4.1 and 4.2, respectively.

$$V_n = V_c + V_s + V_p \tag{4.1}$$

$$V_n = 0.25 f'_c b_v d_v + V_p \tag{4.2}$$

The shear contribution from the vertical or transverse reinforcing steel is calculated using Equation 4.3.

$$V_s = \frac{A_v f_y d_v (\cot\theta + \cot\alpha)\sin\alpha}{s} \tag{4.3}$$

where:

V_p = component in the direction of the applied shear of effective prestressing force(kips)

f'_c = compression strength of concrete (ksi)

b_v = effective web width taken as the minimum web width within the depth d_v (in.)

d_v = effective shear depth as determined as follows (AASHTO Article 5.8.2.9) (in.)

> d_v = effective shear depth taken as the distance, measured perpendicular to the neutral axis, between the resultants of the tensile and compressive forces due to flexure; it need not be taken to be less than the greater of $0.9d_e$ or $0.72h$ (in.)
>
> in which:
>
> $$d_v = \frac{M_n}{A_s f_y + A_{ps} f_{ps}} \tag{4.4}$$
>
> $$d_e = \frac{A_{ps} f_{ps} d_p + A_s f_y d_s}{A_{ps} f_{ps} + A_s f_y} \tag{4.5}$$

s = spacing of the transverse reinforcement

A_v = area of transverse steel within a distance s (in^2)

f_y = yield strength of transverse reinforcement (ksi)

θ = angle of inclination of diagonal compressive stresses (°)

α = angle of inclination of transverse reinforcement within distance s (°)

M_n = nominal moment at the section being considered (kip-in.)

A_s = area if longitudinal steel (in^2)

A_{ps} = area of prestressing steel (in^2)

f_{ps} = force in the prestressing steel (kips)

d_p = depth to the centroid of the prestressing steel (in.)

d_s = depth to the centroid of the longitudinal steel (in.)

According to the AASHTO specifications, there are two different methodologies of calculating the concrete contribution to shear (V_c). The first method (general procedure) comes from a modified compression field theory and assumes that the concrete shear stresses are uniformly distributed over an area b_v in width and d_v in depth. For this method, it is also assumed that the directions of the principal compressive stresses (θ) remain constant over a length d_v, and that the shear strength of the section can be determined by considering the biaxial stress conditions at just one location in the web. AASHTO Equation 5.8.3.3-3 provides the relationship for calculating the magnitude of V_c and is provided in this research as Equation 4.6. The values of β and θ are determined in one of two ways, namely the Empirical Method and the Iterative Method. For this research, the Empirical Method was used and will be presented with the following equations.

$$V_c = 0.0316\beta\sqrt{f'_c}\,b_v d_v \qquad (4.6)$$

For sections containing at least the minimum amount of transverse reinforcement specified in AASHTO Article 5.8.2.5 the value of β may be determined using Equation 4.7.

$$\beta = \frac{4.8}{(1+750\varepsilon_x)} \qquad (4.7)$$

When sections do not contain at least the minimum quantity of shear reinforcement, the value of β should be calculated using Equation 4.8.

$$\beta = \frac{4.8}{1+750\varepsilon_x}\frac{51}{39+s_{xe}} \qquad (4.8)$$

In either case, the value of θ is calculated using of Equation 4.9.

$$\theta = 29 + 3500\varepsilon_x \qquad (4.9)$$

For Equations 4.7-4.9, the strain (ε_x) is defined as the strain in the non-prestressed longitudinal tension reinforcement. The code provides a simplified equation which may be used rather than performing a more detailed and involved analysis. This simplified equation provided as AASHTO Equation 5.8.3.4.2-4 provided in this research as Equation 4.10 to determine ε_x.

$$\varepsilon_x = \frac{\frac{M_u}{d_v} + 0.5N_u + |V_u - V_p| - A_{ps} f_{po}}{E_s A_s + E_p A_{ps}} \tag{4.10}$$

where:

s_{xe} = crack spacing parameter

$$s_{xe} = s_x \frac{1.38}{a_g + 0.63} \tag{4.11}$$

A_c = area of concrete on the flexural tension side of the member (in^2)

A_{ps} = area of prestressing steel on the flexural tension side of the member (in^2)

A_s = area of nonprestressed steel on the flexural tension side of the member at the section under consideration. (in^2)

a_g = maximum aggregate size (in.)

f_{po} = a parameter taken as modulus of elasticity of prestressing tendons multiplied by the locked in difference in strain between the prestressing tendons and the surrounding concrete (ksi). For the usual levels of prestressing, a value of 0.7 f_{pu} will be appropriate for both pretensioned and post-tensioned members

N_u = factored axial force, taken as positive if tensile and negative if compressive (kips)

M_u = factored moment, not to be taken less than $(V_u - V_p)d_v$ (kip-in.)

S_x = the lesser of either dv of the maximum distance between layers of longitudinal crack control reinforcement, where the area of the reinforcement in each layer is not less than $0.003 b_v s_x$

V_u = factored shear force (kips)

The second method (simplified method) for calculating V_c is very similar to the ACI method presented in the next section. In this method, the values of V_c and V_s are calculated differently based on the way the shear cracks develop, namely, flexure-shear cracking or web-shear cracking. If flexure-shear cracks control the design, the value V_{ci} should be used as V_c. However, if web-shear cracks control the design, V_{cw} should be used. V_c is defined to be the lesser of V_{ci} and V_{cw}. In the AASHTO code the requirements are provided in Article 5.8.3.4.3 and provided herein as follows.

$$V_{ci} = 0.02\sqrt{f'_c}b_v d_v + V_d + \frac{V_i M_{cre}}{M_{max}} \geq 0.06\sqrt{f'_c}b_v d_v \qquad (4.12)$$

where:

V_d = shear force at section due to unfactored dead load including both DC and DW (kips)

V_i = factored shear force at section due to externally applied loads occurring simultaneously with M_{max} (kips)

M_{cre} = moment causing flexural cracking at section due to external loads (kip-in.)

$$M_{cre} = S_c\left(f_r + f_{cpe} - \frac{M_{dnc}}{S_{nc}}\right) \qquad (4.13)$$

M_{max} = maximum factored moment at section due to externally applied loads (kip-in.)

f_{cpe} = compressive stress in concrete due to effective prestress forces only (after all losses) at extreme fiber of section where tensile stress is caused by externally applied loads (ksi)

M_{dnc} = total unfactored dead load moment acting on the monolithic or noncomposite section (kip-in.)

S_c = section modulus for the extreme fiber of the composite section where tensile stress is caused by externally applied loads (in^3)

S_{nc} = section modulus for the extreme fiber of the monolithic or noncomposite section where tensile stress is caused by externally applied loads (in^3)

The value V_{cw} is to be calculated according to Equation 4.14. The component of shear resistance provided by the transverse steel shall be computed via Equation 4.3 with cot θ = 1.0 where $V_{ci} < V_{cw}$, and $\cot\theta = 1.0 + 3\left(\frac{f_{pc}}{\sqrt{f'_c}}\right) \leq 1.8$ where $V_{ci} > V_{cw}$.

$$V_{cw} = \left(0.06\sqrt{f'_c} + 0.30 f_{pc}\right)b_v d_v + V_p \qquad (4.14)$$

where:

f_{pc} = compressive stress in concrete (after allowance for all prestress losses) at centroid of cross section resisting externally applied loads or at junction of web and flange when the centroid lies within the flange (ksi). In a composite member, f_{pc} is the resultant compressive stress at the centroid of the composite section, or at junction of web and flange, due to both prestress and moments resisted by precast member acting alone.

For Girders 1 through 6 the calculated shear capacity according to the AASHTO general procedure was calculated to be 47.79-kips. Using the simplified method, a shear value of 82.27-kips was calculated. For Girders 7 and 8 the calculated capacities for shear were calculated as 37.66-kips and 100.28-kips from the general and simplified procedures respectively.

Of the two methods provided by the AASHTO specifications, the simplified method provided a closer estimate of the ultimate shear capacity of the AASHTO Type II bridge girders tested for this research. In general, both methods are very conservative and rely on bending theory. The bending theory is believed to be less correct in the d-regions (a distance equal to the depth of the girder from the face of the support) of concrete beams, especially thin webbed beams. In the d-regions, the shear stresses are not distributed linearly over the depth of the beam according to bending theory, and therefore St. Venant's Principle does not apply. The AASHTO LRFD code, as well as the ACI code, allow for sectional analysis of beams. This is acceptable because the predicted values are conservative. As will be shown in the following section, the ACI 318-08 code for shear calculations outside the d-region is also derived from bending theory and accordingly the predicted shear is also conservative.

4.1.2 Predictive Method ACI 318-08

The ACI code presents two different methods for computing the ultimate shear capacity of prestressed concrete members. The first is described as the approximate method which estimates the contribution of shear strength from the concrete to be a function of the girder shape, applied loads, and concrete strengths. This method can only be used in prestressed members if the effective prestress force is equal to or greater than 40% of the tensile strength of the flexural reinforcement. The nominal shear capacity of a prestressed girder according to ACI Equation 11-9 is provided here as Equation 4.15.

$$V_c = \left(0.6\lambda\sqrt{f'_c} + \frac{700 V_u d_p}{M_u}\right) b_w d \qquad (4.15)$$

This value must be greater than or equal to Equation 4.16,

$$V_c = 2\lambda\sqrt{f'_c} b_w d \qquad (4.16)$$

but must be less than Equation 4.17.

$$V_c = 5\lambda\sqrt{f'_c} b_w d \qquad (4.18)$$

where:

λ = unit weight of concrete modification factor (1 for normal weight concrete)

V_u = the maximum design shear at the section being considered (kips)

M_u = the design moment at the same section occurring simultaneously with V_u (kip-in.)

d_p = the distance from the extreme compression fiber to the centroid of the prestressing strands (in.)

d = the distance from the extreme compression fiber to the centroid of the tension reinforcement (in.)

f'_c = the compressive stress of the concrete (psi)

b_w = web width (in.)

The contribution of shear from the web shear reinforcing steel must be added to the shear contribution of the concrete. ACI Equation 11-15 is recommended to be used to calculate the shear contribution from the stirrups and is provided here as Equation 4.19.

$$V_s = \frac{A_s f_y d}{s} \qquad (4.19)$$

where:

V_s = the shear resistance provided by the transverse shear steel (kips)

A_s = the area of transverse steel (in^2)

f_y = the yield strength of the transverse (ksi)

s = spacing of transverse reinforcement (in.)

The shear capacities were calculated using this approximate method for Girders 1 through 6 as 101.74-kips. This value is approximately 62% of the average measured value of 163.56-kips. For Girders 7 and 8 the approximate method resulted in a calculated shear capacity of 131.09-kips. For Girders 7 and 8 the approximate method underestimated the measured value, yielding only about 50% of the average measured value of 261.50-kips.

The second method recommended by the ACI code is the detailed method in which V_c is taken as the smaller of the calculated values of V_{ci} of V_{cw}. This method may be used for any beam, and must be used when the effective prestress force is less than 40% of the tensile strength of the flexural reinforcement. The term V_{ci} is used to describe the concrete shear strength of a member when the diagonal shear cracks form due to a combination of shear and moment. V_{cw} is used to define the nominal concrete shear strength of a member when the diagonal cracks form due to excessive principal tensile stress in the concrete. V_{ci} can be approximated with ACI Equation 11.3.3.1 which is provided as Equation 4.20.

$$V_{ci} = 0.6\lambda\sqrt{f'_c}\,b_w d_p + V_d + \frac{V_i M_{cre}}{M_{max}} \geq 1.7\lambda\sqrt{f'_c}\,b_w d \tag{4.20}$$

where:

V_d = the shear at the section in question due to service dead load (lbs)

V_i = the shear that occurs simultaneously with M_{max} (lbs)

M_{cr} = the cracking moment (lb-in.)

$$M_{cr} = \left(\frac{I}{y_t}\right)\left(6\lambda\sqrt{f'_c} + f_{pe} - f_d\right) \text{ (lb-in.)} \tag{4.21}$$

I = the moment of inertia of the section that resists the externally applied load (in^4)

Y_t = the distance from the centroidal axis of the gross section (neglecting the reinforcing) to the extreme tension fiber (in.)

f_{pe} = the compressive stress in the concrete due to prestress after all losses at the extreme fiber of the section where the applied loads cause tension (psi)

f_d = the stress due to unfactored dead load at the extreme fiber where the applied loads cause tension (psi)

The equation for V_{cw} provides the shear capacity of the concrete beam in units of pounds as derived from a rather simplified principal tension theory and is provided as Equation 4.22 which comes from ACI Equation 11-22.

$$V_{cw} = \left(3.5\lambda\sqrt{f'_c} + 0.3f_{pc}\right)b_w d_p + V_p \geq 1.5\lambda\sqrt{f'_c}\,b_w d \qquad (4.22)$$

where:

f_{pc} = the calculated compressive stress in the concrete at the centroid of the section resisting the applied loads due to the effective prestress after all losses (psi)

V_p = the vertical component of the effective prestress force at the section of interest (lb)

The value for f_{pc} is to be calculated at the centroid of the composite cross-section unless the centroid falls within the flange, in which case f_{pc} should be computed at the intersection of the web and the flange. ACI 11.3.3.2 states that V_{cw} may be taken as the concrete shear capacity that corresponds to a multiple of dead load plus live load. This results in a calculated principal tensile stress equal to $4\lambda\sqrt{f'_c}$ at the point where f_{pc} is calculated as described above.

For the detailed method, the total shear in a prestressed concrete member must be the sum of the shear contributions from the concrete, the vertical component of the prestressing, and the shear contribution from the web steel. If the effective prestress force is greater than or equal to 40% of the tensile strength of the flexural reinforcement Equation 4.23 (ACI Equation 11-14) is to be used to calculate the required area of shear steel, A_v.

$$A_{v,m} = \left(\frac{A_{ps}}{80}\right)\left(\frac{f_{pu}}{f_{yt}}\right)\left(\frac{s}{d}\right)\sqrt{\frac{d}{b_w}} \qquad (4.23)$$

where:

$A_{v,m}$ = the minimum area of shear steel (in^2)

A_{ps} = the area of prestressing reinforcement in the tensile zone (in^2)

f_{pu} = the ultimate stress of the prestressing reinforcement (psi)

f_{yt} = the yield strength of the mild steel tension reinforcement (psi)

The detailed method provided a computed shear capacity of 90.98-kips for Girders 1 through 6, and 136.75-kips for Girders 7 and 8. These values are only 55.62% and 52.29% of the average measured values for Girders 1 through 6 and Girders 7 and 8 respectively.

As was described previously for the AASHTO method, the ACI design equations were developed using bending theory which has been found to be less accurate in the d-regions of a prestressed concrete beam, and thus provides very conservative values for shear in this region.

4.1.3 Predictive Method Strut-and-Tie Model

Concrete girders can be divided up into B-regions and D-regions. The B-regions are regions in which Bernoulli bending theory applies. In B-regions it is assumed that strains are distributed linearly through the depth of the girder. D-regions are discontinuity or disturbed regions as defined by St. Venant's Principle. Since the design code equations were developed based on bending theory another method needed to be examined which would better describe the types of failures observed in this research. One such method is called the strut-and-tie model. Both the AASHTO and the ACI design codes allow for a strut-and-tie model (STM) to be used in the design of prestressed concrete girders when the critical section is located within a D-region. The governing equations and recommendations on how to apply the STM are found in the appendices of each of the two design codes. STMs are rarely used in design of new girders, but this model does prove very useful in design as well as analysis of prestressed concrete girders. Analysis of concrete girders for shear in the D-region is easily and accurately handled by the strut-and-tie model.

The strut-and-tie model is an idealized model of a girder consisting of struts which are compression members made of concrete parallel to the expected cracks, ties or stirrups which are tension members made of steel analogous to the reinforcement, and nodes made of concrete which are connecting members.

Various types of struts may be used depending on the application. The most common struts are rectangles (prisms), bottles, and fans. The different shapes assume a distribution of the forces corresponding to the shape, and represent compressive stress fields. The compressive stresses act parallel to the longitudinal axis of the strut, causing transverse tension in the strut which can lead to failure.

The node sizes are determined by the bearing area of the load, the bearing area of the support, and the prism of concrete surrounding the tie. Nodes are sections of concrete which connect the strut to the ties. The nodes are idealized as pinned joints. The concrete in and surrounding the node is referred to as the nodal zone. There are three or more forces planer forces that all act through the node and satisfy equilibrium.

Ties act as the reinforcement, whether that is a single layer, or several different layers of reinforcement. The axis of the tie must coincide with the axis of the reinforcement. In a STM the tie consists of the reinforcement plus a prism of concrete concentric with the longitudinal reinforcement making up the width of the tie (Wright and MacGregor, 2009). The node dimensions are developed from the concrete surrounding the tie, which do not carry any load, but aid in transferring the loads.

For this research a strut-and-tie model was developed using two struts and one tie connected at three nodes. This configuration formed a simple triangular truss which was analyzed to obtain ultimate shear values of 138.56-kips and 258.7-kips for Girders 1 through 6 and for Girders 7 and 8, respectively. Some sample calculations are included at the end of Appendix A.

4.1.4 Comparison of Calculated to Measured Shear Capacities

The AASHTO and ACI procedures for calculating the shear capacities of prestressed concrete girders are both based on bending theory, and St. Venant’s Principle. This implies that it is assumed that the shear stresses are distributed linearly through the depth of the beam as long as the load is applied at a distance larger than the depth of the beam or outside the D-region. The eight beams that were tested for this research were tested in the D-region where the shear stresses were believed to not be evenly distributed through the depth of the beam. Having the load applied in the D-region causes the stresses in the girder to be concentrated in some regions, and almost non-existent in other areas due to arching action of the beam. The design codes examined in this research did not take into account the effects of unevenly distributed shear stresses through the depth of the beam. The codes allow the sectional analysis to be done along the length of the girder because the values computed using the design equations are conservative.

The strut-and-tie model used for this research was able to much more accurately predict the ultimate shear capacity of the girders. The strut-and-tie model was very simple while still yielding good results. When analysis is to be done, the STM is far better at predicting the actual strength in the D-regions of reinforced concrete beams.

Table 4.1Calculated shear values

Method	Girders 1-6 Shear (kips)	Percentage of Measured	Girders 7-8 Shear (kips)	Percentage of Measured
AASHTO General	47.79	29.22%	37.66	14.40%
AASHTO Simplified	82.27	50.30%	100.28	38.35%
ACI Simplified	101.74	62.20%	131.09	50.13%
ACI Detailed	90.98	55.62%	136.75	52.29%
Strut-and-Tie	138.56	84.72%	258.7	98.93%
Measured Value	163.56		261.5	

The results calculated for this research are presented in Table 4.1 showing the predicted values as calculated using the methods presented above. The calculated values are also compared to the measured values as a percentage of the measured values.

4.1.5 ASHTO LRFD Predicted Prestress Losses

The AASHTO LRFD bridge design code provides two different methods for predicting the prestress losses in a prestressed concrete girder (AASHTO, 2009). The first is classified as the approximate method which can be used with gross section properties or transformed section properties. The second method is classified as the detailed method with transformed section properties. This section will provide both methods and present the values calculated from each method.

The approximate method, using transformed section properties, automatically takes into account the elastic shortening loss of prestress due to introduction of prestress to the concrete member, as well as any instantaneous gain due to the application of gravity loads. The long-term prestress losses are assumed to be the negative prestress (Δf_{pLT} in ksi) as calculated from Equation 4.24 multiplied by the area of the prestressing tendons (A_{ps} in in^2). These long-term losses include losses that result from creep, shrinkage of the concrete, and relaxation of the prestressing steel.

$$\Delta f_{pLT} = 10.0\frac{f_{pi}A_{ps}}{A_g}\gamma_h\gamma_{st} + 12.0\gamma_h\gamma_{st} + \Delta f_{pR} \tag{4.24}$$

$$\gamma_h = 1.7 - 0.01H \tag{4.25}$$

$$\gamma_{st} = 5/(1 + f'_{ci}) \tag{4.26}$$

where:

f_{pi} = prestressing immediately before transfer (ksi)

A_g = gross area (in^2)

H = average ambient humidity as a percent

f'_{ci} = specified initial concrete compressive strength (ksi)

A_{ps} = the total area of the prestressing steel (in^2)

Δf_{pR} = an estimate of relaxation loss taken as 2.4 for low relaxation strand, 10.0 for stress relieved strand, and in accordance with manufactures recommendations for other types of strand (ksi)

This loss in prestress is applied at the centroid of the prestressing steel area and the transformed concrete section resulting in a prestress force at service. Using the effective prestress force at service, stresses can be easily calculated using the transformed section properties and compared against the design stress limits.

The detailed method is much more involved, but relatively easy to apply. This method entails calculating creep and shrinkage material properties independently. Equation 4.27 should be used to calculate the elastic shortening loss and Equation 4.28 should be used to calculate the prestress losses from the detailed method. The subscript “*id*” is used to denote losses before the deck is made composite, and the subscript “*df*” is used to denote losses that occur after the deck has been made composite until the final time. The bottom fiber stress and the stress at the centroid of the steel can be calculated at different stages of construction. The elastic shortening loss due to initial prestress force and the girder self weight is automatically accounted for, as described above in the simplified method, if transformed section properties are used. Using all of the correction coefficients and the different factors, the prestress loss was calculated as 179.75- kips shown in table 4.2.

$$\Delta f_{pES} = \frac{E_p}{E_{ct}} f_{cgp} \qquad (4.27)$$

where:

E_p = modulus of elasticity of prestressing steel (ksi)

E_{ct} = modulus of elasticity of concrete at transfer or time of load application (ksi)

f_{cgp} = the concrete stress at the center of gravity of the prestressing strands due to prestressing force immediately after transfer and the self-weight of the member at the section of maximum moment (ksi)

$$\Delta f_{pLT} = \left(\Delta f_{pSR} + \Delta f_{pCR} + \Delta f_{pR1}\right)_{id} + \left(\Delta f_{pSD} + \Delta f_{pCD} + \Delta f_{pR2} - \Delta f_{pSS}\right)_{df} \qquad (4.28)$$

where:

Δf_{pSR} = prestress loss due to shrinkage of girder concrete between transfer and deck placement (ksi)

Δf_{pCR} = prestress loss due to creep of girder concrete between transfer and deck placement (ksi)

Δf_{pR1} = prestress loss due to relaxation of prestressing strands between time of transfer and deck placement (ksi)

Δf_{pR2} = prestress loss due to relaxation of prestressing strands in composite section between time of deck placement and final time (ksi)

Δf_{pSD} = prestress loss due to shrinkage of girder concrete between time of deck placement and final time (ksi)

Δf_{pCD} = prestress loss due to creep of girder concrete between time of deck placement and final time (ksi)

Δf_{pSS} = prestress gain due to shrinkage of deck in composite section (ksi)

4.1.6 Comparison of Measured and Calculated Prestress Losses

The effective prestress force which remained in Girders 1 through 6 was calculated as 188.42-kips using the AASHTO LRFD simplified method. Using the simplified method the effective prestress force was 114% of the average measured prestress force in the girders. When the effective prestress force was calculated using the AASHTO LRFD detailed method a value of

Table 4.2 Factors used with AASHTO Detailed Method for P_e

α_g=	1.17	Change in Concrete Stress at the Level of Prestressing Strands:	
K_{td}=	0.55		
K_s=	1.00		
K_{hs}=	1.21	Δf_{cd}=	0.0924415 ksi
K_f=	1.00	Δf_{pc}=	0.7855794 ksi
ε_{bid}=	0.000321	Δp=	-29.183121 kips
K_{la}=	1	Δf_{cb}=	-0.1191112 ksi
K_{hc}=	1.12	α_{gc}=	3.293183
ψ_{bid}=	1.1726337	ε_{bif}=	0.0008718
ψ_{bif}=	2.1320612	k_{la}=	0.6218903
f_{pu}=	250 ksi	ε_{bdf}=	0.000551
f'_{ci}=	4 ksi	ε_{ddf}=	0.0008718
f_{pi}=	175 ksi	K_s=	1.9995044
E_p=	28500 ksi	K_f=	0.748503
$E_{c\ at\ trns}$ =	4027.56 ksi	ψ_{bdf}=	1.9806209
$E_{c\ at\ svc}$ =	4830.55 ksi	ψ_{ddf}=	1.9806209
E_{cd}=	4027.56 ksi	K_{df}=	0.9317569
n_i=	7.08	Shringage Loss:	
n_d=	0.83	Δf_{pSD}=	14.626124 ksi
$n_{service}$=	5.90	Creep Loss Due to Initial Loads:	
A_{ps}=	1.38 in^2	Δf_{pCD1}=	5.5542193 ksi
P_o=	241.5 kips	Creep Loss Due to Deck and SIDL:	
P_i=	241.5 kips		
M_g=	1193.0882 kip-in	Δf_{pCD2}=	-14.907152 ksi
f_{cgp}=	0.8780209 ksi	Relaxation Loss:	
Δf_{pES}=	6.2130983 ksi	Δf_{pR3}=	-5.89 ksi
Transformed section factors between transfer and deck		Prestress Gain Due to Shrinkage of the deck:	
K_{id}=	0.9284207	Δf_{cdf}=	-0.9133993 ksi
Shrinkage Loss:		Δf_{ssp}=	-11.982886 ksi
Δf_{pSR}=	8.4930055 ksi	Total Long-term Stress change between deck placement and final time:	
Creep Loss:			
Δf_{pCR}=	6.7641834 ksi	Δf_{pdf}=	-12.599695 ksi
Relaxation Loss:		The change in the concrete stress at the bottom fiber of the girder due to long-term losses is:	
Δf_{pR2}=	5.89 ksi		
Total Losses:		ΔP=	-17.387579 kips
Δf_{pid}=	21.147189 ksi	Δf_{cb}=	0.0723921 ksi

179.75-kips was found. This was 109% of the average measured prestress force from the cracking tests. Table 4.3 shows four different effective prestress forces. All of the effective prestress forces were compared to the average measured prestress force in Girders 1 through 6. These girders were subjected to severe corrosion during their service life. This corrosion was believed to contribute to the lower than expected effective prestress force. The maximum difference was 23.42-kips, with the bridge plan specifications being the closest at a difference of only 11-kips.

Table 4.3 Effective prestress force comparison

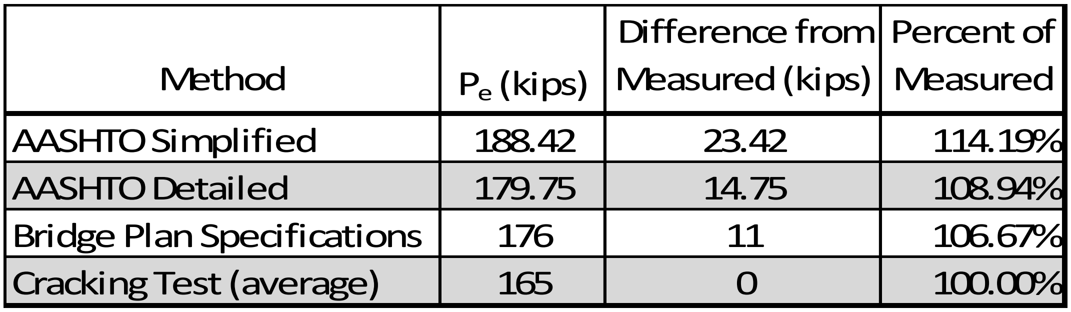

Method	P_e (kips)	Difference from Measured (kips)	Percent of Measured
AASHTO Simplified	188.42	23.42	114.19%
AASHTO Detailed	179.75	14.75	108.94%
Bridge Plan Specifications	176	11	106.67%
Cracking Test (average)	165	0	100.00%

4.2 Introduction to Predictive Methods for Shear Contribution from CFRP

In this chapter, a comparison of two analytical methods that calculate the contribution of the CFRP reinforcement for shear in AASHTO prestressed girders is presented. The general design equation used to calculate the nominal shear capacity of a girder is:

$$V_n = V_c + V_s + V_f \qquad (4.29)$$

where V_c is the shear contribution from the concrete, V_s is the shear contribution from the steel stirrups, and V_f is the shear contribution from the CFRP reinforcement.

There are two methods for calculating the carbon fiber contribution for shear, V_f that will be evaluated in this research. The first method evaluated to calculate V_f is described in ACI 440.2R-8 entitled Guide for the "Design and Construction of Externally Bonded FRP Systems for Strengthening Concrete Structures" (ACI, 2008b). The second method to evaluated V_f is a method presented in a research paper by Hutchinson, Donald, and Rizkalla (1999). Each of these methods are used to calculate the additional contribution of the CFRP reinforcement V_f to the overall nominal shear capacity V_n of the eight tested bridge girders. The nominal shear capacity from the two different methods will then be compared to the ultimate shear capacity found in the experimental program in Chapter 3.

4.2.1 ACI Analytical Method for Vf

The first analytical method that is evaluated for this research is the recommendations found in the ACI 440.2R-08 manual entitled, “Guide for the Design and Construction of Externally Bonded FRP Systems for Strengthening Concrete Structures.” This research covers how the ACI code compares to actual experimental results found in CFRP reinforcement for I-shaped prestressed girders. The reader should note that the ACI code does not have specific design equations for I-shaped sections but in this research an evaluation was performed how the standard rectangular section equations in the code ACI code apply to other shapes. The ACI equation for the contribution of CFRP systems for shear is expressed in Equation 4.30 as:

$$V_f = \psi_f \frac{A_{fv} f_{fe} (\sin\alpha + \cos\alpha) d_f}{s_f} \tag{4.30}$$

where

$\psi_f = 0.85$

Reduction factor for U-wraps

$A_{fv} = 2 n t_f w_f$

Area of CFRP shear reinforcement, in^2

n = number of plies

t_f = thickness of CFRP sheet, in.

w_f = width of CFRP strip, in.

$f_{fe} = \varepsilon_{fe} E_f$ Tensile Stress

E_f = Tensile Modulus

$\varepsilon_{fe} = K_v \varepsilon_{fu} \leq 0.004$ Max. effective strain

ε_{fu} = design rupture strain, in/in

$K_v = \frac{k_1 k_2 L_e}{468 \varepsilon_{fu}} \leq 0.75$

Bond reduction Coefficient, in.-lb units

$L_e = \frac{2500}{(n t_f E_f)^{0.58}}$

Active bond length, in.-lb units

$k_1 = \left(\frac{f'_c}{4000}\right)^{2/3}$

Bond reduction Coefficient, in.-lb units

α = angle of CFRP fiber orientation

S_f = Space of CFRP strips, in.

$$k_2=\frac{d_f-L_e}{d_f}$$

Bond reduction Coef., in.-lb units

d_f =Effective depth of CFRP reinforcement, in.

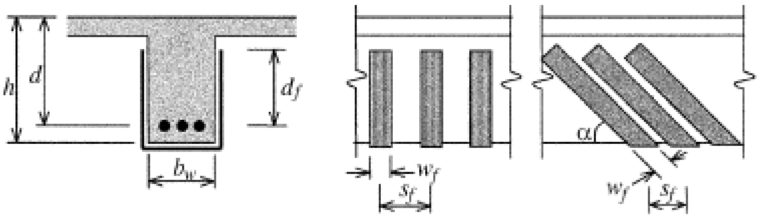

Figure 4.1 Dimensional variables for CFRP shear reinforcement design found in ACI 440.2R-08.

The equation presented above is presented in more detail in the ACI 440.2R-08. Equation 4.30 was developed based on U-wraps, calculated using standard units, while the code found in the ACI is used for both full wraps and U-wraps in both metric and standard units.

Table 4.4 Calculated results for ACI analytical methods for Vf

ACI Design Equation Results						
Method	Girder 2	Girder 3	Girder 4	Girder 5	Girder 6	Girder 8
ACI Vf (kips)	84.00	63.72	63.72	57.93	63.72	55.82
df (in)	28.80	28.80	28.80	28.80	28.80	27.80
wf (in)	20	10	10	10	10	10
Sf (in)	20.00	18.64	18.64	14.50	18.64	14.50
α (deg)	90.00	45.00	45.00	90.00	45.00	90.00
f'c (psi)	7000	7000	7000	7000	7000	7000
Le (in)	1.35	1.35	1.35	1.35	1.35	1.35
k1	1.45	1.45	1.45	1.45	1.45	1.45
k2	0.95	0.95	0.95	0.95	0.95	0.95
Kv	0.24	0.24	0.24	0.24	0.24	0.24
efe	0.004	0.004	0.004	0.004	0.004	0.004
n	1	1	1	1	1	1

Afv (in^2)	0.52	0.26	0.26	0.26	0.26	0.26
tf (in)	0.013	0.013	0.013	0.013	0.013	0.013
ffe (ksi)	131.98	131.98	131.98	131.98	131.98	131.98

The results for the ACI method in Table 4.4 are the calculated results for the shear contribution of CFRP reinforcement Vf, using the ACI equation explained in Section 4.1. The ACI code is used for the design of girders with rectangular sections and the research presented is how the equations can apply to I-shaped girders. In Table 4.4 are the results of the ACI code for I-shaped girders.

4.2.2 Analytical Method in Hutchinson, Donald, and Rizkalla (1999) for Vf

In a research paper entitled "FRP for Shear Strengthening of AASHTO Bridge Girders" by Hutchinson, Donald, and Rizkalla (1999), the authors present an alternative rational method to the ACI procedure to calculate the additional contribution of a CFRP system for shear reinforcement. This contribution due to the CFRP reinforcement is calculated using the following expression:

$$V_{fmax} = \frac{\varepsilon_{fave} E_f 2 n_f t_f w_f d_f}{s_f} (\cot\theta + \cot\alpha_f) \sin\alpha_f \qquad (4.31)$$

where

E_f= Tensile Modulus

t_f= Thickness of sheet

n_f = Number of layers

d_f= Length from top of flange to the centroid of longitudinal steel in bottom flange

d= Length from centroid of longitudinal steel to top of beam (or top of deck if deck exists)

s_f = Length of spacing from edge of one strip to the same edge of next strip

θ= Assumed crack angle (30-degrees)

w_f= Width of sheet

α_f= Angle of orientation of CFRP fibers

where:

from the longitudinal direction of beam

$$\epsilon_{fave}=\epsilon_{fmax}\frac{[\left(\frac{d}{2}\right)+0.5\left(d_f-\frac{d}{2}\right)]}{d_f}$$

ϵ_{fave}= Average CFRP strain for I-shaped sections

ϵ_{fmax}=.004 (diagonal strips 45-degrees)

ϵ_{fmax}=.0028 (Vertical strips)

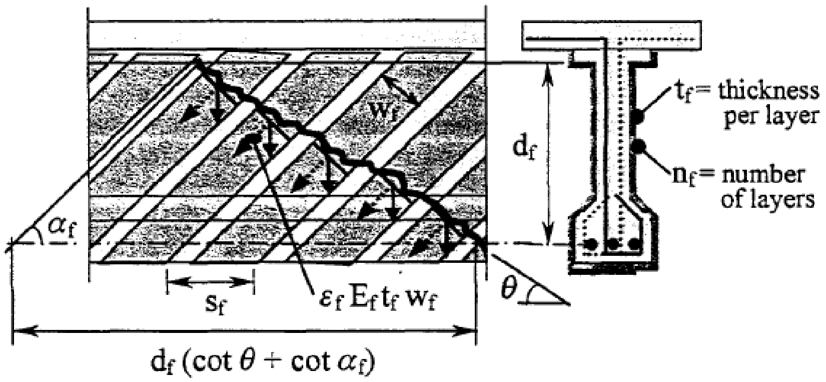

w_f
d_f
t_f= thickness per layer
n_f= number of layers
α_f
s_f
$\varepsilon_f E_f t_f w_f$
θ
$d_f (\cot\theta + \cot\alpha_f)$

Figure 4.2 Dimensional variables for CFRP shear reinforcement design found in Hutchinson, Donald, and Rizkalla (1999).

Table 4.5 lists the calculated results for the shear contribution of the CFRP reinforcement for I-shaped girders using the method presented in Hutchinson, Donald, and Rizkalla (1999) that is explained above.

Table 4.5 Results for method in Hutchinson, Donald, and Rizkalla (1999) for Vf

Analytical method in Hutchinson, Donald, and Rizkalla (1999)						
	Girder 2	Girder 3	Girder 4	Girder 5	Girder 6	Girder 8
Vf (kips)	90.50	51.75	51.75	62.41	51.75	62.41
d (in)	39.00	39.00	39.00	39.00	39.00	39.00
df (in)	24.00	24.00	24.00	24.00	24.00	24.00
wf (in)	20.00	10.00	10.00	10.00	10.00	10.00
Sf (in)	20.00	18.64	18.64	14.50	18.64	18.64
tf (in)	0.013	0.013	0.013	0.013	0.013	0.013
n (ply)	1	1	1	1	1	1
Lfe (in)	37.73	37.73	37.73	37.73	37.73	37.73
efmax	0.003	0.003	0.003	0.003	0.003	0.003
efave	0.0025	0.0025	0.0025	0.0025	0.0025	0.0025
θ (deg)	30	30	30	30	30	30
α (deg)	90	45	45	90	45	90

4.2.3 Comparison of Analytical Models for Vf and measured Vf

The calculated magnitudes of Vf for both methods were found to compare well with the measured values of shear but the effectiveness of their predictions were dependent on the CFRP reinforcement configuration. The analytical and measured values of additional shear capacity are compared in Table 4.6. This section will evaluate each CFRP reinforcement configuration and how it compared to both analytical predictive models when compared to the shear capacity of the control.

Girder 1. There was no CFRP reinforcement applied to this girder. The average measured shear capacity of this girder was used for comparison of Girder 2 through 6 results. The average shear capacity of Girder 7 was 163.37 kips.

Girder 2. The CFRP configuration for this girder was found to be effective in providing additional shear capacity but was also found to be extremely sensitive to the application process which led to even decreases in shear capacity. This sensitivity has been attributed from the anchorage system which involved cutting one inch grooves into the girder (see Chapter 3 for detail). For Test 2A the CFRP reinforcement provided an additional shear force of 92.11 kips. The ACI model predicted the CFRP reinforcement would yield 84 kips while the Hutchinson, Donald, and Rizkalla (1999) model predicted a 90.5 kip increase. For this test both models were close and conservative but the Hutchinson, Donald, and Rizkalla (1999) model predicted 98% of the actual shear capacity increase while the ACI predicted 92.2% . It must be noted that for Test 2B there was a decrease in shear capacity for one of the tests. This decrease is believed to be due to the sensitivity of the configuration and the required cuts for the anchorage system.

Girder 3. The CFRP reinforcement configuration on this girder was found to increase the shear capacity and was found to be more consistent in comparison to Girder 2. This consistency is believed to be due to the horizontal strip of CFRP placed over the diagonal stirrups. The average increase of shear capacity from the two tests on Girder 3 was 39.7 kips. The ACI model predicted the CFRP reinforcement would yield 63.72 kips while the Hutchinson, Donald, and Rizkalla (1999) model predicted a 51.75 kip increase. For this test both models overestimated the increased shear capacity. The difference is believed to be due the shape of the girder causing early debonding. The actual increased shear capacity was only 62.3% of the ACI analytical prediction and 76.7% of the Hutchinson, Donald, and Rizkalla (1999) analytical prediction.

Girder 4. The CFRP reinforcement configuration for this girder was similar to Girder 3 but with the absence of the horizontal anchorage strip. It was expected that this capacity would be less than Girder 3. The decrease in the additional shear capacity for this girder was evidence that the horizontal strip for anchorage was successful in increasing the capacity of the diagonal and vertical strips. The average increase of shear capacity from the two tests on Girder 4 was 13.64 kips. The ACI model predicted the CFRP reinforcement would yield 63.72 kips while the Hutchinson, Donald, and Rizkalla (1999) model predicted a 51.75 kip increase. The analytical methods predicted the same increase in shear capacity as Girder 3 even though Girder 4 did not have the anchorage system. For this test both models overestimated the increased shear capacity. The actual increased shear capacity was only 21.4% of the ACI analytical prediction and 26.35% of the Hutchinson, Donald, and Rizkalla (1999) analytical prediction.

Girder 5. The CFRP reinforcement configuration of Girder 5 provided a large increase in shear capacity for both tests. Due to its consistency and ease in application this girder was selected as the most effective reinforcement configuration and the same configuration was applied again on Girder 8. The analytical calculations were also found to be effective in predicting the increase in magnitude of shear capacity. The average increase of shear capacity from the two shear tests on Girder 5 was 61.43 kips. The ACI model predicted the CFRP reinforcement capacity at 57.93 kips while the Hutchinson, Donald, and Rizkalla (1999) model predicted a 62.41 kip capacity increase. For this test, both predictive methods underestimated the measured shear capacity of the CFRP reinforcement. Both models were close and conservative but the Hutchinson, Donald, and Rizkalla (1999) method predicted 94.3% of the actual shear capacity increase while the ACI predicted 101.6%. The Hutchinson, Donald, and Rizkalla (1999) predictive method was found to be only 5.7% over conservative for this girder, while the ACI method only overestimated by 1.6%.

Girder 6. The CFRP configuration for this girder was found to be effective in providing additional shear capacity but similar to Girder 2 was also found to be extremely sensitive to the application process which led to decrease in shear capacity for one test. This is the same issue that was found in the CFRP reinforcement configuration on Girder 2. This sensitivity has been attributed from the anchorage system which involved cutting one inch grooves into the girder at the interface of the web and bottom flange (see Chapter 3 for detail). For Test 6A, the CFRP reinforcement provided an additional shear force of 84.49 kips. The ACI model predicted the CFRP reinforcement would add an additional 63.72 kips while the Hutchinson, Donald, and Rizkalla (1999) method predicted a 51.75 kip increase. For this test both models were close but very conservative. The Hutchinson, Donald, and Rizkalla (1999) model predicted an increase of 61.25% of the actual shear capacity while the ACI methodology predicted an increase of 75.42%.

Girder 7. There was no CFRP reinforcement applied to this girder. The average measured shear capacity of this girder was used for comparison of Girder 8 results. The average shear capacity of Girder 7 was 261.50 kips.

Girder 8. The CFRP reinforcement configuration for Girder 8 provided a large increase in shear capacity for both tests. Due to the consistency and ease in application on Girder 5 the same configuration was applied and tested on Girder 8. The analytical models were also found to be effective in predicting the increase in shear capacity of Girder 5. The average increase of shear capacity from the two tests on Girder 8 was 48.46 kips. The ACI methodology predicted the CFRP reinforcement would provide an additional capacity of 55.82 kips while the Hutchinson, Donald, and Rizkalla (1999) methodology predicted a 62.41 kip increase. For this test both models overestimated the increased shear capacity. The actual increased shear capacity was only 86.82% of the ACI analytical prediction and 77.65% of the Hutchinson, Donald, and Rizkalla (1999) analytical prediction.

The success of the predictive methodologies was dependent on the CFRP reinforcement configurations. The configurations of Girder 5 and 8 were found to be most consistent in matching the predictive methodologies and most consistent in increasing the shear capacity. For Girders 5 and 8 the average increase in shear capacity due to the same configurations, was 54.96 kips. The ACI predicted an average increase for girders 5 and 8 of 56.88 kips while the Hutchinson, Donald, and Rizkalla (1999) model predicted 62.41 kips. The ACI method overestimated by 3.5% while the Hutchinson, Donald, and Rizkalla (1999) overestimated the average measured increases by 13.55%.

Table 4.6 Results of actual Vf and analytical methods for Vf

Method (kips)	Test 1A	Test 1B	Test 2A	Test 2B	Test 3A	Test 3B	Test 4A	Test 4B
Vn	150.28	176.86	255.68	162.70	197.02	209.50	179.61	174.80
Vf (actual)	0	0	92.11	-0.87	33.45	45.93	16.04	11.23
Vf (ACI)	0	0	84.00	84.00	63.72	63.72	63.72	63.72
Vf (hut. et al.)	0	0	90.50	90.50	51.75	51.75	51.75	51.75

Method (kips)	Test 5A	Test 5B	Test 6A	Test 6B	Test 7A	Test 7B	Test 8A	Test 8B
Vn	225.07	224.94	248.06	151.79	263.36	259.63	311.93	307.97
Vf (actual)	61.52	61.37	84.49	-11.78	0	0	50.44	46.48
Vf(ACI)	57.93	57.93	63.72	63.72	0	0	55.82	55.82
Vf(hut. et al.)	62.41	62.41	51.75	51.75	0	0	62.41	62.41

5.0 SUMMARY AND CONCLUSIONS

5.1 Summary

As bridges age and deteriorate, their capacities tend to decrease and are difficult to predict. This fact coupled with larger and larger loads being applied to the nation's bridges has lead to much research and implementation of retrofitting and strengthening of in-service bridge girders. The tendency is to reinforce bridge girders primarily in flexure. This increase in flexural capacity leads to a stiffer girder which can result in shear being the failure mode of the girder. With added load and flexure strengthening, understanding of the shear behavior becomes increasingly more important. To this end, research was conducted on two different types of AASHTO Type II reinforced prestressed concrete bridge girders that were over 40 years old to determine their existing shear capacities at the end of the girders where water had damaged them extensively. The measured values were compared against the predicted values using the AASHTO LRFD shear design code as well as the ACI-318 shear design specifications.

Two separate groups of girders were tested from two different decommissioned bridges. Girders 1 through 6 had an in-service span length of 22-ft 3-in, and Girders 7 and 8 had an in-service span length of 34.5-ft. The girders were simply supported and loaded at a distance of 48 inches (d + 1-ft) from the supports with a single point load. Each end of each girder was tested independently of the other. This caused the overall span lengths to vary from end to end; as one end was tested through failure, it became necessary to move the corresponding support, locating it under a section of the girder which was still intact. The measured shear capacities for Girders 1 through 6 and 7 and 8 respectively were 163.56-kips and 261.50-kips.

Carbon Fiber Reinforced Polymers are being found to be effective in retrofitting highway bridges for many different applications. The focus of this research was to investigate how a CFRP fabric system can be applied for shear reinforcement to the deteriorated ends of I-shaped prestressed concrete girders. There are inherent difficulties in applying CFRP to typical precast sections. To provide insight on how CFRP behaves on I-shape cross-sections, five different configurations of the CFRP fabric were tested. Of the five different configurations, two anchorage systems were implemented to increase the shear capacity of the CFRP. Each girder was then tested to failure in shear to quantify the increased shear capacity. During the load test, deflections, and strains were measured to provide conclusive evidence of the influence of the CFRP on shear capacity.

Another aspect of the research was to investigate how two different theoretical models that predicted the increase in shear capacity from the CFRP system. The first method evaluated to calculate Vf is found in ACI 440.2R-8 entitled Guide for the "Design and Construction of Externally Bonded FRP Systems for Strengthening Concrete Structures". The second method to evaluated Vf is a method presented in a research paper entitled "FRP for Shear Strengthening of AASHTO Bridge Girders" by Hutchinson, Donald, and Rizkalla (1999). The calculated results for the two methods were then compared to the actual increased shear capacity.

5.2 Conclusions on Existing Shear Capacity

In the d-region of a prestressed concrete beam the shear capacity is not accurately predicted using standard equations from the current design codes. In order to accurately predict the ultimate shear capacity of a prestressed concrete girder another approach needs to be taken. One other approach examined in this research was a strut-and-tie model, which much more accurately predicted the ultimate shear capacity. The strut-and-tie model was found to be within about 15 percent of the measured values. Further details are given below.

5.2.1 Comparison with AASHTO LRFD

Both the General and Simplified methods provided by the AASHTO LRFD bridge design code provided conservative values of the ultimate shear capacity. The AASHTO Design specifications were developed using bending theory with the assumption that plane sections remain plane. The shear load, as tested in this research, was right at the boundary and therefore St. Venant's Principle was not likely valid. The AASHTO specifications allow for sectional design because it is known that the values calculated for the shear capacity near the supports will be conservative. The average measured shear for Girders 1 through 6 was 163.56-kips where the General Method produced a calculated shear capacity of 47.79-kips, and the Simplified Method resulted in a calculated shear capacity of 82.27-kips. For Girders 7 and 8 the General Method resulted in a calculated shear capacity of 37.66-kips and the Simplified Method resulted in a calculated shear capacity of 100.28-kips. When tested in the lab the average shear capacity of Girders 7 and 8 was 261.50-kips.

5.2.3 Comparison with ACI318-08

The ACI-318 design code was developed based on bending theory assuming that plane sections remain plane. As was described for the AASHTO specifications, these assumptions have been shown to not be valid near the supports of a girder. The ACI-318 code also allows for sectional analysis near the supports of a beam with the understanding the calculated shear capacities will be conservative near the supports, which was shown from the results of this research. For Girders 1 through 6 the ACI Simplified Method and Detailed Method produced values of the shear capacity as 101.74-kips and 90.98-kips, respectively. The average measured value was 163.56-kips. For the longer girders, Girders 7 and 8, the Simplified Method resulted in a calculated value of 131.09-kips, and the Detailed Method gave a calculated value of 136.75-kips. The average measured shear value for Girders 7 and 8 was 261.50-kips.

5.2.4 Comparison with the Strut-and-Tie Model

The strut-and-tie model which is not based on bending theory or St. Venant's Principle was developed for the girders tested in this research. The model consisted of two main compression struts and a tension tie connected at the nodes. This model was very simple in nature, yet yielded much more accurate results. For Girders 1 through 6 the STM produced an ultimate shear capacity of 138.56-kips which is 84.72% of the average measured value. For Girders 7 and 8 the STM gave an ultimate shear capacity of 258.7-kips. The STM was 98.93% of the average measured value of 261.50-kips for Girders 7 and 8.

5.2.5 Cracking Test

Cracking tests were carried out on Girders 1 through 6 to determine the residual prestressing force in the girders. This was done by initially cracking the simply supported beams by means of a single point load applied at mid-span. Once the crack was located and marked, strain gauges were placed across and to either side of the crack on the bottom flange of the girder. The girder was then reloaded at mid-span while load and strain were recorded. The strain was then plotted vs. load and the decompression load was obtained from the response. The decompression load was used to calculate the prestressing force. The average existing prestressing force for Girders 1 through 6 was 165.0-kips.

5.2.6 Comparison of Prestress Losses

AASHTO prestress loss equations were used to compare against the measured values. The AASHTO LRFD specifications (AASHTO, 2009) were used as a guide for these calculations. The two methods utilized herein were the Approximate Method using transformed section properties and the Detailed Method with transformed section properties. Using the Approximate Method, the effective prestress force at service was calculated as 188.42-kips. The Detailed Method produced a calculated effective prestress force of 179.74-kips. The bridge plans specified an effective prestress force after all losses of 176.00-kips. The effective prestress force obtained from the cracking test was 165.0. All of the predictive methods under-predicted the effective prestress force. This was likely due to the excessive corrosion of the steel in the girders.

5.3 Conclusions on CFRP Reinforcement

The experimental program consisting of the load testing of five different CFRP reinforcement configurations was found to increase the shear capacity of the AASHTO I-shaped prestressed girders. The magnitude of the increased shear capacity was found to be highly dependent on the CFRP reinforcement configuration and anchorage system. The theoretical models effectiveness in predicting the increased shear capacity was also highly dependent on the CFRP reinforcement configuration and anchorage system. The CFRP reinforcement was able to allow for larger deflections before failure. From the strain measurements it was concluded that the CFRP fabric was not overstressed and failed due to debonding.

5.3.1 Effects of CFRP Configurations on Increased Capacity

The increased shear capacity was highly dependent on the configuration of the CFRP reinforcement. CFRP has a more difficult time resisting shear forces of I-shaped girders due to the large normal forces developed in the web to flange corners. In order to help resist these normal forces, two different anchorage systems were applied to four different CFRP sheet configurations. One girder was reinforced without an anchorage system to provide comparative results with the girders with anchorage systems.

Girder 4 was reinforced with diagonal (45 degrees) CFRP fabric stirrups but without an anchorage system. The result when loaded to failure was an increase of only 13.64 kips in shear capacity. Girder 3 had the same diagonal CFRP fabric stirrups as Girder 4 but had a horizontal strip of CFRP fabric applied over the diagonal strips for anchorage, resulting in an increased shear capacity of 39.69 kips which is 26.05 kips larger than Girder 4 without the anchorage. This is conclusive evidence that the horizontal anchorage system greatly increases the capacity of the CFRP reinforcement.

Girder 2 was reinforced with diagonal (45 degrees) CFRP fabric stirrups but with the inserted CFRP laminate anchorage system at the web to flange corner. The result when loaded to failure was an increase of 92.11 kips for the first test and a decrease of 0.87 kips of shear capacity for the second test. Girder 6 had the same anchorage system but had vertical wraps of CFRP fabric for the whole shear span. The result for the first test increased the shear capacity by 84.49 kips and decreased the shear capacity by 11.78 kips for the second test. Both of these configurations had the potential to have high increases in shear capacity but were found to be very sensitive to the anchorage system cutes and unreliable. The imbedded anchorage system which involved cutting a 1 inch slit into the girder at the web to flange corner weakened the girder for two of the four tests and is concluded to be the cause of a very sensitive system.

Girders 5 and 8 had vertical CFRP fabric stirrups and a horizontal strip of CFRP fabric over the vertical stirrups. This configuration was found to be the most reliable and consistent in increasing the shear capacity. The four tests on Girders 5 and 8 produced an average increased shear capacity of 55.70 kips. The CFRP reinforcement configuration on Girders 5 and 8 were also the easiest to apply due to its simplicity in design.

Overall, the CFRP fabric reinforcement was found to be successful in increasing the shear capacity of AASHTO prestressed I-shaped girders. The configuration on Girders 5 and 8, which consisted of vertical stirrups and a horizontal strip placed over the vertical stirrups for anchorage, was found to produce the largest consistent increase in shear capacity consistently. This configuration was also the easiest to apply and can be credited for its consistency. Therefore, this CFRP reinforcement configuration was found to be the most effective in increasing the shear capacity of AASHTO prestressed I-shaped girders.

5.3.2 Observations from CFRP Theoretical Models

The theoretical models for predicting the total shear capacity V_n, were found to be very conservative and can mainly be contributed to the conservatism in calculating V_c and V_s, which made it more challenging to compare the two V_f theoretical models. We were able to find conclusive evidence when comparing the actual V_f against the two predictive models for V_f.

The ACI method overestimated Girders 3, 4, and 8 by 37.7%, 78.6%, and 13.18% respectively and underestimated Girders 2, 5, and 6 by 7.9%, 7.96% and 24.42% respectively. The Hutchinson, Donald, and Rizkalla (1999) method overestimated Girders 3, 4, and 8 by 23.3%, 73.65%, and 22.35%, respectively, and underestimated Girders 2, 5, and 6 by 1.75%, 0.84% and 22.35%, respectively. Both methods for predicting the shear contribution of the CFRP fabric were found to be conservative and over conservative for the same reinforcement configurations.

The CFRP reinforcement configuration on Girders 5 and 8 were found to be most consistent and reliable in increasing the shear capacity. When comparing the average actual shear capacity increase of 55.70 kips, the ACI estimated 56.88 kips which is only a 2.11% overestimation, while the Hutchinson, Donald, and Rizkalla (1999) method estimated 62.41 which is a 12.05% overestimation. Therefore, the ACI method was found to be the most accurate in predicting the increased shear capacity of AASHTO prestressed I-shaped girders with this configuration and anchorage system.

5.3.3 Observations from Deflections

During each girder test of the shear load vs deflection, curves were monitored and compared against the unreinforced shear load vs deflection curves. The comparisons concluded that the CFRP reinforcement acted compositely with the girder and allowed for increased deflections. This provided a failure that was less brittle when loaded and failed in shear.

5.3.4 Observations from Strains

During the load testing, strains were measured at various locations on the CFRP fabric that provided evidence that this external reinforcement was resisting the applied shear load. It was also observed that the maximum strain observed yielded a stress of half the maximum allowable stress in the CFRP C160 fabric. This provides evidence the system failed due to delamination and concrete surface rupture. The CF130 fabric which is half the thickness of the CF160 fabric, would have also been adequate in providing a similar increased shear capacity for the I-shaped girders since its failure mechanism was not fiber rupture.

5.4 Recommendations for Future Work on Predicting Shear Capacity

This research investigated the near support shear capacity of prestressed reinforced concrete AASHTO Type II girders with the load applied at a distance of d+1-ft. The girders failed in a typical shear manner, but the design codes did not closely predict this kind of shear failure.

Future research needs to be done to determine equations for the shear capacity at near support regions of prestressed concrete AASHTO Type girders. Such equations could prove especially useful in bridges where large forces result from live loads being located near the support.

Other types of prestressed concrete girders should be tested in a similar manner to generalize the results and types of shear failures. By testing various shapes with differing levels of prestressing and shear reinforcement, it can be shown whether or not the design codes are adequate for specific shapes or if the results are all very conservative regardless of shape. Having a better understanding of the shear failures of different shapes of girders would provide useful information as methods are developed to increase the existing shear capacities of prestressed concrete girders.

5.5 Recommendations for Application of CFRP Shear Reinforcement

This research was funded by the UDOT with the goal of finding a solution for increasing the shear capacity of deteriorated AASHTO prestressed I-shaped girders. The experimental program consisted of testing various forms of application of a CFRP fabric system provided by The Chemical Company (BASF). The following summary was found to be the most effective application for increased shear capacity of I-shaped girders retrofitted with a CFRP fabric system and what analytical model would best fit that configuration.

The simplest configuration to apply was also found to be the most effective in increasing the shear capacity. The recommended configuration was on Girders 5 and 8 which consisted of four vertical strips 10 inches wide spaced at 4.5 inches and a horizontal strip 15 inches in height and 63 inches in length placed over the vertical strips along the web (see Section 3.5.1 for detail). This configuration is very simply to apply which leaves little room for error, making it more reliable. The configurations with angled stirrups are harder to apply and since they cannot be continuous they must be overlapped on the bottom of the girder. The anchorage requiring a cut in the girder (Girders 2 and 6) made the system very sensitive and more difficult to apply, making the system response uncertain. The recommended configuration was also found to be consistent over its four individual tests.

Another observation was that during testing, the highest observed stress in the CFRP CF160 fabric was approximately 297 ksi, which is roughly half the max stress of 550 ksi. This shows that the CF130 fabric which is half the thickness of the CF160 fabric could have been used and produced the same capacity. This would have also made the theoretical models more conservative but producing the same actual increased capacity. The recommendation that is proposed then is that for smaller girders where the depth or bond lengths are smaller the CF130 fabric would be sufficient but for girders with larger depths or bond lengths, the CF160 would be more effective.

The ACI method for calculating the predicted shear capacity of the CFRP, V_f, found in ACI 440.2R-8 entitled Guide for the "Design and Construction of Externally Bonded FRP Systems for Strengthening Concrete Structures" was found to be the most accurate for predicting the recommended CFRP reinforcement configuration. It overestimated the actual increased shear capacity by only 2.11% and with reduction factors it would fall below the design code requirements.

REFERENCES

AASHTO. 2009. AASHTO LRFD bridge design specifications. Fourth edition, 2009 Interim. Washington DC.

ACI Committee 318. 2008a. Building code requirements for structural concrete (ACI 318-08) and commentary. American Concrete Institute. Farmington Hills, MI, 465 p.

ACI Committee 440. 2008b. Guide for the design and construction of externally bonded FRP systems for strengthening concrete structures (ACI 440.2R-08) and Commentary. Farmington Hills, MI: American Concrete Institute, 465.

Adhikary, B. B., and H. Mutsuyoshi. 2004. Behavior of concrete beams strengthened in shear with carbon-fiber sheets. ASCE, Journal of Composites for Construction, V. 8, No. 3, pp. 258-264.

AISC. 2007. Steel Construction Manual. 13. United States of America.

Carolin, A., and B. Täljsten. 2005. Experimental study of strengthening for increased shear bearing capacity. ASCE, Journal of Composites for Construction, 9:6(488).

Deniaud, C., and J.J.R., Cheng. 2004. Simplified shear design method for concrete beams strengthened with fiber reinforced polymer sheets. Journal of Composites for Construction, ASCE 8(5): 425–433.

Diagana, C., A. Li, B. Gedalia, and Y. Dlemas. 2003. Shear strengthening effectiveness with CFF strips. Eng Struct (25), pp. 507–516.

Elzanaty, Ashraf H., A. H. Nilson, and F. O. Slate. 1986. Shear capacity of reinforced concrete beams using high-strength concrete. ACI Journal, January-February. 290-296.

Hutchinson, R., D. Donald, and S. Rizkalla. 1999. FRP for Shear Strengthening of AASHTO Bridge Girders. Proceedings of the Structural Faults and Repair '99, London, England, July, CD ROM.

Kaufman, Keith, and J. A. Ramirez. 1988. Re-evaluation of the ultimate shear behavior of high-strength concrete prestressed I-beams. ACI Structural Journal (May-June): 295-303.

Khalifa, A., W.J. Gold, A. Nanni, and A.M.I. Aziz. 1998. Contribution of externally bonded FRP to shear capacity of RC flexural members. Journal of Composites for Construction, ASCE 2(4): 195–202.

Kordina, K., J. Hegger, and M. Tuetsch. 1989. Shear strength of prestressed concrete beams with unbonded tendons. ACI Structural Journal 86, (2): 143-149.

MacGregor, James G., M. A. Sozen, and C. P. Siess. 1965. Strength of prestressed concrete beams with web reinforcement. Journal of the American Concrete Institute (December): 1503-1519.

Oh, Byung Hwan, and K. S. Kim. 2004. "Shear behavior of full-scale post-tensioned prestressed concrete bridge girders." ACI Structural Journal 101, (2). 176-182.

Saqan, Elias I., and R. J. Frosch. 2009. Influence of flexural reinforcement on shear strength of prestressed concrete beams. ACI Structural Journal 106(1): 60-68.

Utah State Department of Highways Structural Division. 1967. I-415: 45th South to I-80 4430 South Over I-415. Drawing F-156. September 19. Salt Lake City, Utah.

Wright, James K., and J. G. MacGregor. 2009. Reinfroced concrete. Fifth edition. Prentice Hall, Upper Saddle River, New Jersey

Zhang, Z., and C.T. Hsu. 2005. Shear strengthening of reinforced concrete beams using carbon-fiber-reinforced polymer laminates. Journal of Composites for Construction 9(2): 158–169.

APPENDICES

APPENDIX A

Section Properties, Bridge Plans, and CFRP Properties and Application

Table A.1 Girder section properties

Beam	Area (In^2)	e (in)	Y (in)	I (in^4)	Distance to Crack (in)	Length of Beam (in)
1	433.5	8.405	19.41	79821	132.5	268.5
2	429	8.144	19.14	77629	121.5	268.5
3	441	8.837	19.84	83539	124	268.5
4	400	6.352	17.35	63725	120.5	268.5
5	429	8.144	19.14	77629	124	268.5
6	429	8.144	19.14	77629	121	268.5

Table A.2 Calculation of effective prestress force

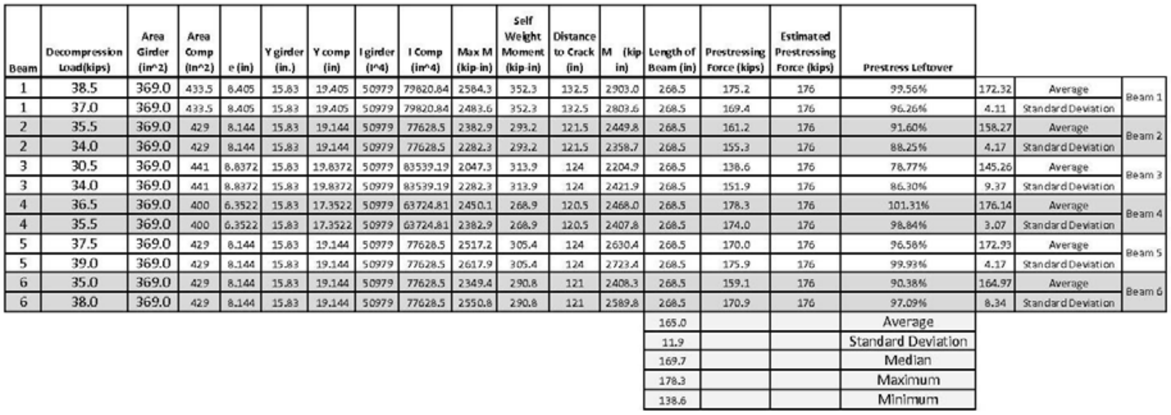

Beam	Decompression Load(kips)	Area Girder (in^2)	Area Comp (In^2)	e (in)	Y girder (in.)	Y comp (in)	I girder (I^4)	I Comp (in^4)	Max M (kip-in)	Self Weight Moment (kip-in)	Distance to Crack (in)	M (kip-in)	Length of Beam (in)	Prestressing Force (kips)	Estimated Prestressing Force (kips)	Prestress Leftover			
1	38.5	369.0	433.5	8.405	15.83	19.405	50979	79820.84	2584.3	352.3	132.5	2903.0	268.5	175.2	176	99.56%	172.32	Average	Beam 1
1	37.0	369.0	433.5	8.405	15.83	19.405	50979	79820.84	2483.6	352.3	132.5	2803.6	268.5	169.4	176	96.26%	4.11	Standard Deviation	
2	35.5	369.0	429	8.144	15.83	19.144	50979	77628.5	2382.9	293.2	121.5	2449.8	268.5	161.2	176	91.60%	158.27	Average	Beam 2
2	34.0	369.0	429	8.144	15.83	19.144	50979	77628.5	2282.3	293.2	121.5	2358.7	268.5	155.3	176	88.25%	4.17	Standard Deviation	
3	30.5	369.0	441	8.8372	15.83	19.8372	50979	83539.19	2047.3	313.9	124	2204.9	268.5	138.6	176	78.77%	145.26	Average	Beam 3
3	34.0	369.0	441	8.8372	15.83	19.8372	50979	83539.19	2282.3	313.9	124	2421.9	268.5	151.9	176	86.30%	9.37	Standard Deviation	
4	36.5	369.0	400	6.3522	15.83	17.3522	50979	63724.81	2450.1	268.9	120.5	2468.0	268.5	178.3	176	101.31%	176.14	Average	Beam 4
4	35.5	369.0	400	6.3522	15.83	17.3522	50979	63724.81	2382.9	268.9	120.5	2407.8	268.5	174.0	176	98.84%	3.07	Standard Deviation	
5	37.5	369.0	429	8.144	15.83	19.144	50979	77628.5	2517.2	305.4	124	2630.4	268.5	170.0	176	96.58%	172.93	Average	Beam 5
5	39.0	369.0	429	8.144	15.83	19.144	50979	77628.5	2617.9	305.4	124	2723.4	268.5	175.9	176	99.93%	4.17	Standard Deviation	
6	35.0	369.0	429	8.144	15.83	19.144	50979	77628.5	2349.4	290.8	121	2408.3	268.5	159.1	176	90.38%	164.97	Average	Beam 6
6	38.0	369.0	429	8.144	15.83	19.144	50979	77628.5	2550.8	290.8	121	2589.8	268.5	170.9	176	97.09%	8.34	Standard Deviation	
													165.0			Average			
													11.9			Standard Deviation			
													169.7			Median			
													178.3			Maximum			
													138.6			Minimum			

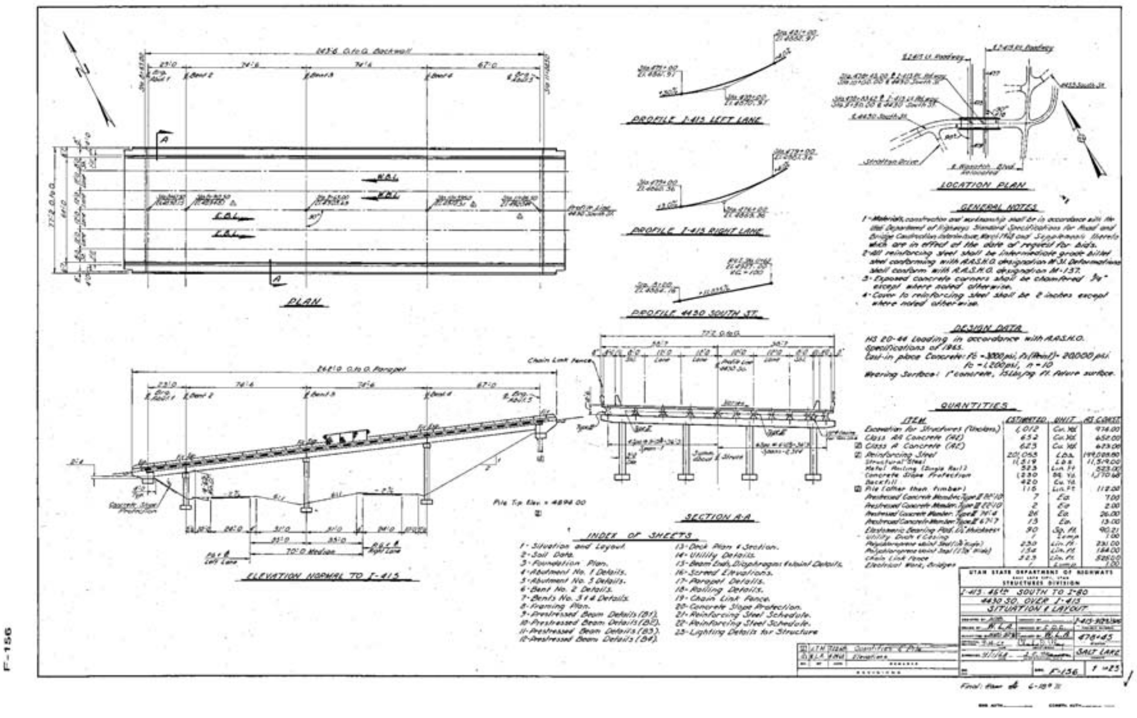
PLAN
PROFILE I-415 LEFT LANE
PROFILE I-415 RIGHT LANE
PROFILE 4430 SOUTH ST.
LOCATION PLAN
GENERAL NOTES
DESIGN DATA
QUANTITIES
SECTION A-A
ELEVATION NORMAL TO I-415
INDEX OF SHEETS
UTAH STATE DEPARTMENT OF HIGHWAYS
STRUCTURES DIVISION
I-415 45th SOUTH TO I-80
4430 SO. OVER I-415
SITUATION & LAYOUT
478+45
SALT LAKE
F-156
1 of 23
F-156

Figure A.1 Bridge plans page 1 of 23.

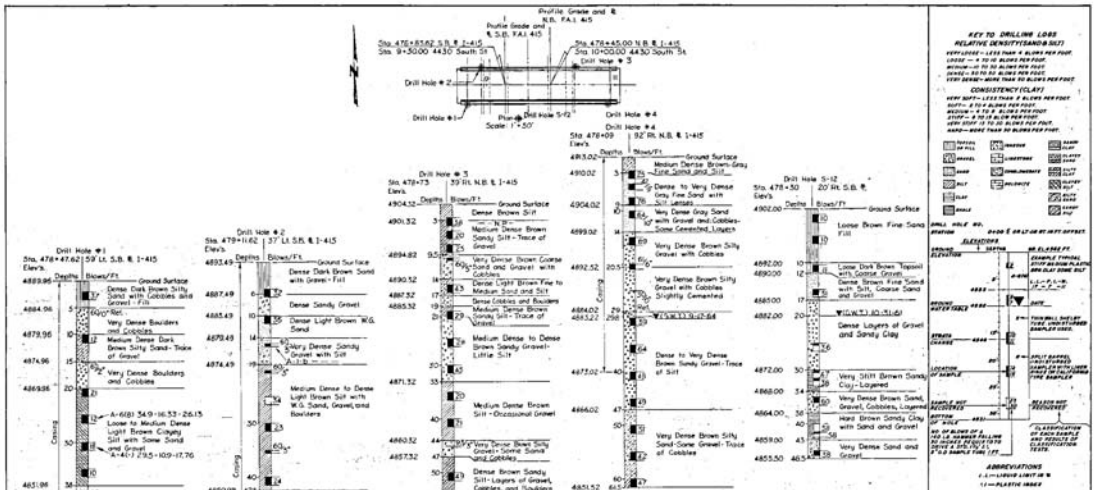
Drill Hole #1
Drill Hole #2
Drill Hole #3
Drill Hole #4
Drill Hole S-12
KEY TO DRILLING LOGS
RELATIVE DENSITY (SAND & SILT)
CONSISTENCY (CLAY)
ABBREVIATIONS
Note: Drill Hole # S-12 performed by Meissner Engineers, Inc. October 30 and October 31, 1961
Profile Scale: 1" = 6'
UTAH STATE DEPARTMENT OF HIGHWAYS
MATERIALS AND RESEARCH DIVISION
I-415 45th SOUTH TO I-80
4430 SO. STREET OVER FAI 415
DRILLING LOGS
SALT LAKE
F-156
2 of 23

Figure A.2 Bridge plans page 2 of 23.

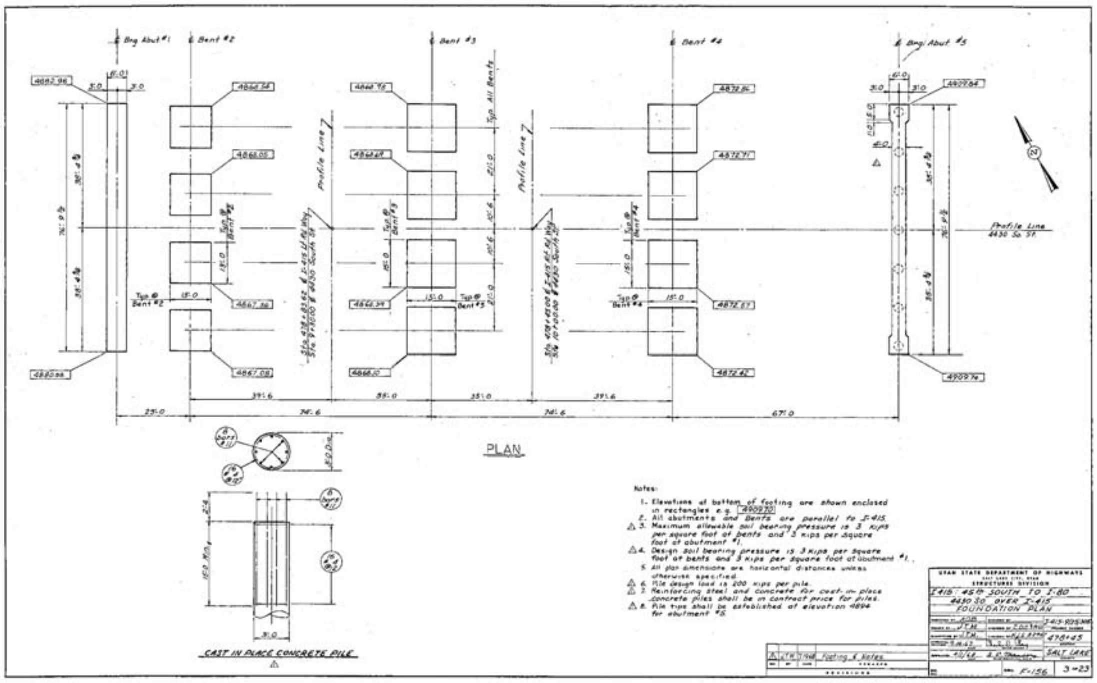
PLAN
CAST IN PLACE CONCRETE PILE
Profile Line 4430 So. St.
UTAH STATE DEPARTMENT OF HIGHWAYS
STRUCTURES DIVISION
I-415: 45th SOUTH TO I-80
4430 SO. OVER I-415
FOUNDATION PLAN
SALT LAKE
F-156
3 of 23

Figure A.3 Bridge plans page 3 of 23.

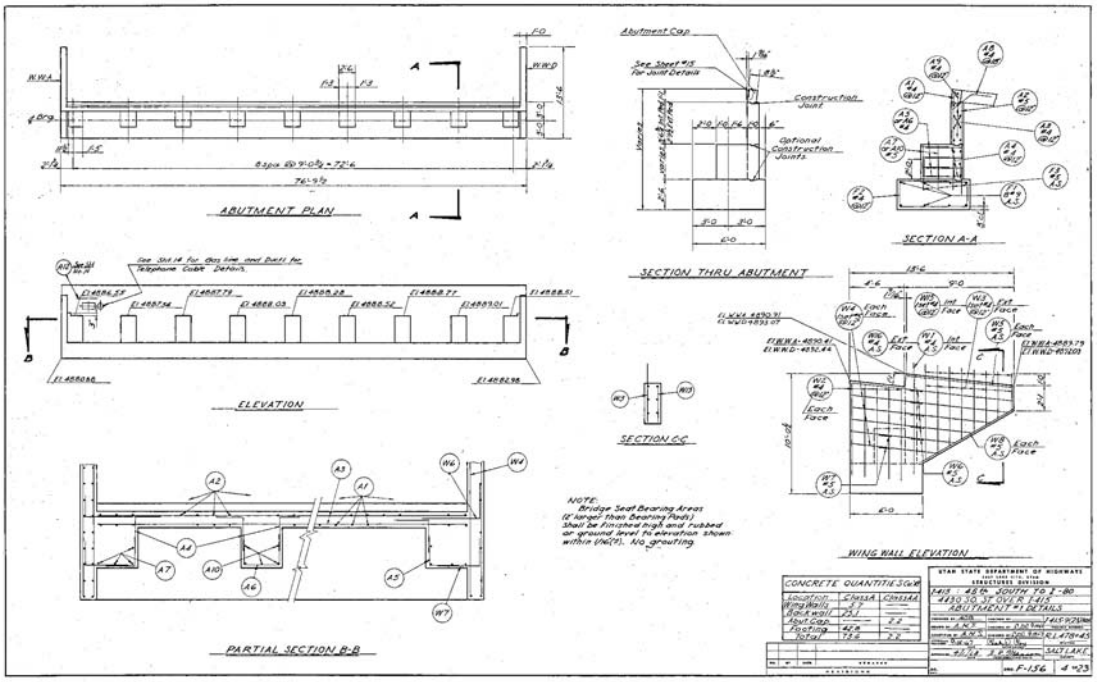
ABUTMENT PLAN
SECTION THRU ABUTMENT
SECTION A-A
ELEVATION
SECTION C-C
PARTIAL SECTION B-B
WING WALL ELEVATION
CONCRETE QUANTITIES
UTAH STATE DEPARTMENT OF HIGHWAYS
STRUCTURES DIVISION
I-415: 45th SOUTH TO I-80
4430 SO. ST. OVER I-415
ABUTMENT #1 DETAILS
SALT LAKE
F-156
4 of 23

Figure A.4 Bridge plans page 4 of 23.

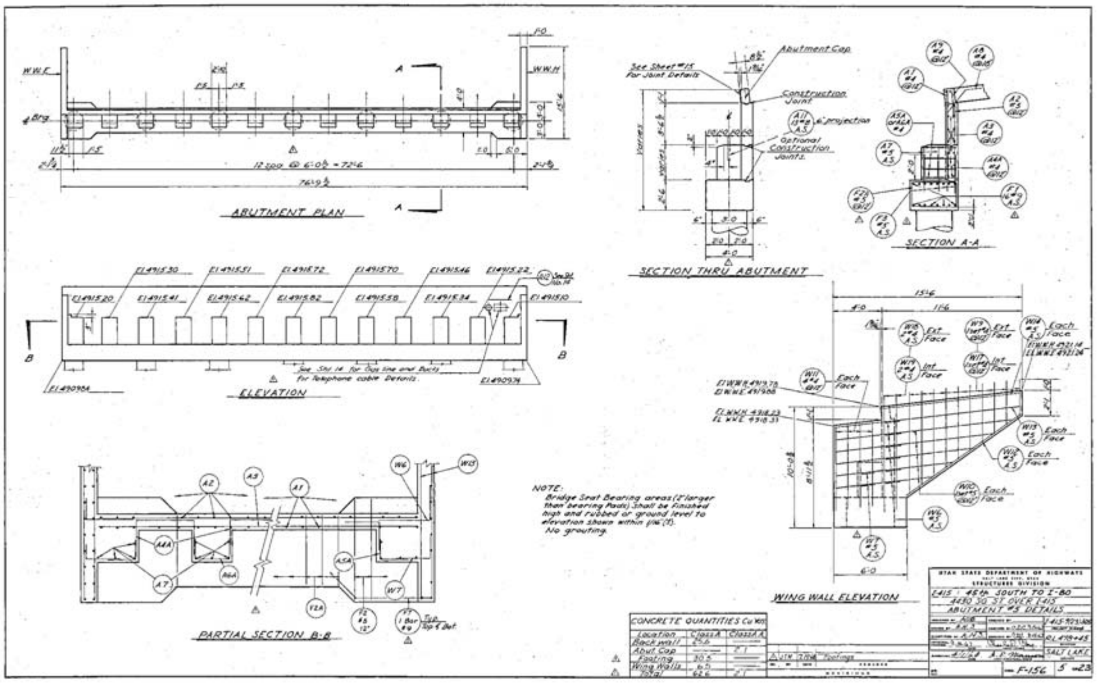
ABUTMENT PLAN
12 spa @ 6'-0½" = 72'-6
76'-9½
ELEVATION
See Sht 14 for Gas line and Ducts for Telephone cable Details
PARTIAL SECTION B-B
SECTION THRU ABUTMENT
Abutment Cap
Construction Joint
Optional Construction Joints
SECTION A-A
WING WALL ELEVATION
NOTE:
Bridge Seat Bearing areas (2" larger than bearing Pads) Shall be Finished high and rubbed or ground level to elevation shown within 1/16"(±).
No grouting.
CONCRETE QUANTITIES Cu Yds
Location | Class A | Class A
Back wall | 25.6
Abut Cap | | 2.1
Footing | 30.5
Wing Walls | 6.5
Total | 62.6 | 2.1
UTAH STATE DEPARTMENT OF HIGHWAYS
SALT LAKE CITY, UTAH
STRUCTURES DIVISION
I-415 : 45th SOUTH TO I-80
4430 SO ST OVER I-415
ABUTMENT #5 DETAILS
SALT LAKE
F-156
5 of 23

Figure A.5 Bridge plans page 5 of 23.

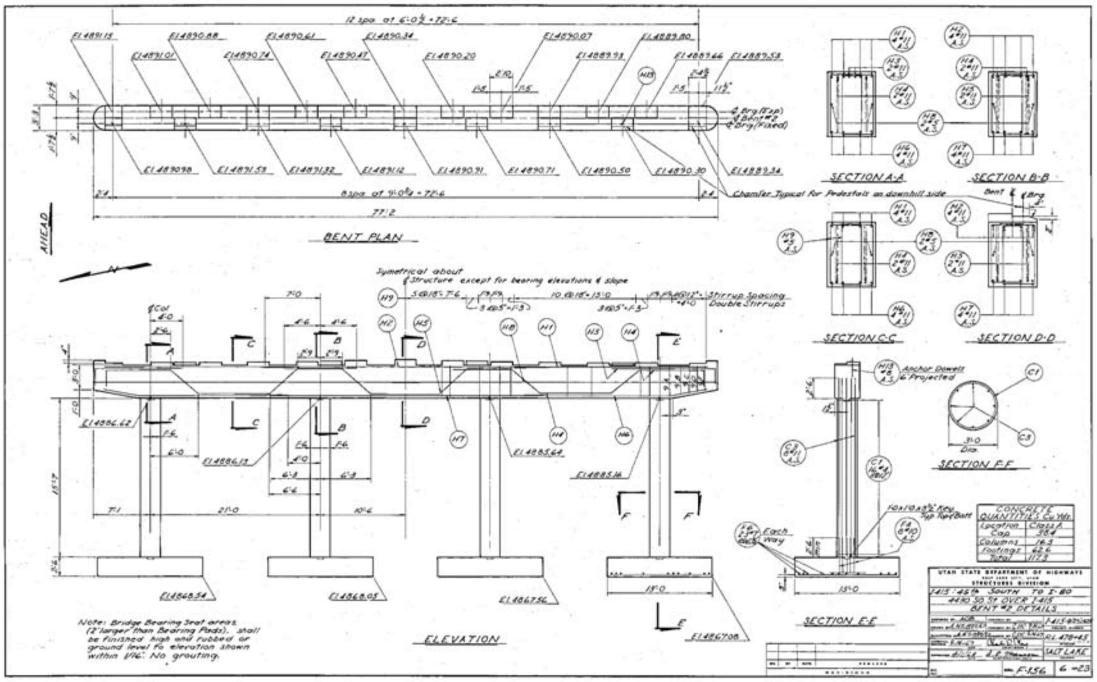
12 spa at 6'-0½" = 72'-6
8 spa at 9'-0¾" = 72'-6
77'-2
BENT PLAN
AHEAD
Chamfer Typical for Pedestals on downhill side
Symmetrical about ℄ Structure except for bearing elevations & slope
Stirrup Spacing Double Stirrups
ELEVATION
Note: Bridge Bearing Seat areas (2" larger than Bearing Pads) shall be Finished high and rubbed or ground level to elevation shown within 1/16". No grouting.
SECTION A-A
SECTION B-B
SECTION C-C
SECTION D-D
SECTION E-E
SECTION F-F
Anchor Dowels 6" Projected
10x10x3½" Key Typ Top & Bott
Each Way
15'-0
3'-0 Dia.
CONCRETE QUANTITIES Cu Yds
Location | Class A
Cap | 38.4
Columns | 16.3
Footings | 62.6
Total | 117.3
UTAH STATE DEPARTMENT OF HIGHWAYS
SALT LAKE CITY, UTAH
STRUCTURES DIVISION
I-415 : 45th SOUTH TO I-80
4430 SO ST OVER I-415
BENT #2 DETAILS
SALT LAKE
F-156
6 of 23

Figure A.6 Bridge plans page 6 of 23.

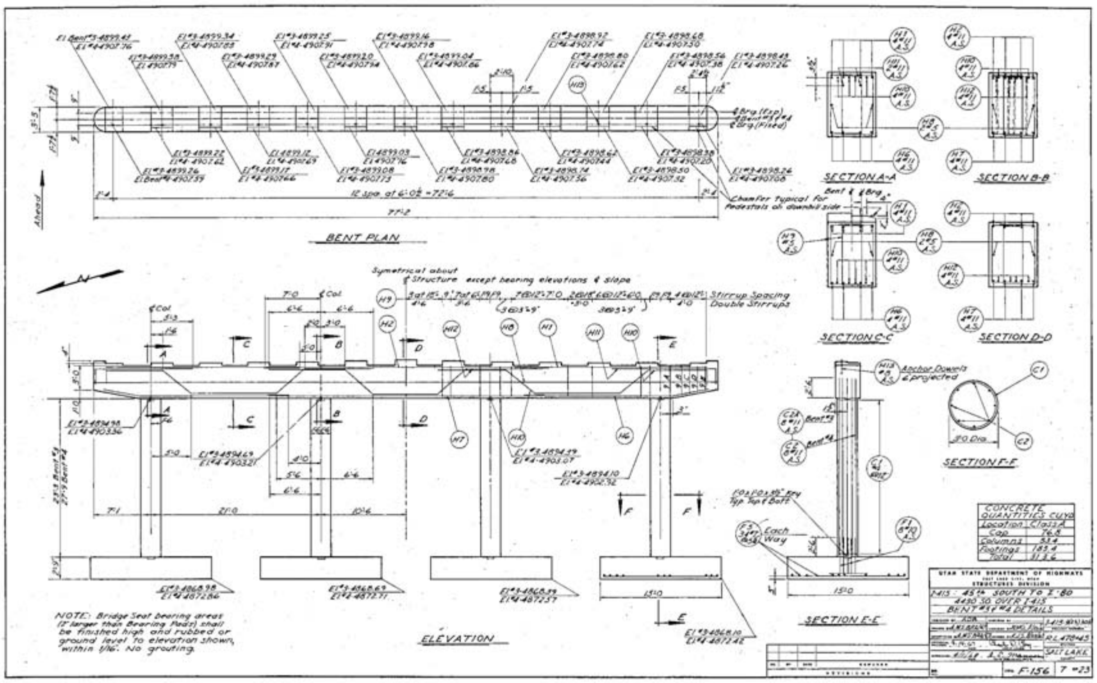
BENT PLAN
ELEVATION
SECTION A-A
SECTION B-B
SECTION C-C
SECTION D-D
SECTION E-E
SECTION F-F
Ahead
12 spa. at 6'-0½ = 72'-6
77'-2
Symetrical about ℄ Structure except bearing elevations & slope
Stirrup Spacing Double Stirrups
Anchor Dowels ℄ projected
3'-0 Dia.
NOTE: Bridge Seat bearing areas (2" larger than Bearing Pads) shall be finished high and rubbed or ground level to elevation shown, within 1/16". No grouting.
CONCRETE QUANTITIES CU.YD.
Location | Class A
Cap | 76.8
Columns | 51.4
Footings | 183.4
Total | 311.6
UTAH STATE DEPARTMENT OF HIGHWAYS
SALT LAKE CITY, UTAH
STRUCTURES DIVISION
I-415: 45th SOUTH TO I-80
4430 SO. OVER I-415
BENT #3 & #4 DETAILS
RL 470+45
SALT LAKE
F-156
7 of 23

Figure A.7 Bridge plans page 7 of 23.

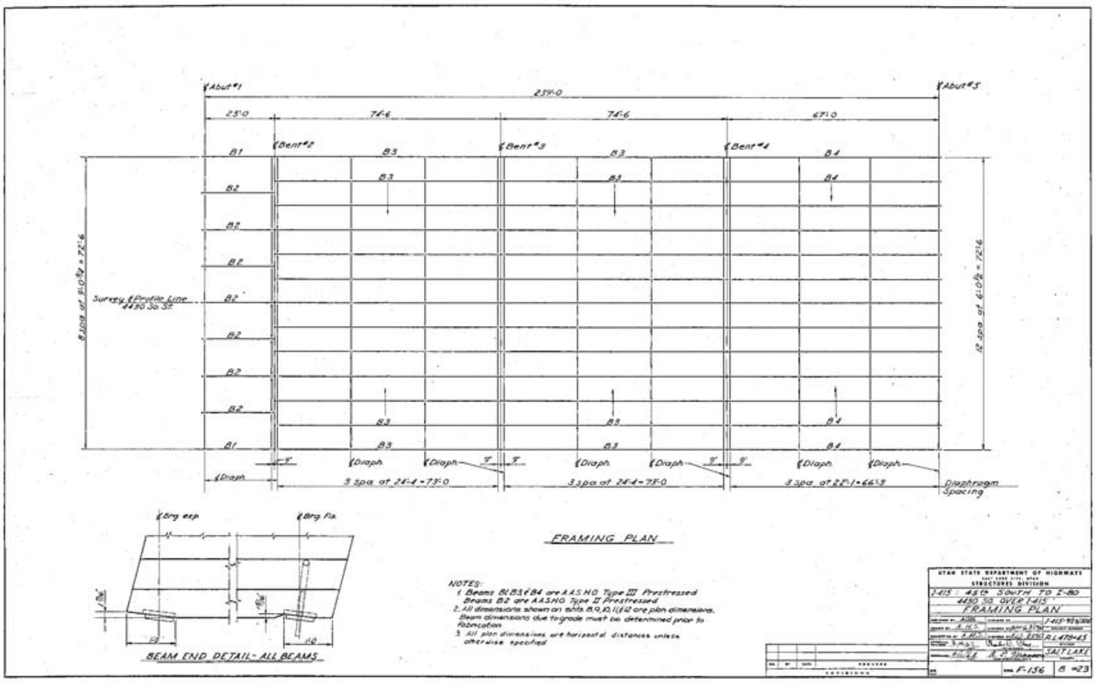
℄ Abut #1
℄ Abut #5
239'-0
25'-0
74'-6
74'-6
67'-0
℄ Bent #2
℄ Bent #3
℄ Bent #4
B1
B2
B3
B4
8 spa. at 9'-0½ = 72'-6
12 spa. at 6'-0½ = 72'-6
Survey ℄ Profile Line 4430 So. St.
℄ Diaph.
3 spa. at 24'-4 = 73'-0
3 spa. at 24'-4 = 73'-0
3 spa. at 22'-1 = 66'-3
Diaphragm Spacing
℄ Brg. exp.
℄ Brg. fix.
BEAM END DETAIL - ALL BEAMS
FRAMING PLAN
NOTES:
1. Beams B1, B3 & B4 are A.A.S.H.O. Type III Prestressed. Beams B2 are A.A.S.H.O. Type II Prestressed.
2. All dimensions shown on shts. 8, 9, 10, 11 & 12 are plan dimensions. Beam dimensions due to grade must be determined prior to fabrication.
3. All plan dimensions are horizontal distances unless otherwise specified.
UTAH STATE DEPARTMENT OF HIGHWAYS
SALT LAKE CITY, UTAH
STRUCTURES DIVISION
I-415: 45th SOUTH TO I-80
4430 SO. OVER I-415
FRAMING PLAN
RL 470+45
SALT LAKE
F-156
8 of 23

Figure A.8 Bridge plans page 8 of 23.

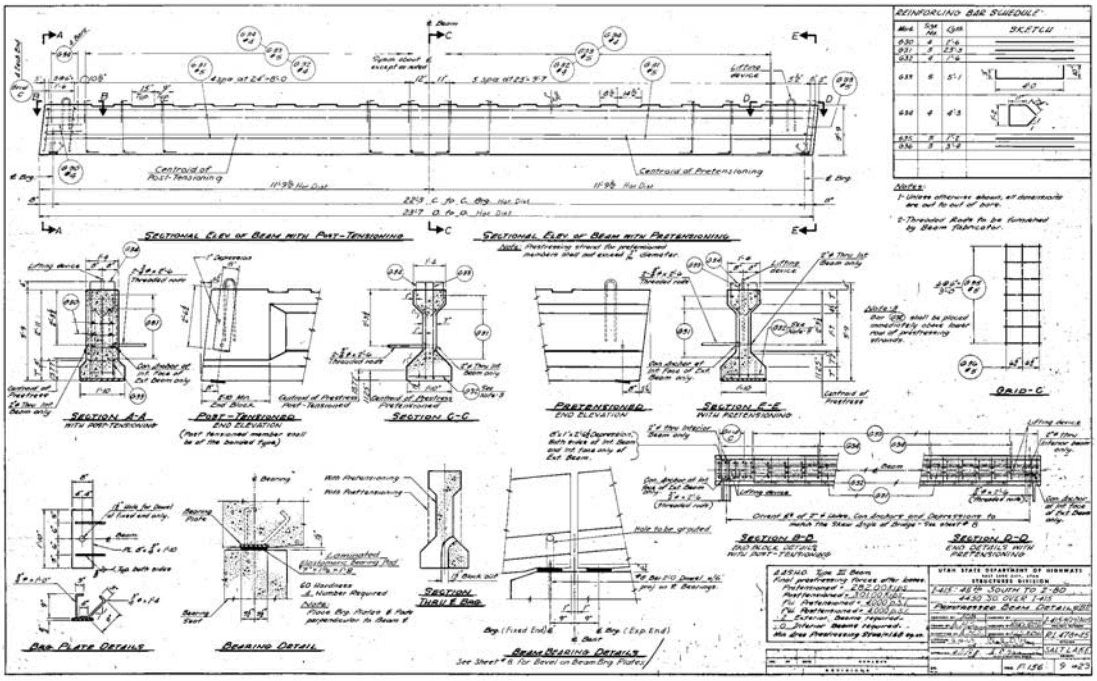
REINFORCING BAR SCHEDULE
SECTIONAL ELEV OF BEAM WITH POST-TENSIONING
SECTIONAL ELEV OF BEAM WITH PRETENSIONING
SECTION A-A
POST-TENSIONED
SECTION C-C
PRETENSIONED
SECTION E-E
GRID-C
SECTION B-B
SECTION D-D
BRG. PLATE DETAILS
BEARING DETAIL
SECTION THRU ℄ BRG.
BEAM BEARING DETAILS
UTAH STATE DEPARTMENT OF HIGHWAYS
STRUCTURES DIVISION
PRESTRESSED BEAM DETAILS
SALT LAKE
F-156
9 of 23

Figure A.9 Bridge plans page 9 of 23.

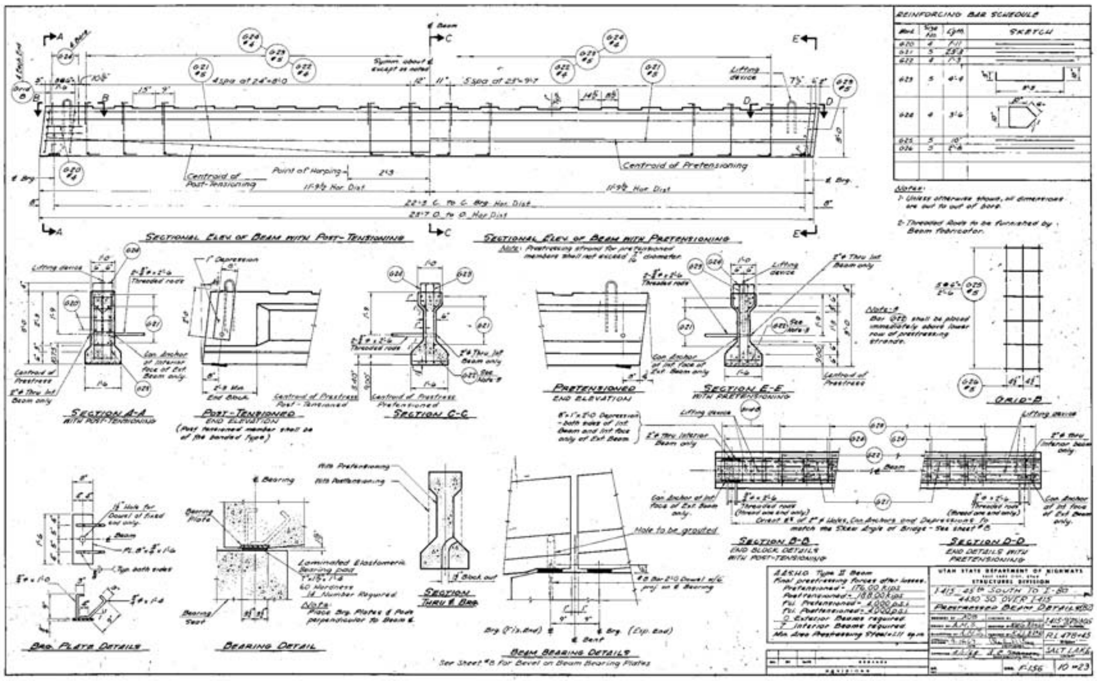
REINFORCING BAR SCHEDULE
SECTIONAL ELEV OF BEAM WITH POST-TENSIONING
SECTIONAL ELEV OF BEAM WITH PRETENSIONING
SECTION A-A
POST-TENSIONED
SECTION C-C
PRETENSIONED
SECTION E-E
GRID-B
SECTION B-B
SECTION D-D
BRG. PLATE DETAILS
BEARING DETAIL
SECTION THRU ℄ BRG.
BEAM BEARING DETAILS
UTAH STATE DEPARTMENT OF HIGHWAYS
STRUCTURES DIVISION
PRESTRESSED BEAM DETAILS
SALT LAKE
F-156
10 of 23

Figure A.10 Bridge plans page 10 of 23.

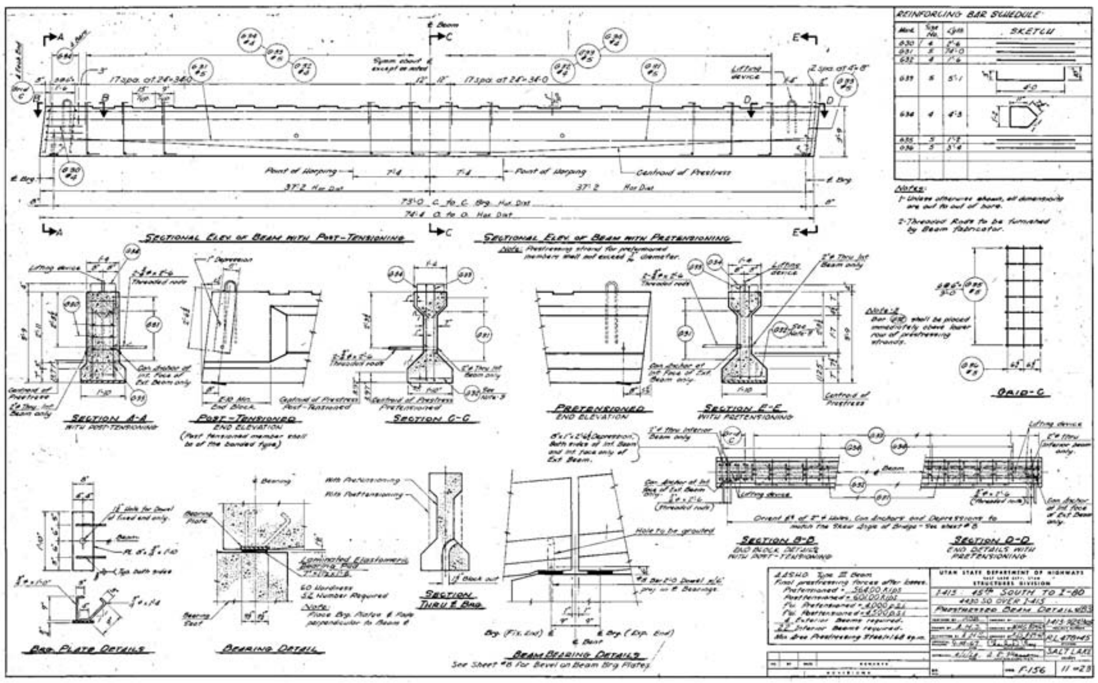
REINFORCING BAR SCHEDULE
SKETCH
SECTIONAL ELEV OF BEAM WITH POST-TENSIONING
SECTIONAL ELEV OF BEAM WITH PRETENSIONING
Point of Harping
Centroid of Prestress
73'-0 C to C Brg. Hor Dist
74'-4 O to O Hor Dist
SECTION A-A
WITH POST-TENSIONING
POST-TENSIONED
END ELEVATION
SECTION C-C
PRETENSIONED
END ELEVATION
SECTION E-E
WITH PRETENSIONING
GRID-C
SECTION B-B
END BLOCK DETAILS WITH POST-TENSIONING
SECTION D-D
END DETAILS WITH PRETENSIONING
BRG. PLATE DETAILS
BEARING DETAIL
SECTION THRU ℄ BRG.
BEAM BEARING DETAILS
See Sheet #8 For Bevel on Beam Brg Plates
UTAH STATE DEPARTMENT OF HIGHWAYS
STRUCTURES DIVISION
I-415 : 45th SOUTH TO I-80
4430 SO OVER I-415
PRESTRESSED BEAM DETAILS
SALT LAKE
F-156
11 of 23

Figure A.11 Bridge plans page 11 of 23.

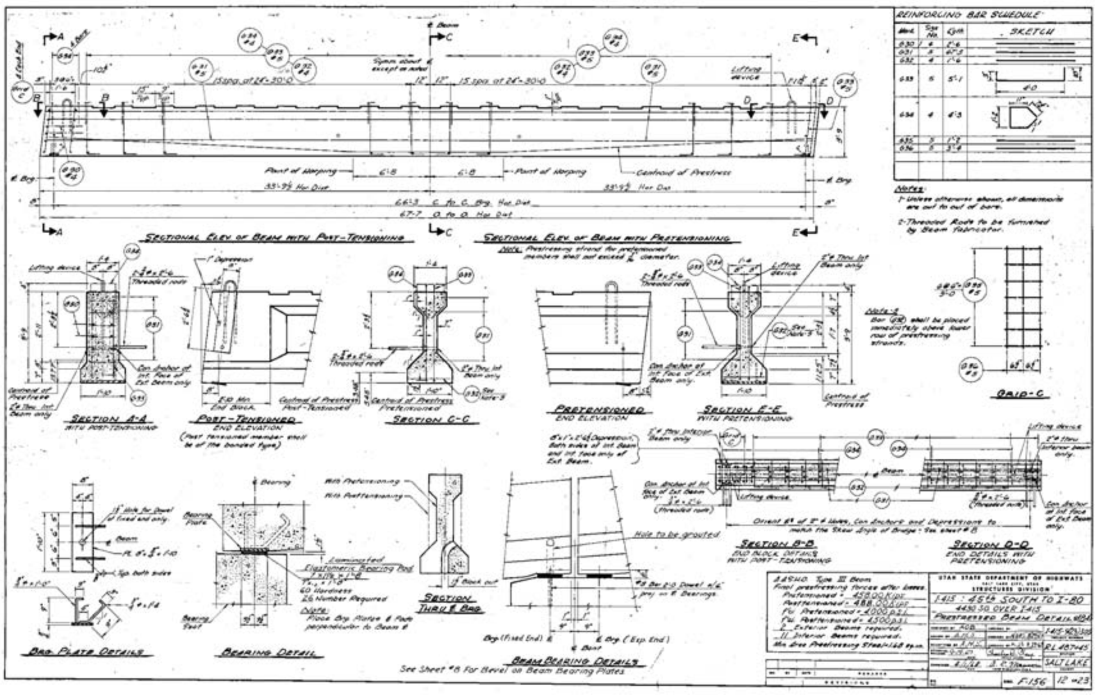
REINFORCING BAR SCHEDULE
SKETCH
SECTIONAL ELEV OF BEAM WITH POST-TENSIONING
SECTIONAL ELEV OF BEAM WITH PRETENSIONING
Point of Harping
Centroid of Prestress
66'-3 C to C Brg. Hor Dist
67'-7 O to O Hor Dist
SECTION A-A
WITH POST-TENSIONING
POST-TENSIONED
END ELEVATION
SECTION C-C
PRETENSIONED
END ELEVATION
SECTION E-E
WITH PRETENSIONING
GRID-C
SECTION B-B
END BLOCK DETAILS WITH POST-TENSIONING
SECTION D-D
END DETAILS WITH PRETENSIONING
BRG. PLATE DETAILS
BEARING DETAIL
SECTION THRU ℄ BRG.
BEAM BEARING DETAILS
See Sheet #8 For Bevel on Beam Bearing Plates
UTAH STATE DEPARTMENT OF HIGHWAYS
STRUCTURES DIVISION
I-415 : 45th SOUTH TO I-80
4430 SO OVER I-415
PRESTRESSED BEAM DETAILS
SALT LAKE
F-156
12 of 23

Figure A.12 Bridge plans page 12 of 23.

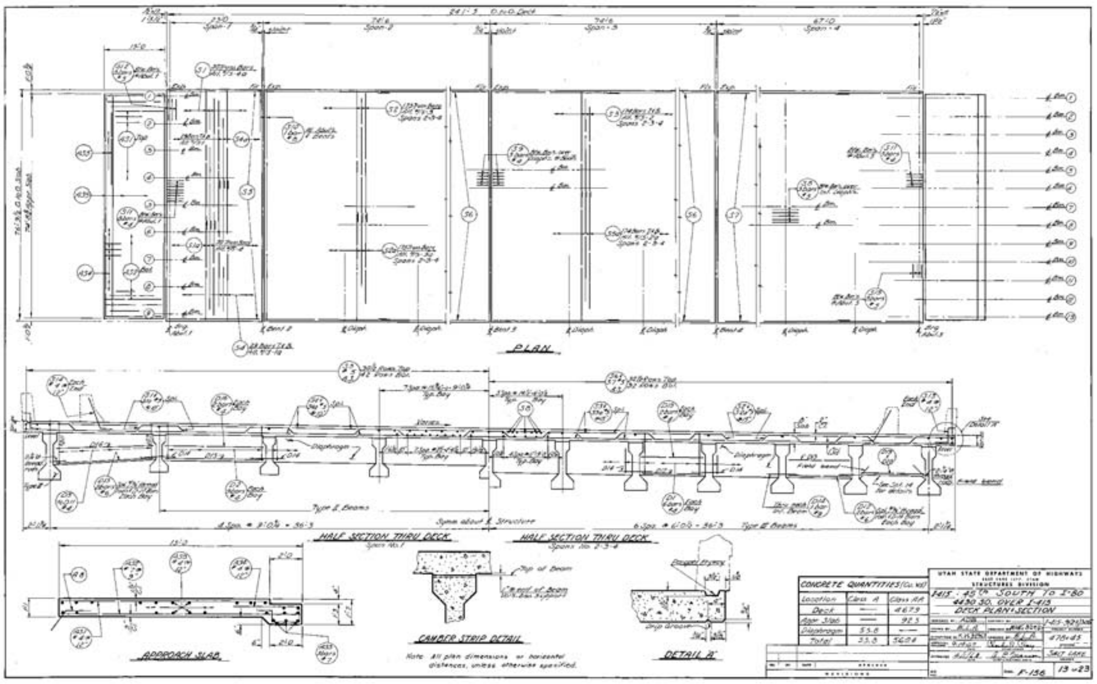
PLAN
HALF SECTION THRU DECK
HALF SECTION THRU DECK
APPROACH SLAB
CAMBER STRIP DETAIL
DETAIL A
CONCRETE QUANTITIES
UTAH STATE DEPARTMENT OF HIGHWAYS
STRUCTURES DIVISION
I-415 - 45th SOUTH TO I-80
4430 SO. OVER I-415
DECK PLAN & SECTION
F-156
13 of 23

Figure A.13 Bridge plans page 13 of 23.

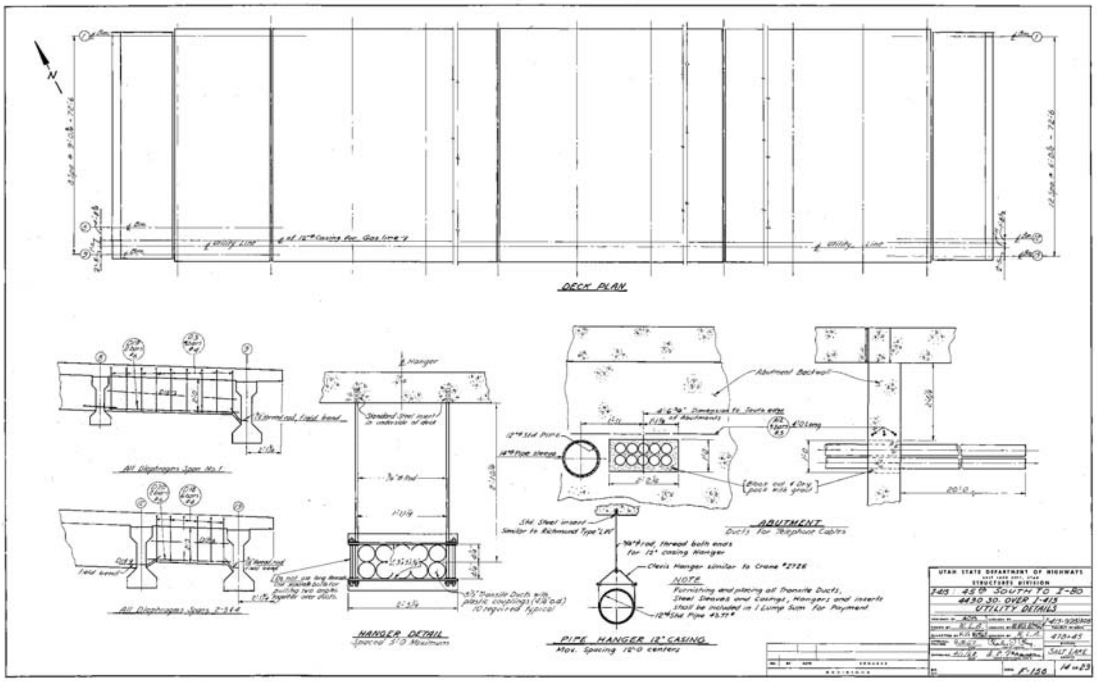
DECK PLAN
All Diaphragms Span No. 1
All Diaphragms Spans 2-3 & 4
HANGER DETAIL
PIPE HANGER 12" CASING
ABUTMENT
Ducts for Telephone Cables
UTAH STATE DEPARTMENT OF HIGHWAYS
STRUCTURES DIVISION
I-415 - 45th SOUTH TO I-80
4430 SO. OVER I-415
UTILITY DETAILS
F-156
14 of 23

Figure A.14 Bridge plans page 14 of 23.

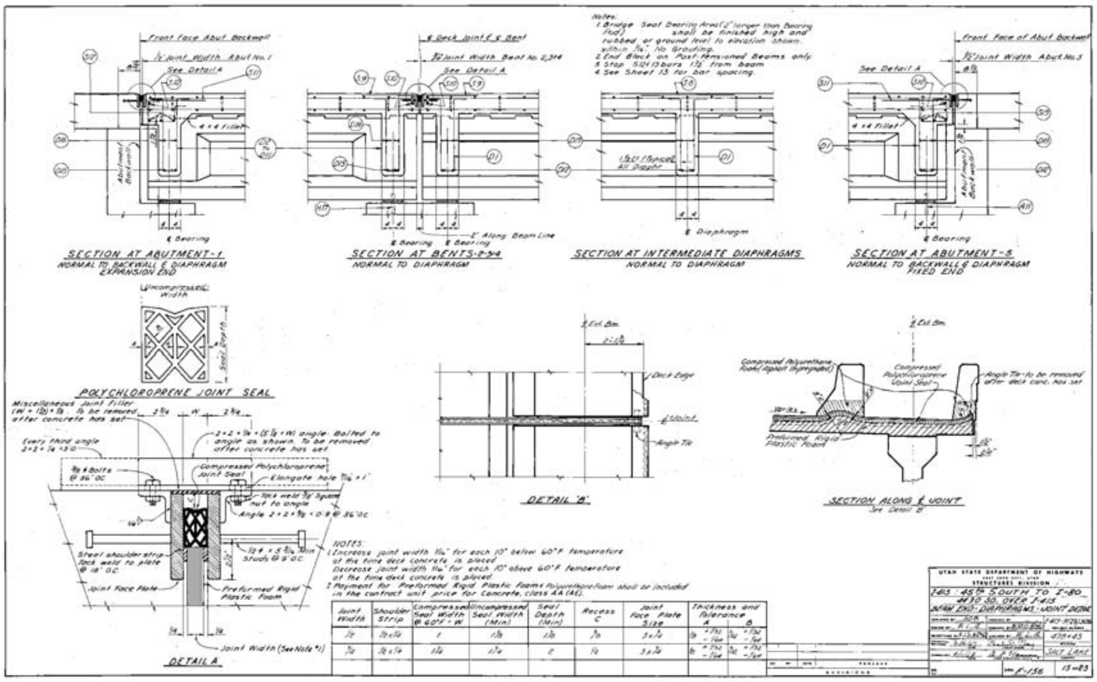
SECTION AT ABUTMENT-1
NORMAL TO BACKWALL & DIAPHRAGM
EXPANSION END
SECTION AT BENTS-2-3-4
NORMAL TO DIAPHRAGM
SECTION AT INTERMEDIATE DIAPHRAGMS
NORMAL TO DIAPHRAGM
SECTION AT ABUTMENT-5
NORMAL TO BACKWALL & DIAPHRAGM
FIXED END
POLYCHLOROPRENE JOINT SEAL
DETAIL A
DETAIL 'B'
SECTION ALONG ℄ JOINT
UTAH STATE DEPARTMENT OF HIGHWAYS
STRUCTURES DIVISION
I-415 45th SOUTH TO I-80
4430 SO. OVER I-415
SALT LAKE
F-156
15-23

Figure A.15 Bridge plans page 15 of 23.

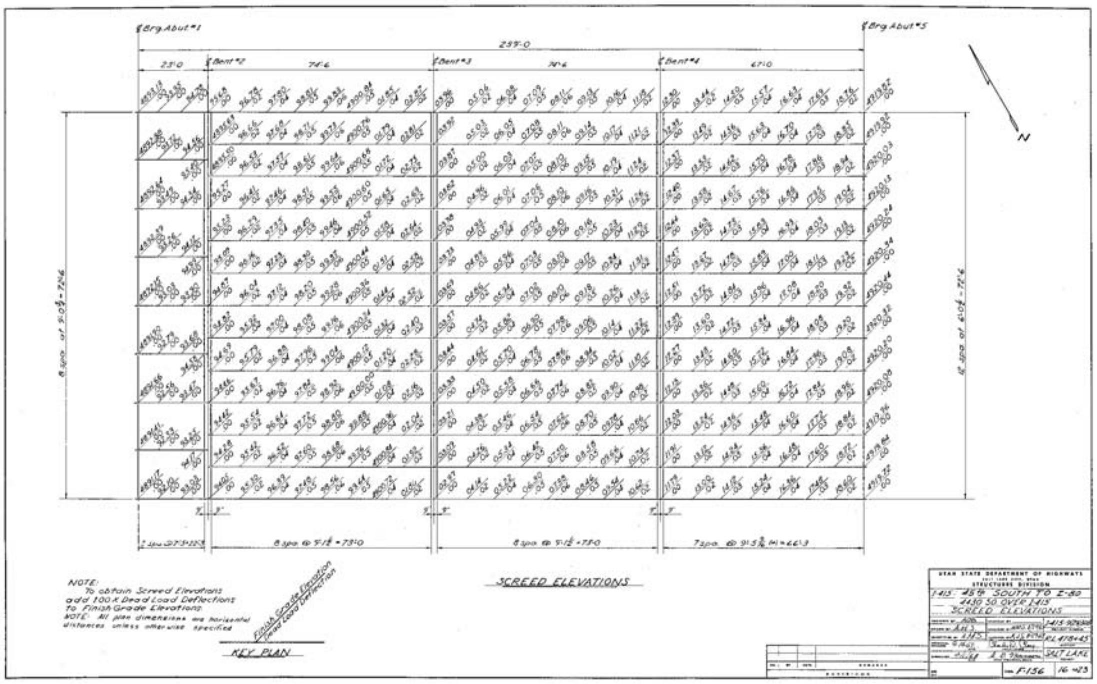
℄ Brg. Abut. #1
℄ Brg. Abut. #5
255'-0
℄ Bent #2
℄ Bent #3
℄ Bent #4
SCREED ELEVATIONS
KEY PLAN
N
UTAH STATE DEPARTMENT OF HIGHWAYS
STRUCTURES DIVISION
I-415 45th SOUTH TO I-80
4430 SO. OVER I-415
SCREED ELEVATIONS
SALT LAKE
F-156
16-23

Figure A.16 Bridge plans page 16 of 23.

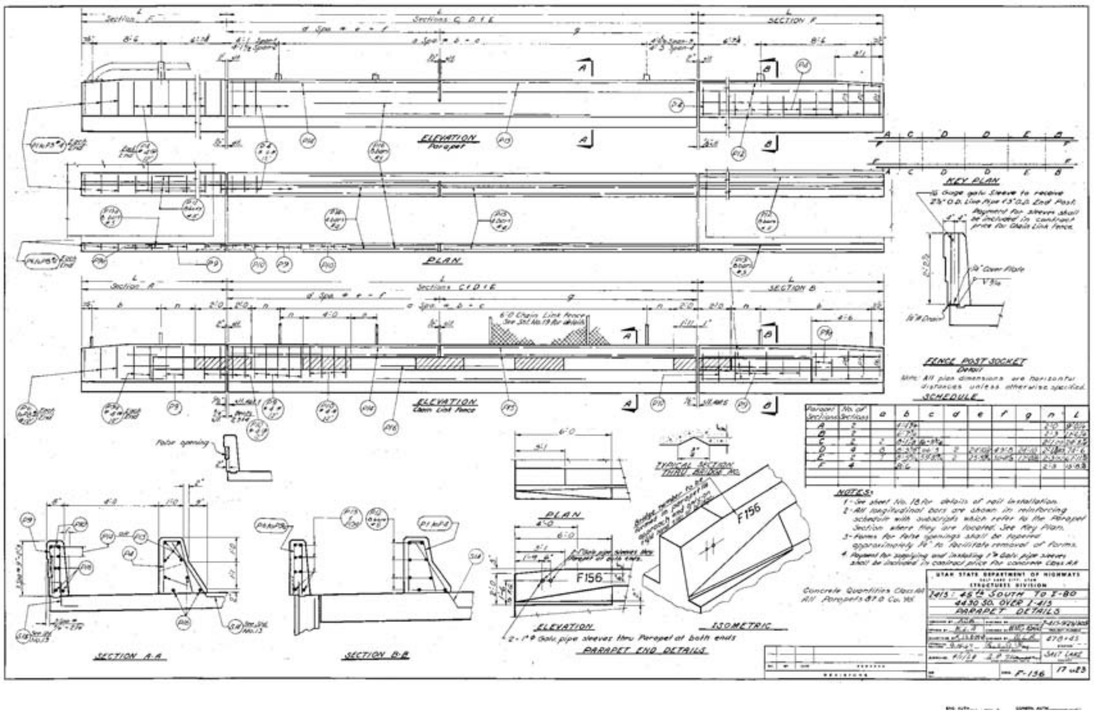
ELEVATION Parapet
PLAN
ELEVATION Chain Link Fence
KEY PLAN
FENCE POST SOCKET Detail
SCHEDULE
NOTES:
SECTION A-A
SECTION B-B
PLAN
ELEVATION
ISOMETRIC
PARAPET END DETAILS
TYPICAL SECTION
F156
UTAH STATE DEPARTMENT OF HIGHWAYS
STRUCTURES DIVISION
I-415: 45th SOUTH TO I-80
4430 SO. OVER I-415
PARAPET DETAILS
F-156
17 of 23

Figure A.17 Bridge plans page 17 of 23.

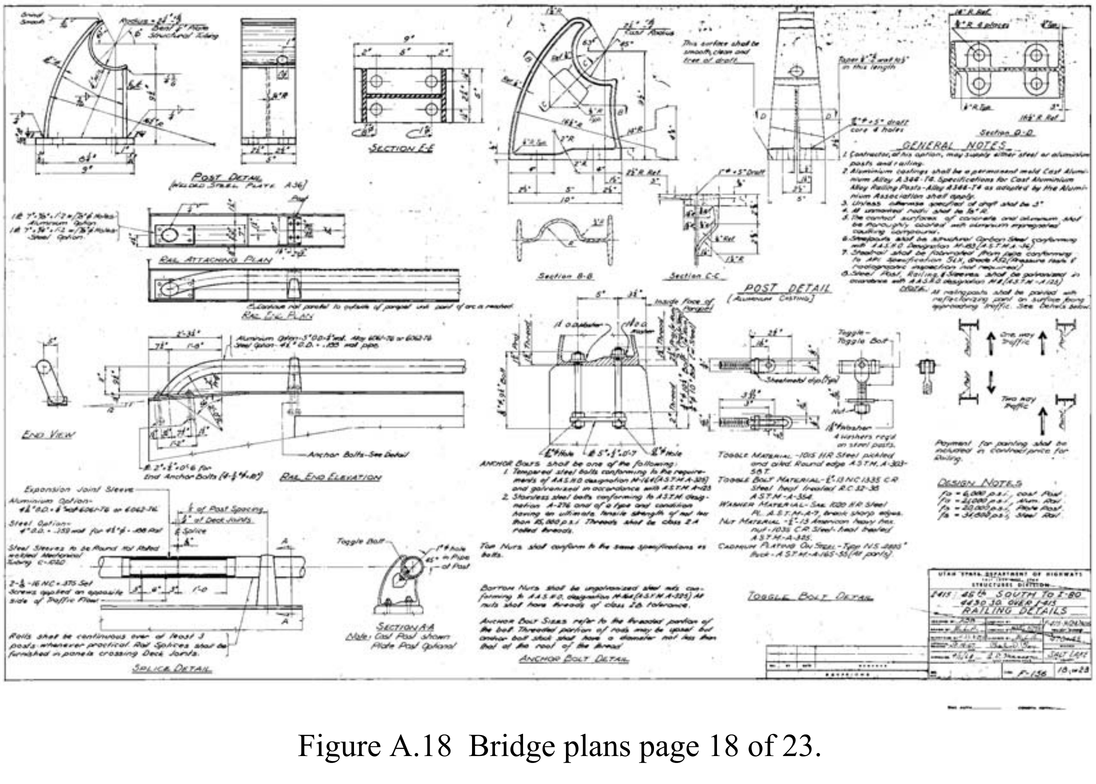
POST DETAIL
(WELDED STEEL PLATE A36)
SECTION E-E
RAIL ATTACHING PLAN
RAIL END PLAN
Section B-B
Section C-C
POST DETAIL
(Aluminum Casting)
GENERAL NOTES
Section D-D
END VIEW
RAIL END ELEVATION
SPLICE DETAIL
SECTION A-A
ANCHOR BOLT DETAIL
TOGGLE BOLT DETAIL
DESIGN NOTES
UTAH STATE DEPARTMENT OF HIGHWAYS
STRUCTURES DIVISION
I-415: 45th SOUTH TO I-80
4430 SO. OVER I-415
RAILING DETAILS
F-156
18 of 23

Figure A.18 Bridge plans page 18 of 23.

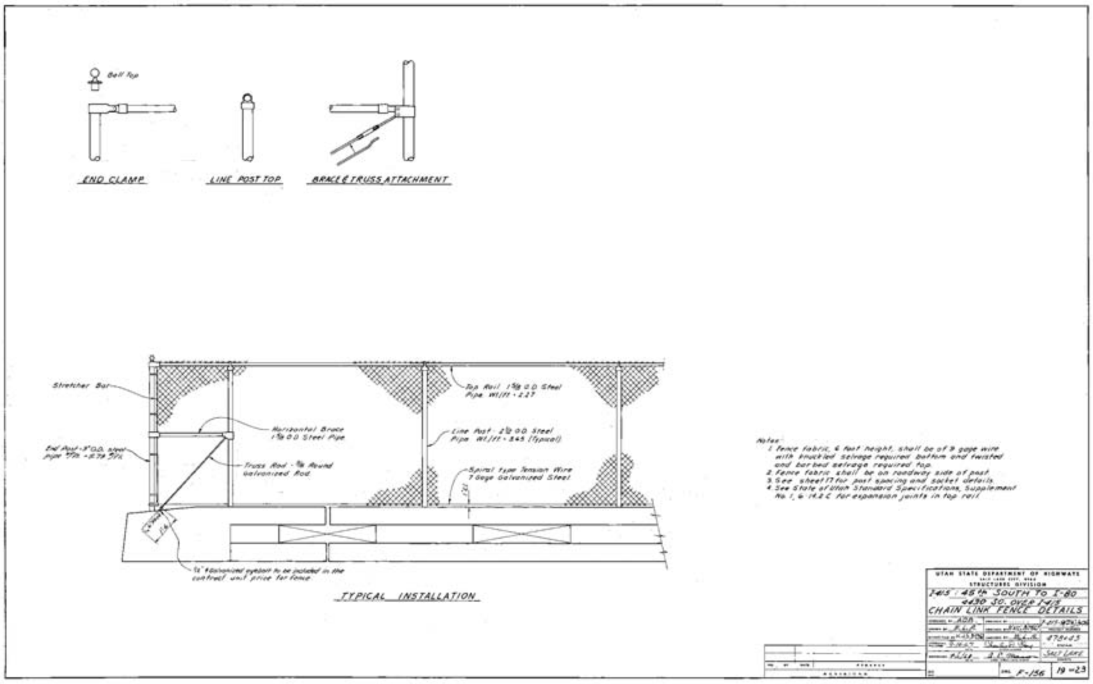

Bell Top
END CLAMP
LINE POST TOP
BRACE & TRUSS ATTACHMENT
Stretcher Bar
End Post - 3" O.D. steel pipe
Horizontal Brace 1⅝ O.D. Steel Pipe
Truss Rod - ⅜ Round Galvanized Rod
Top Rail 1⅝ O.D. Steel Pipe Wt/ft = 2.27
Line Post - 2½ O.D. Steel Pipe Wt/ft - 3.65 (Typical)
Spiral type Tension Wire 7 Gage Galvanized Steel
⅝" galvanized eyebolt to be included in the contract unit price for fence
TYPICAL INSTALLATION
Notes:
1. Fence fabric, 6 foot height, shall be of 9 gage wire with knuckled selvage required bottom and twisted and barbed selvage required top.
2. Fence fabric shall be on roadway side of post.
3. See sheet 17 for post spacing and socket details.
4. See State of Utah Standard Specifications, Supplement No. 1, 6-14.2 C for expansion joints in top rail.
UTAH STATE DEPARTMENT OF HIGHWAYS
STRUCTURES DIVISION
I-415 : 45th SOUTH TO I-80
4430 SO. OVER I-415
CHAIN LINK FENCE DETAILS
478+43
SALT LAKE
F-156
19 - 23

Figure A.19 Bridge plans page 19 of 23.

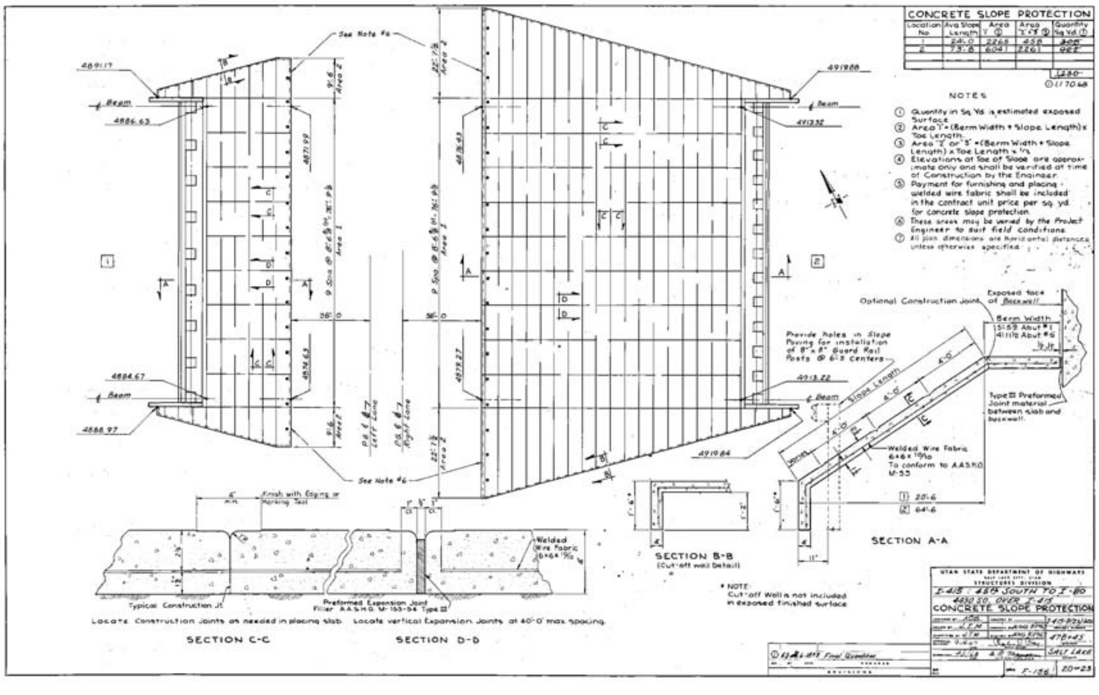

CONCRETE SLOPE PROTECTION
Location No | Avg Slope Length | Area 1 ② | Area 2 + 3 ③ | Quantity Sq Yd ①
1 | 24.0 | 2265 | 458 | ~~305~~
2 | 73-6 | 6041 | 2261 | ~~922~~
~~1230~~
① 1170.68
NOTES
① Quantity in Sq. Yds is estimated exposed Surface.
② Area 1 = (Berm Width + Slope Length) x Toe Length.
③ Area 2 or 3 = (Berm Width + Slope Length) x Toe Length x ½.
④ Elevations at Toe of Slope are approximate only and shall be verified at time of Construction by the Engineer.
⑤ Payment for furnishing and placing welded wire fabric shall be included in the contract unit price per sq. yd. for concrete slope protection.
⑥ These areas may be varied by the Project Engineer to suit field conditions.
⑦ All plan dimensions are horizontal distances unless otherwise specified.
See Note #6
Beam
4891.17
4886.63
4884.67
4886.97
4919.88
4913.22
4919.84
Area 1
Area 2
Area 3
P.G. & #7 Left Lane
P.G. & #7 Right Lane
Optional Construction Joint
Exposed face of Backwall
Berm Width
5'-5⅞ Abut #1
4'-11½ Abut #6
Provide holes in Slope Paving for installation of 8" x 8" Guard Rail Posts @ 6'-3 Centers
Slope Length
Type III Preformed Joint material between slab and backwall.
Welded Wire Fabric 6x6 x 10/10 To conform to A.A.S.H.O. M-55
SECTION A-A
SECTION B-B (Cut-off wall Detail)
* NOTE: Cut-off Wall is not included in exposed finished surface.
Finish with Edging or Marking Tool
Welded Wire Fabric 6x6 x 10/10
Typical Construction Jt.
Preformed Expansion Joint Filler A.A.S.H.O. M-153-54 Type III
Locate Construction Joints as needed in placing slab. Locate vertical Expansion Joints at 40'-0" max. spacing.
SECTION C-C
SECTION D-D
① Final Quantities
UTAH STATE DEPARTMENT OF HIGHWAYS
STRUCTURES DIVISION
I-415 : 45th SOUTH TO I-80
4430 SO. OVER I-415
CONCRETE SLOPE PROTECTION
478+43
SALT LAKE
F-156
20 - 23

Figure A.20 Bridge plans page 20 of 23.

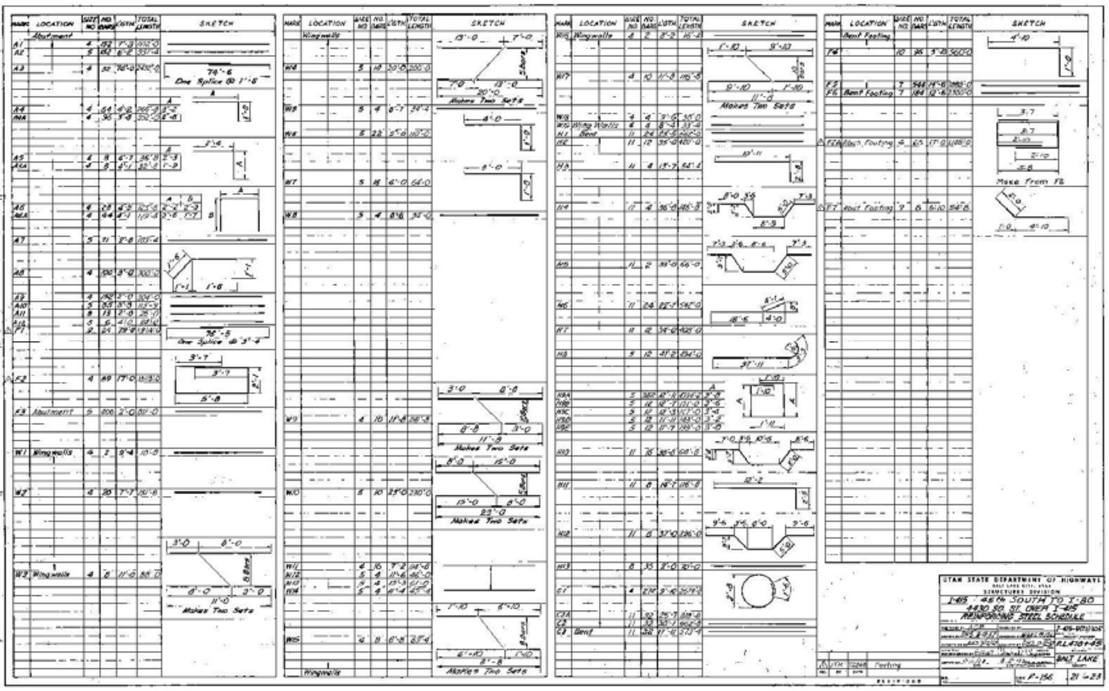
UTAH STATE DEPARTMENT OF HIGHWAYS
SALT LAKE CITY, UTAH
STRUCTURES DIVISION
I-15 45th SOUTH TO I-80
4430 SO. ST. OVER I-215
REINFORCING STEEL SCHEDULE
SALT LAKE
F-156
21 of 23

Figure A.21 Bridge plans page 21 of 23.

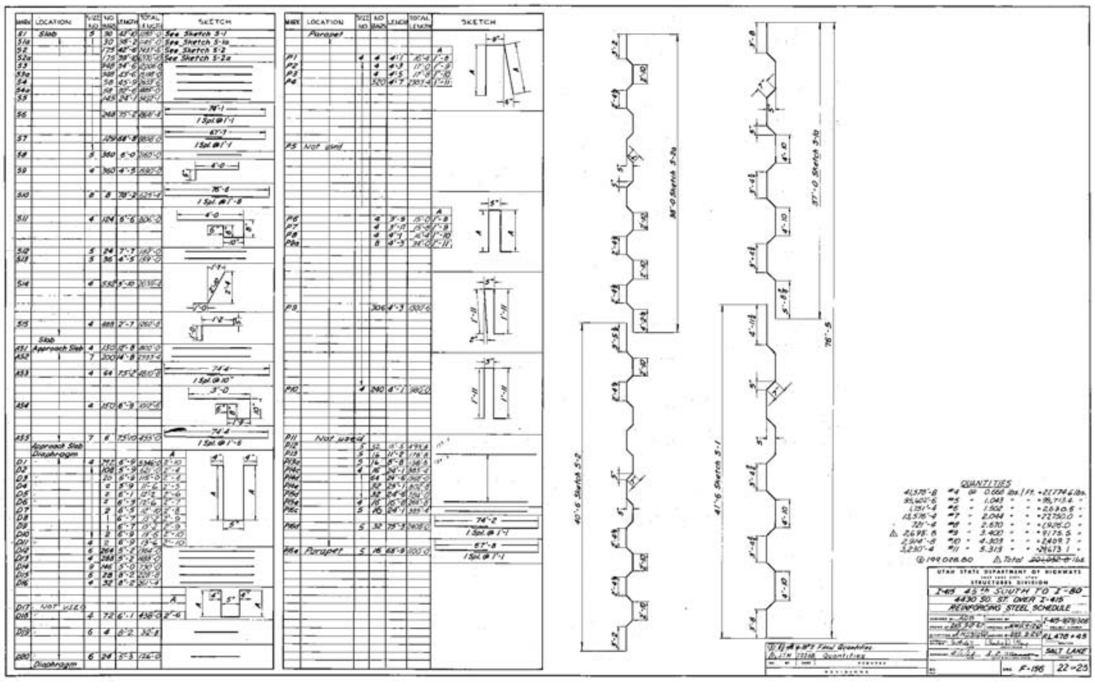
QUANTITIES
UTAH STATE DEPARTMENT OF HIGHWAYS
STRUCTURES DIVISION
I-15 45th SOUTH TO I-80
4430 SO. ST. OVER I-215
REINFORCING STEEL SCHEDULE
SALT LAKE
F-156
22 of 23

Figure A.22 Bridge plans page 22 of 23.

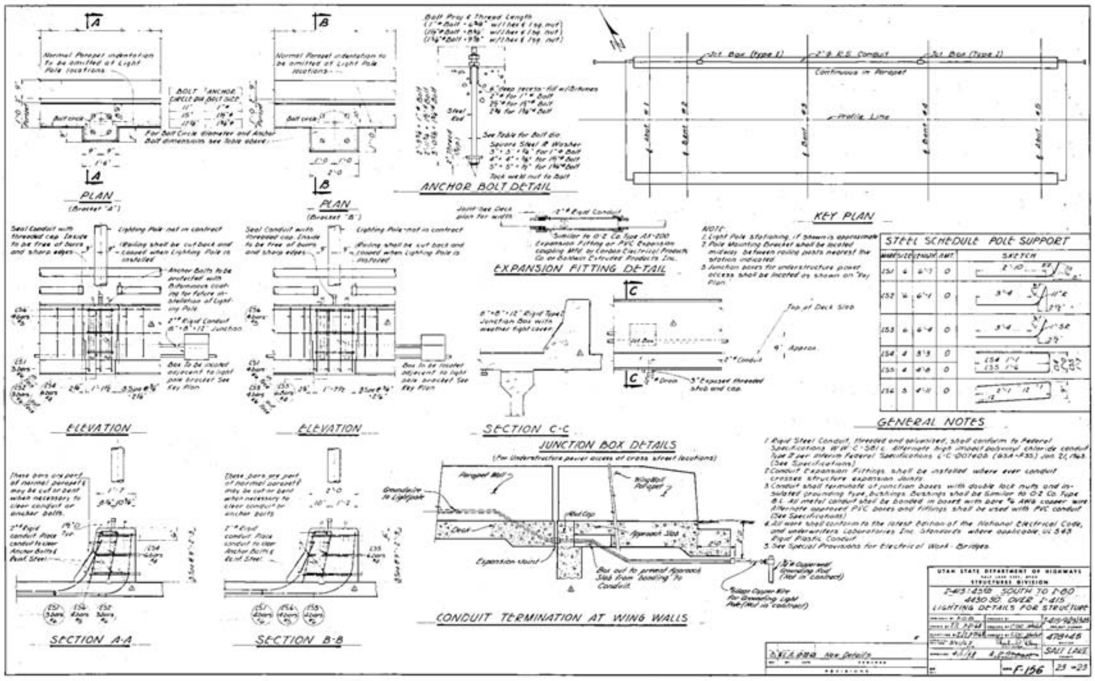
PLAN
(Bracket "A")
PLAN
(Bracket "B")
ANCHOR BOLT DETAIL
KEY PLAN
EXPANSION FITTING DETAIL
STEEL SCHEDULE POLE SUPPORT
ELEVATION
ELEVATION
SECTION C-C
GENERAL NOTES
JUNCTION BOX DETAILS
(For Understructure power access of cross street locations)
3. Conduit shall terminate at junction boxes with double lock nuts and insulated grounding type bushings. Bushings shall be Similar to O-Z Co. Type B.L. All metal conduit shall be bonded in boxes with bare #6 AWG copper wire. Alternate approved PVC boxes and fittings shall be used with PVC conduit (See Specifications)
4. All work shall conform to the latest Edition of the National Electrical Code, and underwriters Laboratories Inc. Standards where applicable, UL 543 Rigid Plastic Conduit
5. See Special Provisions for Electrical Work - Bridges.
SECTION A-A
SECTION B-B
CONDUIT TERMINATION AT WING WALLS
UTAH STATE DEPARTMENT OF HIGHWAYS
SALT LAKE CITY, UTAH
STRUCTURES DIVISION
I-415: 4550 SOUTH TO I-80
4430 SO. OVER I-415
LIGHTING DETAILS FOR STRUCTURE
478+45
SALT LAKE
New Details
REVISIONS
F-156
23 - 23

Figure A.23 Bridge plans page 23 of 23.

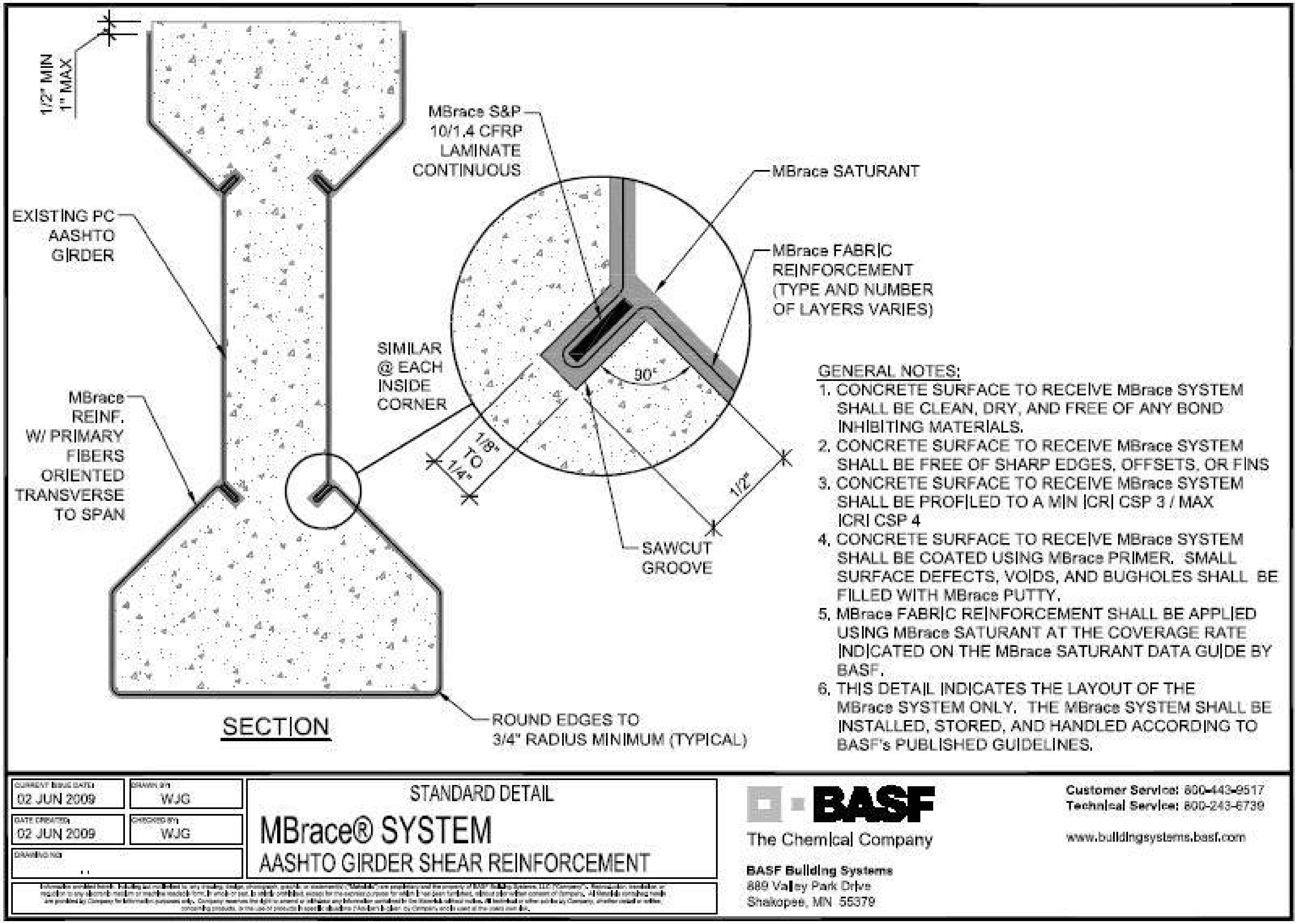
1/2" MIN
1" MAX
EXISTING PC AASHTO GIRDER
MBrace REINF. W/ PRIMARY FIBERS ORIENTED TRANSVERSE TO SPAN
MBrace S&P 10/1.4 CFRP LAMINATE CONTINUOUS
SIMILAR @ EACH INSIDE CORNER
MBrace SATURANT
MBrace FABRIC REINFORCEMENT (TYPE AND NUMBER OF LAYERS VARIES)
90°
1/8" TO 1/4"
1/2"
SAWCUT GROOVE
ROUND EDGES TO 3/4" RADIUS MINIMUM (TYPICAL)
SECTION
CURRENT ISSUE DATE
02 JUN 2009
DRAWN BY
WJG
DATE CREATED
02 JUN 2009
CHECKED BY
WJG
DRAWING NO.
STANDARD DETAIL
MBrace® SYSTEM
AASHTO GIRDER SHEAR REINFORCEMENT
BASF
The Chemical Company
BASF Building Systems
889 Valley Park Drive
Shakopee, MN 55379
Customer Service: 800-443-9517
Technical Service: 800-243-6739
www.buildingsystems.basf.com

GENERAL NOTES:

1. CONCRETE SURFACE TO RECEIVE MBrace SYSTEM SHALL BE CLEAN, DRY, AND FREE OF ANY BOND INHIBITING MATERIALS.
2. CONCRETE SURFACE TO RECEIVE MBrace SYSTEM SHALL BE FREE OF SHARP EDGES, OFFSETS, OR FINS
3. CONCRETE SURFACE TO RECEIVE MBrace SYSTEM SHALL BE PROFILED TO A MIN ICRI CSP 3 / MAX ICRI CSP 4
4. CONCRETE SURFACE TO RECEIVE MBrace SYSTEM SHALL BE COATED USING MBrace PRIMER. SMALL SURFACE DEFECTS, VOIDS, AND BUGHOLES SHALL BE FILLED WITH MBrace PUTTY.
5. MBrace FABRIC REINFORCEMENT SHALL BE APPLIED USING MBrace SATURANT AT THE COVERAGE RATE INDICATED ON THE MBrace SATURANT DATA GUIDE BY BASF.
6. THIS DETAIL INDICATES THE LAYOUT OF THE MBrace SYSTEM ONLY. THE MBrace SYSTEM SHALL BE INSTALLED, STORED, AND HANDLED ACCORDING TO BASF's PUBLISHED GUIDELINES.

Figure A.24 Embedment anchorage detail.

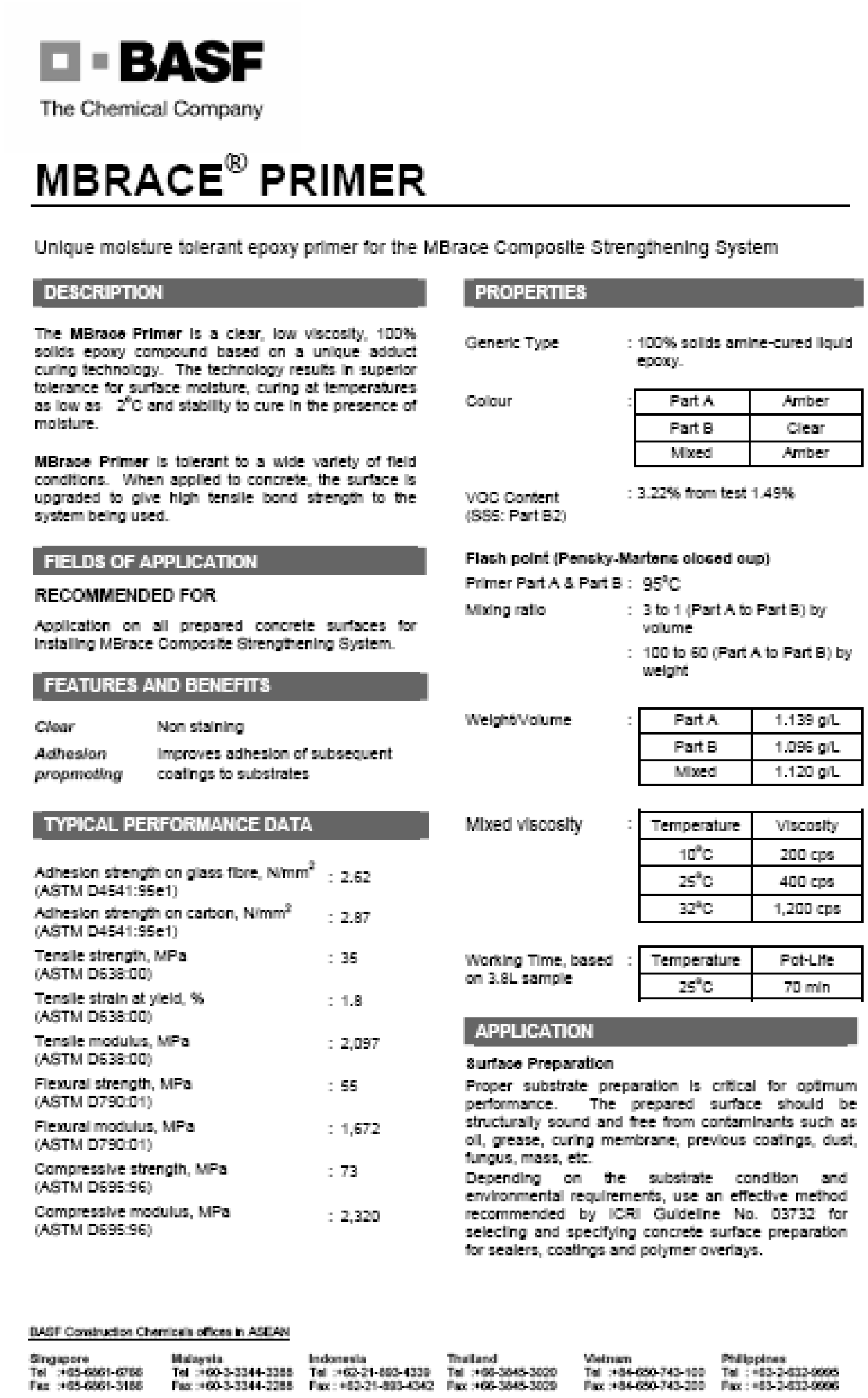

BASF
The Chemical Company

MBRACE® PRIMER

Unique moisture tolerant epoxy primer for the MBrace Composite Strengthening System

DESCRIPTION

The **MBrace Primer** is a clear, low viscosity, 100% solids epoxy compound based on a unique adduct curing technology. The technology results in superior tolerance for surface moisture, curing at temperatures as low as 2°C and stability to cure in the presence of moisture.

MBrace Primer is tolerant to a wide variety of field conditions. When applied to concrete, the surface is upgraded to give high tensile bond strength to the system being used.

FIELDS OF APPLICATION

RECOMMENDED FOR

Application on all prepared concrete surfaces for installing MBrace Composite Strengthening System.

FEATURES AND BENEFITS

Clear	Non staining
Adhesion propmoting	Improves adhesion of subsequent coatings to substrates

TYPICAL PERFORMANCE DATA

Adhesion strength on glass fibre, N/mm² (ASTM D4541:95e1)	: 2.62
Adhesion strength on carbon, N/mm² (ASTM D4541:95e1)	: 2.87
Tensile strength, MPa (ASTM D638:00)	: 35
Tensile strain at yield, % (ASTM D638:00)	: 1.8
Tensile modulus, MPa (ASTM D638:00)	: 2,097
Flexural strength, MPa (ASTM D790:01)	: 55
Flexural modulus, MPa (ASTM D790:01)	: 1,672
Compressive strength, MPa (ASTM D695:96)	: 73
Compressive modulus, MPa (ASTM D695:96)	: 2,320

PROPERTIES

Generic Type : 100% solids amine-cured liquid epoxy.

Colour :

Part A	Amber
Part B	Clear
Mixed	Amber

VOC Content (SS5: Part B2) : 3.22% from test 1.49%

Flash point (Pensky-Martens closed cup)

Primer Part A & Part B : 95°C

Mixing ratio : 3 to 1 (Part A to Part B) by volume
: 100 to 60 (Part A to Part B) by weight

Weight/Volume :

Part A	1.139 g/L
Part B	1.096 g/L
Mixed	1.120 g/L

Mixed viscosity :

Temperature	Viscosity
10°C	200 cps
25°C	400 cps
32°C	1,200 cps

Working Time, based on 3.8L sample :

Temperature	Pot-Life
25°C	70 min

APPLICATION

Surface Preparation

Proper substrate preparation is critical for optimum performance. The prepared surface should be structurally sound and free from contaminants such as oil, grease, curing membrane, previous coatings, dust, fungus, mass, etc.

Depending on the substrate condition and environmental requirements, use an effective method recommended by ICRI Guideline No. 03732 for selecting and specifying concrete surface preparation for sealers, coatings and polymer overlays.

BASF Construction Chemicals offices in ASEAN

Singapore	Malaysia	Indonesia	Thailand	Vietnam	Philippines
Tel :+65-6861-6766	Tel :+60-3-3344-3388	Tel :+62-21-893-4339	Tel :+66-3845-3020	Tel :+84-650-743-100	Tel : +63-2-632-9995
Fax :+65-6861-3186	Fax :+60-3-3344-2288	Fax : +62-21-893-4342	Fax :+66-3845-3029	Fax :+84-650-743-200	Fax : +63-2-632-9996

Figure A.25 Primer specifications page 1.

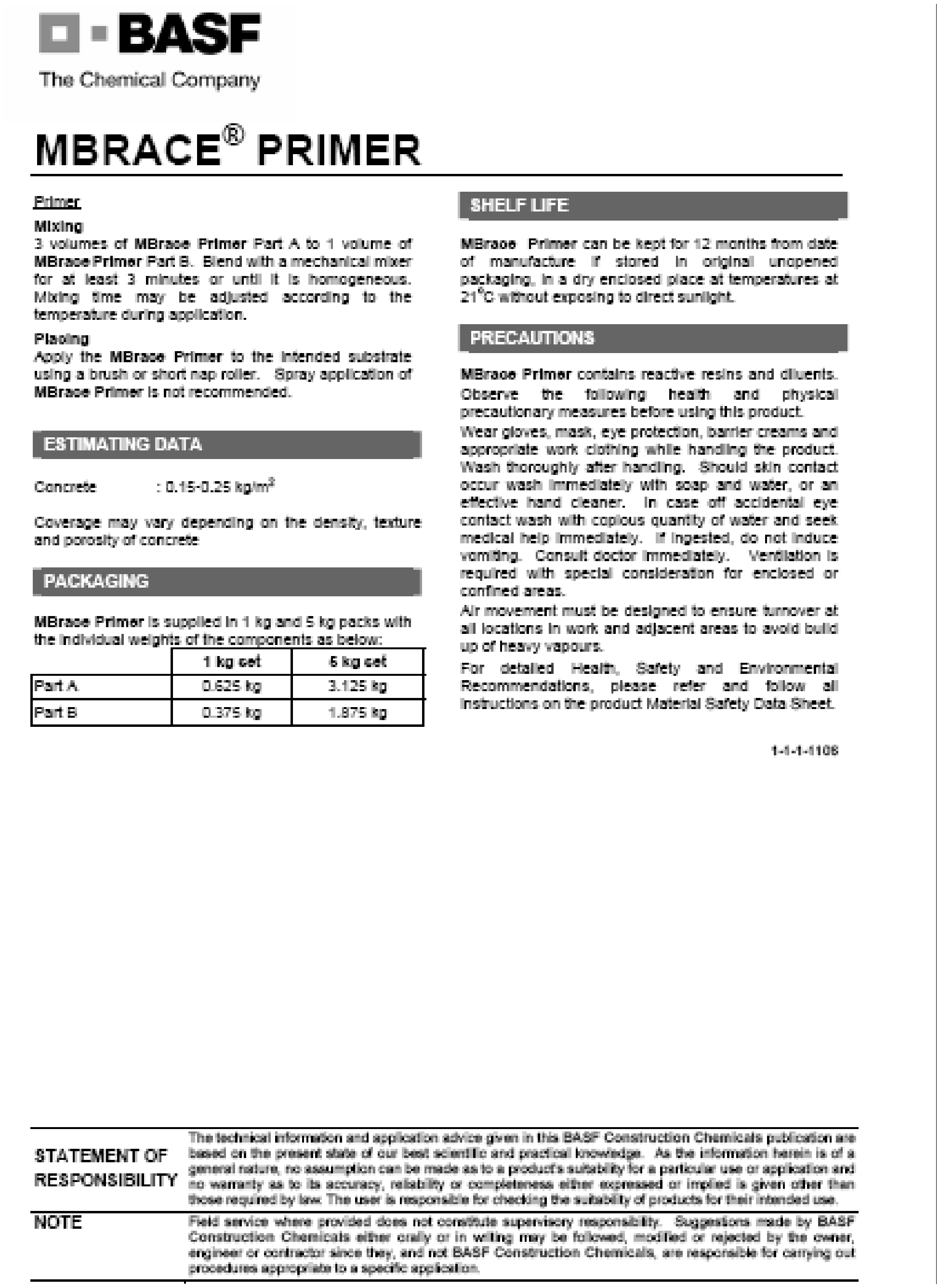

BASF
The Chemical Company

MBRACE® PRIMER

Primer

Mixing

3 volumes of **MBrace Primer** Part A to 1 volume of **MBrace Primer** Part B. Blend with a mechanical mixer for at least 3 minutes or until it is homogeneous. Mixing time may be adjusted according to the temperature during application.

Placing

Apply the **MBrace Primer** to the intended substrate using a brush or short nap roller. Spray application of **MBrace Primer** is not recommended.

ESTIMATING DATA

Concrete : 0.15-0.25 kg/m^2

Coverage may vary depending on the density, texture and porosity of concrete

PACKAGING

MBrace Primer is supplied in 1 kg and 5 kg packs with the individual weights of the components as below:

	1 kg set	5 kg set
Part A	0.625 kg	3.125 kg
Part B	0.375 kg	1.875 kg

SHELF LIFE

MBrace Primer can be kept for 12 months from date of manufacture if stored in original unopened packaging, in a dry enclosed place at temperatures at 21°C without exposing to direct sunlight.

PRECAUTIONS

MBrace Primer contains reactive resins and diluents. Observe the following health and physical precautionary measures before using this product.

Wear gloves, mask, eye protection, barrier creams and appropriate work clothing while handling the product. Wash thoroughly after handling. Should skin contact occur wash immediately with soap and water, or an effective hand cleaner. In case off accidental eye contact wash with copious quantity of water and seek medical help immediately. If ingested, do not induce vomiting. Consult doctor immediately. Ventilation is required with special consideration for enclosed or confined areas.

Air movement must be designed to ensure turnover at all locations in work and adjacent areas to avoid build up of heavy vapours.

For detailed Health, Safety and Environmental Recommendations, please refer and follow all instructions on the product Material Safety Data Sheet.

1-1-1-1106

STATEMENT OF RESPONSIBILITY	The technical information and application advice given in this BASF Construction Chemicals publication are based on the present state of our best scientific and practical knowledge. As the information herein is of a general nature, no assumption can be made as to a product's suitability for a particular use or application and no warranty as to its accuracy, reliability or completeness either expressed or implied is given other than those required by law. The user is responsible for checking the suitability of products for their intended use.
NOTE	Field service where provided does not constitute supervisory responsibility. Suggestions made by BASF Construction Chemicals either orally or in writing may be followed, modified or rejected by the owner, engineer or contractor since they, and not BASF Construction Chemicals, are responsible for carrying out procedures appropriate to a specific application.

Figure A.26 Primer specifications page 2.

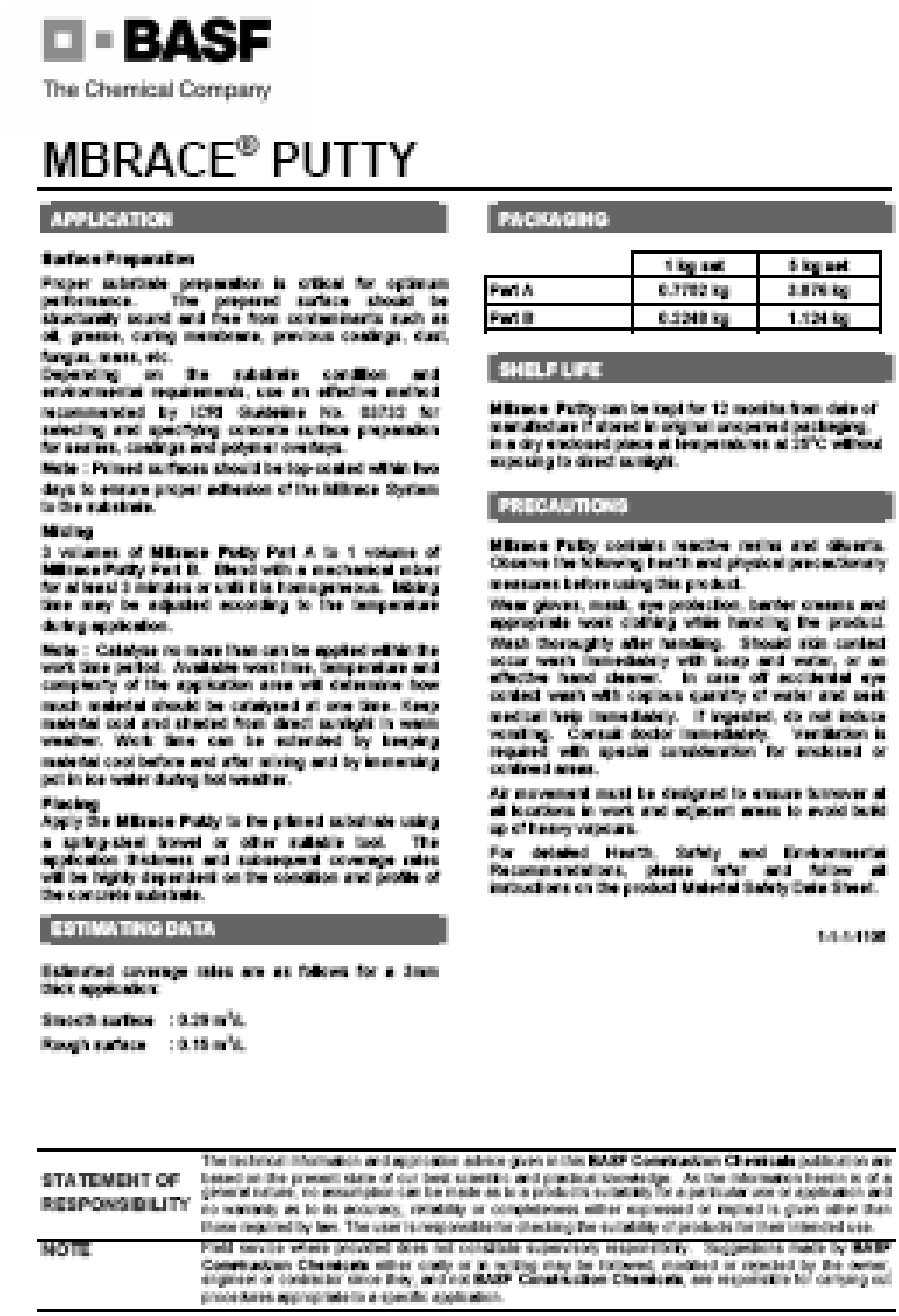

BASF
The Chemical Company

MBRACE® PUTTY

APPLICATION

Surface Preparation

Proper substrate preparation is critical for optimum performance. The prepared surface should be structurally sound and free from contaminants such as oil, grease, curing membrane, previous coatings, dust, fungus, moss, etc.
Depending on the substrate condition and environmental requirements, use an effective method recommended by ICRI Guideline No. 03732 for selecting and specifying concrete surface preparation for sealers, coatings and polymer overlays.

Note : Primed surfaces should be top-coated within two days to ensure proper adhesion of the Mbrace System to the substrate.

Mixing
3 volumes of **Mbrace Putty Part A** to 1 volume of **Mbrace Putty Part B**. Blend with a mechanical mixer for at least 3 minutes or until it is homogeneous. Mixing time may be adjusted according to the temperature during application.

Note : Catalyse no more than can be applied within the work time period. Available work time, temperature and complexity of the application area will determine how much material should be catalysed at one time. Keep material cool and shaded from direct sunlight in warm weather. Work time can be extended by keeping material cool before and after mixing and by immersing pot in ice water during hot weather.

Placing
Apply the **Mbrace Putty** to the primed substrate using a spring-steel trowel or other suitable tool. The application thickness and subsequent coverage rates will be highly dependent on the condition and profile of the concrete substrate.

ESTIMATING DATA

Estimated coverage rates are as follows for a 3mm thick application:

Smooth surface : 0.29 m²/L
Rough surface : 0.15 m²/L

PACKAGING

	1 kg set	5 kg set
Part A	0.7752 kg	3.876 kg
Part B	0.2248 kg	1.124 kg

SHELF LIFE

Mbrace Putty can be kept for 12 months from date of manufacture if stored in original unopened packaging, in a dry enclosed place at temperatures at 35°C without exposing to direct sunlight.

PRECAUTIONS

Mbrace Putty contains reactive resins and diluents. Observe the following health and physical precautionary measures before using this product.

Wear gloves, mask, eye protection, barrier creams and appropriate work clothing while handling the product. Wash thoroughly after handling. Should skin contact occur wash immediately with soap and water, or an effective hand cleaner. In case of accidental eye contact wash with copious quantity of water and seek medical help immediately. If ingested, do not induce vomiting. Consult doctor immediately. Ventilation is required with special consideration for enclosed or confined areas.

Air movement must be designed to ensure turnover at all locations in work and adjacent areas to avoid build up of heavy vapours.

For detailed Health, Safety and Environmental Recommendations, please refer and follow all instructions on the product Material Safety Data Sheet.

1-1-5/1130

STATEMENT OF RESPONSIBILITY	The technical information and application advice given in this **BASF Construction Chemicals** publication are based on the present state of our best scientific and practical knowledge. As the information herein is of a general nature, no assumption can be made as to a product's suitability for a particular use or application and no warranty as to its accuracy, reliability or completeness either expressed or implied is given other than those required by law. The user is responsible for checking the suitability of products for their intended use.
NOTE	Field service where provided does not constitute supervisory responsibility. Suggestions made by **BASF Construction Chemicals** either orally or in writing may be followed, modified or rejected by the owner, engineer or contractor since they, and not **BASF Construction Chemicals**, are responsible for carrying out procedures appropriate to a specific application.

Figure A.27 Putty specifications.

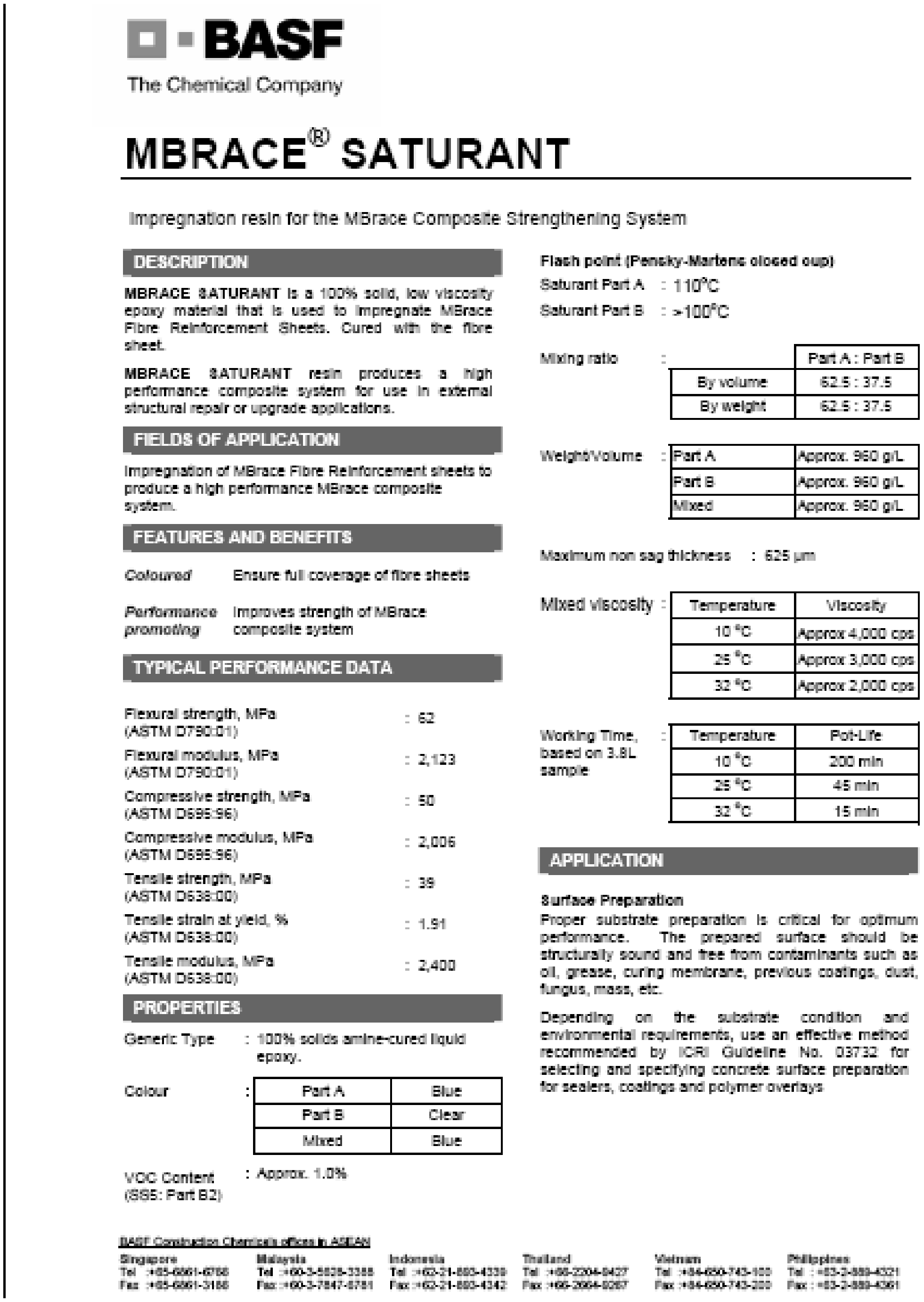

BASF
The Chemical Company

MBRACE® SATURANT

Impregnation resin for the MBrace Composite Strengthening System

DESCRIPTION

MBRACE SATURANT is a 100% solid, low viscosity epoxy material that is used to impregnate MBrace Fibre Reinforcement Sheets. Cured with the fibre sheet.

MBRACE SATURANT resin produces a high performance composite system for use in external structural repair or upgrade applications.

FIELDS OF APPLICATION

Impregnation of MBrace Fibre Reinforcement sheets to produce a high performance MBrace composite system.

FEATURES AND BENEFITS

Coloured	Ensure full coverage of fibre sheets
Performance promoting	Improves strength of MBrace composite system

TYPICAL PERFORMANCE DATA

Flexural strength, MPa (ASTM D790:01)	: 62
Flexural modulus, MPa (ASTM D790:01)	: 2,123
Compressive strength, MPa (ASTM D695:96)	: 50
Compressive modulus, MPa (ASTM D695:96)	: 2,006
Tensile strength, MPa (ASTM D638:00)	: 39
Tensile strain at yield, % (ASTM D638:00)	: 1.91
Tensile modulus, MPa (ASTM D638:00)	: 2,400

PROPERTIES

Generic Type : 100% solids amine-cured liquid epoxy.

Colour :

Part A	Blue
Part B	Clear
Mixed	Blue

VOC Content (SS5: Part B2) : Approx. 1.0%

Flash point (Pensky-Martens closed cup)
Saturant Part A : 110°C
Saturant Part B : >100°C

Mixing ratio :

	Part A : Part B
By volume	62.5 : 37.5
By weight	62.5 : 37.5

Weight/Volume :

Part A	Approx. 960 g/L
Part B	Approx. 960 g/L
Mixed	Approx. 960 g/L

Maximum non sag thickness : 625 µm

Mixed viscosity :

Temperature	Viscosity
10 °C	Approx 4,000 cps
25 °C	Approx 3,000 cps
32 °C	Approx 2,000 cps

Working Time, based on 3.8L sample :

Temperature	Pot-Life
10 °C	200 min
25 °C	45 min
32 °C	15 min

APPLICATION

Surface Preparation
Proper substrate preparation is critical for optimum performance. The prepared surface should be structurally sound and free from contaminants such as oil, grease, curing membrane, previous coatings, dust, fungus, moss, etc.

Depending on the substrate condition and environmental requirements, use an effective method recommended by ICRI Guideline No. 03732 for selecting and specifying concrete surface preparation for sealers, coatings and polymer overlays

Figure A.28 Saturant specifications page 1.

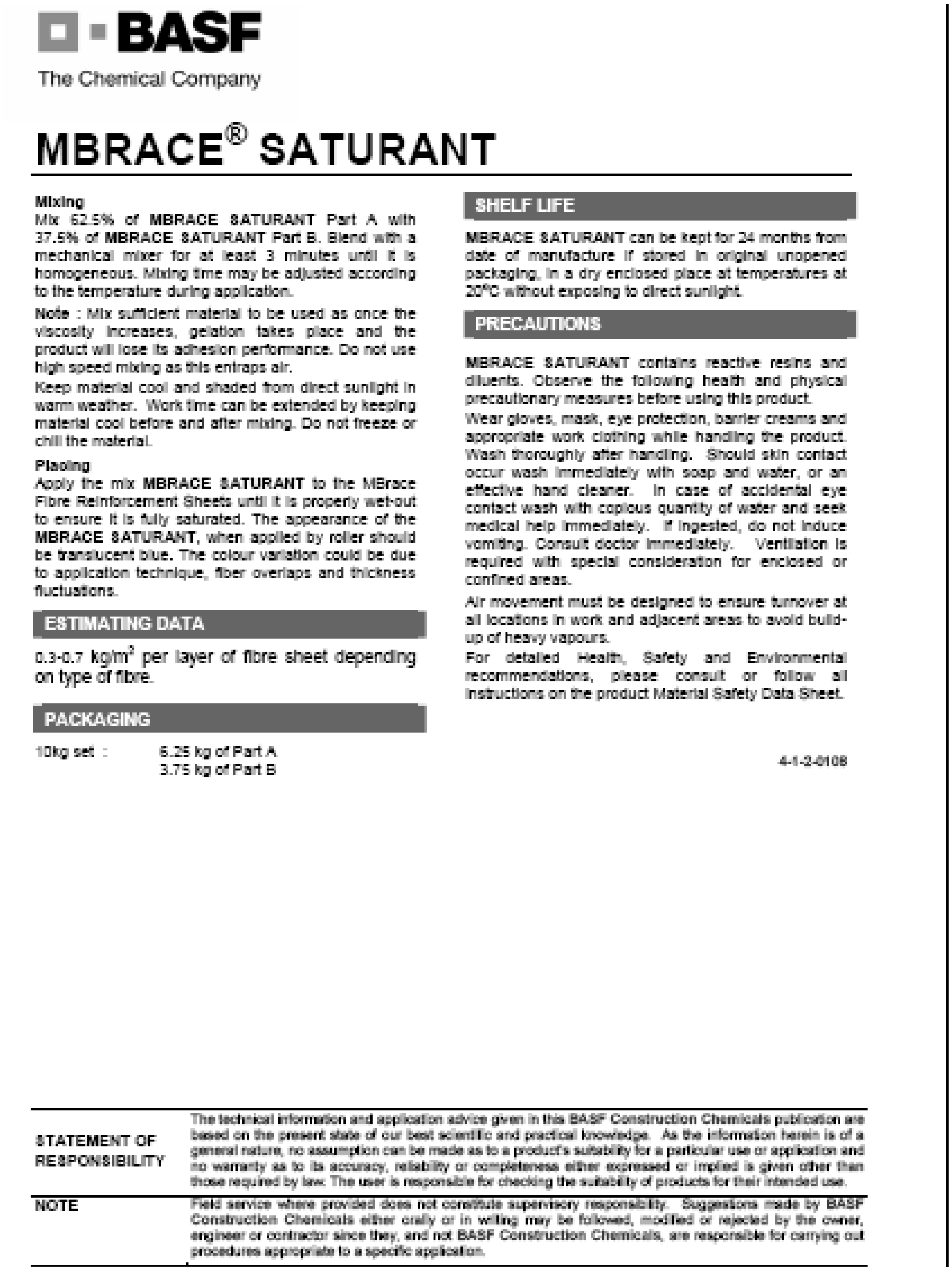

BASF
The Chemical Company

MBRACE® SATURANT

Mixing

Mix 62.5% of **MBRACE SATURANT** Part A with 37.5% of **MBRACE SATURANT** Part B. Blend with a mechanical mixer for at least 3 minutes until it is homogeneous. Mixing time may be adjusted according to the temperature during application.

Note : Mix sufficient material to be used as once the viscosity increases, gelation takes place and the product will lose its adhesion performance. Do not use high speed mixing as this entraps air.

Keep material cool and shaded from direct sunlight in warm weather. Work time can be extended by keeping material cool before and after mixing. Do not freeze or chill the material.

Placing

Apply the mix **MBRACE SATURANT** to the MBrace Fibre Reinforcement Sheets until it is properly wet-out to ensure it is fully saturated. The appearance of the **MBRACE SATURANT**, when applied by roller should be translucent blue. The colour variation could be due to application technique, fiber overlaps and thickness fluctuations.

ESTIMATING DATA

0.3-0.7 kg/m^2 per layer of fibre sheet depending on type of fibre.

PACKAGING

10kg set : 6.25 kg of Part A
3.75 kg of Part B

SHELF LIFE

MBRACE SATURANT can be kept for 24 months from date of manufacture if stored in original unopened packaging, in a dry enclosed place at temperatures at 20°C without exposing to direct sunlight.

PRECAUTIONS

MBRACE SATURANT contains reactive resins and diluents. Observe the following health and physical precautionary measures before using this product.

Wear gloves, mask, eye protection, barrier creams and appropriate work clothing while handling the product. Wash thoroughly after handling. Should skin contact occur wash immediately with soap and water, or an effective hand cleaner. In case of accidental eye contact wash with copious quantity of water and seek medical help immediately. If ingested, do not induce vomiting. Consult doctor immediately. Ventilation is required with special consideration for enclosed or confined areas.

Air movement must be designed to ensure turnover at all locations in work and adjacent areas to avoid build-up of heavy vapours.

For detailed Health, Safety and Environmental recommendations, please consult or follow all instructions on the product Material Safety Data Sheet.

4-1-2-0108

STATEMENT OF RESPONSIBILITY	The technical information and application advice given in this BASF Construction Chemicals publication are based on the present state of our best scientific and practical knowledge. As the information herein is of a general nature, no assumption can be made as to a product's suitability for a particular use or application and no warranty as to its accuracy, reliability or completeness either expressed or implied is given other than those required by law. The user is responsible for checking the suitability of products for their intended use.
NOTE	Field service where provided does not constitute supervisory responsibility. Suggestions made by BASF Construction Chemicals either orally or in writing may be followed, modified or rejected by the owner, engineer or contractor since they, and not BASF Construction Chemicals, are responsible for carrying out procedures appropriate to a specific application.

Figure A.29 Saturant specifications page 2.

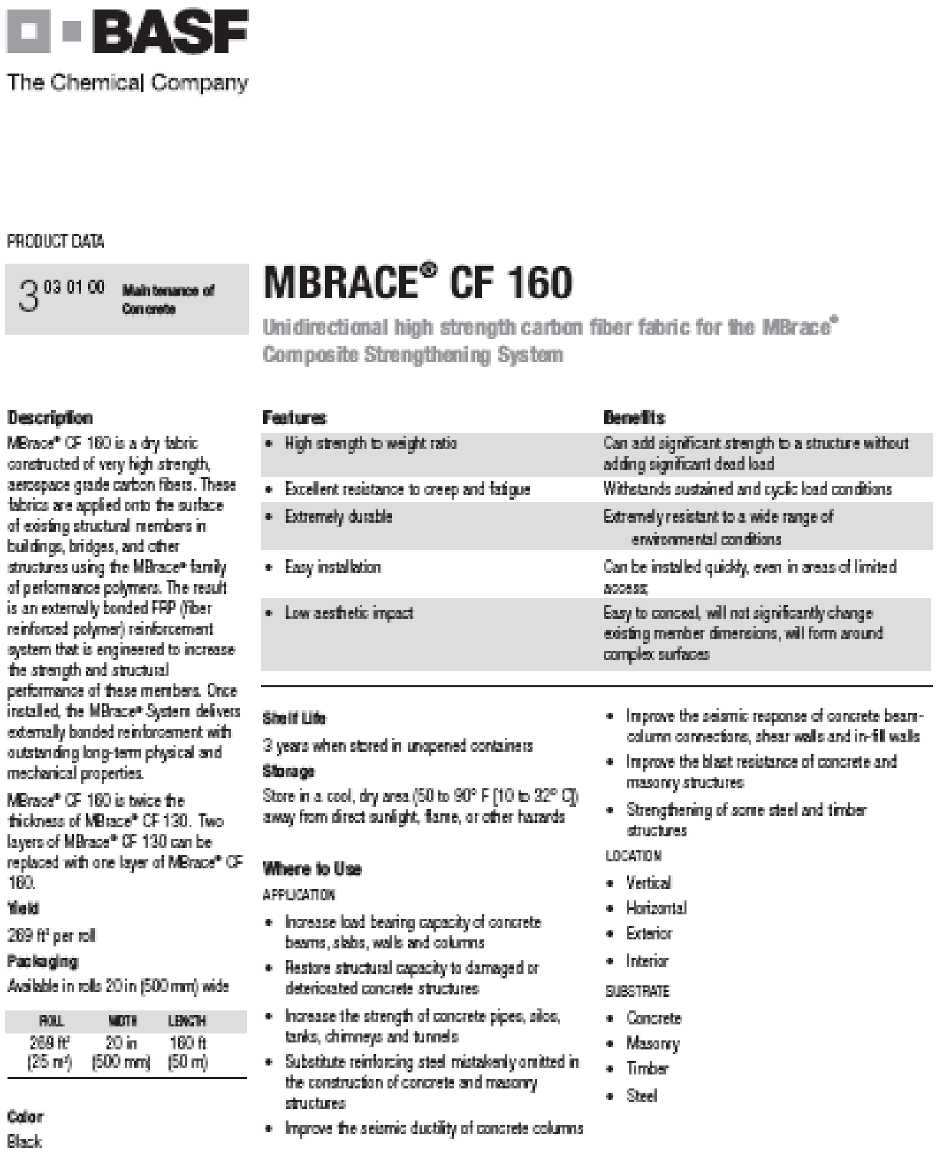

BASF
The Chemical Company

PRODUCT DATA

3 03 01 00 **Maintenance of Concrete**

MBRACE® CF 160

Unidirectional high strength carbon fiber fabric for the MBrace® Composite Strengthening System

Description

MBrace® CF 160 is a dry fabric constructed of very high strength, aerospace grade carbon fibers. These fabrics are applied onto the surface of existing structural members in buildings, bridges, and other structures using the MBrace® family of performance polymers. The result is an externally bonded FRP (fiber reinforced polymer) reinforcement system that is engineered to increase the strength and structural performance of these members. Once installed, the MBrace® System delivers externally bonded reinforcement with outstanding long-term physical and mechanical properties.

MBrace® CF 160 is twice the thickness of MBrace® CF 130. Two layers of MBrace® CF 130 can be replaced with one layer of MBrace® CF 160.

Yield

269 ft^2 per roll

Packaging

Available in rolls 20 in (500 mm) wide

ROLL	WIDTH	LENGTH
269 ft^2 (25 m^2)	20 in (500 mm)	160 ft (50 m)

Color

Black

Features	Benefits
• High strength to weight ratio	Can add significant strength to a structure without adding significant dead load
• Excellent resistance to creep and fatigue	Withstands sustained and cyclic load conditions
• Extremely durable	Extremely resistant to a wide range of environmental conditions
• Easy installation	Can be installed quickly, even in areas of limited access;
• Low aesthetic impact	Easy to conceal, will not significantly change existing member dimensions, will form around complex surfaces

Shelf Life

3 years when stored in unopened containers

Storage

Store in a cool, dry area (50 to 90° F [10 to 32° C]) away from direct sunlight, flame, or other hazards

Where to Use

APPLICATION

- Increase load bearing capacity of concrete beams, slabs, walls and columns
- Restore structural capacity to damaged or deteriorated concrete structures
- Increase the strength of concrete pipes, silos, tanks, chimneys and tunnels
- Substitute reinforcing steel mistakenly omitted in the construction of concrete and masonry structures
- Improve the seismic ductility of concrete columns
- Improve the seismic response of concrete beam-column connections, shear walls and in-fill walls
- Improve the blast resistance of concrete and masonry structures
- Strengthening of some steel and timber structures

LOCATION

- Vertical
- Horizontal
- Exterior
- Interior

SUBSTRATE

- Concrete
- Masonry
- Timber
- Steel

Figure A.30 CF 160 fabric specification page 1.

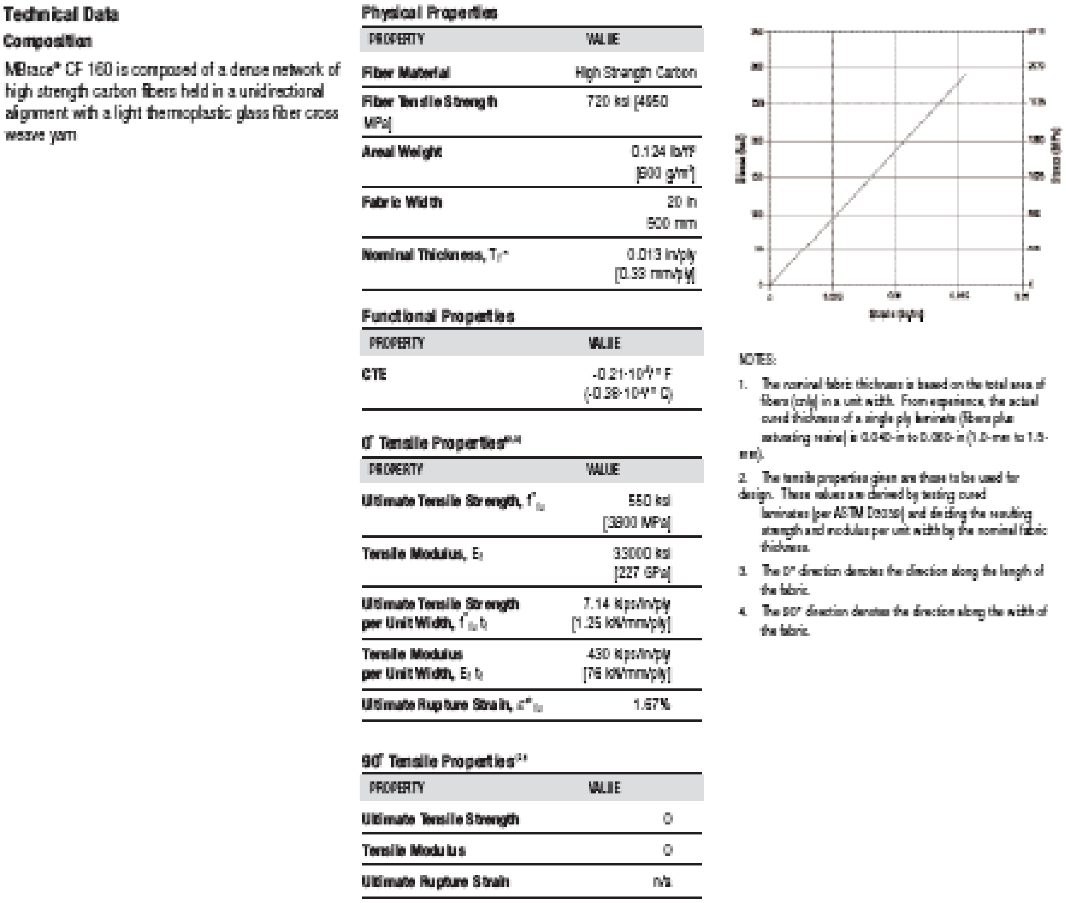
Stress (ksi)
Stress (MPa)
Strain (in/in)

Technical Data

Composition

MBrace® CF 160 is composed of a dense network of high strength carbon fibers held in a unidirectional alignment with a light thermoplastic glass fiber cross weave yarn

Physical Properties

PROPERTY	VALUE
Fiber Material	High Strangth Carbon
Fiber Tensile Strength	720 ksi [4950 MPa]
Areal Weight	0.124 lb/ft² [600 g/m²]
Fabric Width	20 in 500 mm
Nominal Thickness, T_f*	0.013 in/ply [0.33 mm/ply]

Functional Properties

PROPERTY	VALUE
CTE	$-0.21 \cdot 10^{-6}/°$ F ($-0.38 \cdot 10^{-6}/°$ C)

0° Tensile Properties[2,4]

PROPERTY	VALUE
Ultimate Tensile Strength, f^*_{fu}	550 ksi [3800 MPa]
Tensile Modulus, E_f	33000 ksi [227 GPa]
Ultimate Tensile Strength per Unit Width, $f^*_{fu}\ t_f$	7.14 kips/in/ply [1.25 kN/mm/ply]
Tensile Modulus per Unit Width, $E_f\ t_f$	430 kips/in/ply [76 kN/mm/ply]
Ultimate Rupture Strain, ε^*_{fu}	1.67%

90° Tensile Properties[2,4]

PROPERTY	VALUE
Ultimate Tensile Strength	0
Tensile Modulus	0
Ultimate Rupture Strain	n/a

NOTES:

1. The nominal fabric thickness is based on the total area of fibers (only) in a unit width. From experience, the actual cured thickness of a single ply laminate (fibers plus saturating resins) is 0.040-in to 0.060-in (1.0-mm to 1.5-mm).
2. The tensile properties given are those to be used for design. These values are derived by testing cured laminates (per ASTM D3039) and dividing the resulting strength and modulus per unit width by the nominal fabric thickness.
3. The 0° direction denotes the direction along the length of the fabric.
4. The 90° direction denotes the direction along the width of the fabric.

Figure A.31 CF 160 Fabric Specifications Page 2.

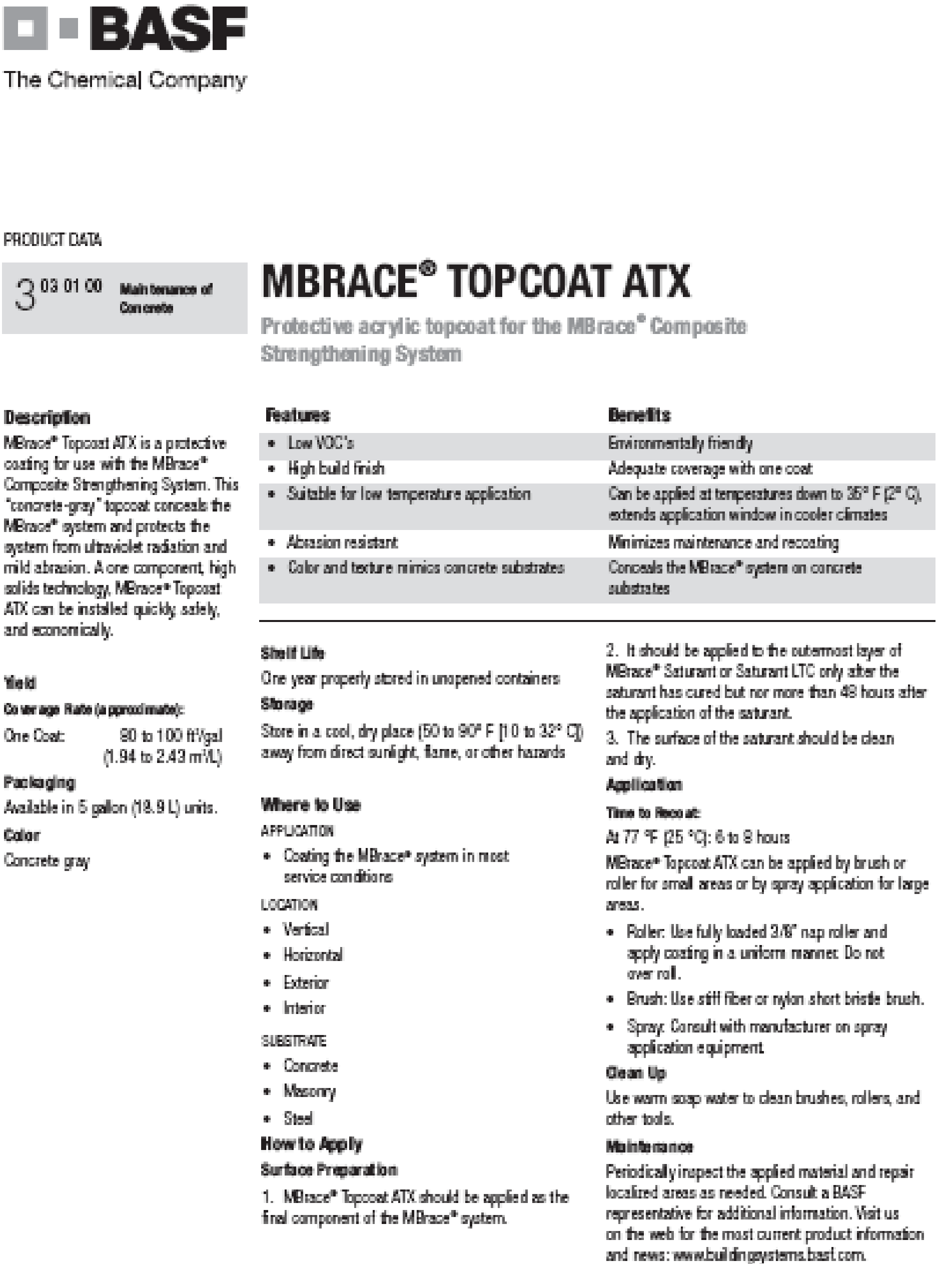

BASF

The Chemical Company

PRODUCT DATA

3 03 01 00 **Maintenance of Concrete**

MBRACE® TOPCOAT ATX

Protective acrylic topcoat for the MBrace® Composite Strengthening System

Description

MBrace® Topcoat ATX is a protective coating for use with the MBrace® Composite Strengthening System. This "concrete-gray" topcoat conceals the MBrace® system and protects the system from ultraviolet radiation and mild abrasion. A one component, high solids technology, MBrace® Topcoat ATX can be installed quickly, safely, and economically.

Yield

Coverage Rate (approximate):

One Coat: 90 to 100 ft^2/gal (1.94 to 2.43 m^2/L)

Packaging

Available in 5 gallon (18.9 L) units.

Color

Concrete gray

Features	Benefits
• Low VOC's	Environmentally friendly
• High build finish	Adequate coverage with one coat
• Suitable for low temperature application	Can be applied at temperatures down to 35° F (2° C), extends application window in cooler climates
• Abrasion resistant	Minimizes maintenance and recoating
• Color and texture mimics concrete substrates	Conceals the MBrace® system on concrete substrates

Shelf Life

One year properly stored in unopened containers

Storage

Store in a cool, dry place (50 to 90° F [10 to 32° C]) away from direct sunlight, flame, or other hazards

Where to Use

APPLICATION

- Coating the MBrace® system in most service conditions

LOCATION

- Vertical
- Horizontal
- Exterior
- Interior

SUBSTRATE

- Concrete
- Masonry
- Steel

How to Apply

Surface Preparation

1. MBrace® Topcoat ATX should be applied as the final component of the MBrace® system.
2. It should be applied to the outermost layer of MBrace® Saturant or Saturant LTC only after the saturant has cured but nor more than 48 hours after the application of the saturant.
3. The surface of the saturant should be clean and dry.

Application

Time to Recoat:

At 77 °F (25 °C): 6 to 8 hours

MBrace® Topcoat ATX can be applied by brush or roller for small areas or by spray application for large areas.

- Roller: Use fully loaded 3/8" nap roller and apply coating in a uniform manner. Do not over roll.
- Brush: Use stiff fiber or nylon short bristle brush.
- Spray: Consult with manufacturer on spray application equipment.

Clean Up

Use warm soap water to clean brushes, rollers, and other tools.

Maintenance

Periodically inspect the applied material and repair localized areas as needed. Consult a BASF representative for additional information. Visit us on the web for the most current product information and news: www.buildingsystems.basf.com.

Figure A.32 Topcoat specifications page 1.

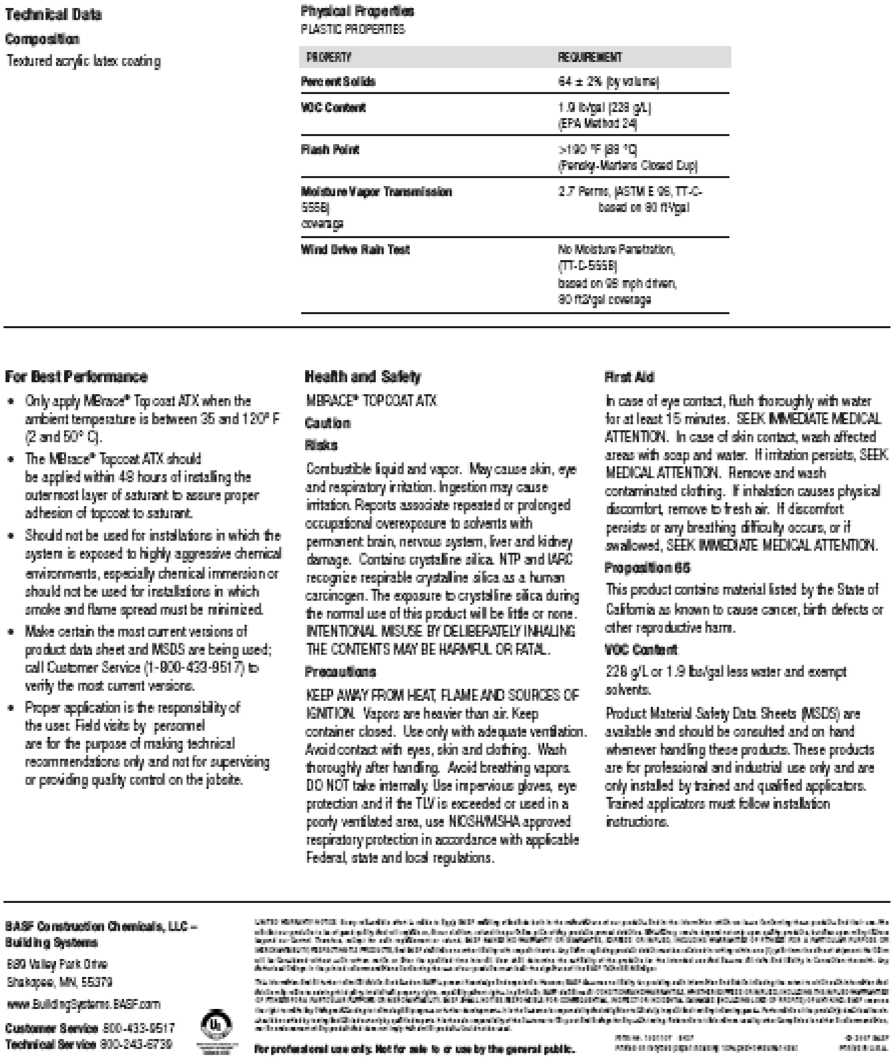

Technical Data

Composition

Textured acrylic latex coating

Physical Properties

PLASTIC PROPERTIES

PROPERTY	REQUIREMENT
Percent Solids	64 ± 2% (by volume)
VOC Content	1.9 lb/gal (228 g/L) (EPA Method 24)
Flash Point	>190 °F (88 °C) (Pensky-Martens Closed Cup)
Moisture Vapor Transmission 5558) coverage	2.7 Perms, (ASTM E 96, TT-C- based on 80 ft²/gal
Wind Drive Rain Test	No Moisture Penetration, (TT-C-555B) based on 98 mph driven, 80 ft2/gal coverage

For Best Performance

- Only apply MBrace® Topcoat ATX when the ambient temperature is between 35 and 120° F (2 and 50° C).
- The MBrace® Topcoat ATX should be applied within 48 hours of installing the outermost layer of saturant to assure proper adhesion of topcoat to saturant.
- Should not be used for installations in which the system is exposed to highly aggressive chemical environments, especially chemical immersion or should not be used for installations in which smoke and flame spread must be minimized.
- Make certain the most current versions of product data sheet and MSDS are being used; call Customer Service (1-800-433-9517) to verify the most current versions.
- Proper application is the responsibility of the user. Field visits by personnel are for the purpose of making technical recommendations only and not for supervising or providing quality control on the jobsite.

Health and Safety

MBRACE® TOPCOAT ATX

Caution

Risks

Combustible liquid and vapor. May cause skin, eye and respiratory irritation. Ingestion may cause irritation. Reports associate repeated or prolonged occupational overexposure to solvents with permanent brain, nervous system, liver and kidney damage. Contains crystalline silica. NTP and IARC recognize respirable crystalline silica as a human carcinogen. The exposure to crystalline silica during the normal use of this product will be little or none. INTENTIONAL MISUSE BY DELIBERATELY INHALING THE CONTENTS MAY BE HARMFUL OR FATAL.

Precautions

KEEP AWAY FROM HEAT, FLAME AND SOURCES OF IGNITION. Vapors are heavier than air. Keep container closed. Use only with adequate ventilation. Avoid contact with eyes, skin and clothing. Wash thoroughly after handling. Avoid breathing vapors. DO NOT take internally. Use impervious gloves, eye protection and if the TLV is exceeded or used in a poorly ventilated area, use NIOSH/MSHA approved respiratory protection in accordance with applicable Federal, state and local regulations.

First Aid

In case of eye contact, flush thoroughly with water for at least 15 minutes. SEEK IMMEDIATE MEDICAL ATTENTION. In case of skin contact, wash affected areas with soap and water. If irritation persists, SEEK MEDICAL ATTENTION. Remove and wash contaminated clothing. If inhalation causes physical discomfort, remove to fresh air. If discomfort persists or any breathing difficulty occurs, or if swallowed, SEEK IMMEDIATE MEDICAL ATTENTION.

Proposition 65

This product contains material listed by the State of California as known to cause cancer, birth defects or other reproductive harm.

VOC Content

228 g/L or 1.9 lbs/gal less water and exempt solvents.

Product Material Safety Data Sheets (MSDS) are available and should be consulted and on hand whenever handling these products. These products are for professional and industrial use only and are only installed by trained and qualified applicators. Trained applicators must follow installation instructions.

BASF Construction Chemicals, LLC – Building Systems

889 Valley Park Drive
Shakopee, MN, 55379
www.BuildingSystems.BASF.com

Customer Service 800-433-9517
Technical Service 800-243-6739

For professional use only. Not for sale to or use by the general public.

Figure A.33 Topcoat specifications page 2.

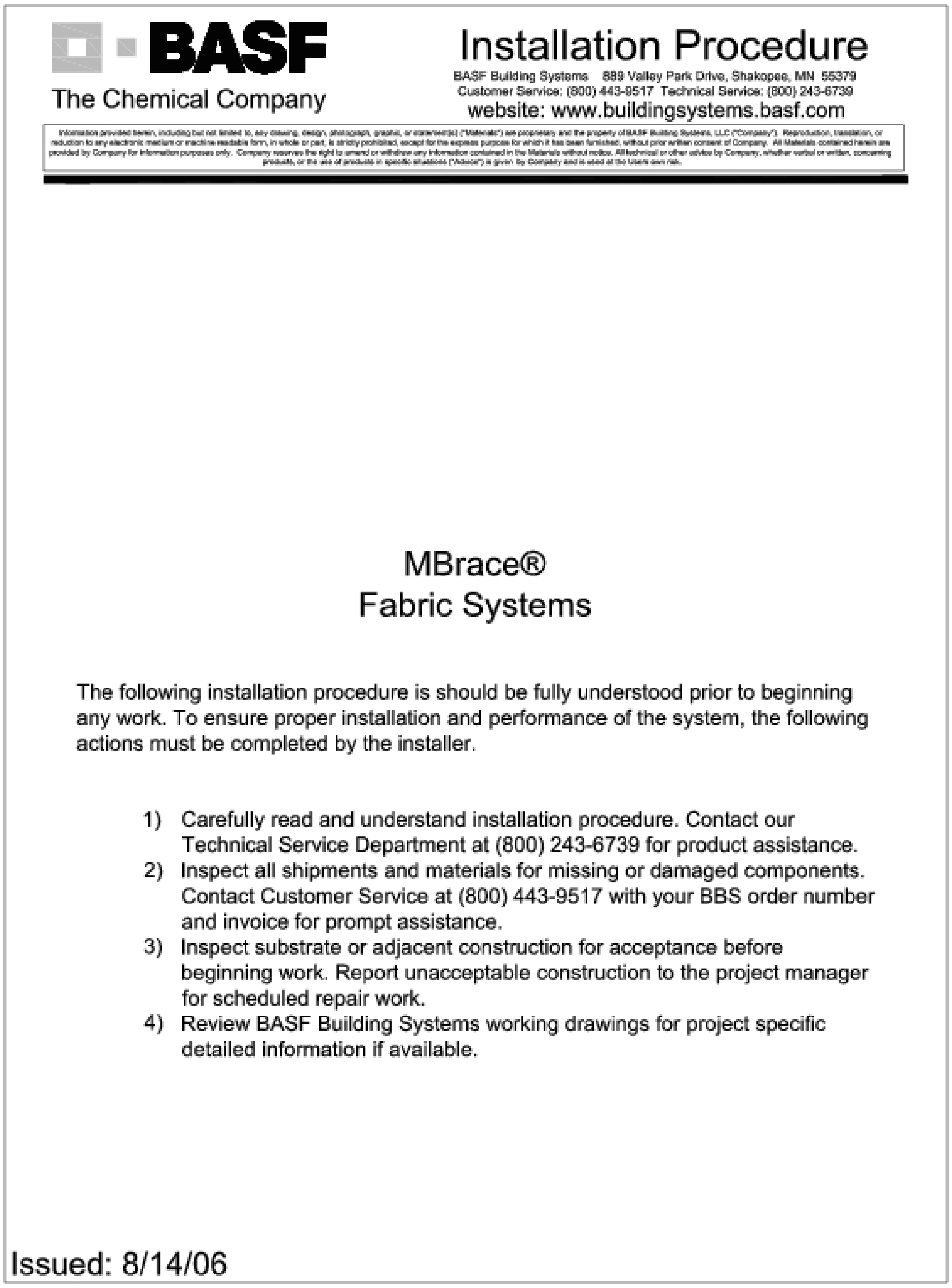

BASF
The Chemical Company

Installation Procedure

BASF Building Systems 889 Valley Park Drive, Shakopee, MN 55379
Customer Service: (800) 443-9517 Technical Service: (800) 243-6739
website: www.buildingsystems.basf.com

Information provided herein, including but not limited to, any drawing, design, photograph, graphic, or statement(s) ("Materials") are proprietary and the property of BASF Building Systems, LLC ("Company"). Reproduction, translation, or reduction to any electronic medium or machine readable form, in whole or part, is strictly prohibited, except for the express purpose for which it has been furnished, without prior written consent of Company. All Materials contained herein are provided by Company for information purposes only. Company reserves the right to amend or withdraw any information contained in the Materials without notice. All technical or other advice by Company, whether verbal or written, concerning products, or the use of products in specific situations ("Advice") is given by Company and is used at the Users own risk.

MBrace®
Fabric Systems

The following installation procedure is should be fully understood prior to beginning any work. To ensure proper installation and performance of the system, the following actions must be completed by the installer.

1) Carefully read and understand installation procedure. Contact our Technical Service Department at (800) 243-6739 for product assistance.
2) Inspect all shipments and materials for missing or damaged components. Contact Customer Service at (800) 443-9517 with your BBS order number and invoice for prompt assistance.
3) Inspect substrate or adjacent construction for acceptance before beginning work. Report unacceptable construction to the project manager for scheduled repair work.
4) Review BASF Building Systems working drawings for project specific detailed information if available.

Issued: 8/14/06

Figure A.34 Application instructions page 1.

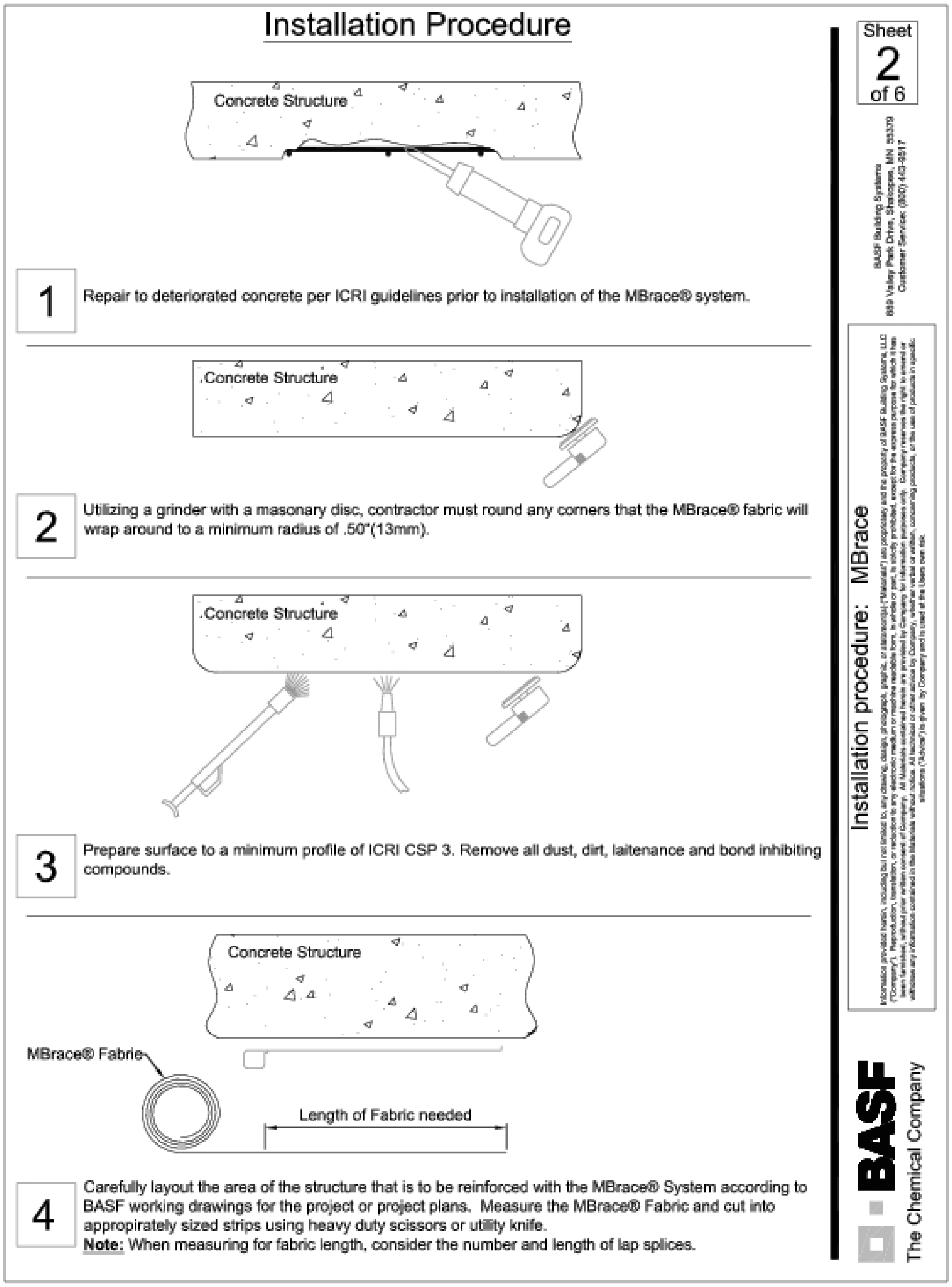

Concrete Structure
Concrete Structure
Concrete Structure
Concrete Structure
MBrace® Fabric
Length of Fabric needed

Installation Procedure

1 Repair to deteriorated concrete per ICRI guidelines prior to installation of the MBrace® system.

2 Utilizing a grinder with a masonary disc, contractor must round any corners that the MBrace® fabric will wrap around to a minimum radius of .50"(13mm).

3 Prepare surface to a minimum profile of ICRI CSP 3. Remove all dust, dirt, laitenance and bond inhibiting compounds.

4 Carefully layout the area of the structure that is to be reinforced with the MBrace® System according to BASF working drawings for the project or project plans. Measure the MBrace® Fabric and cut into appropirately sized strips using heavy duty scissors or utility knife.
Note: When measuring for fabric length, consider the number and length of lap splices.

Sheet 2 of 6

BASF Building Systems
889 Valley Park Drive, Shakopee, MN 55379
Customer Service: (800) 433-9517

Installation procedure: MBrace

BASF
The Chemical Company

Figure A.35 Application instructions page 2.

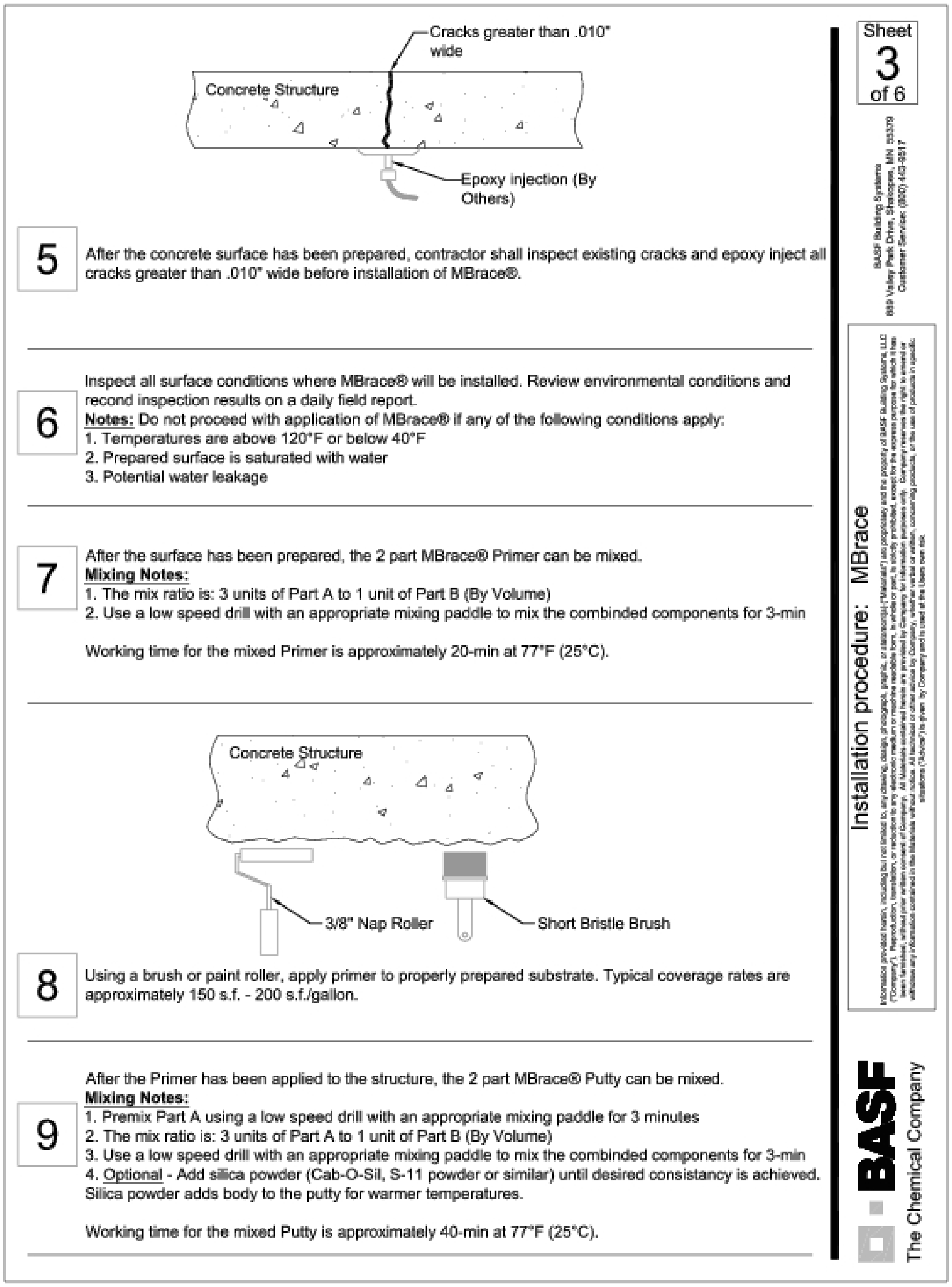
Cracks greater than .010" wide
Concrete Structure
Epoxy injection (By Others)
Concrete Structure
3/8" Nap Roller
Short Bristle Brush

Sheet 3 of 6

Installation procedure: MBrace

BASF Building Systems
889 Valley Park Drive, Shakopee, MN 55379
Customer Service: (800) 433-9517

The Chemical Company

5 After the concrete surface has been prepared, contractor shall inspect existing cracks and epoxy inject all cracks greater than .010" wide before installation of MBrace®.

6 Inspect all surface conditions where MBrace® will be installed. Review environmental conditions and recond inspection results on a daily field report.

Notes: Do not proceed with application of MBrace® if any of the following conditions apply:

1. Temperatures are above 120°F or below 40°F
2. Prepared surface is saturated with water
3. Potential water leakage

7 After the surface has been prepared, the 2 part MBrace® Primer can be mixed.

Mixing Notes:

1. The mix ratio is: 3 units of Part A to 1 unit of Part B (By Volume)
2. Use a low speed drill with an appropriate mixing paddle to mix the combinded components for 3-min

Working time for the mixed Primer is approximately 20-min at 77°F (25°C).

8 Using a brush or paint roller, apply primer to properly prepared substrate. Typical coverage rates are approximately 150 s.f. - 200 s.f./gallon.

9 After the Primer has been applied to the structure, the 2 part MBrace® Putty can be mixed.

Mixing Notes:

1. Premix Part A using a low speed drill with an appropriate mixing paddle for 3 minutes
2. The mix ratio is: 3 units of Part A to 1 unit of Part B (By Volume)
3. Use a low speed drill with an appropriate mixing paddle to mix the combinded components for 3-min
4. Optional - Add silica powder (Cab-O-Sil, S-11 powder or similar) until desired consistancy is achieved. Silica powder adds body to the putty for warmer temperatures.

Working time for the mixed Putty is approximately 40-min at 77°F (25°C).

Figure A.36 Application instructions page 3.

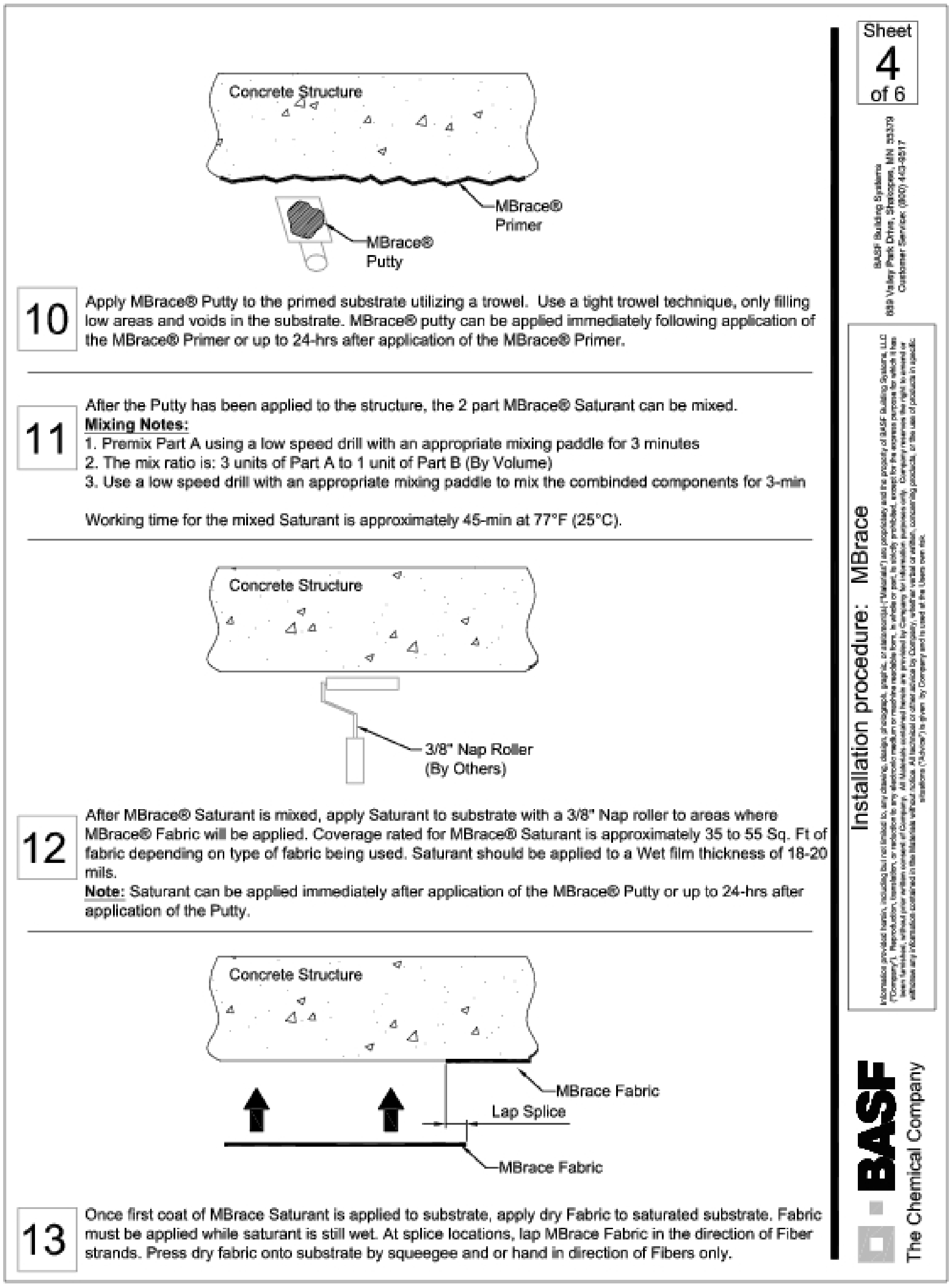
Concrete Structure
MBrace® Primer
MBrace® Putty
Concrete Structure
3/8" Nap Roller (By Others)
Concrete Structure
MBrace Fabric
Lap Splice
MBrace Fabric

Sheet 4 of 6

BASF Building Systems
889 Valley Park Drive, Shakopee, MN 55379
Customer Service: (800) 433-9517

Installation procedure: MBrace

BASF The Chemical Company

10 Apply MBrace® Putty to the primed substrate utilizing a trowel. Use a tight trowel technique, only filling low areas and voids in the substrate. MBrace® putty can be applied immediately following application of the MBrace® Primer or up to 24-hrs after application of the MBrace® Primer.

11 After the Putty has been applied to the structure, the 2 part MBrace® Saturant can be mixed.

Mixing Notes:

1. Premix Part A using a low speed drill with an appropriate mixing paddle for 3 minutes
2. The mix ratio is: 3 units of Part A to 1 unit of Part B (By Volume)
3. Use a low speed drill with an appropriate mixing paddle to mix the combinded components for 3-min

Working time for the mixed Saturant is approximately 45-min at 77°F (25°C).

12 After MBrace® Saturant is mixed, apply Saturant to substrate with a 3/8" Nap roller to areas where MBrace® Fabric will be applied. Coverage rated for MBrace® Saturant is approximately 35 to 55 Sq. Ft of fabric depending on type of fabric being used. Saturant should be applied to a Wet film thickness of 18-20 mils.

Note: Saturant can be applied immediately after application of the MBrace® Putty or up to 24-hrs after application of the Putty.

13 Once first coat of MBrace Saturant is applied to substrate, apply dry Fabric to saturated substrate. Fabric must be applied while saturant is still wet. At splice locations, lap MBrace Fabric in the direction of Fiber strands. Press dry fabric onto substrate by squeegee and or hand in direction of Fibers only.

Figure A.37 Application instructions page 4.

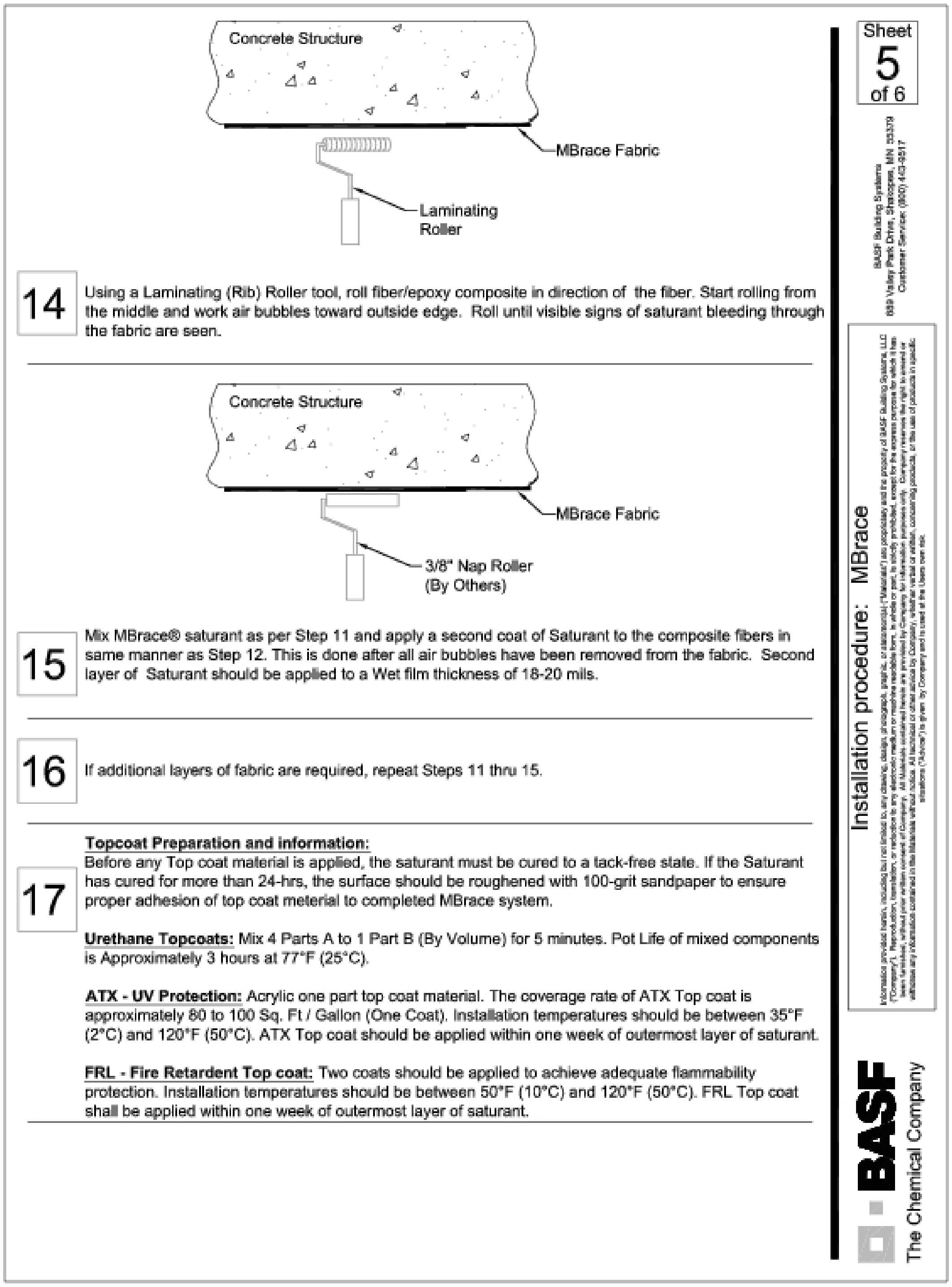
Concrete Structure
MBrace Fabric
Laminating Roller
Concrete Structure
MBrace Fabric
3/8" Nap Roller (By Others)

Sheet 5 of 6

BASF Building Systems
889 Valley Park Drive, Shakopee, MN 55379
Customer Service: (800) 433-9517

Installation procedure: MBrace

BASF The Chemical Company

14 Using a Laminating (Rib) Roller tool, roll fiber/epoxy composite in direction of the fiber. Start rolling from the middle and work air bubbles toward outside edge. Roll until visible signs of saturant bleeding through the fabric are seen.

15 Mix MBrace® saturant as per Step 11 and apply a second coat of Saturant to the composite fibers in same manner as Step 12. This is done after all air bubbles have been removed from the fabric. Second layer of Saturant should be applied to a Wet film thickness of 18-20 mils.

16 If additional layers of fabric are required, repeat Steps 11 thru 15.

17 **Topcoat Preparation and information:**
Before any Top coat material is applied, the saturant must be cured to a tack-free state. If the Saturant has cured for more than 24-hrs, the surface should be roughened with 100-grit sandpaper to ensure proper adhesion of top coat meterial to completed MBrace system.

Urethane Topcoats: Mix 4 Parts A to 1 Part B (By Volume) for 5 minutes. Pot Life of mixed components is Approximately 3 hours at 77°F (25°C).

ATX - UV Protection: Acrylic one part top coat material. The coverage rate of ATX Top coat is approximately 80 to 100 Sq. Ft / Gallon (One Coat). Installation temperatures should be between 35°F (2°C) and 120°F (50°C). ATX Top coat should be applied within one week of outermost layer of saturant.

FRL - Fire Retardent Top coat: Two coats should be applied to achieve adequate flammability protection. Installation temperatures should be between 50°F (10°C) and 120°F (50°C). FRL Top coat shall be applied within one week of outermost layer of saturant.

Figure A.38 Application instructions page 5.

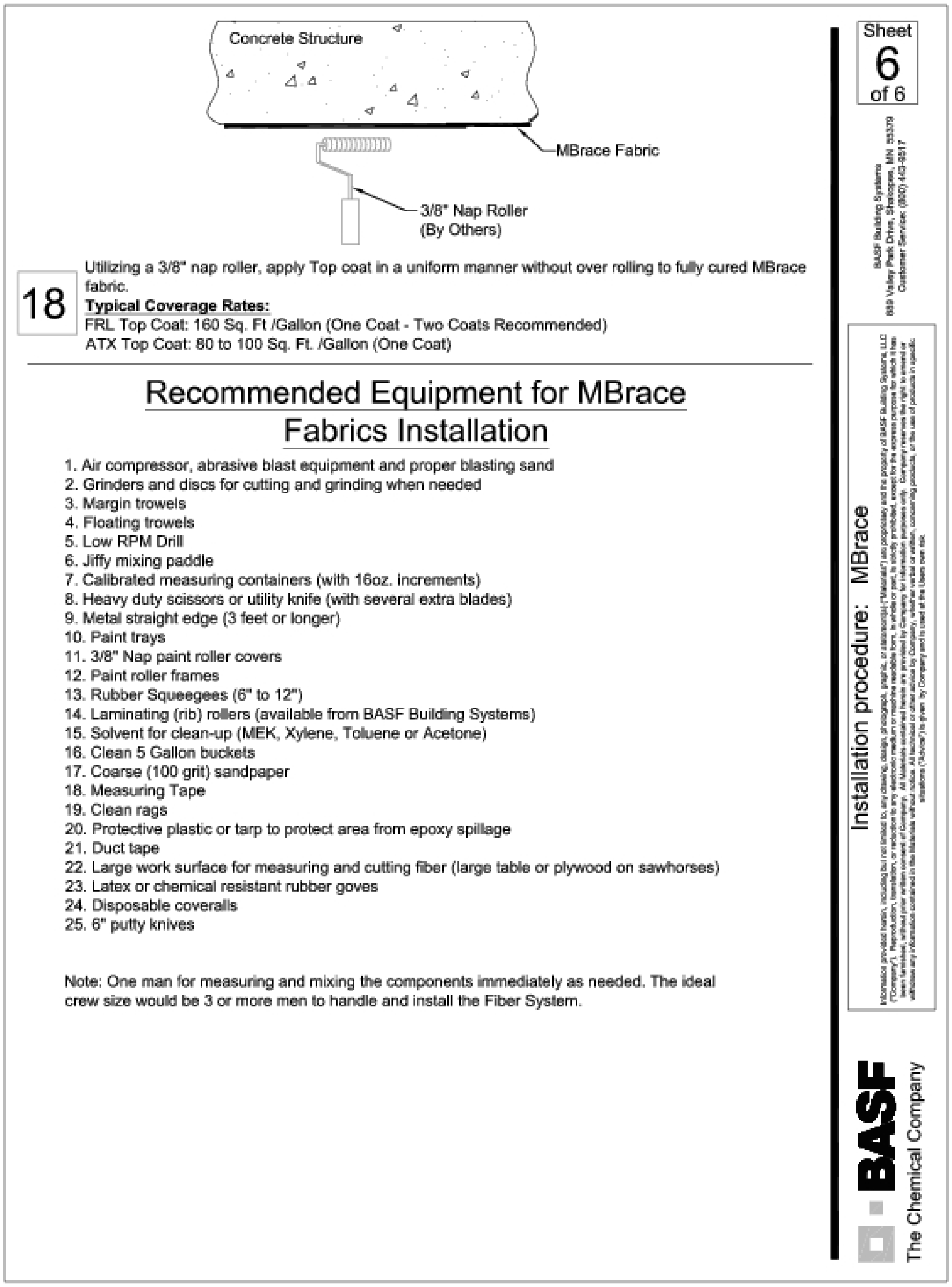
Concrete Structure
MBrace Fabric
3/8" Nap Roller
(By Others)

18

Utilizing a 3/8" nap roller, apply Top coat in a uniform manner without over rolling to fully cured MBrace fabric.

Typical Coverage Rates:
FRL Top Coat: 160 Sq. Ft /Gallon (One Coat - Two Coats Recommended)
ATX Top Coat: 80 to 100 Sq. Ft. /Gallon (One Coat)

Recommended Equipment for MBrace Fabrics Installation

1. Air compressor, abrasive blast equipment and proper blasting sand
2. Grinders and discs for cutting and grinding when needed
3. Margin trowels
4. Floating trowels
5. Low RPM Drill
6. Jiffy mixing paddle
7. Calibrated measuring containers (with 16oz. increments)
8. Heavy duty scissors or utility knife (with several extra blades)
9. Metal straight edge (3 feet or longer)
10. Paint trays
11. 3/8" Nap paint roller covers
12. Paint roller frames
13. Rubber Squeegees (6" to 12")
14. Laminating (rib) rollers (available from BASF Building Systems)
15. Solvent for clean-up (MEK, Xylene, Toluene or Acetone)
16. Clean 5 Gallon buckets
17. Coarse (100 grit) sandpaper
18. Measuring Tape
19. Clean rags
20. Protective plastic or tarp to protect area from epoxy spillage
21. Duct tape
22. Large work surface for measuring and cutting fiber (large table or plywood on sawhorses)
23. Latex or chemical resistant rubber goves
24. Disposable coveralls
25. 6" putty knives

Note: One man for measuring and mixing the components immediately as needed. The ideal crew size would be 3 or more men to handle and install the Fiber System.

Sheet
6
of 6

BASF Building Systems
889 Valley Park Drive, Shakopee, MN 55379
Customer Service: (800) 433-9517

Installation procedure: MBrace

Information provided herein, including but not limited to, any drawing, design, photograph, graphic, or statement(s) ("Materials") are proprietary and the property of BASF Building Systems, LLC ("Company"). Reproduction, translation, or reduction to any electronic medium or machine readable form, in whole or part, is strictly prohibited, except for the express purpose for which it has been furnished, without prior written consent of Company. All Materials contained herein are provided by Company for information purposes only. Company reserves the right to amend or withdraw any information contained in the Materials without notice. All technical or other advice by Company, whether verbal or written, concerning products, or the use of products in specific situations ("Advice") is given by Company and is used at the Users own risk.

BASF
The Chemical Company

Figure A.39 Application instructions page 6.

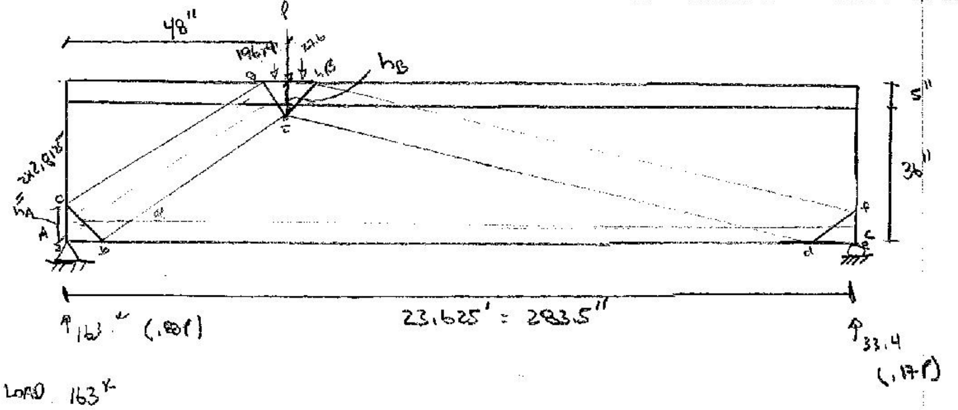
48"
P
196.4k
22.6
6.6
hB
a
e
5"
36"
232.8185
hA
A
c
b
d
f
e
163 k (.83P)
23.625' = 283.5"
33.4
(.17P)

LOAD 163^k

Plate 8 inches

Self Weight (neglect) $V = \frac{wL}{2} = \frac{.384(23.625)}{2} = 4.536^k$

Nodal Zone

Node A (C-C-T Node)

$f_{ce} = .85 \beta_n f'_c$

$= .85(.8)(7100) = 4828$ psi

NODE B (C-C-C Node)

$f_{ce} = .85 \beta_n f'_c = .85(1.0)(7100) = 6035$ psi

NODE C (C-C-T Node)

$f_{ce} = .85 \beta_n f'_c$

$= (.85)(.8)(7100) = 4828$ psi

Moment

$M = 196.4^k (48") = 9427.2$ k-in at loading plane

$M = F \times$ lever ARM

2

AT Node B horizontal Force

$F = 6035\,psi\,(h_B)(t) = 6035\,psi\,(h_B)(6\,in) = 36{,}210\ h_B\ (K/in)$

M = F X lever ARM

$9427.2\ K\text{-}in = 36.210\ h_B\left(41 - 2.8125 - \frac{h_B}{2}\right)$

$h_B = 7.57\ in.$

Force in tie AC

$$F = \overset{\sigma}{6035}\,(\overset{h}{7.57})(\overset{t}{6}) = 274.0\,K$$

(compare w/ capacity of prestressing steel)

Initial
Angle of STRUT α_{AB}

$\frac{6035\,psi}{6}$

$163K = 6035(6)(w_t)$
$w_t = 4.5$

$$\alpha = \tan^{-1}\left(\frac{41 - \frac{7.57}{2} - 2.8125}{48 - 4 - \frac{8}{2}}\right) = 46.687$$

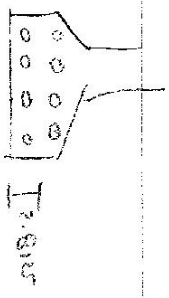

163

Therefore force in Diagonal STRUTS

$$\sin 39.49 = \frac{163}{F_{AB}}$$

$F_{AB} = 256.3\ K$

Angle of STRUT β_{CB}

$$\beta = \tan^{-1}\left(\frac{41 - \frac{5.51}{2} - 2.8125}{23.5.5}\right) = 8.56\,0$$

Therefore force in Diagonal STRUT CB

$$\sin 8.56 = \frac{33.4}{F_{CB}} =$$

$F_{CB} = 224.39\ K$

Check strength of nodal zones

Nodal zone A

Face ac (should be satisfied)

$F = .85\beta_n f'_c A_{nz}$

$= .85(.8)(7100)(8)(5.625) = 217.26^K$

Face ab

$F = .85\beta_n f'_c A_{nz}$ width of plate

$= .85(.8)(7100)(8)(8) = 309^K$ ^{K}

Reaction support $163^K < 309^K \therefore$ OK

check diagonal strut

$F^{AB} = f_{ce} A_{cs}$

.6 (without reinforcement satisfying ACI A 3.3)

$f_{ce} = .85\beta_s f'_c$

$= .85(.6)(7100) = 3621$ psi

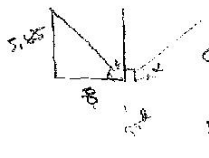

$c = \sqrt{5.625^2 + 8^2} = 9.78$ in

$F_{AB} = 3621(9.78\text{ in})(6\text{ in}) = 212.5$ kips

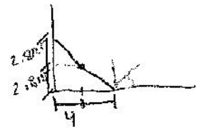

$\sin(39.49) = \frac{\text{REACTION}}{\text{STRUT}}$

STRUT FORCE = $\frac{163}{\sin 40.697}$

= 249.97K

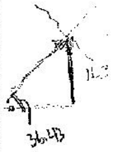

Reaction = $\sin 40.697(212.5)$ = $\underline{\underline{138.56^{K}}}$

W/ minimum Reinforcement

$f_{ce} = .85(.75)(7100) = 4526$ psi

$F_{AB} = 4526(9.78)(6) = 265.6^{K}$

Reaction = $\sin(36.43)(265.6) = \underline{\underline{157.7^{K}}}$

APPENDIX B

Load vs. Strain and Load vs. Deflection Charts

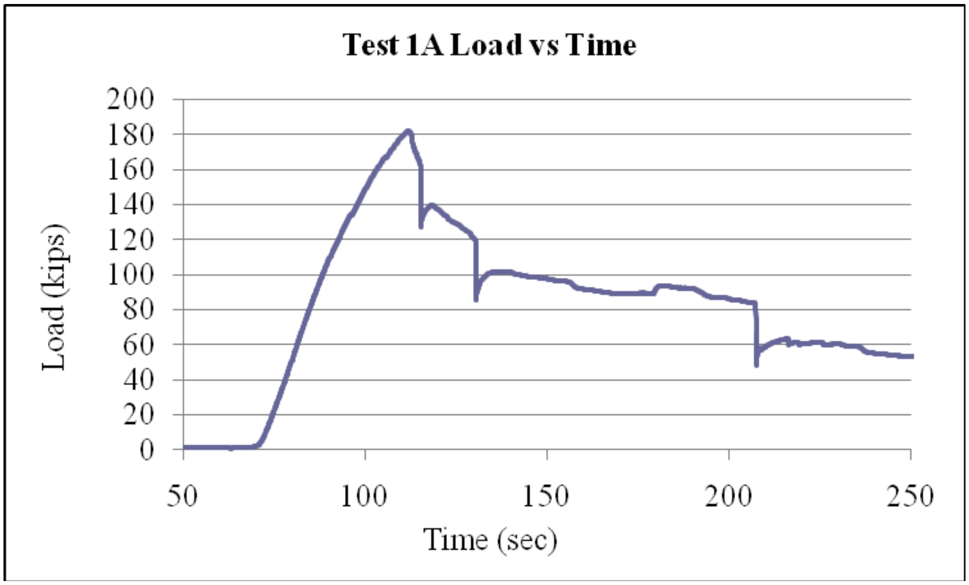

Figure B.1 Test 1A Load vs Time.

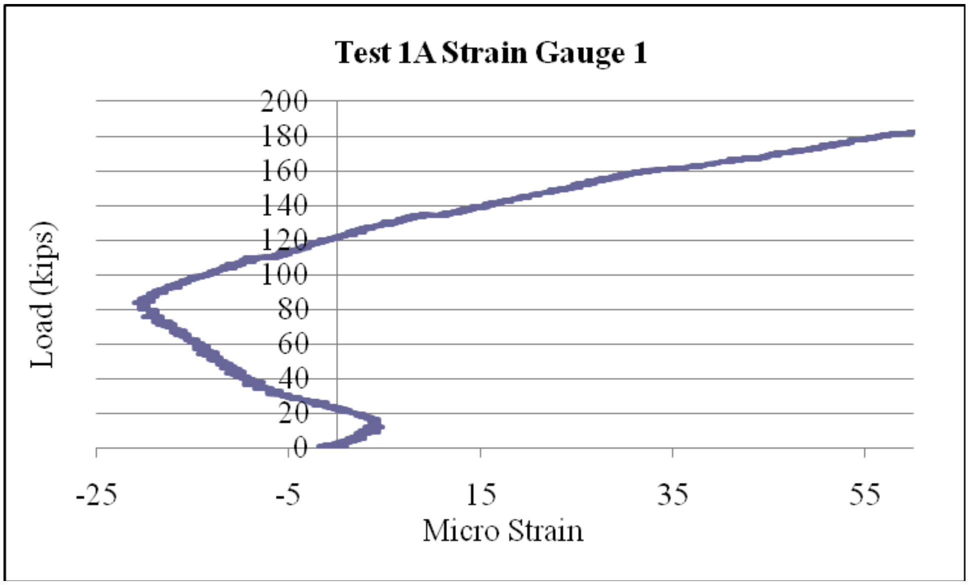

Figure B.2 Test 1A Strain Gauge 1.

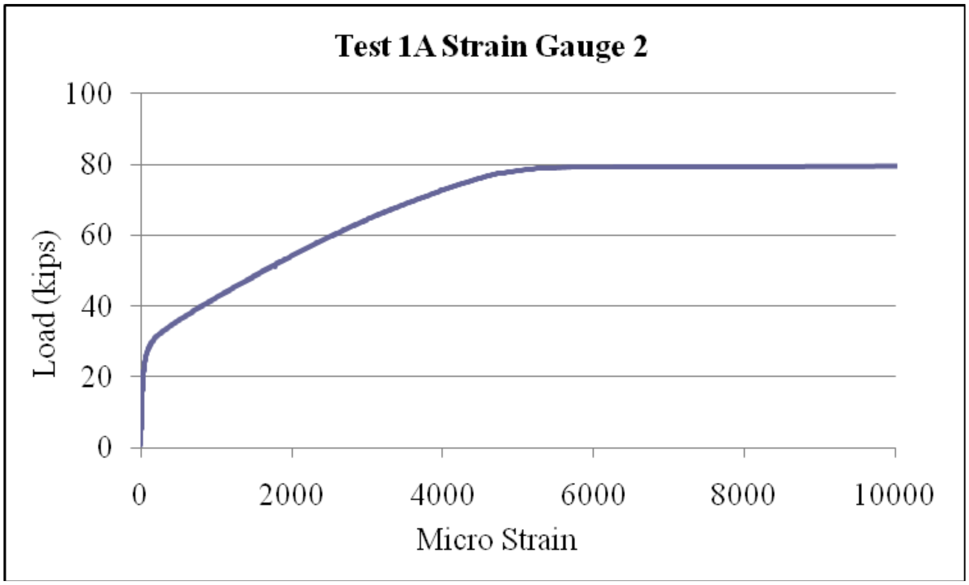

Figure B.3 Test 1A Strain Gauge 2.

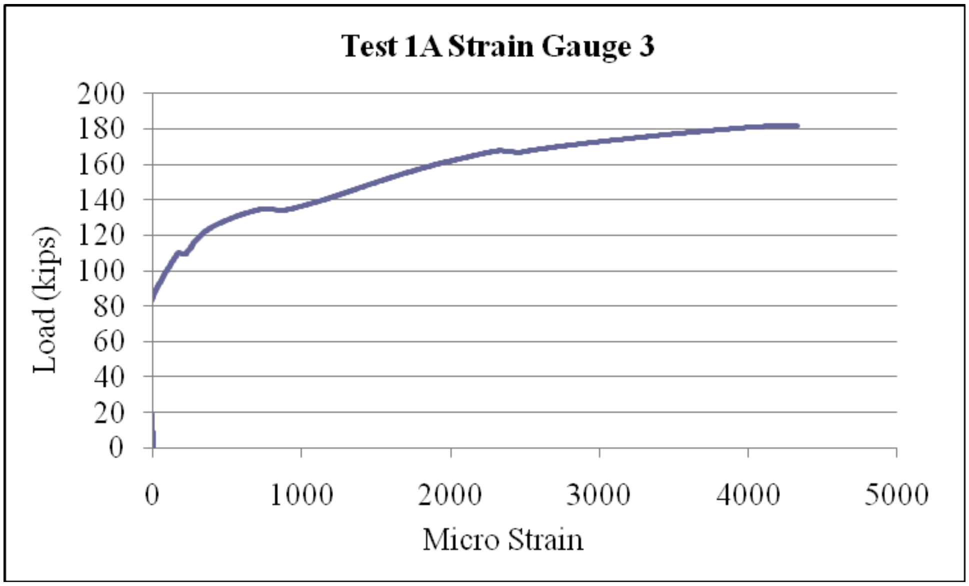

Figure B.4 Test 1A Strain Gauge 3.

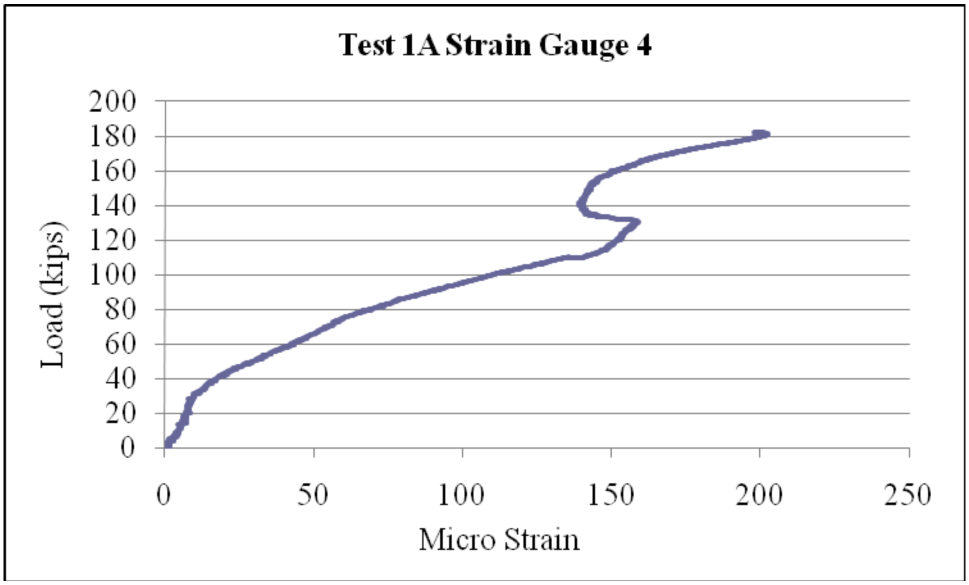

Figure B.5 Test 1A Strain Gauge 4.

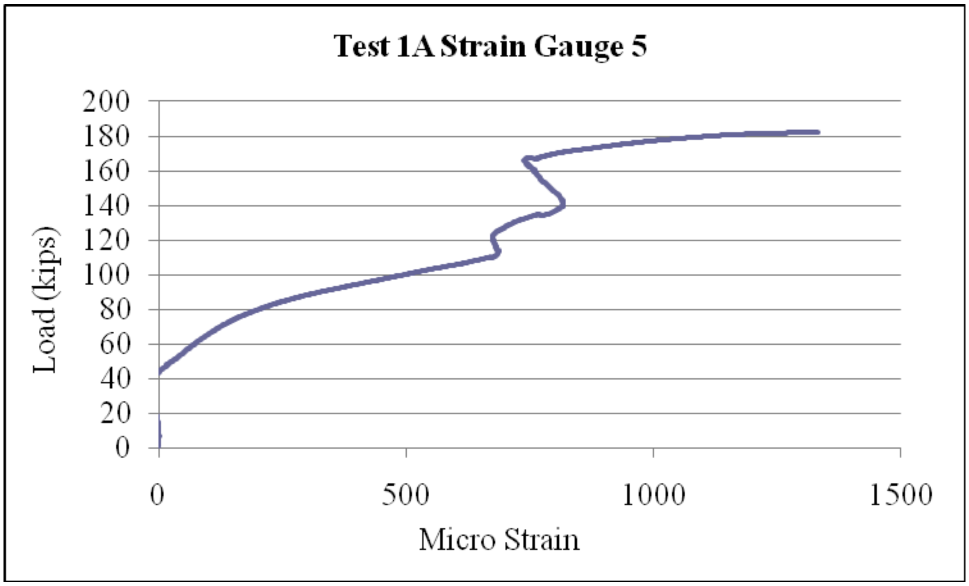

Figure B.6 Test 1A Strain Gauge 5.

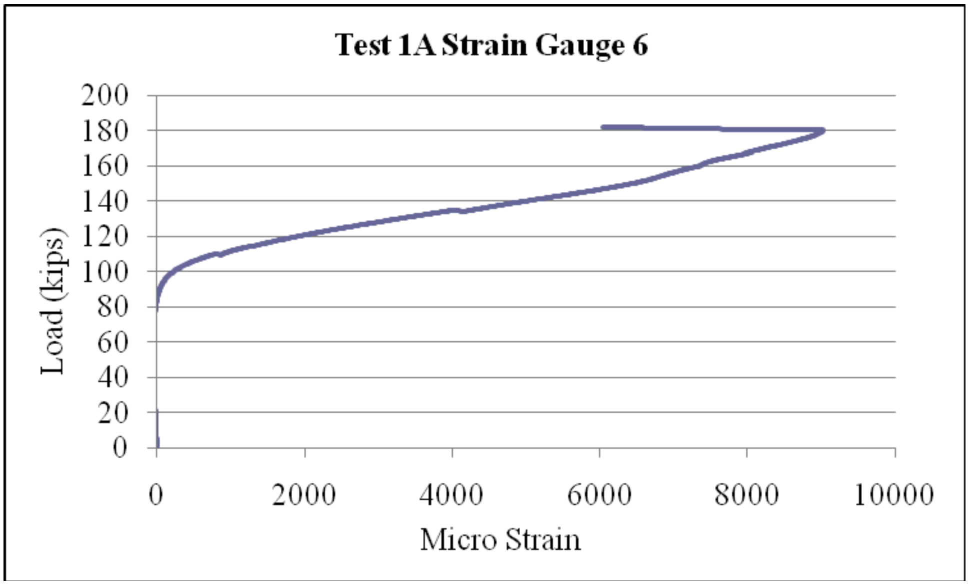

Figure B.7 Test 1A Strain Gauge 6.

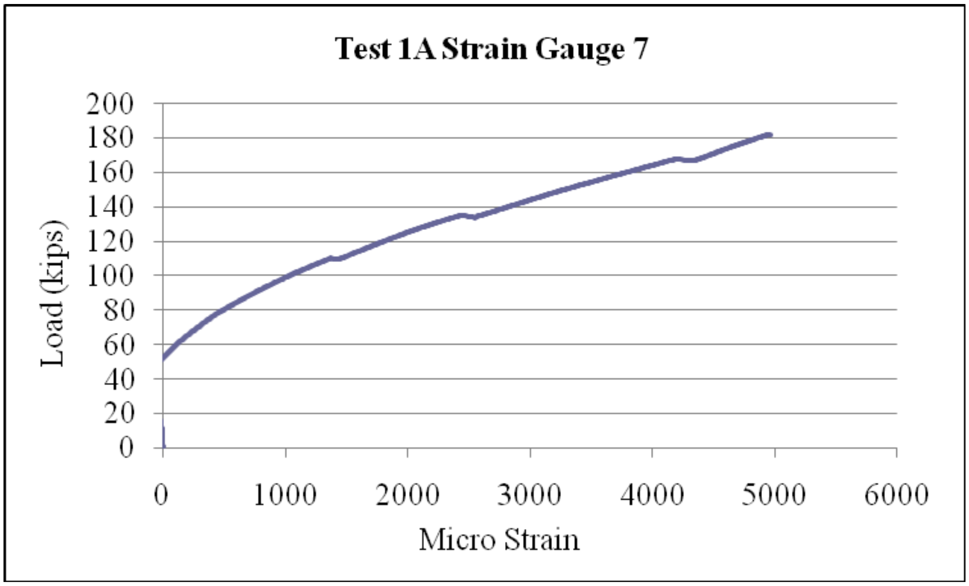

Figure B.8 Test 1A Strain Gauge 7.

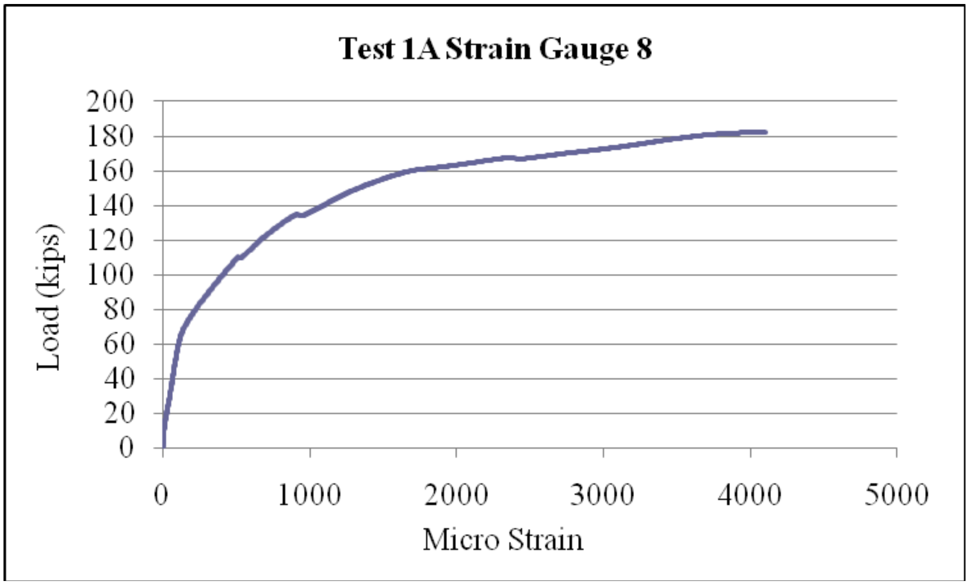

Figure B.9 Test 1A Strain Gauge 8.

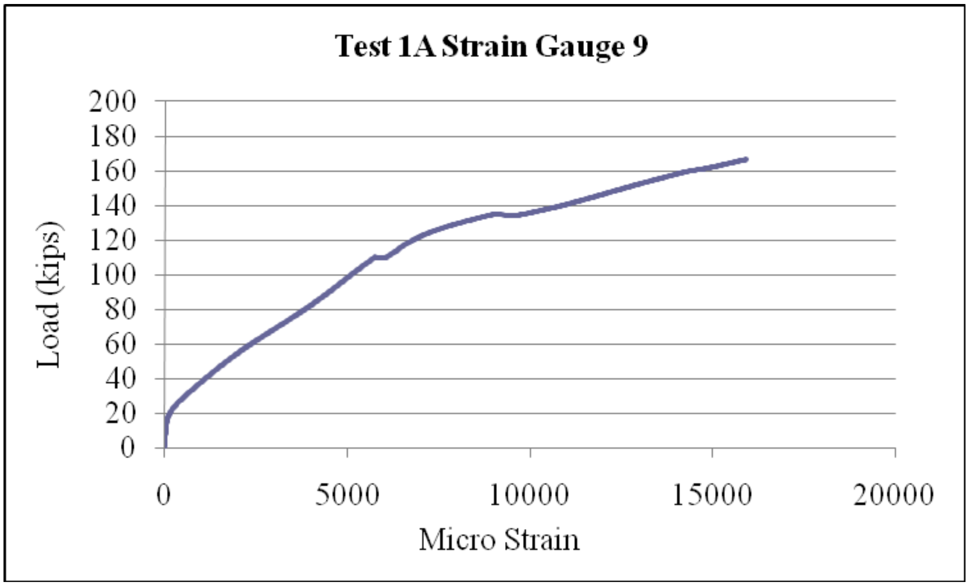

Figure B.10 Test 1A Strain Gauge 9.

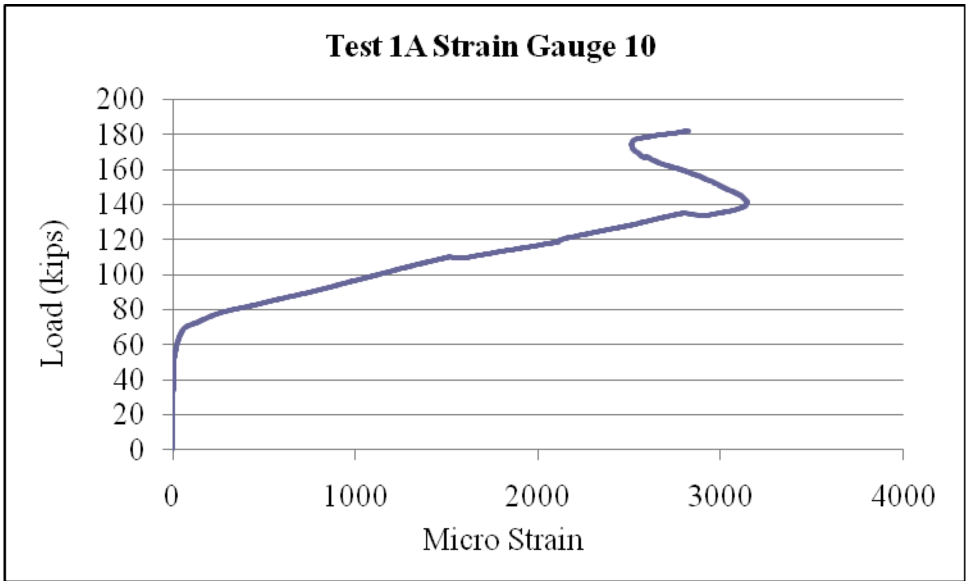

Figure B.11 Test 1A Strain Gauge 10.

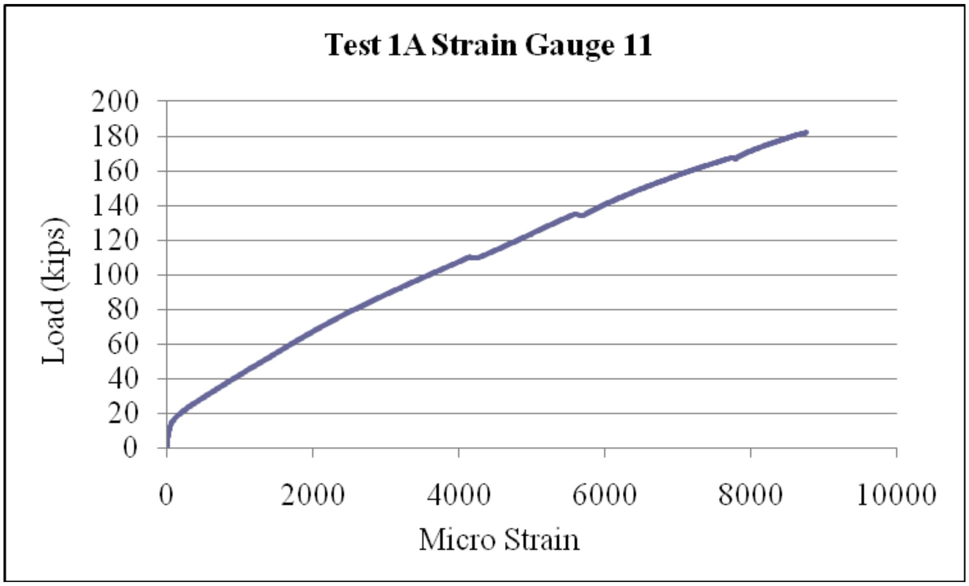

Figure B.12 Test 1A Strain Gauge 11.

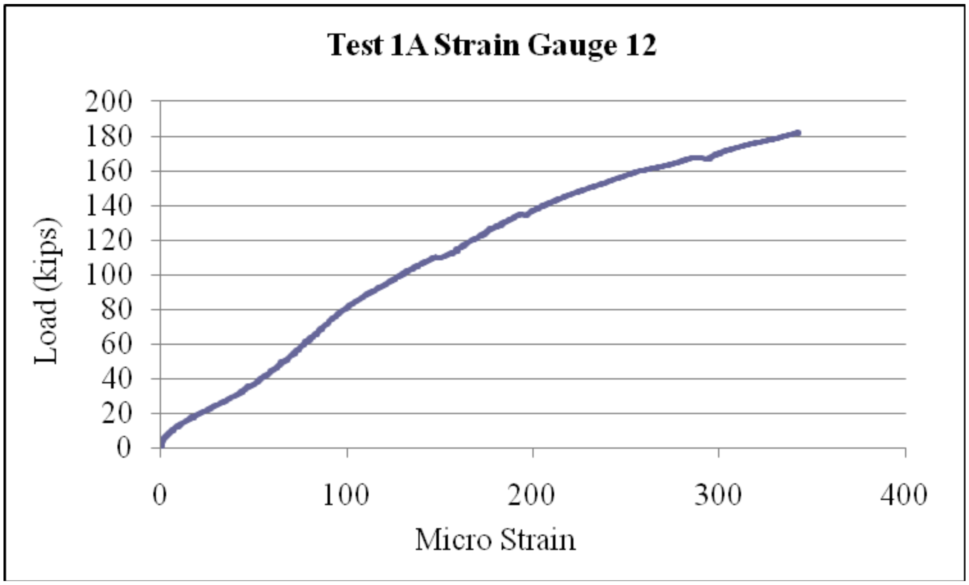

Figure B.13 Test 1A Strain Gauge 12.

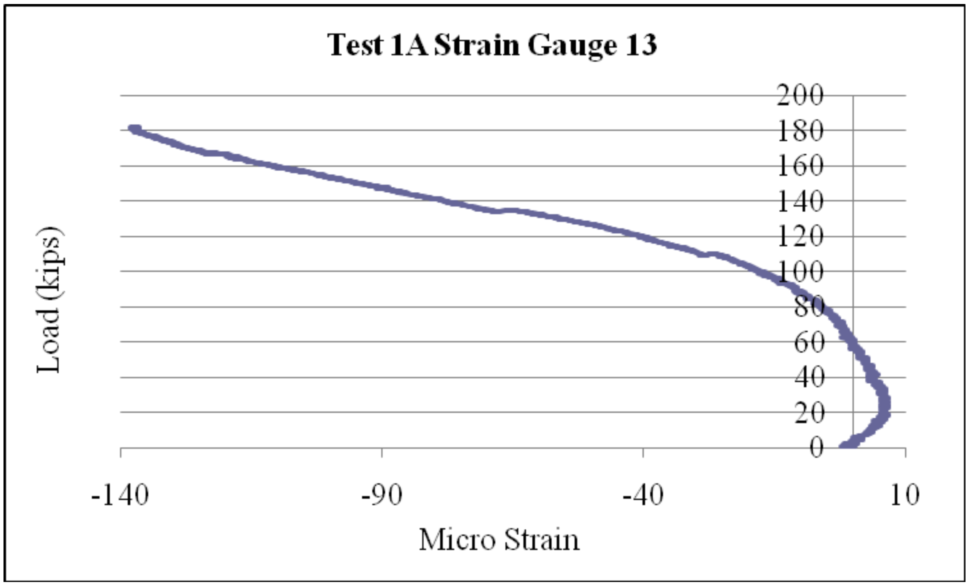

Figure B.14 Test 1A Strain Gauge 13.

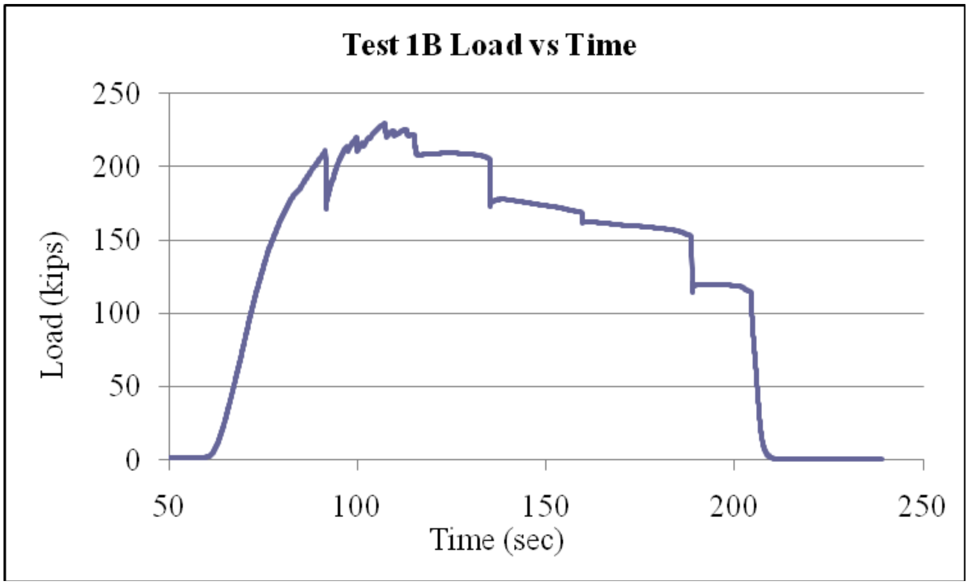

Figure B.15 Test 1B Load vs Time.

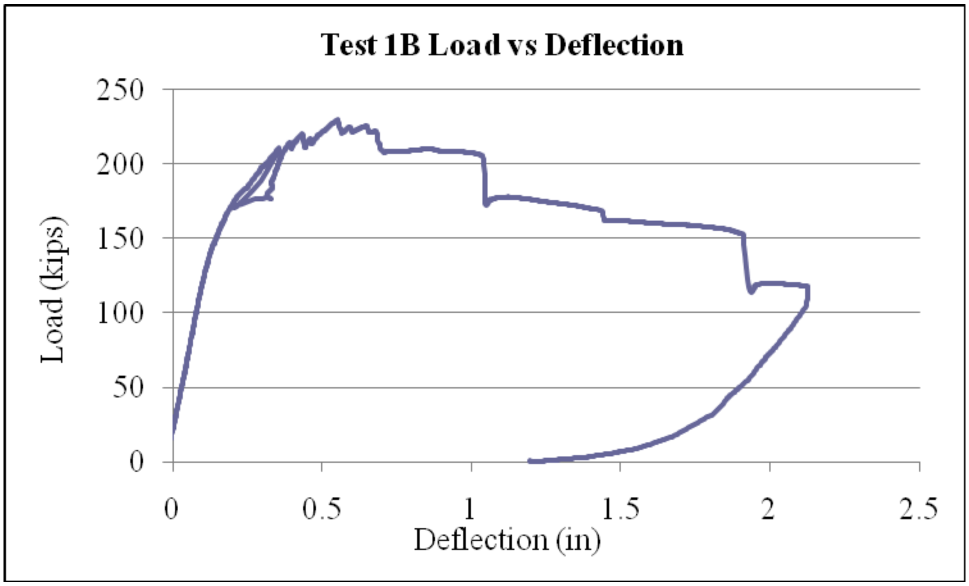

Figure B.16 Test 1B Load vs Deflection.

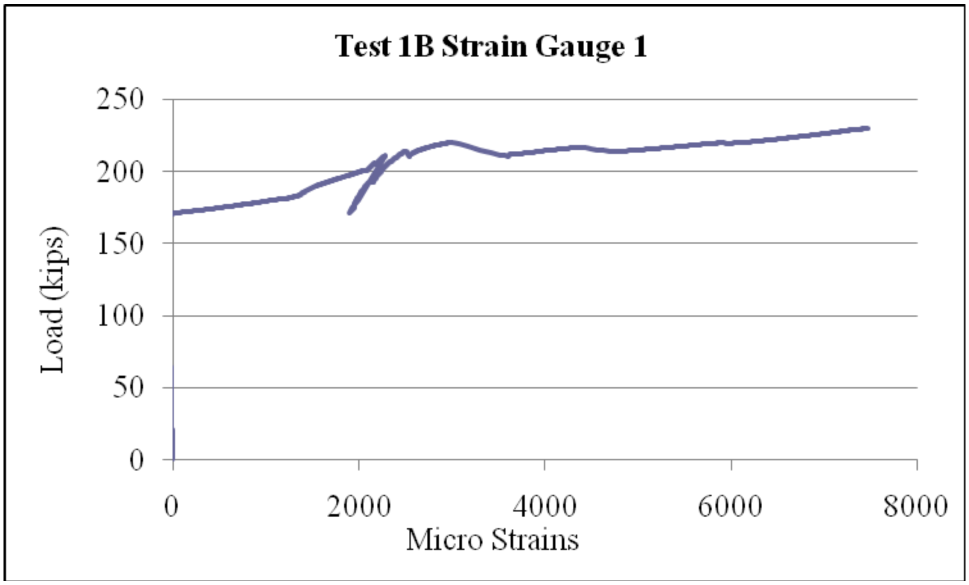

Figure B.17 Test 1B Strain Gauge 1.

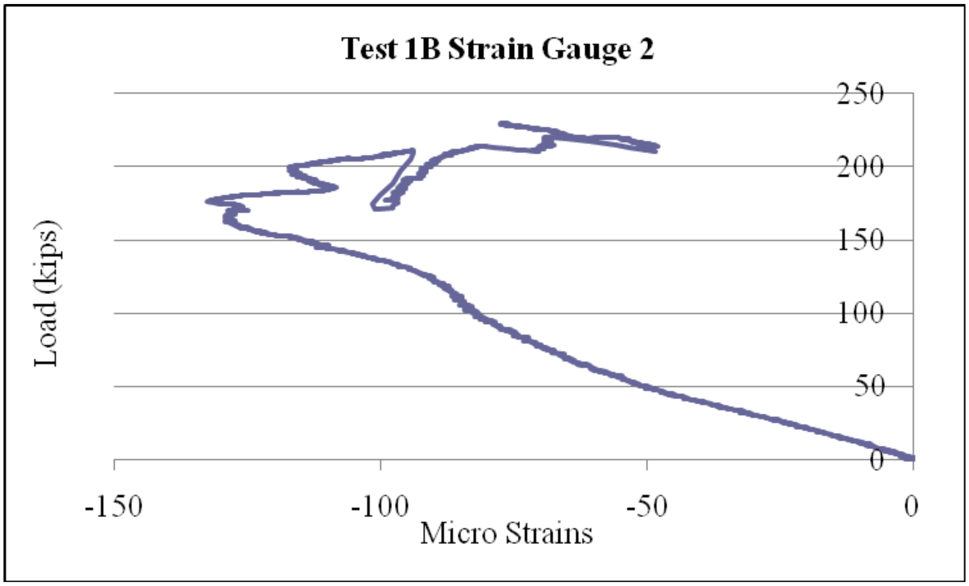

Figure B.18 Test 1B Strain Gauge 2.

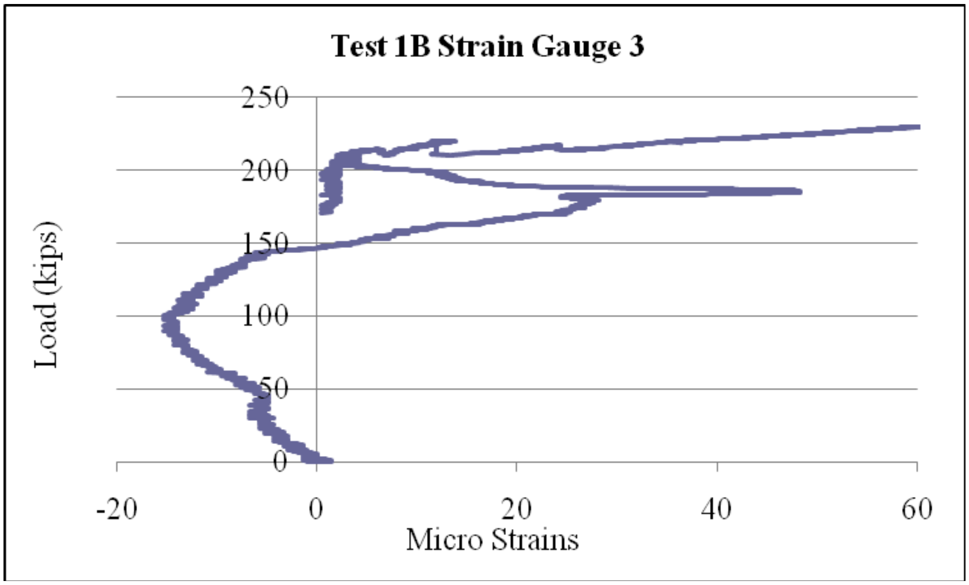

Figure B.19 Test 1B Strain Gauge 3.

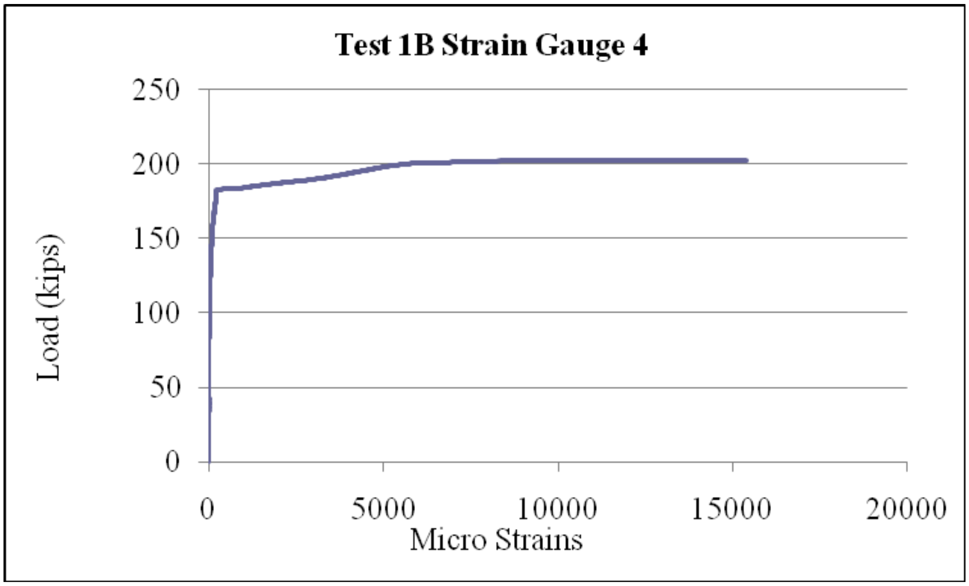

Figure B.20 Test 1B Strain Gauge 4.

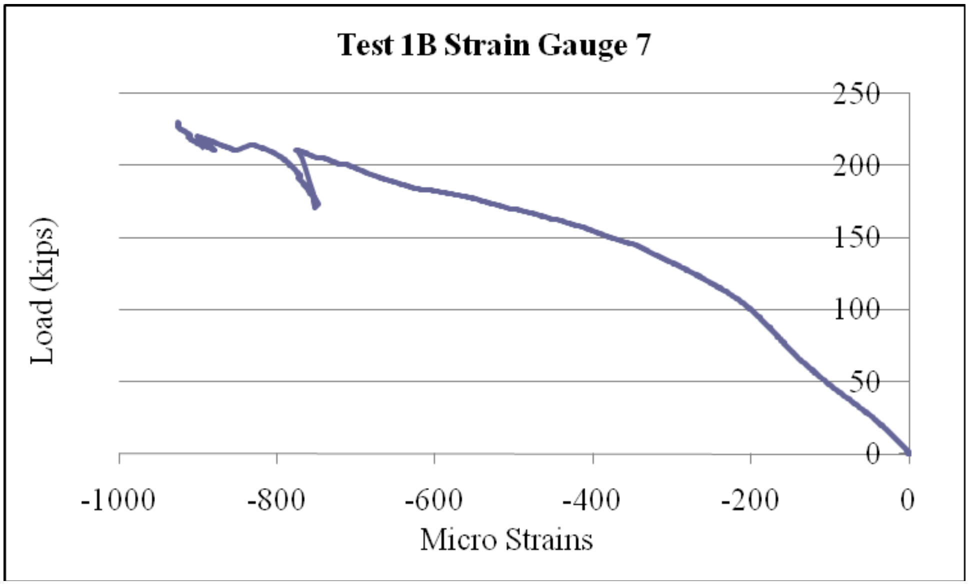

Figure B.21 Test 1B Strain Gauge 7.

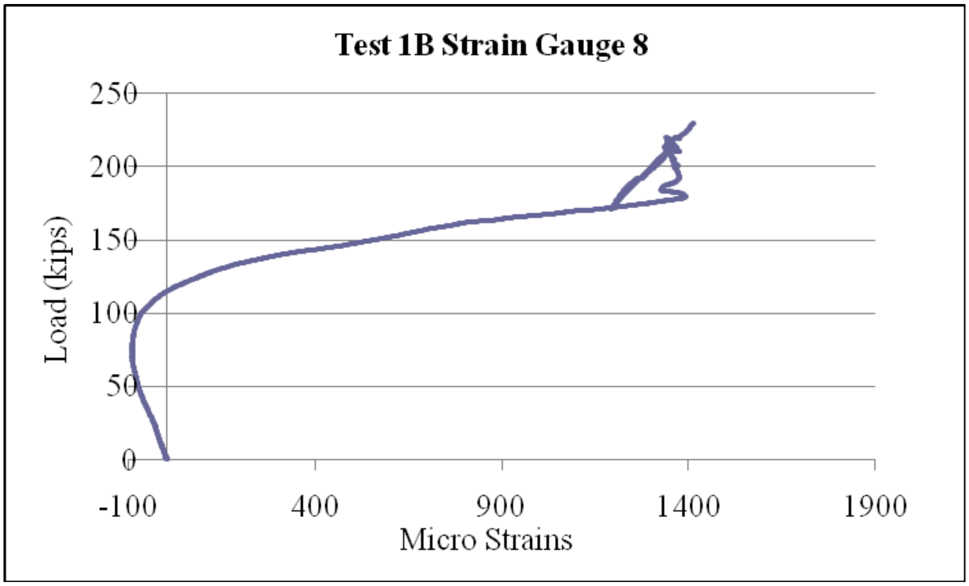

Figure B.22 Test 1B Strain Gauge 8

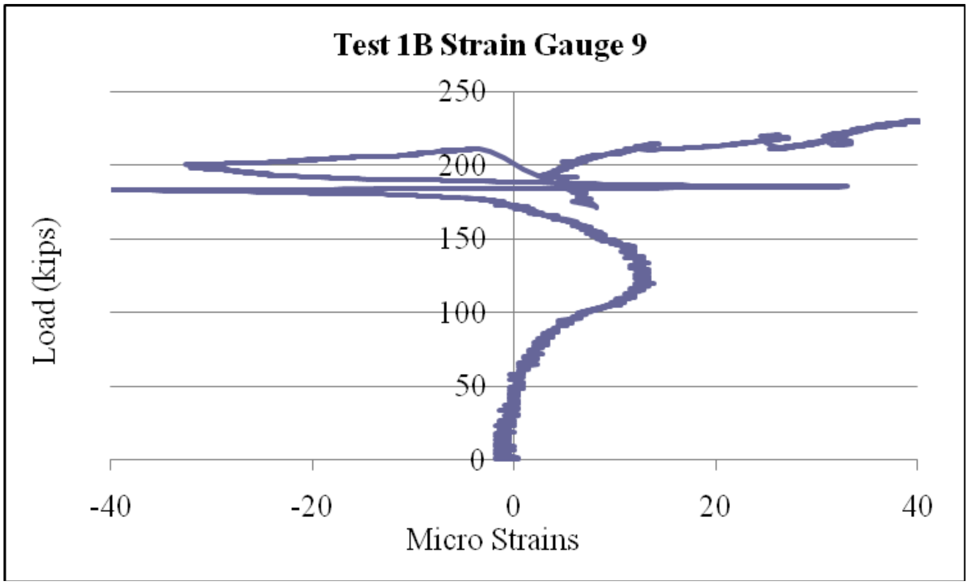

Figure B.23 Test 1B Strain Gauge 9.

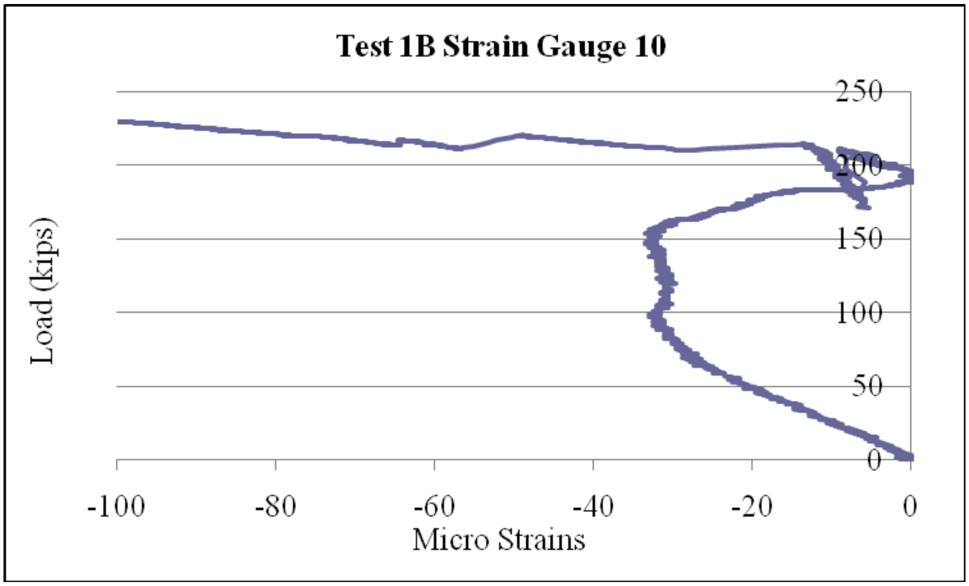

Figure B.24 Test 1B Strain Gauge 10.

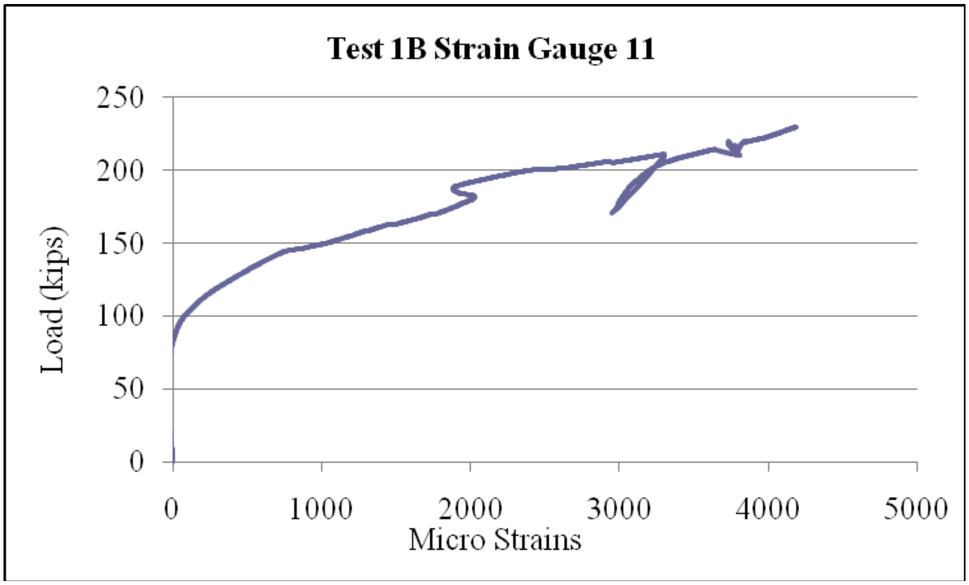

Figure B.25 Test 1B Strain Gauge 11

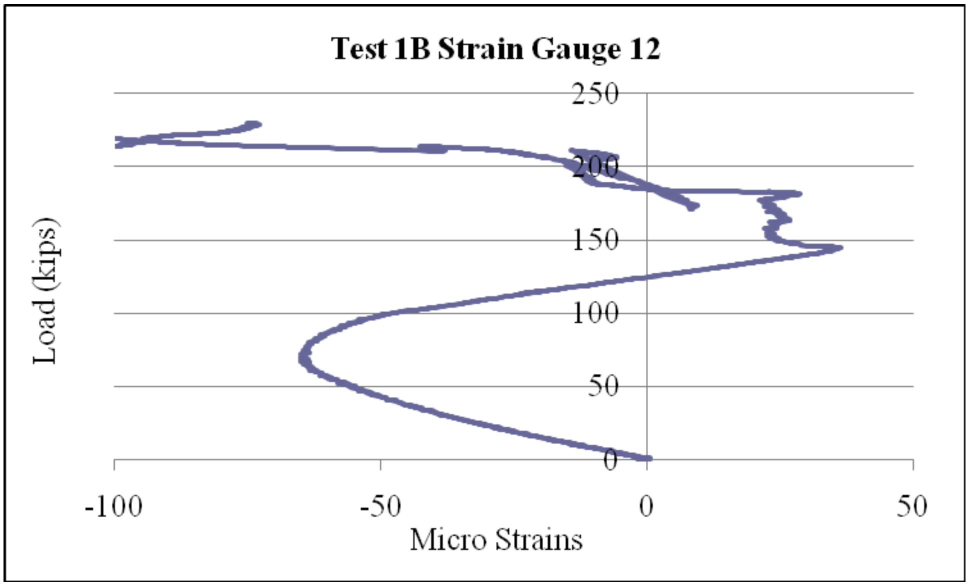

Figure B.26 Test 1B Strain Gauge 12.

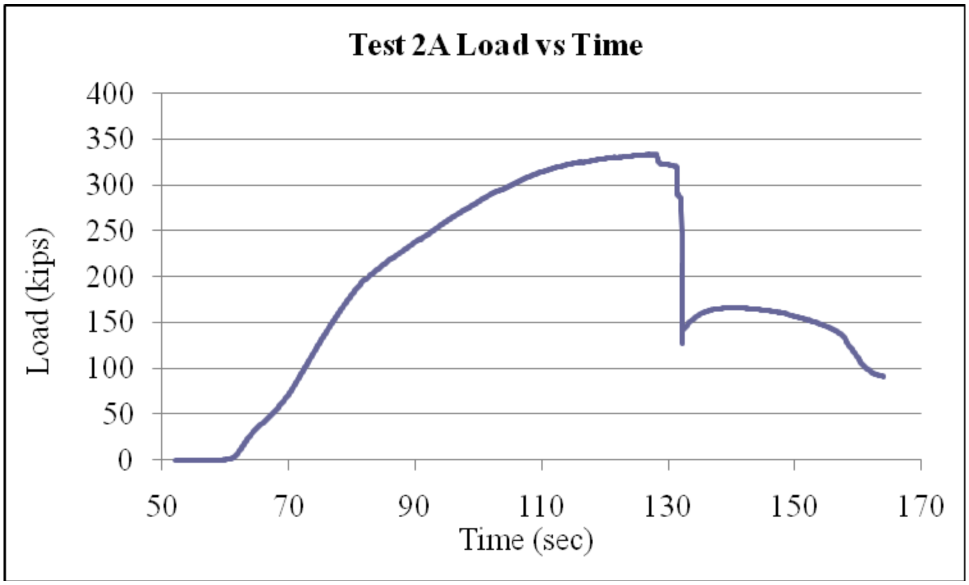

Figure B.27 Test 2A Load vs Time.

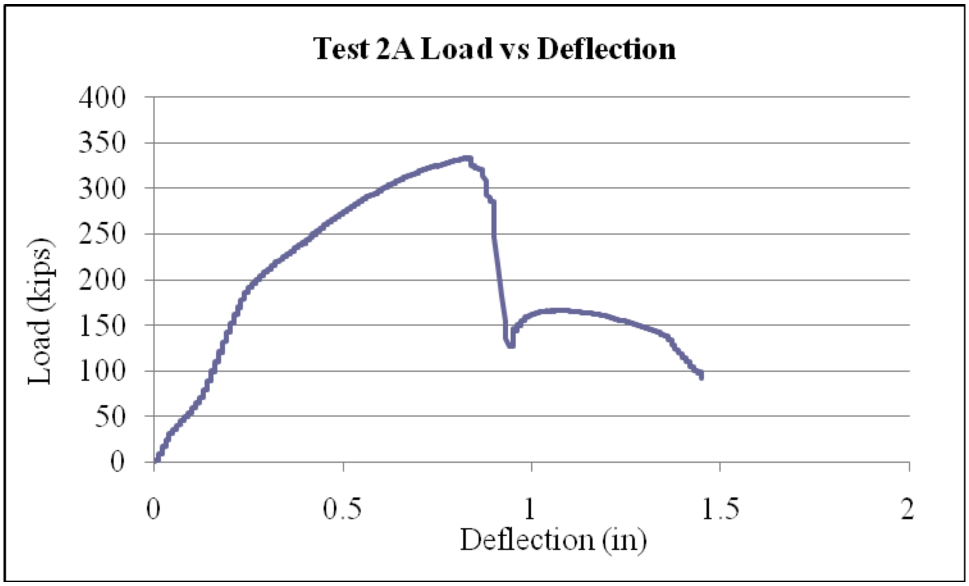

Figure B.28 Test 2A Load vs Deflection.

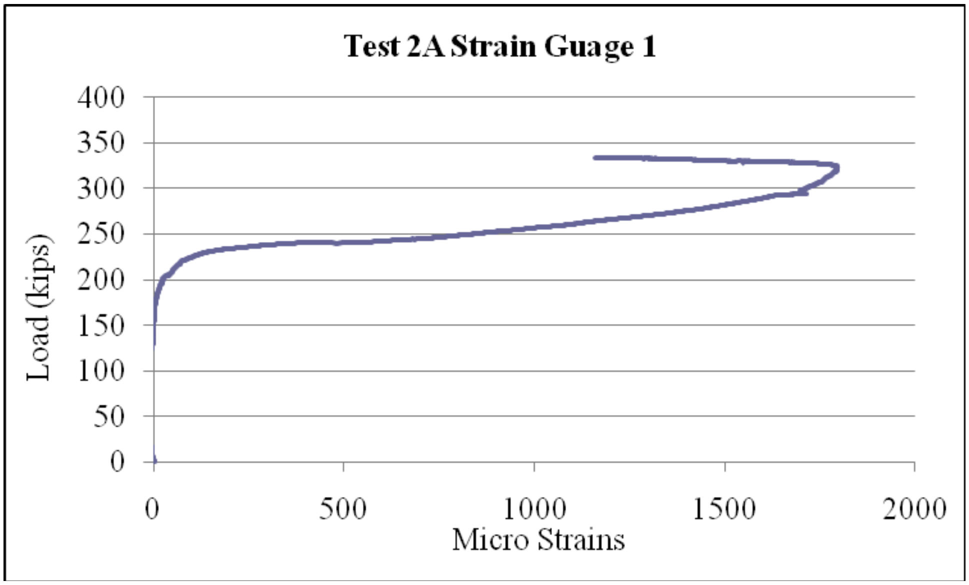

Figure B.29 Test 2A Strain Gauge 1.

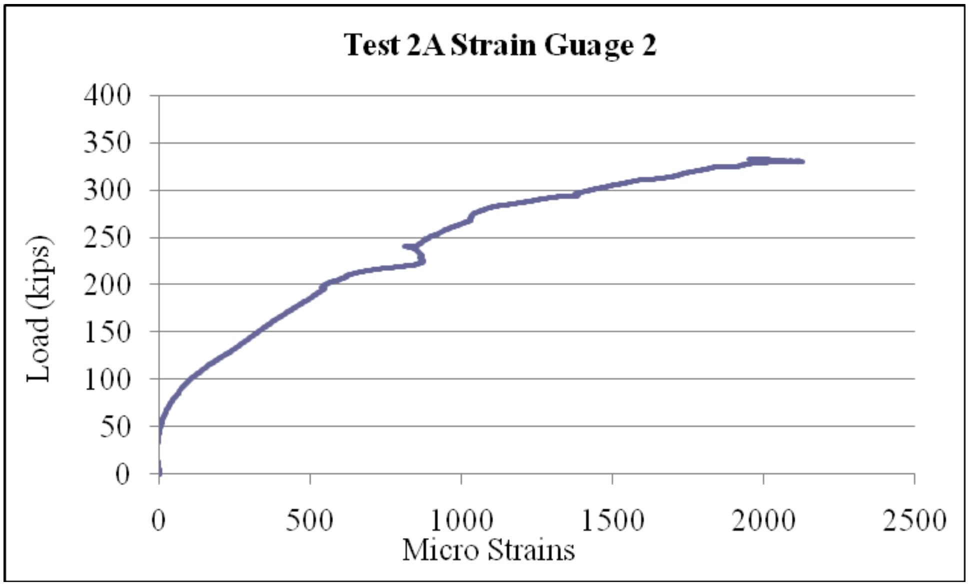

Figure B.30 Test 2A Strain Gauge 2.

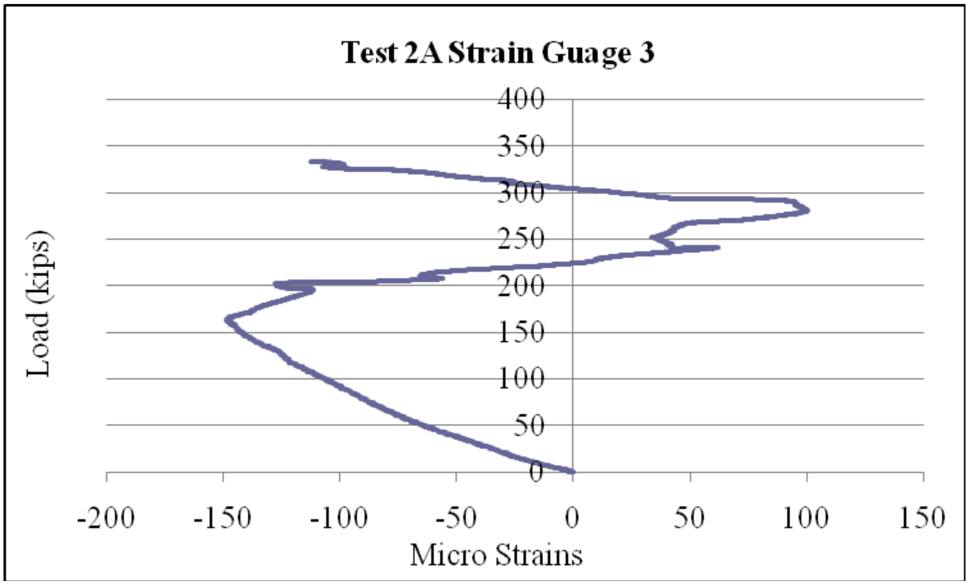

Figure B.31 Test 2A Strain Gauge 3.

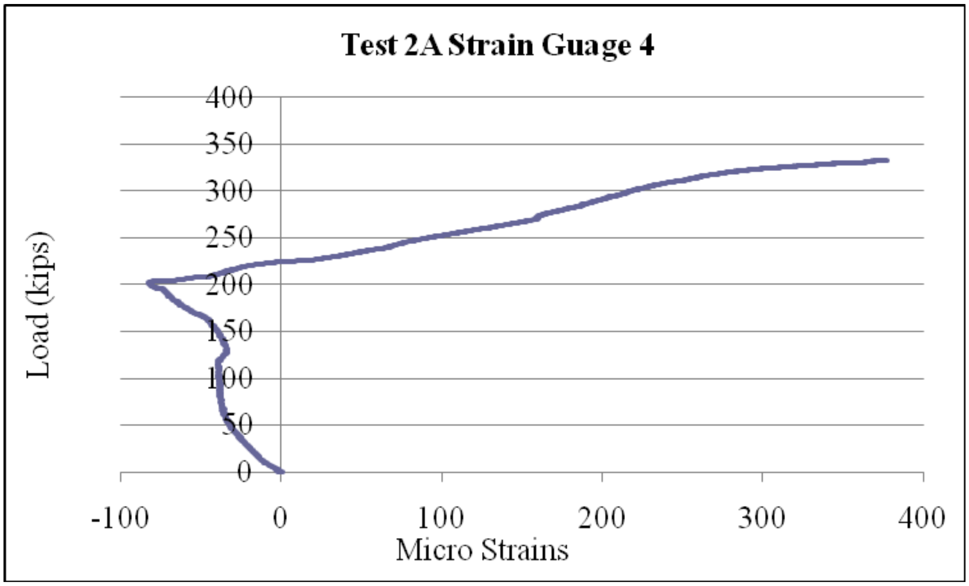

Figure B.32 Test 2A Strain Gauge 4.

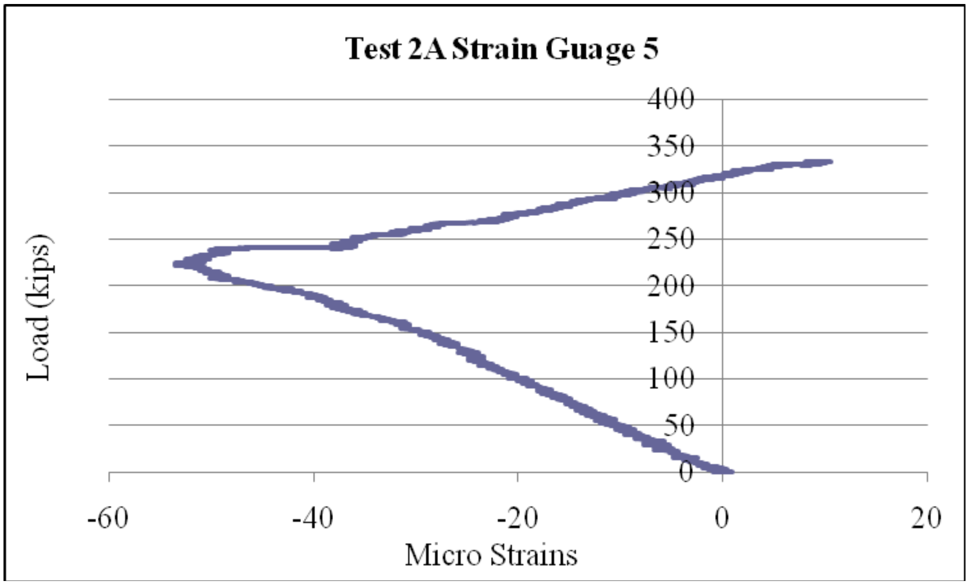

Figure B.33 Test 2A Strain Gauge 5.

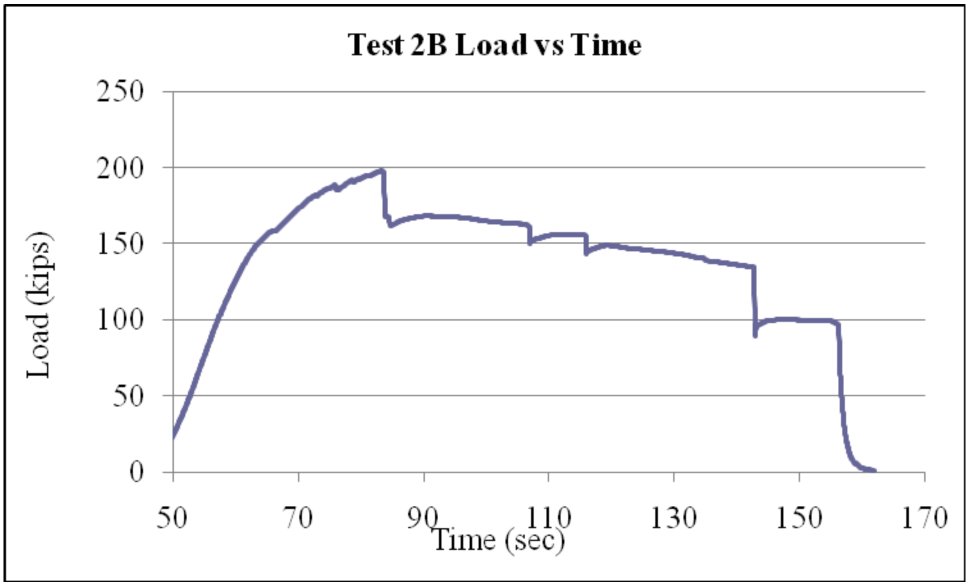

Figure B.34 Test 2B Load vs Time.

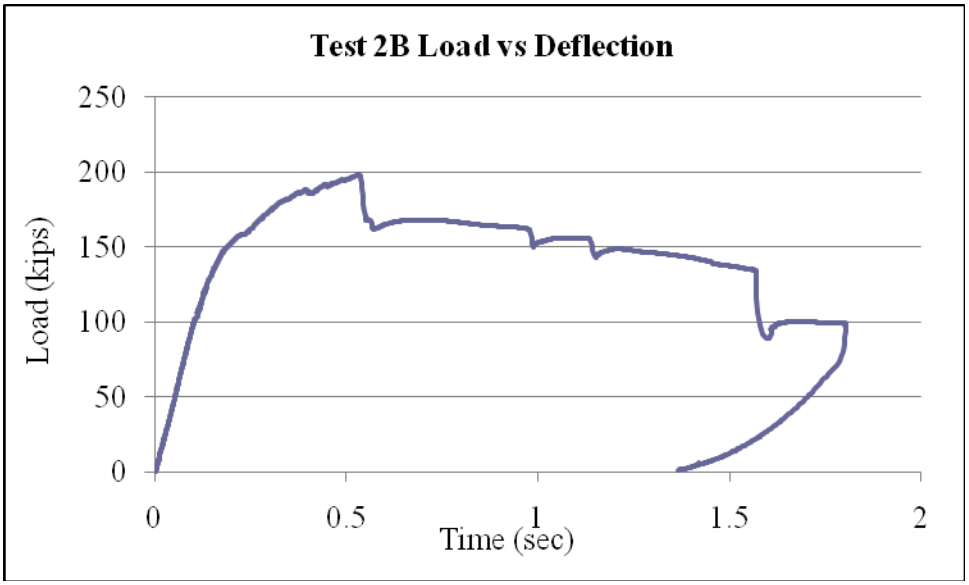

Figure B.35 Test 2B Load vs Deflection.

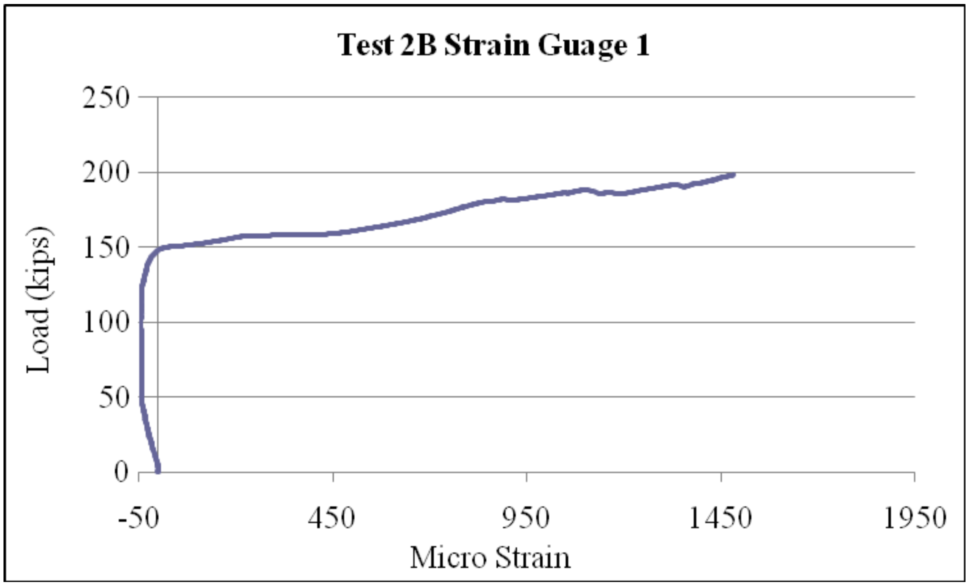

Figure B.36 Test 2B Strain Gauge 1.

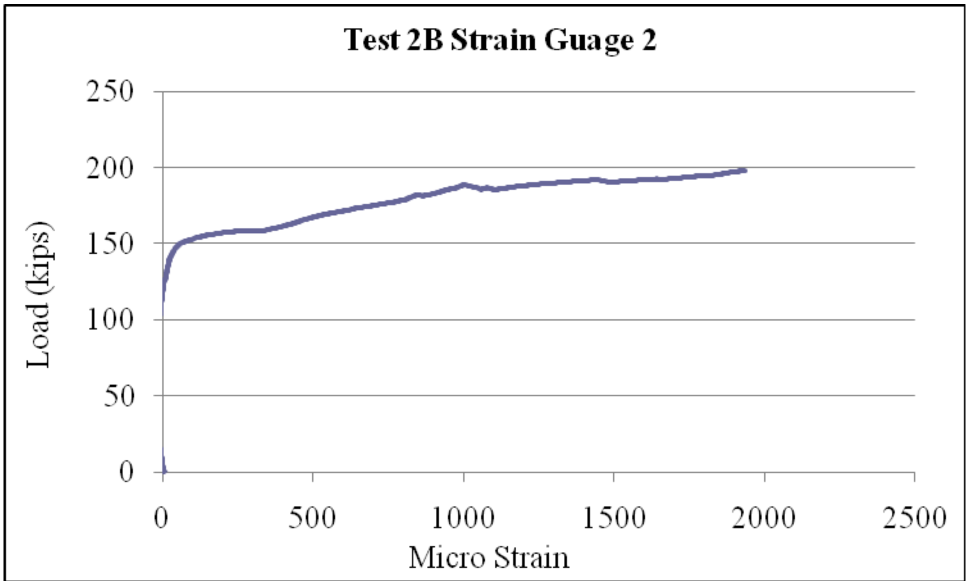

Figure B.37 Test 2B Strain Gauge 2.

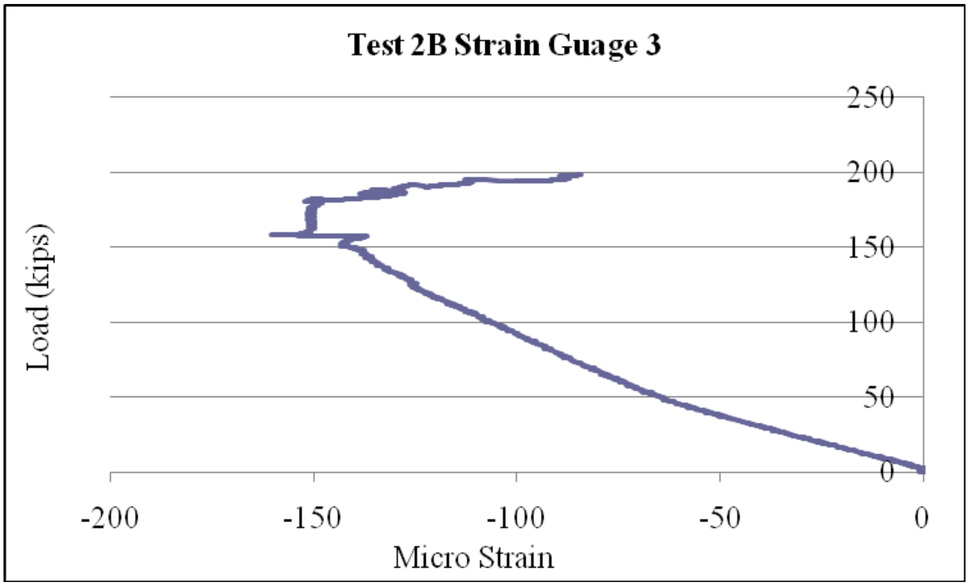

Figure B.38 Test 2B Strain Gauge 3.

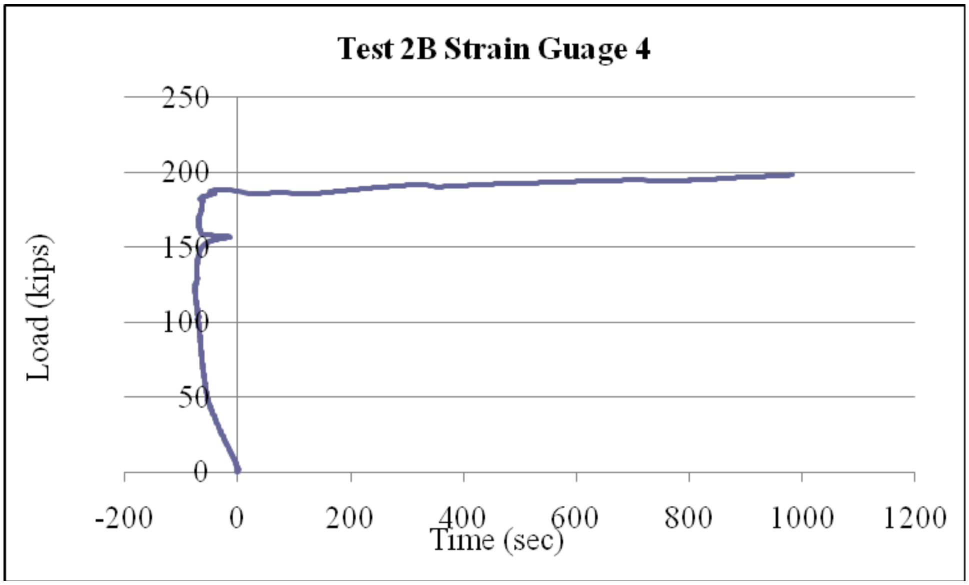

Figure B.39 Test 2B Strain Gauge 4.

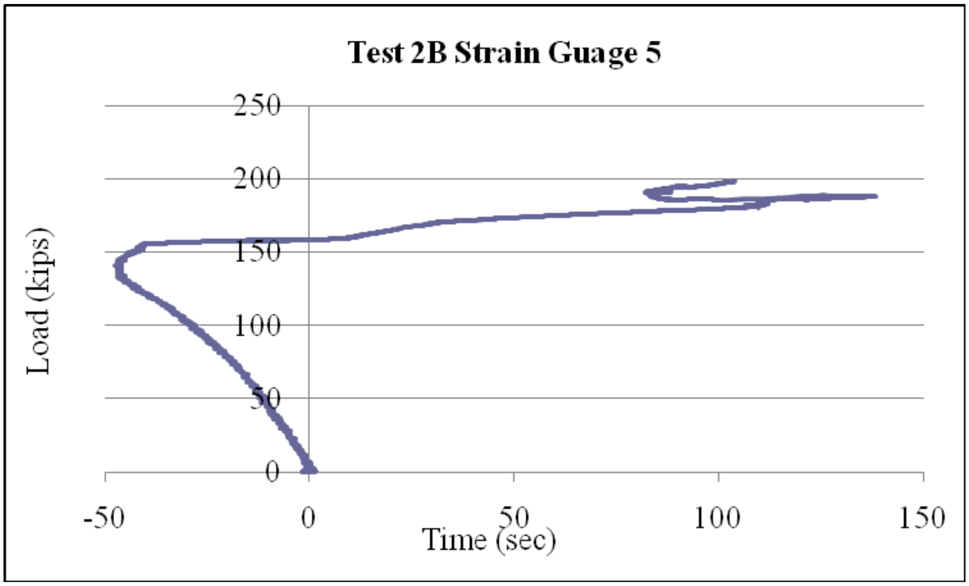

Figure B.40 Test 2B Strain Gauge 5.

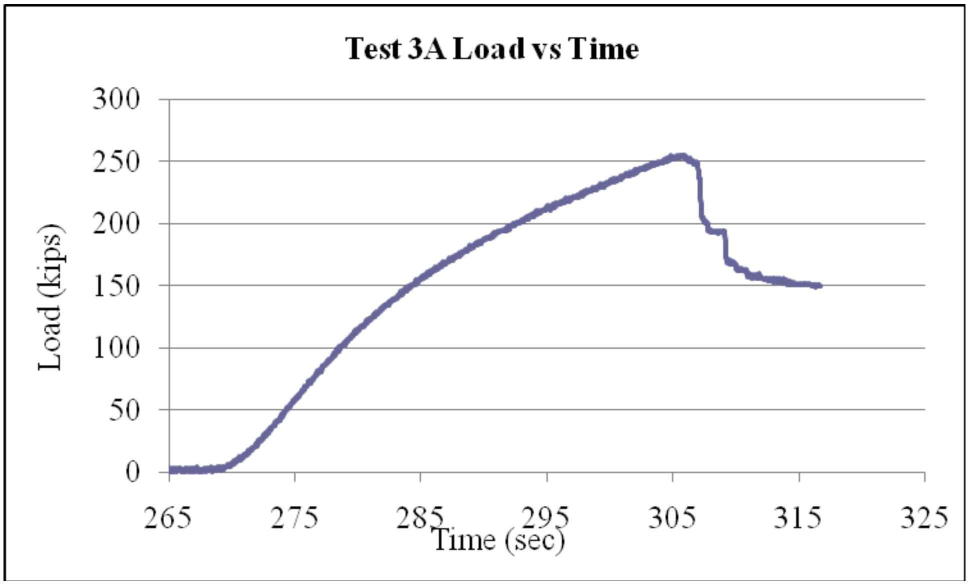

Figure B.41 Test 3A Load vs Time.

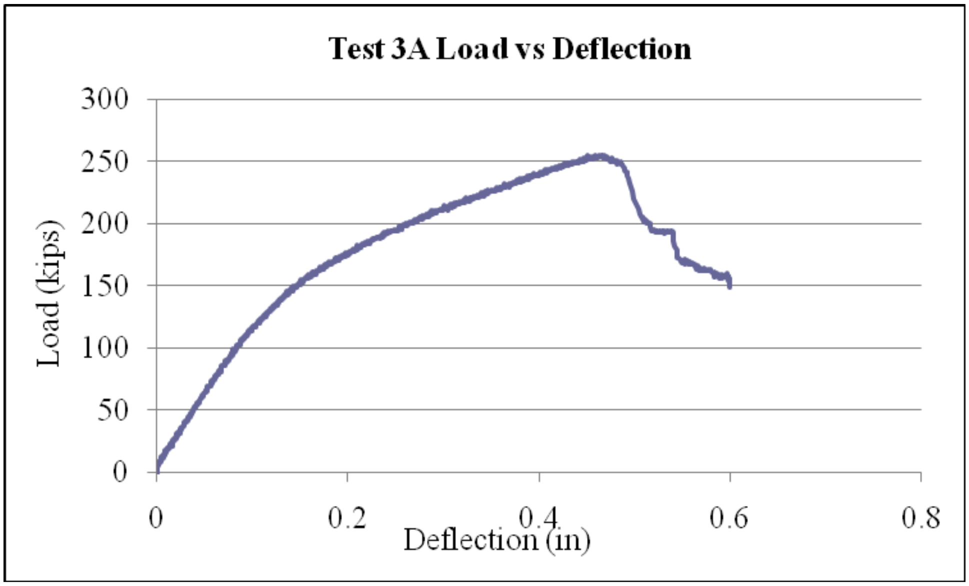

Figure B.42 Test 3A Load vs Deflection.

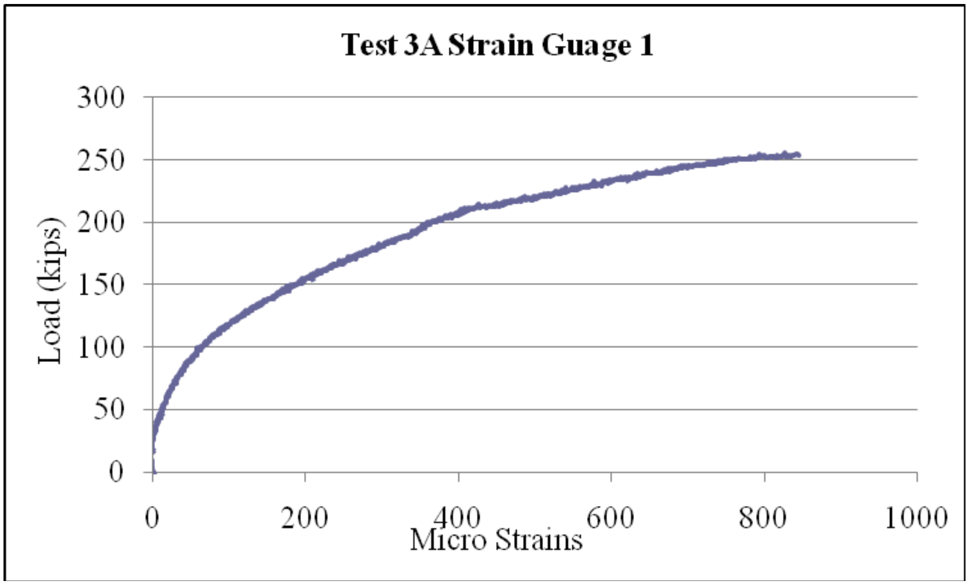

Figure B.43 Test 3A Strain Gauge 1.

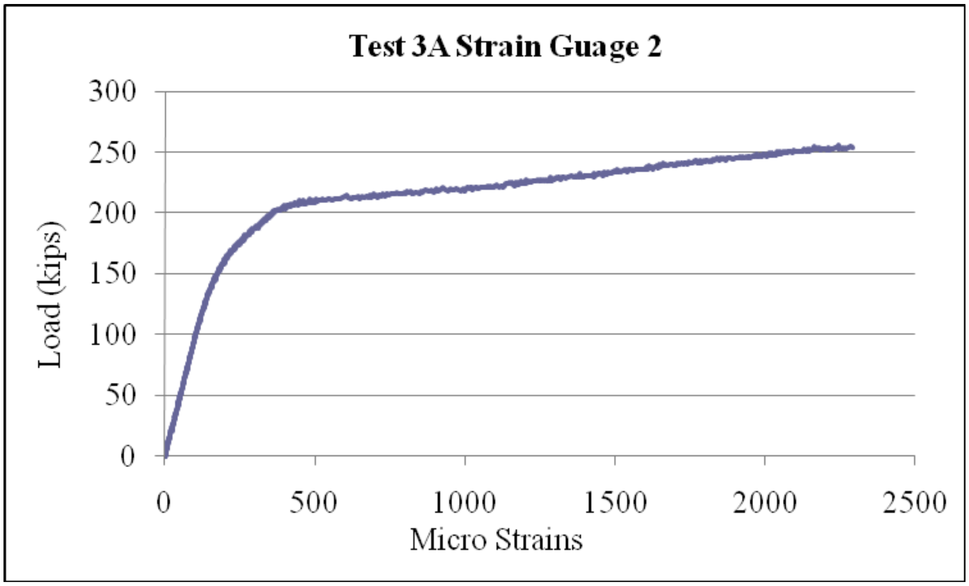

Figure B.44 Test 3A Strain Gauge 2.

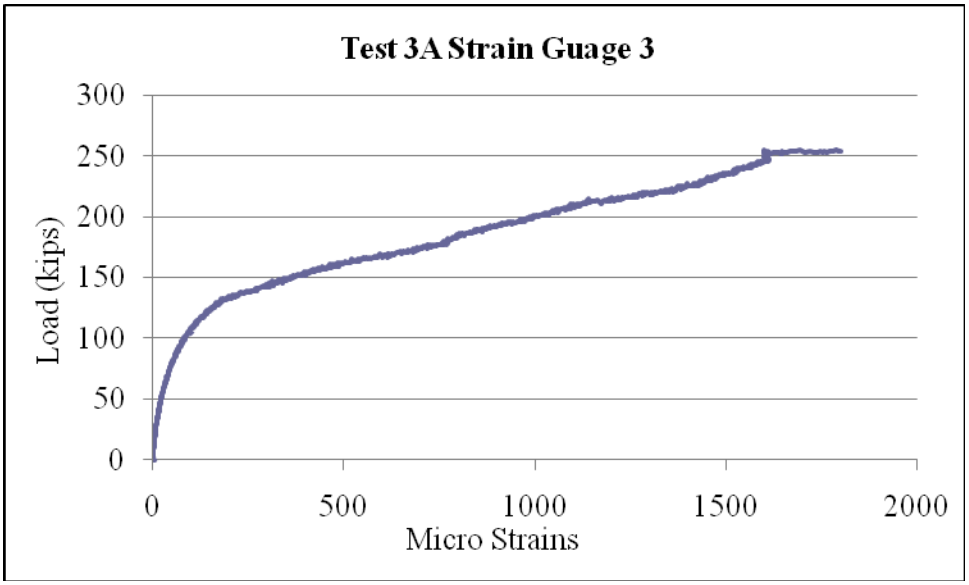

Figure B.45 Test 3A Strain Gauge 3.

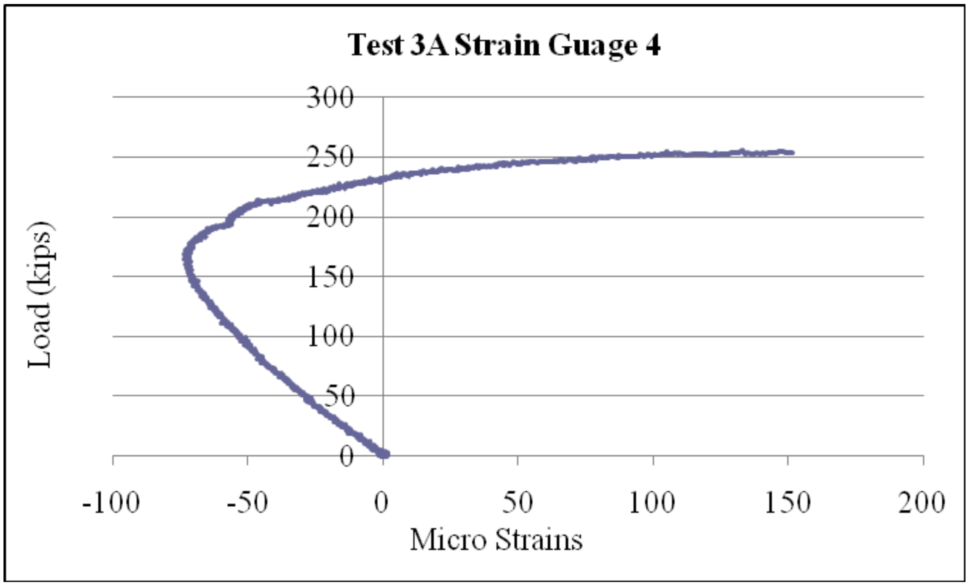

Figure B.46 Test 3A Strain Gauge 4.

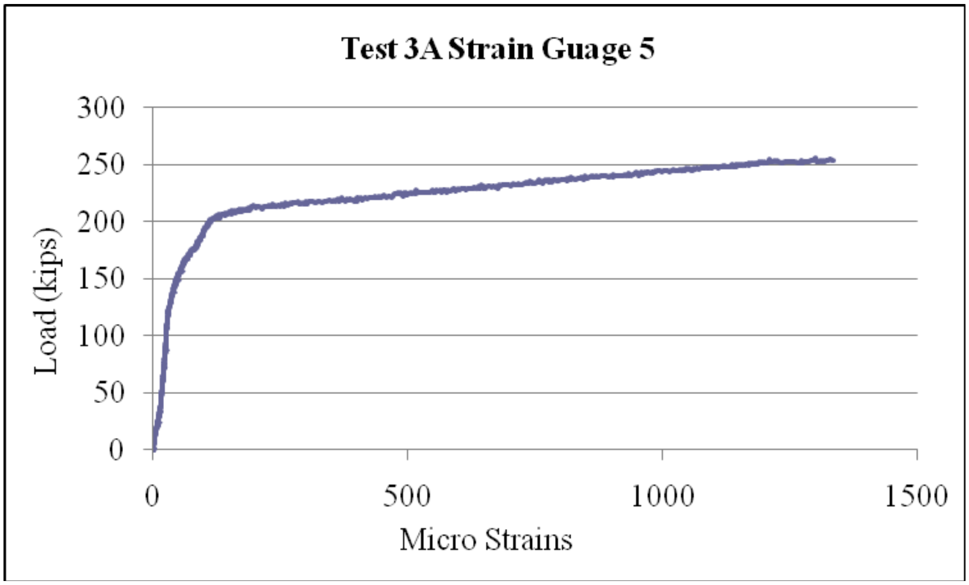

Figure B.47 Test 3A Strain Gauge 5.

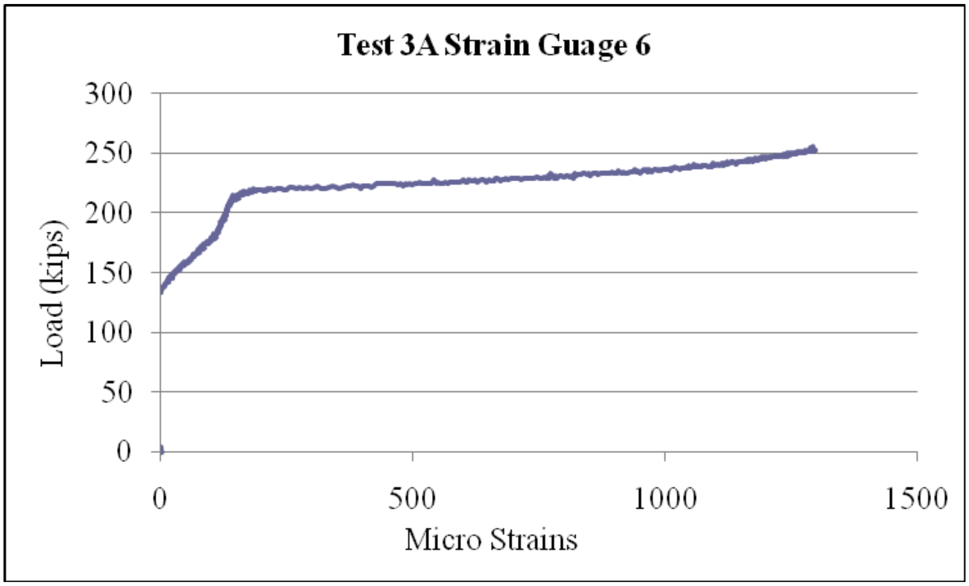

Figure B.48 Test 3A Strain Gauge 6.

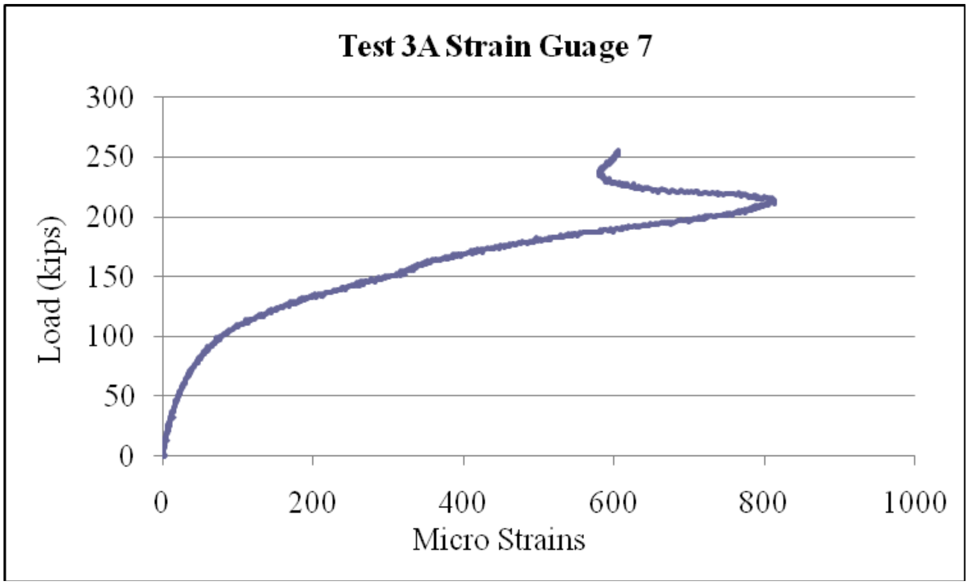

Figure B.49 Test 3A Strain Gauge 7.

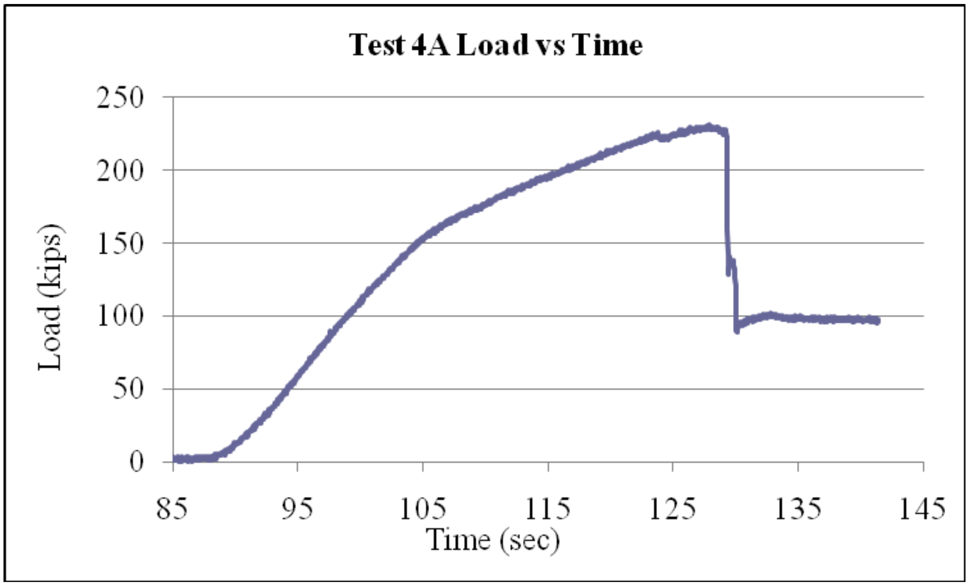

Figure B.50 Test 4A Load vs Time.

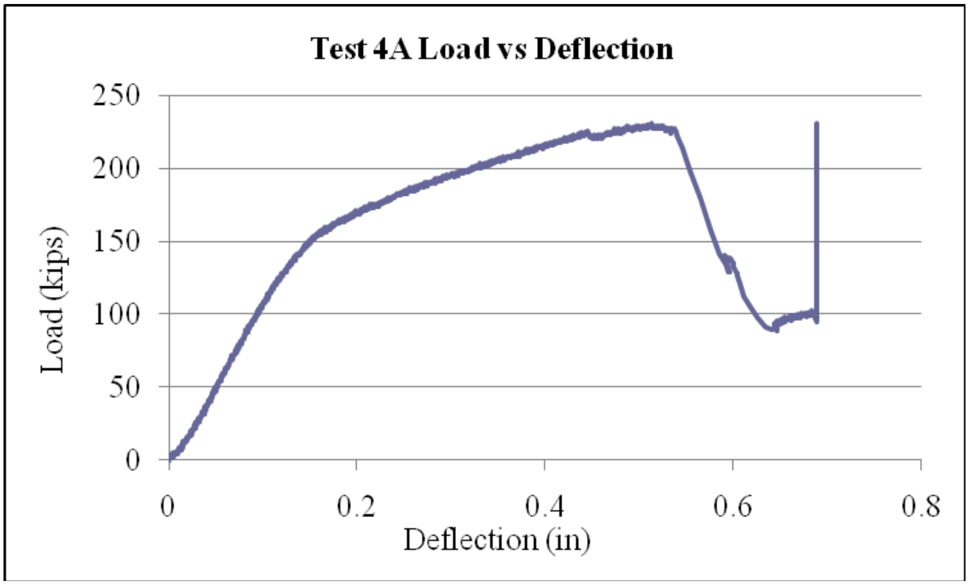

Figure B.51 Test 4A Load vs Deflection.

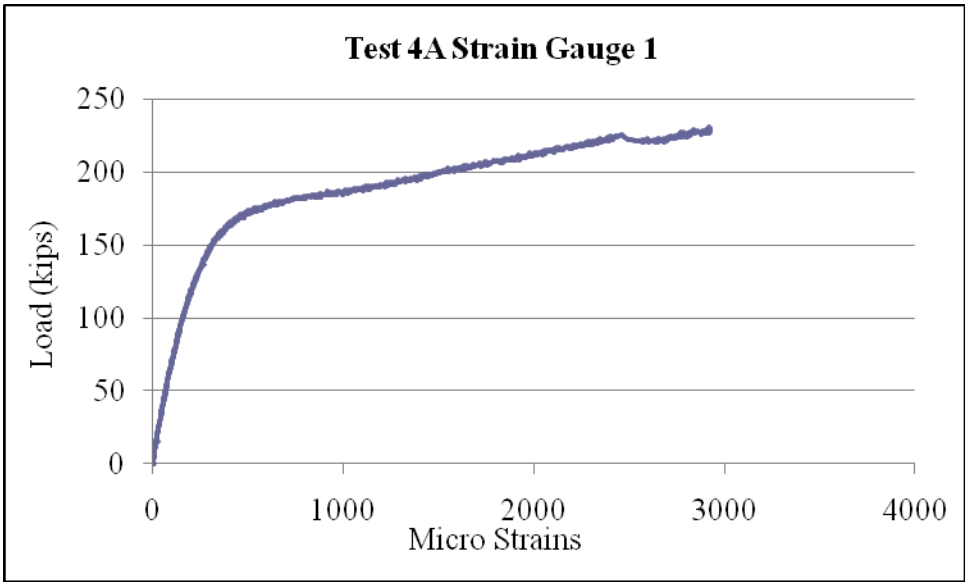

Figure B.52 Test 4A Strain Gauge 1.

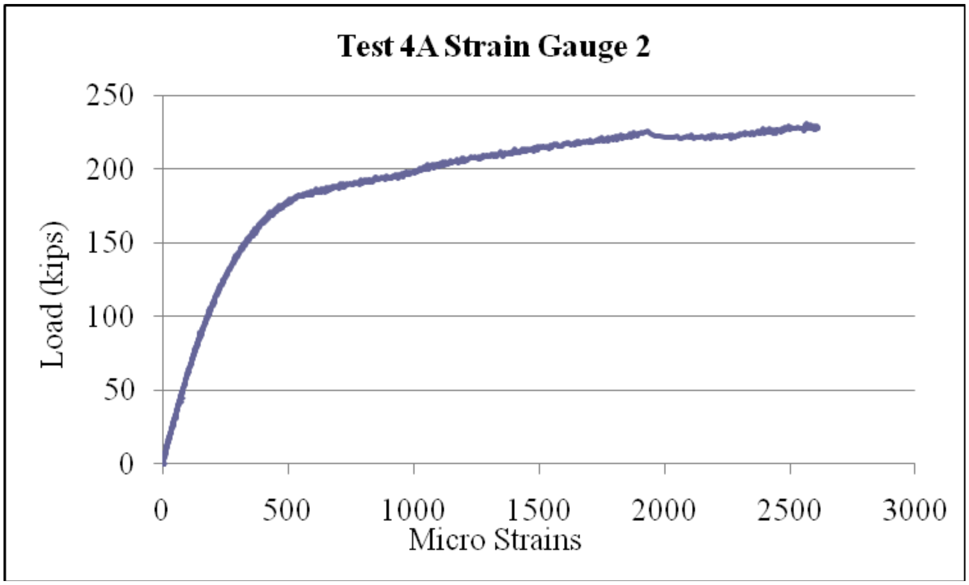

Figure B.53 Test 4A Strain Gauge 2.

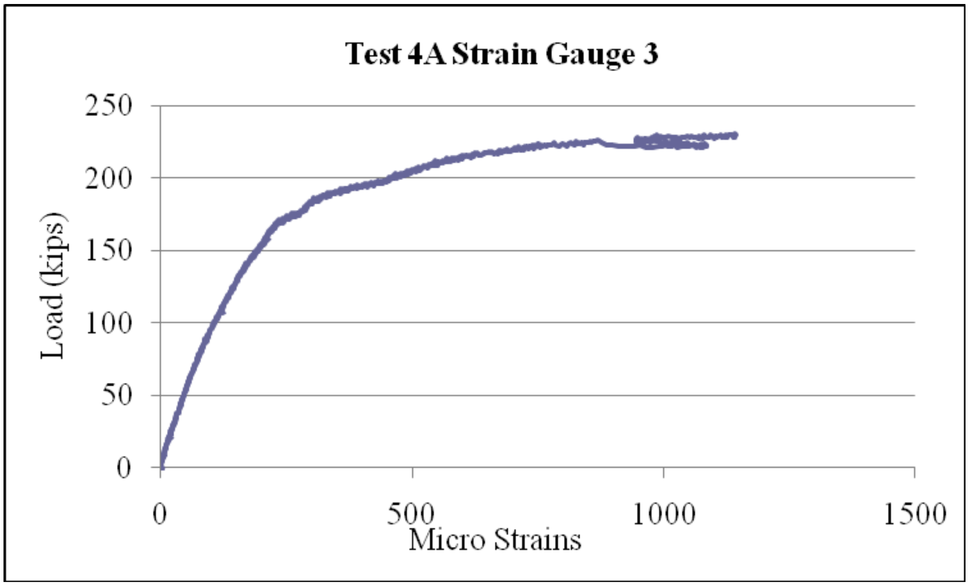

Figure B.54 Test 4A Strain Gauge 3.

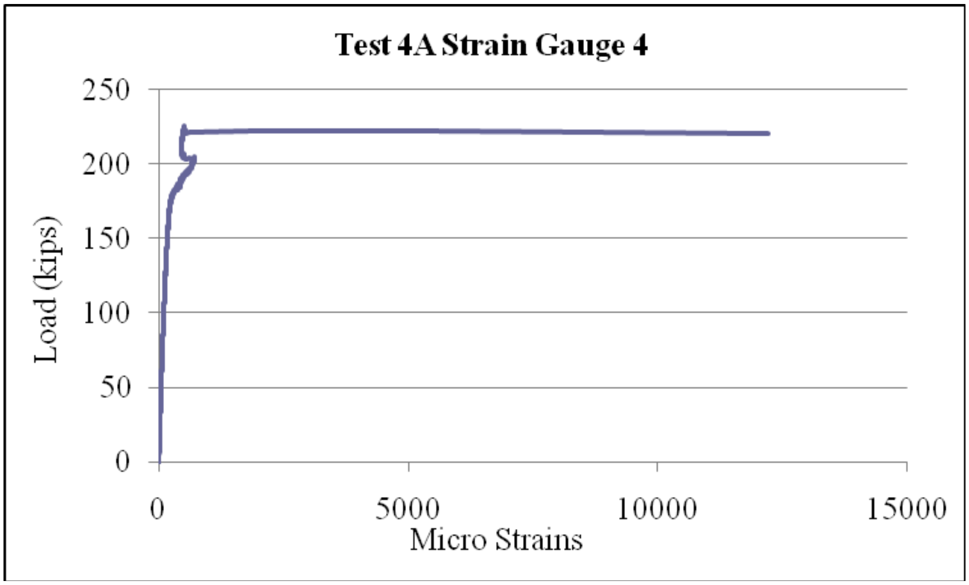

Figure B.55 Test 4A Strain Gauge 4.

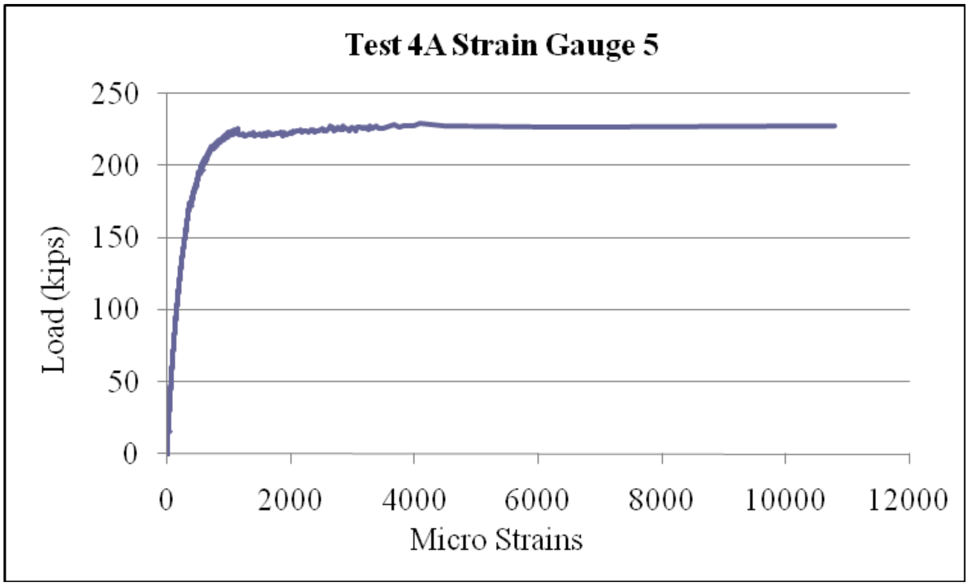

Figure B.56 Test 4A Strain Gauge 5.

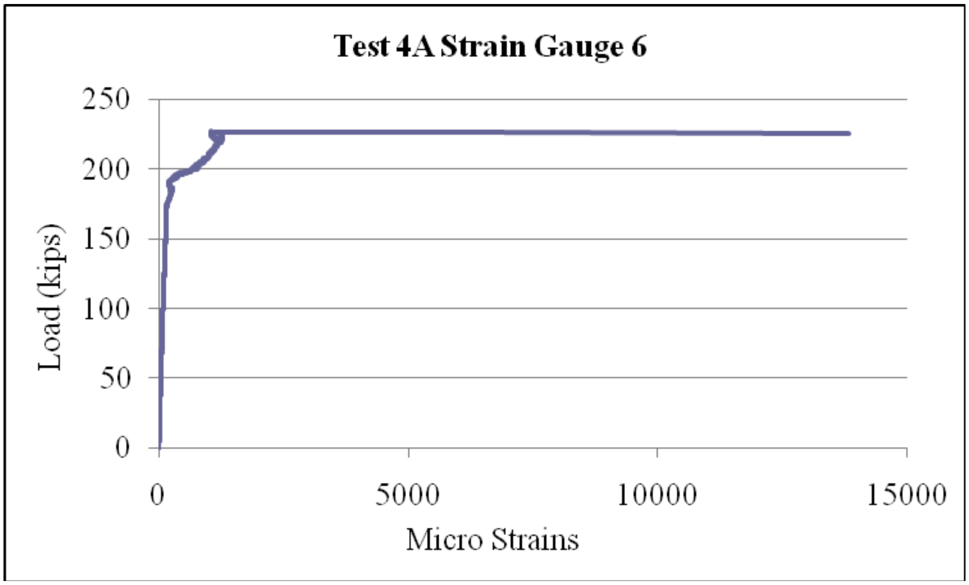

Figure B.57 Test 4A Strain Gauge 6.

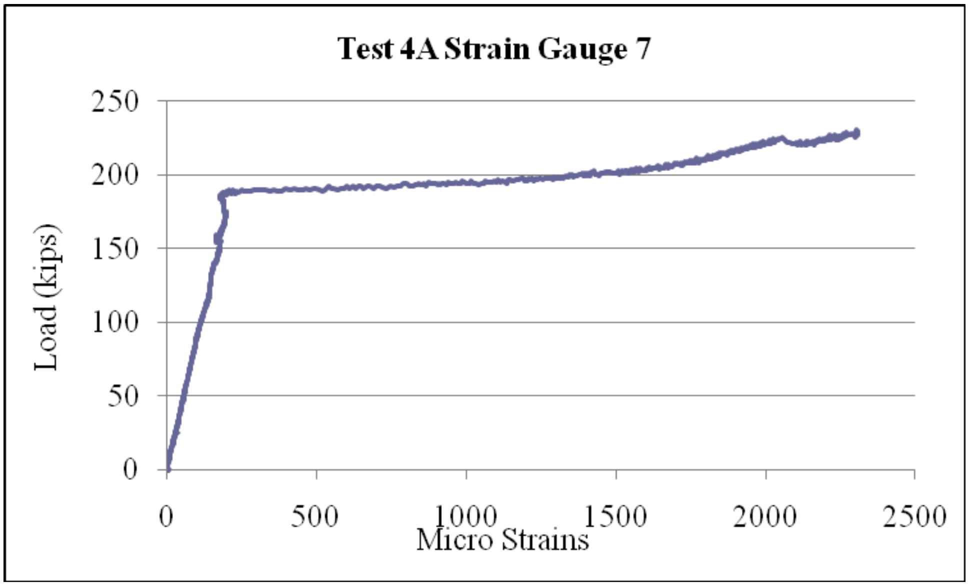

Figure B.58 Test 4A Strain Gauge 7.

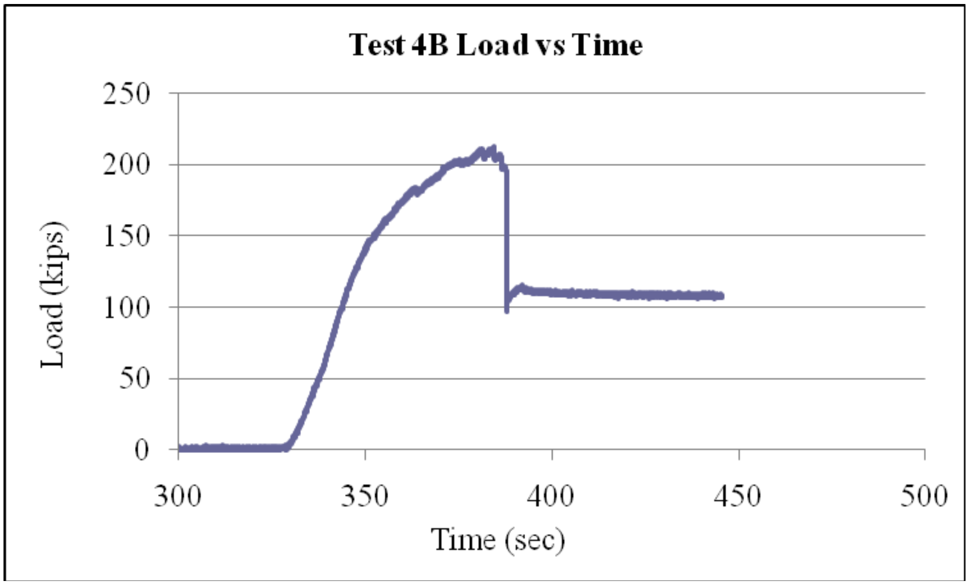

Figure B.59 Test 4B Load vs Time.

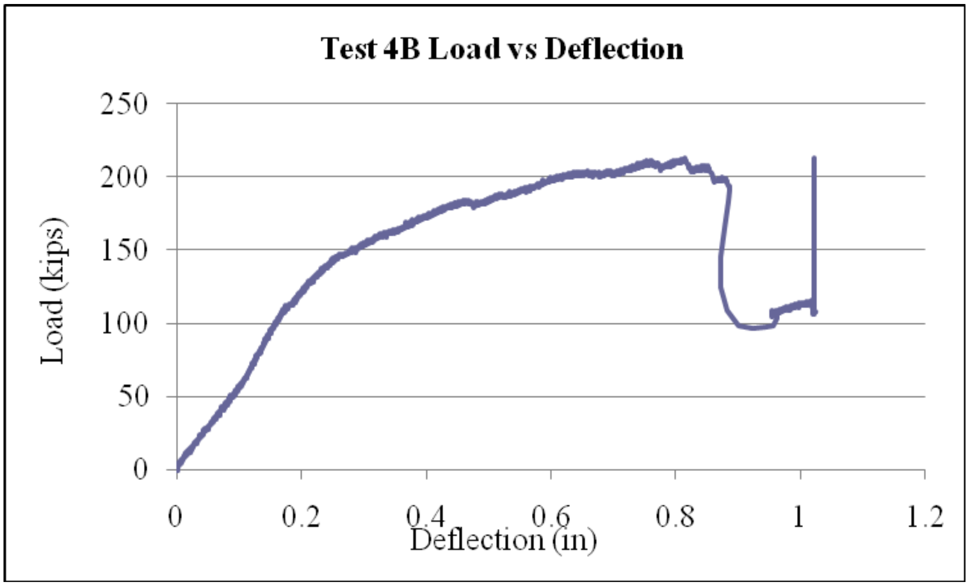

Figure B.60 Test 4B Load vs Deflection.

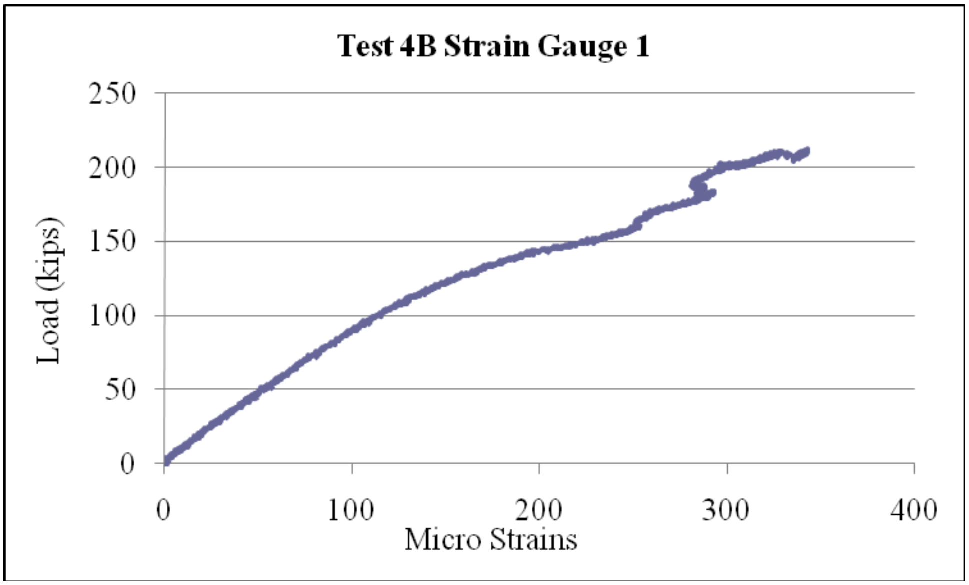

Figure B.61 Test 4B Strain Gauge 1.

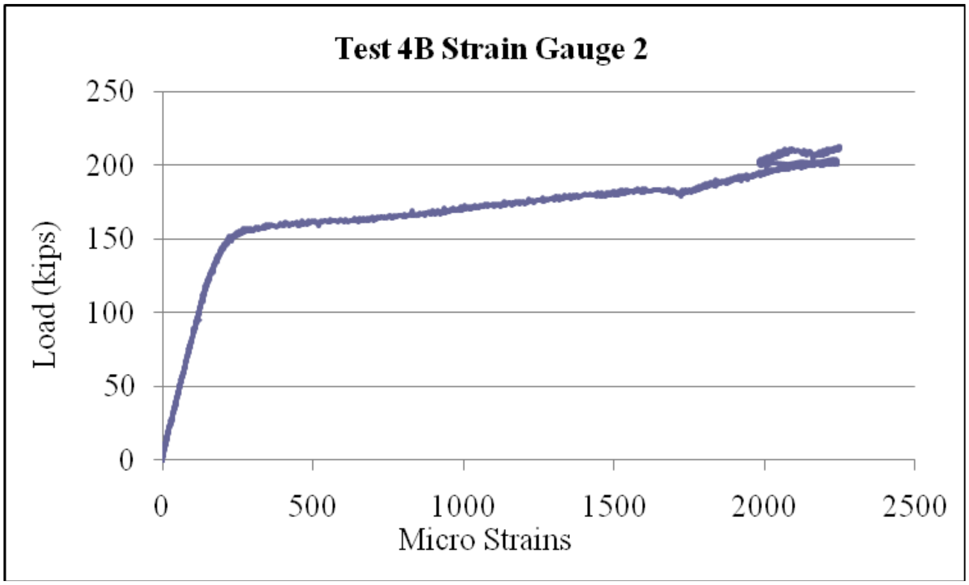

Figure B.62 Test 4B Strain Gauge 2.

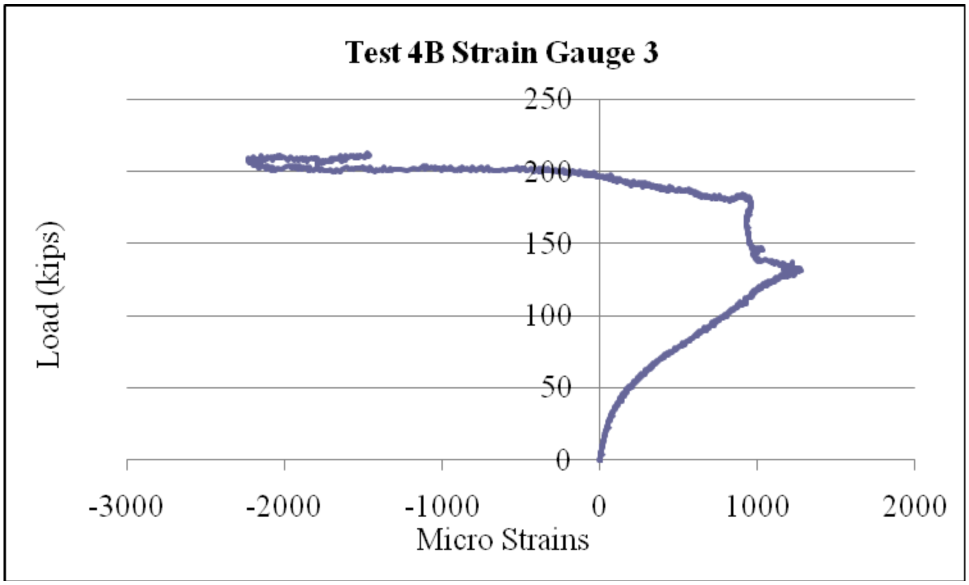

Figure B.63 Test 4B Strain Gauge 3.

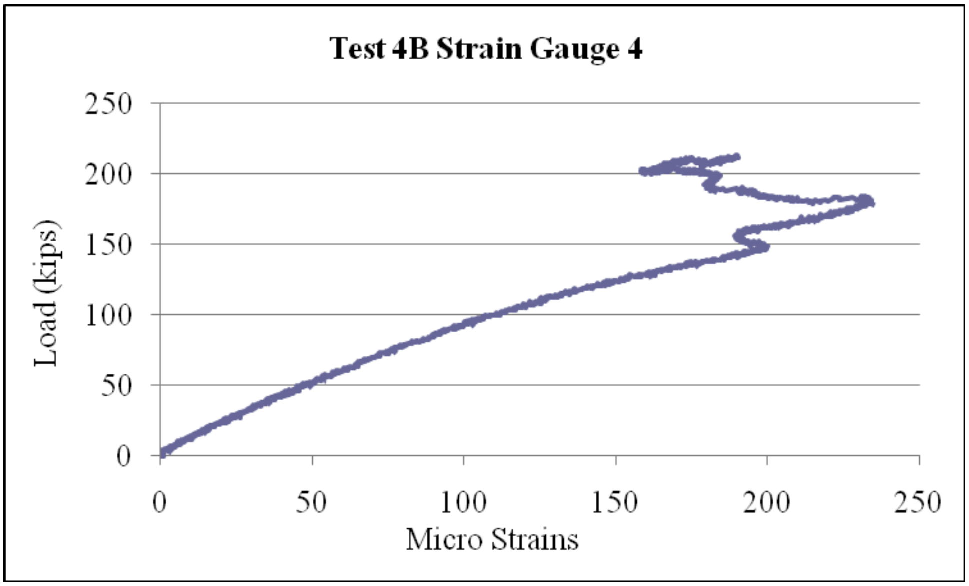

Figure B.64 Test 4B Strain Gauge 4.

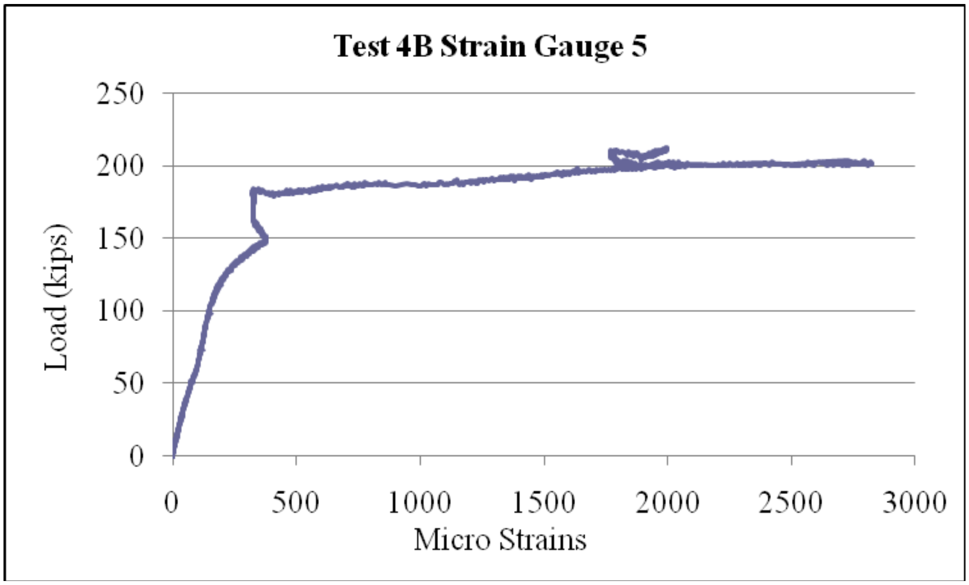

Figure B.65 Test 4B Strain Gauge 5.

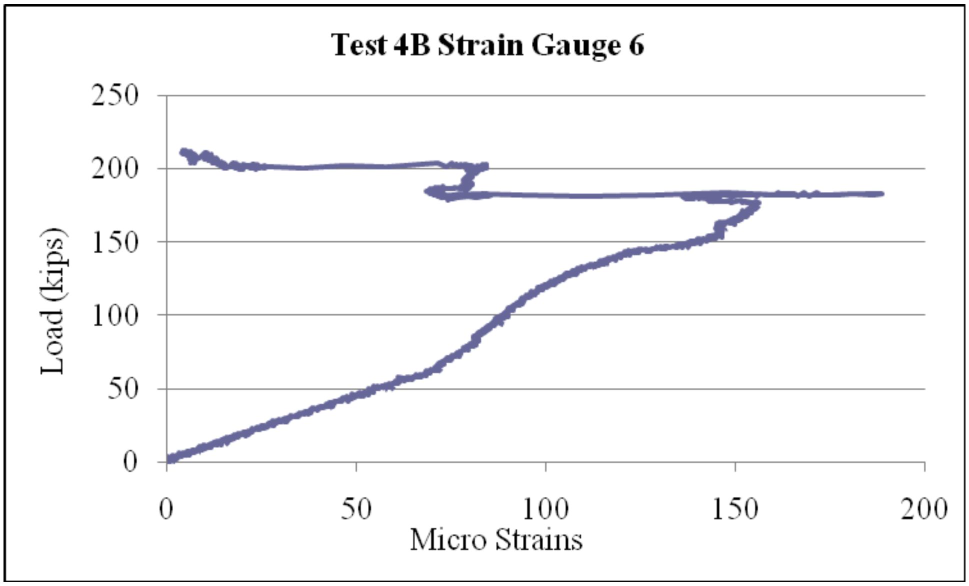

Figure B.66 Test 4B Strain Gauge 6.

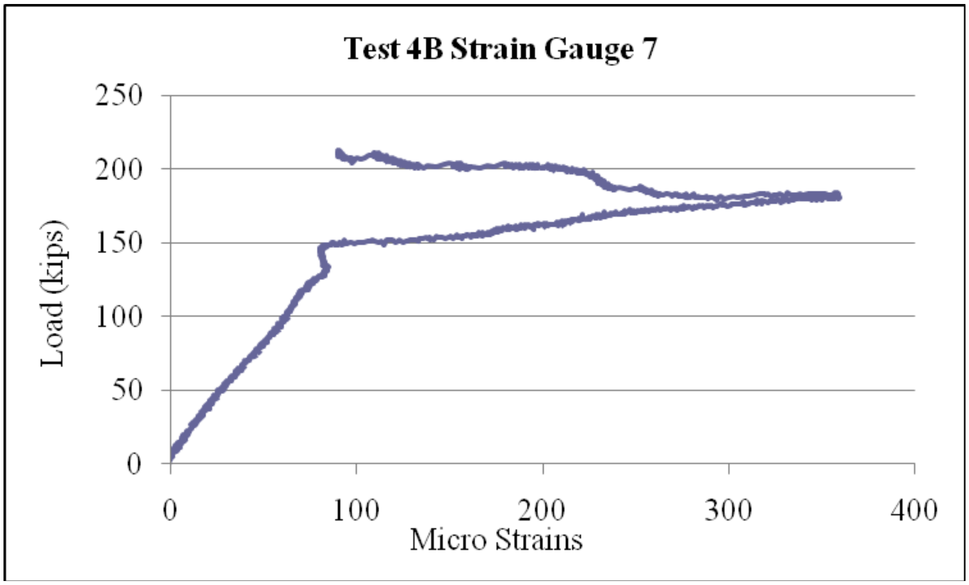

Figure B.67 Test 4B Strain Gauge 7.

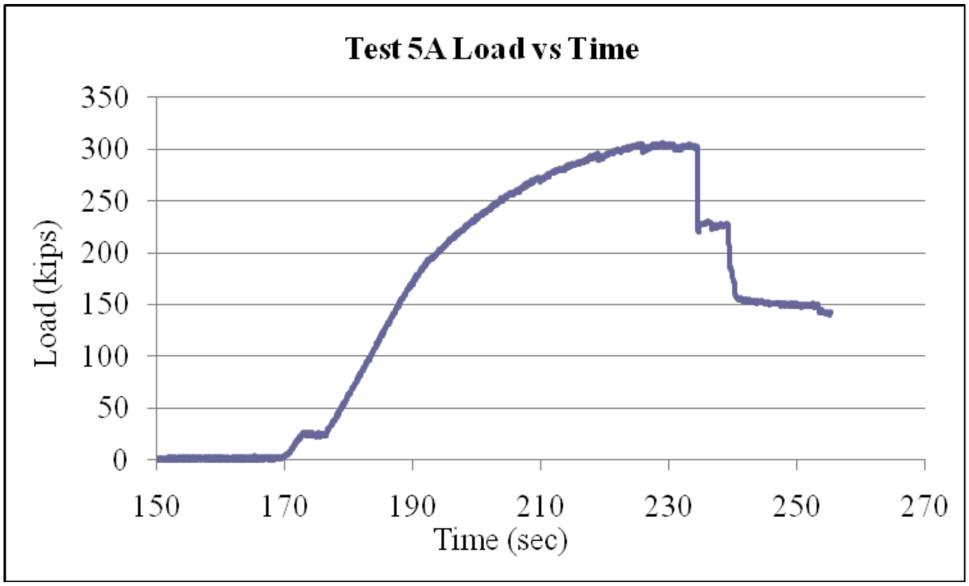

Figure B.68 Test 5A Load vs Time.

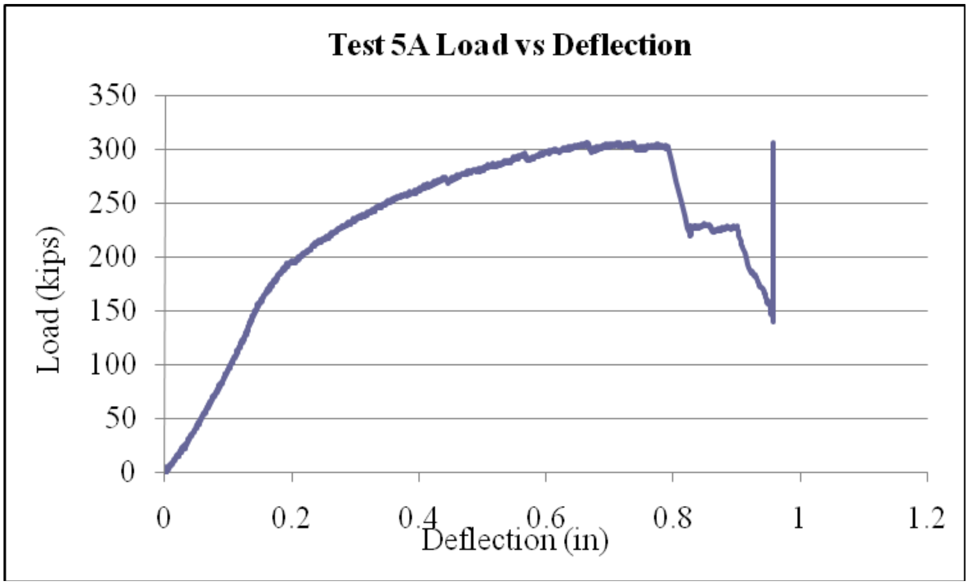

Figure B.69 Test 5A Load vs Deflection.

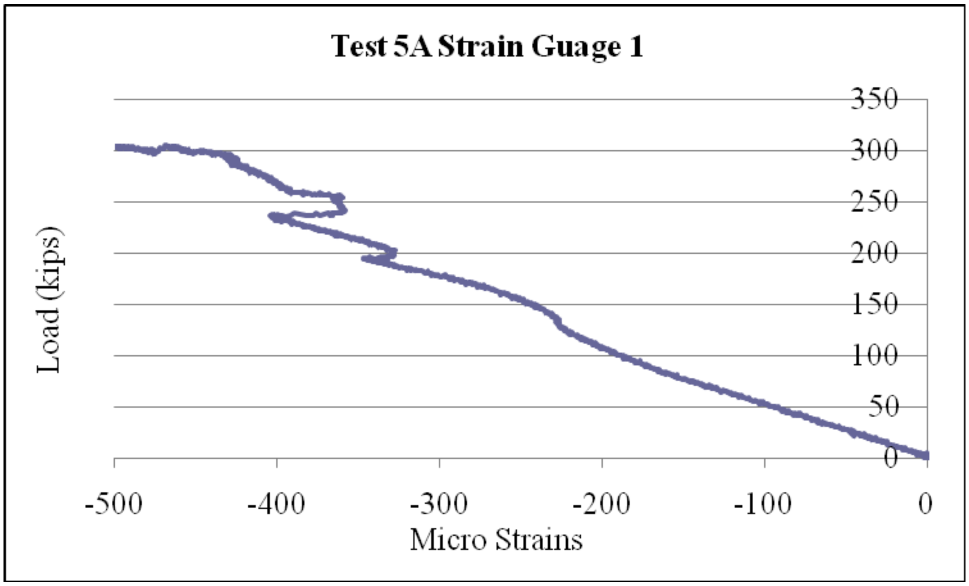

Figure B.70 Test 5A Strain Gauge 1.

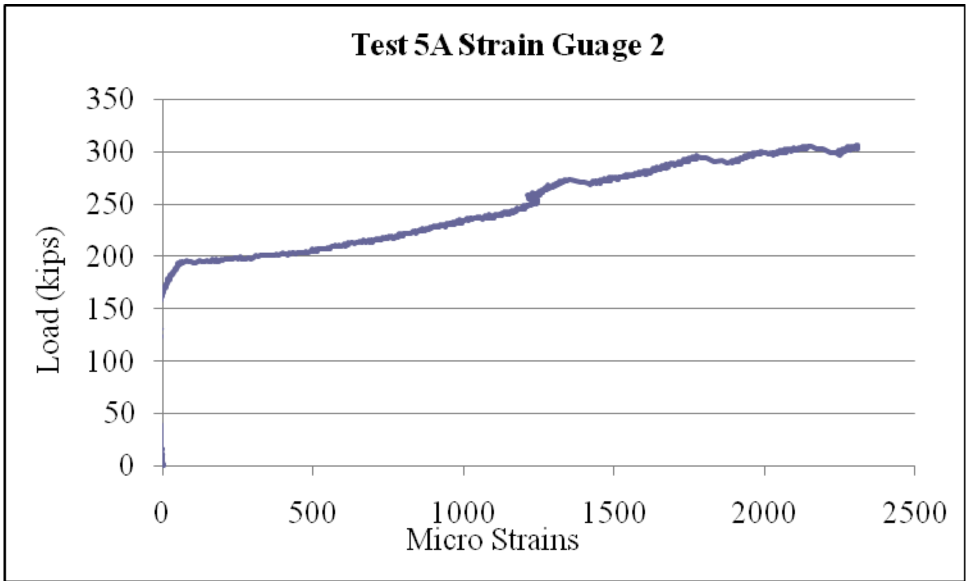

Figure B.71 Test 5A Strain Gauge 2.

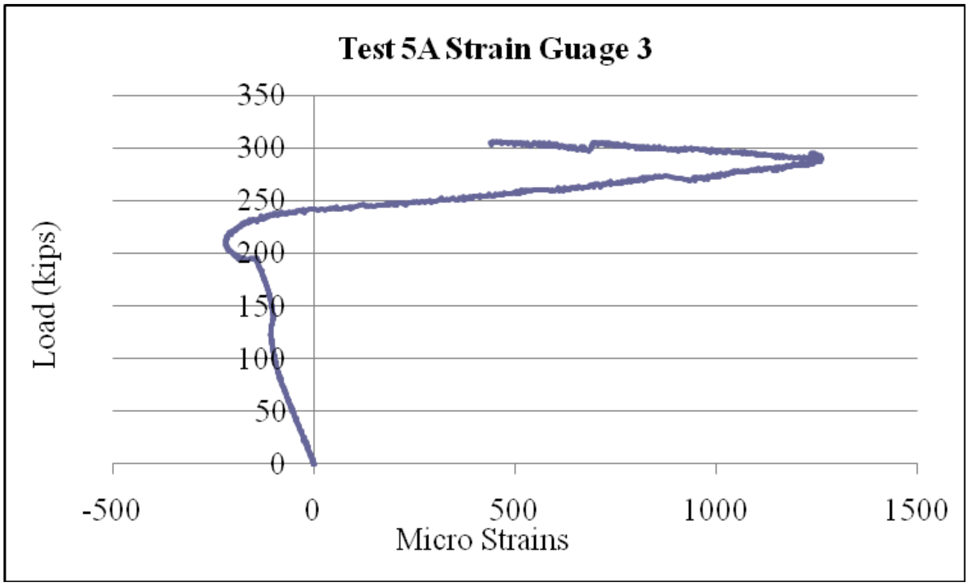

Figure B.72 Test 5A Strain Gauge 3.

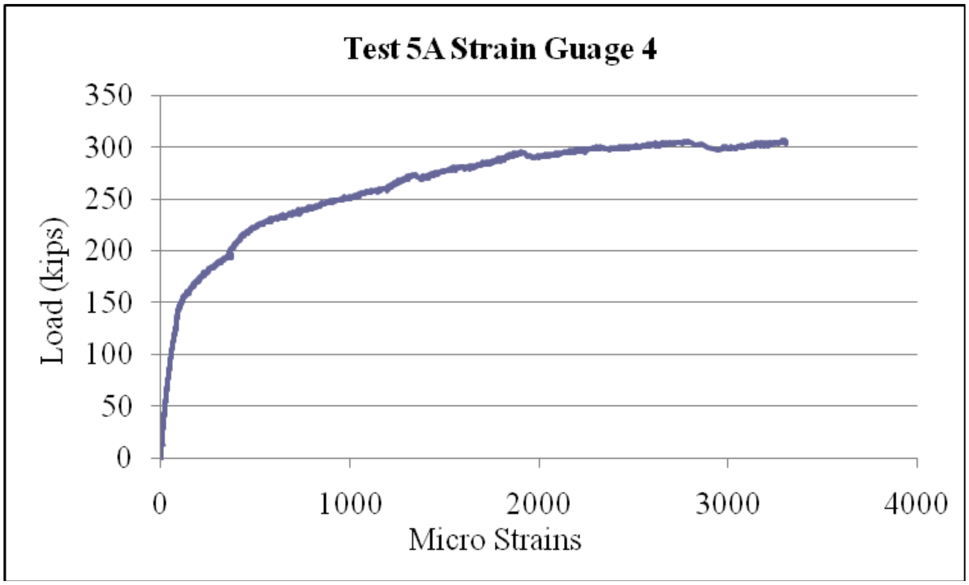

Figure B.73 Test 5A Strain Gauge 4.

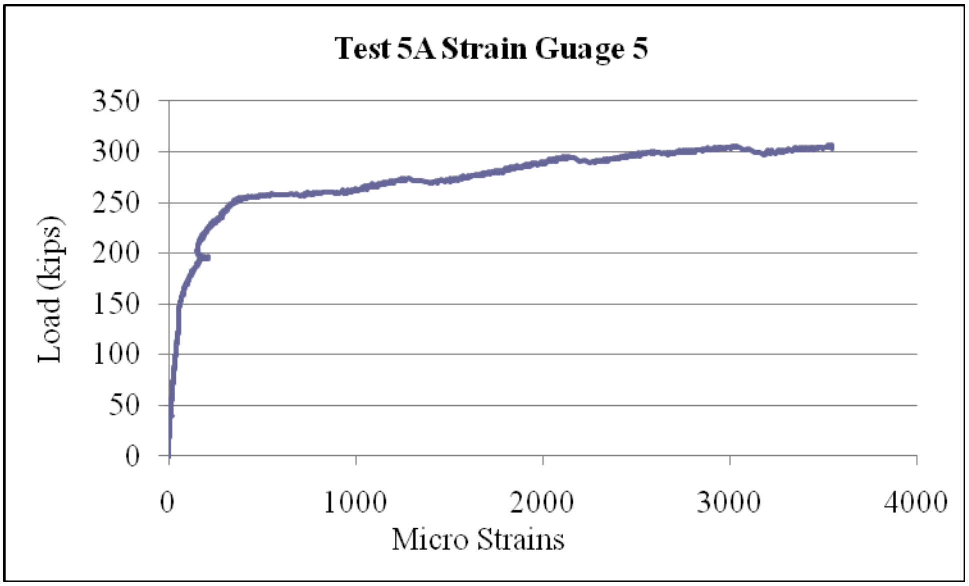

Figure B.74 Test 5A Strain Gauge 5.

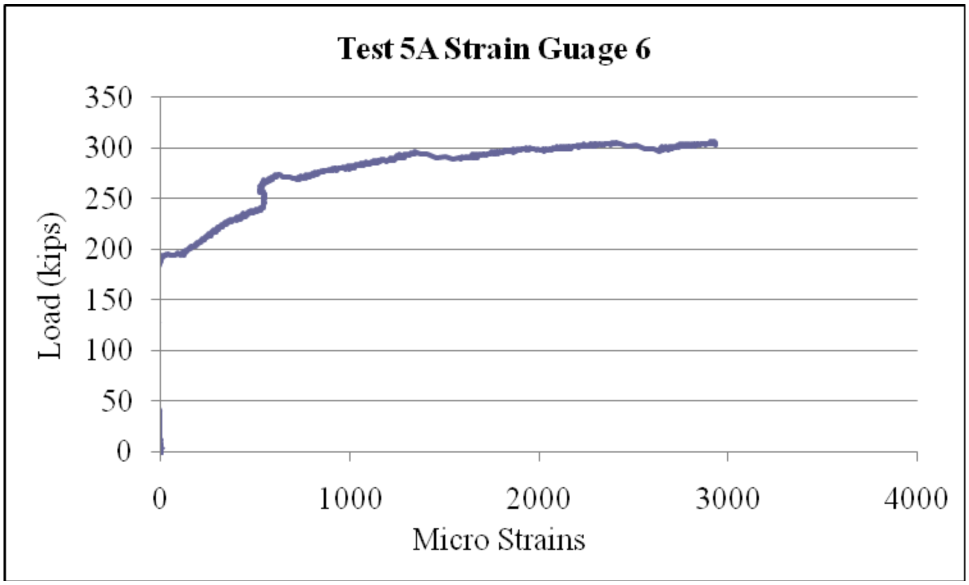

Figure B.75 Test 5A Strain Gauge 6.

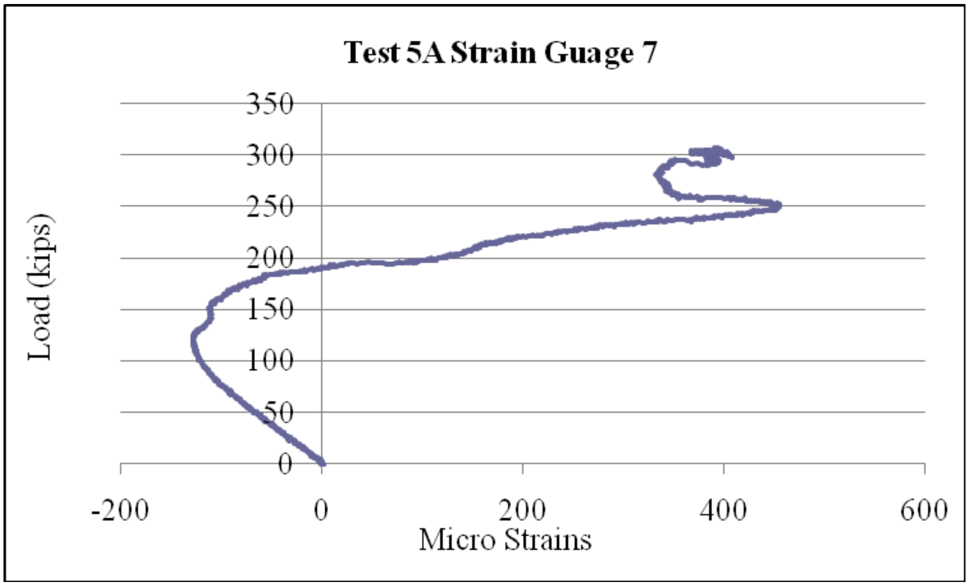

Figure B.76 Test 5A Strain Gauge 7.

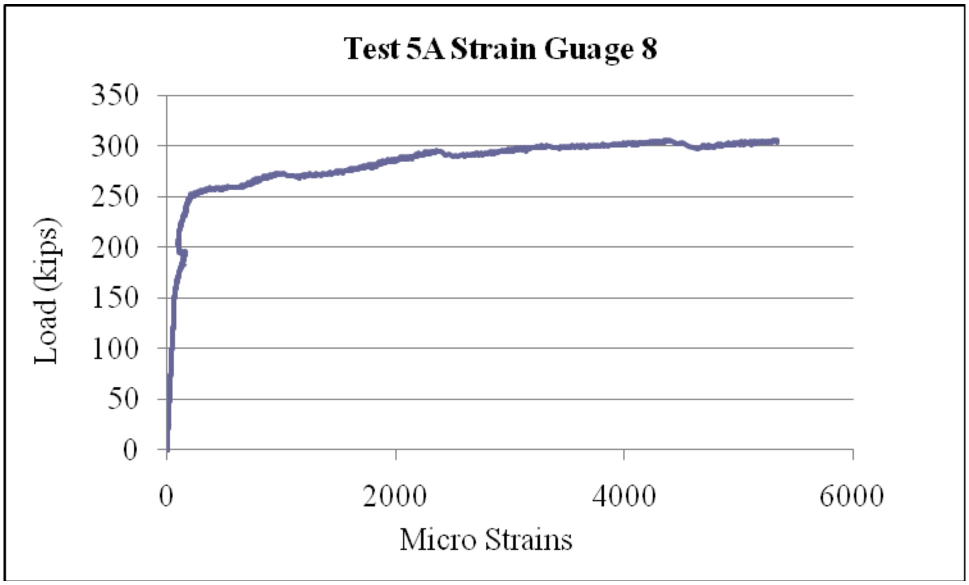

Figure B.77 Test 5A Strain Gauge 8.

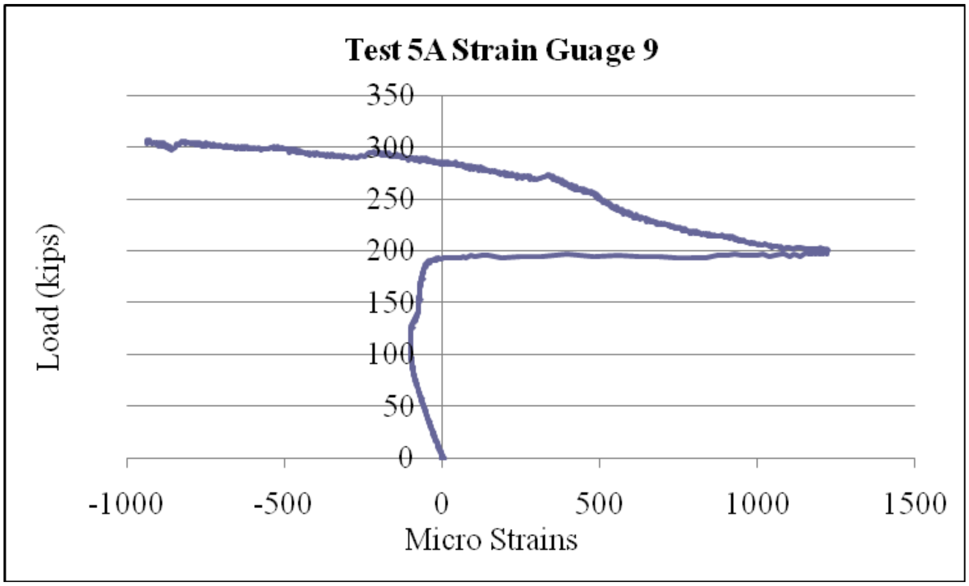

Figure B.78 Test 5A Strain Gauge 9.

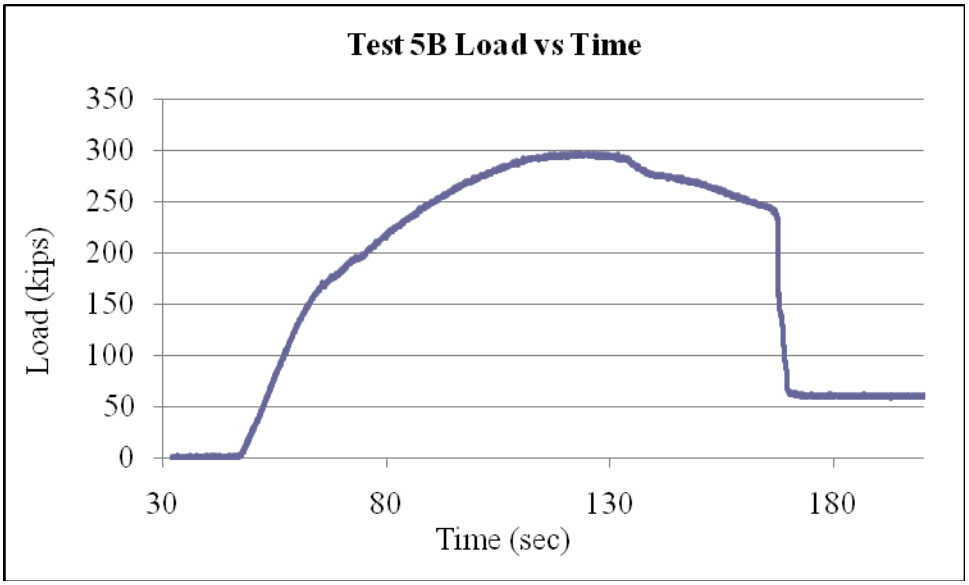

Figure B.79 Test 5B Load vs Time.

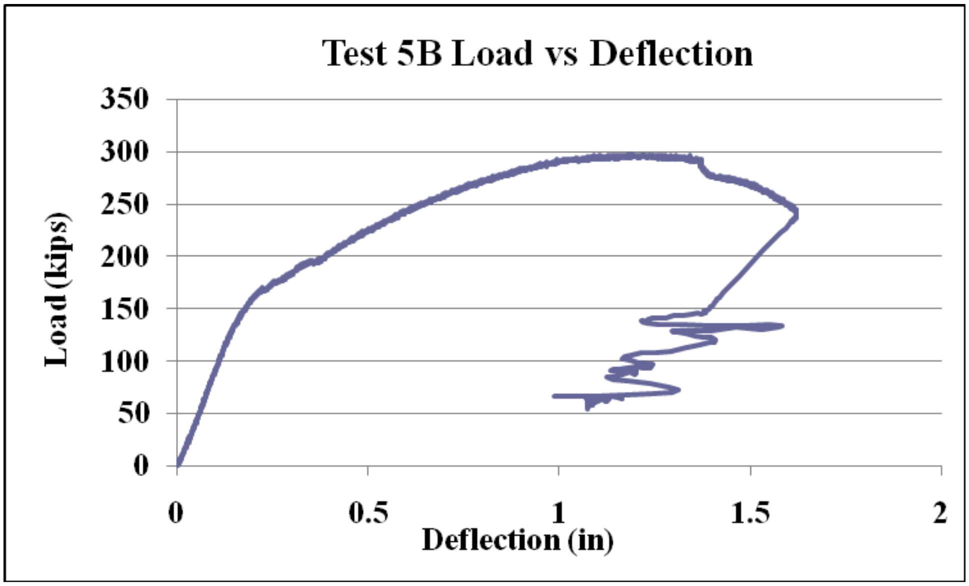

Figure B.80 Test 5B Load vs Deflection.

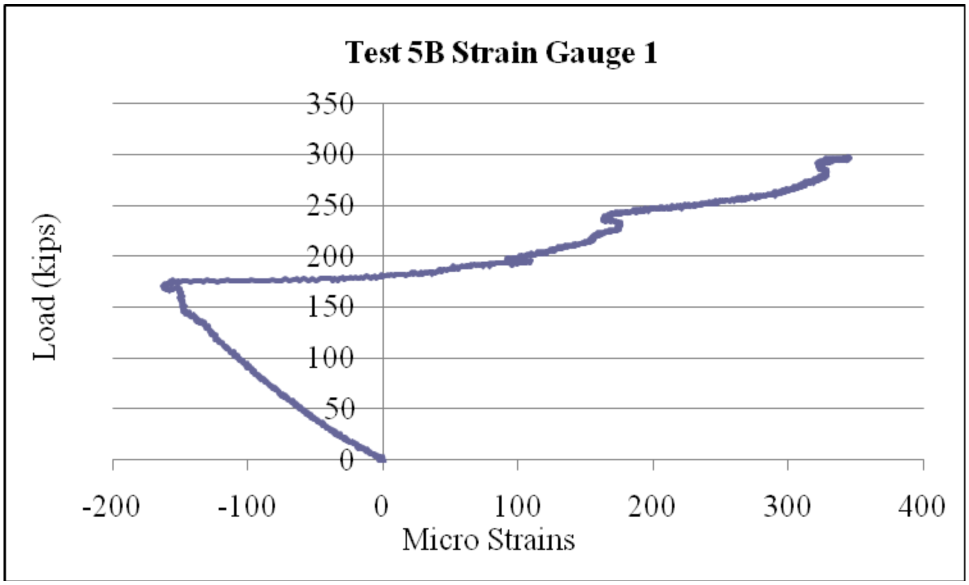

Figure B.81 Test 5B Strain Gauge 1.

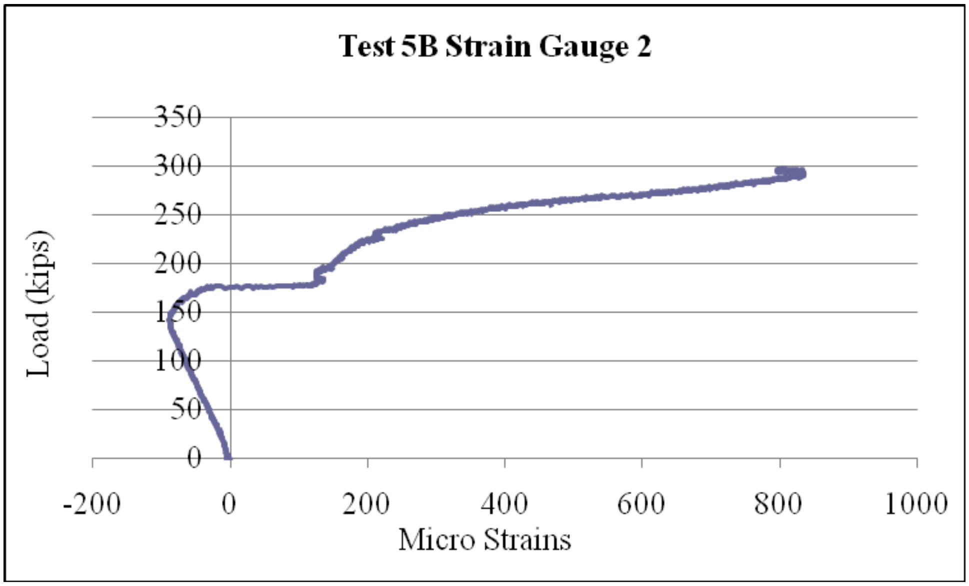

Figure B.82 Test 5B Strain Gauge 2.

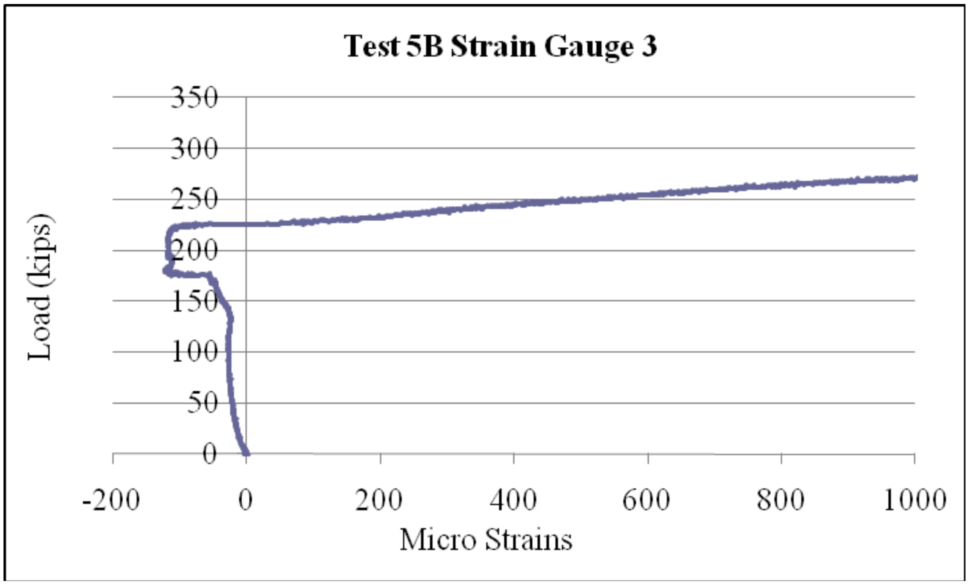

Figure B.83 Test 5B Strain Gauge 3.

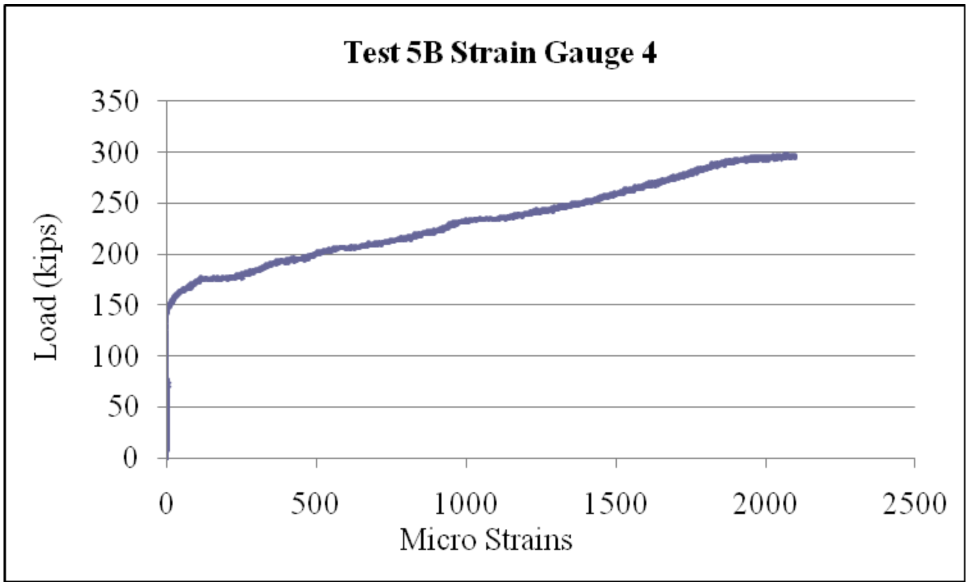

Figure B.84 Test 5B Strain Gauge 4.

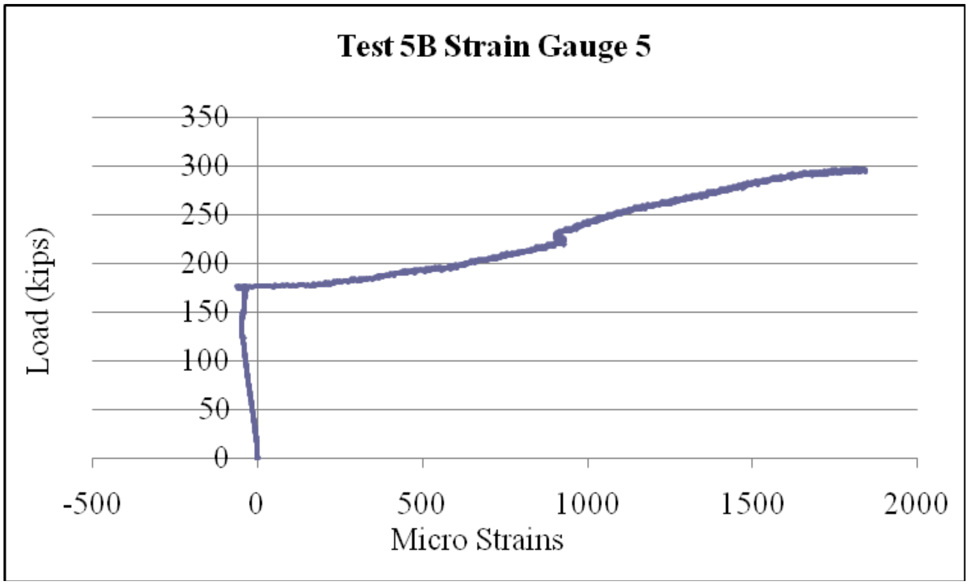

Figure B.85 Test 5B Strain Gauge 5.

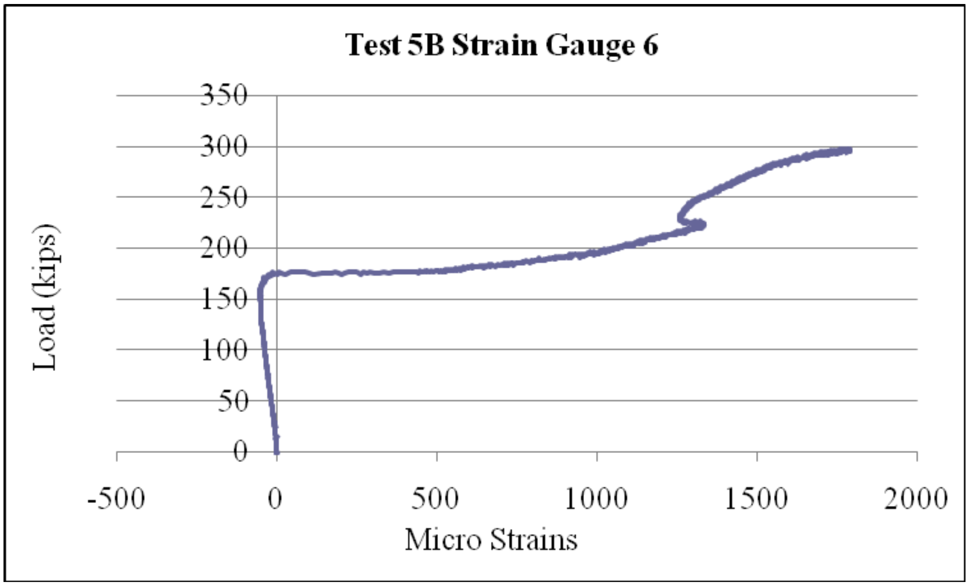

Figure B.86 Test 5B Strain Gauge 6.

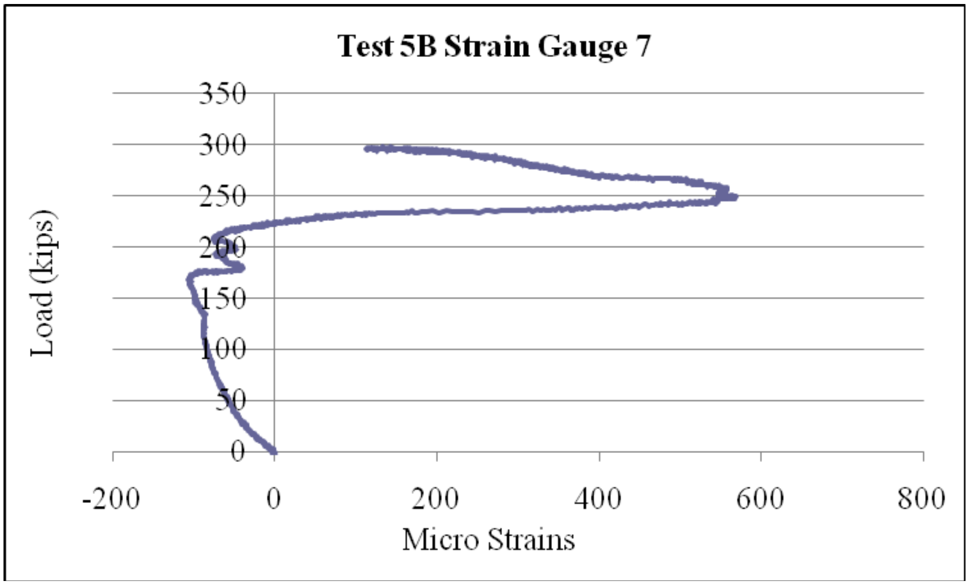

Figure B.87 Test 5B Strain Gauge 7.

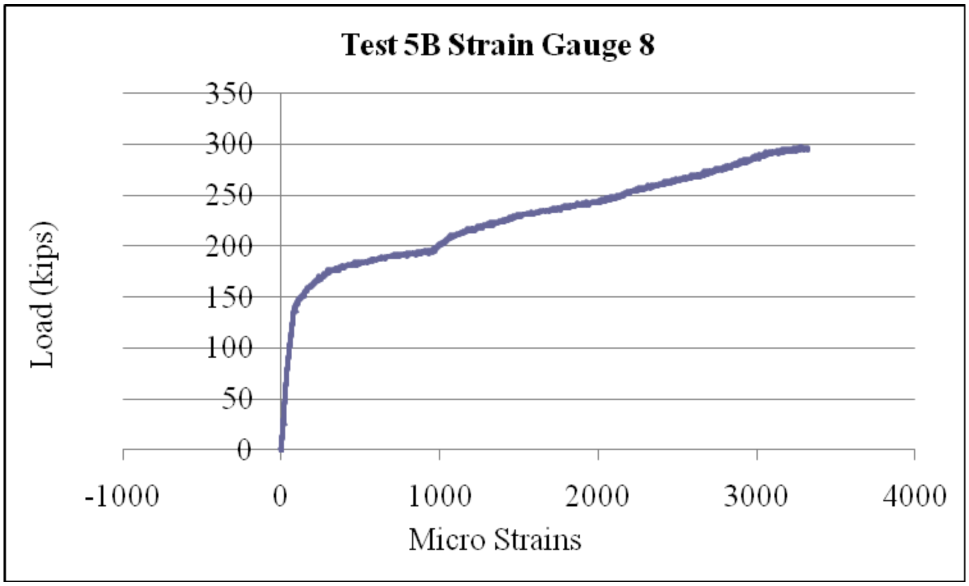

Figure B.88 Test 5B Strain Gauge 8.

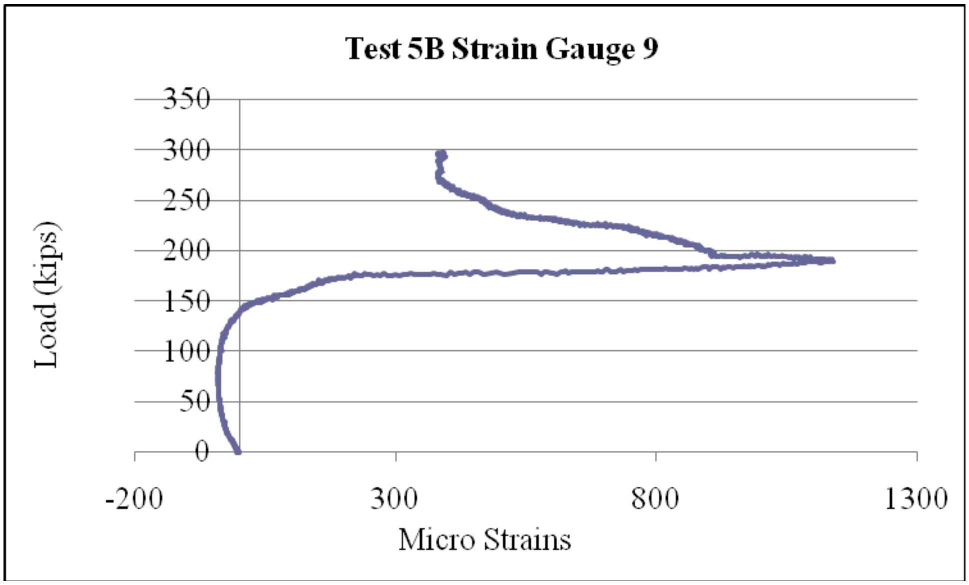

Figure B.89 Test 5B Strain Gauge 9.

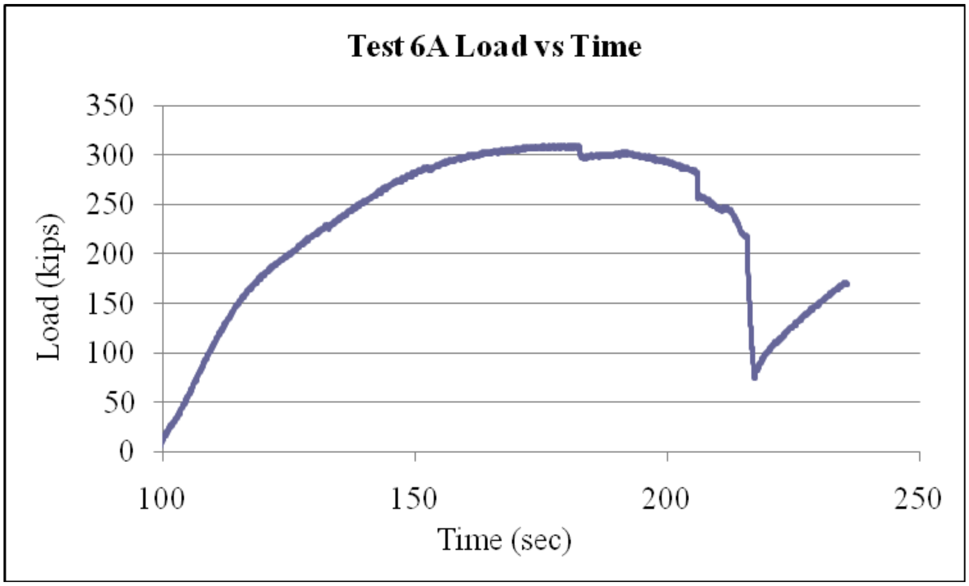

Figure B.90 Test 6A Load vs Time.

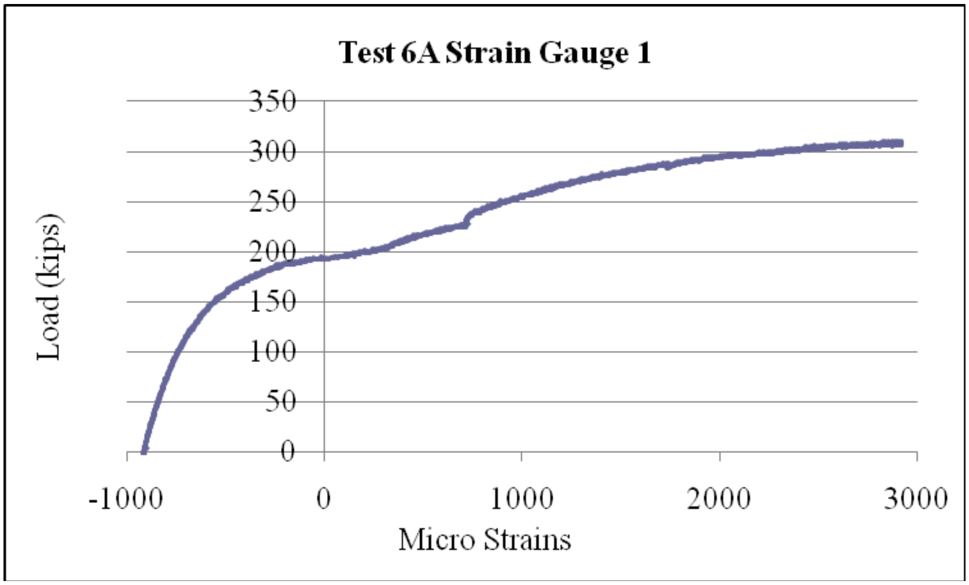

Figure B.91 Test 6A Strain Gauge 1.

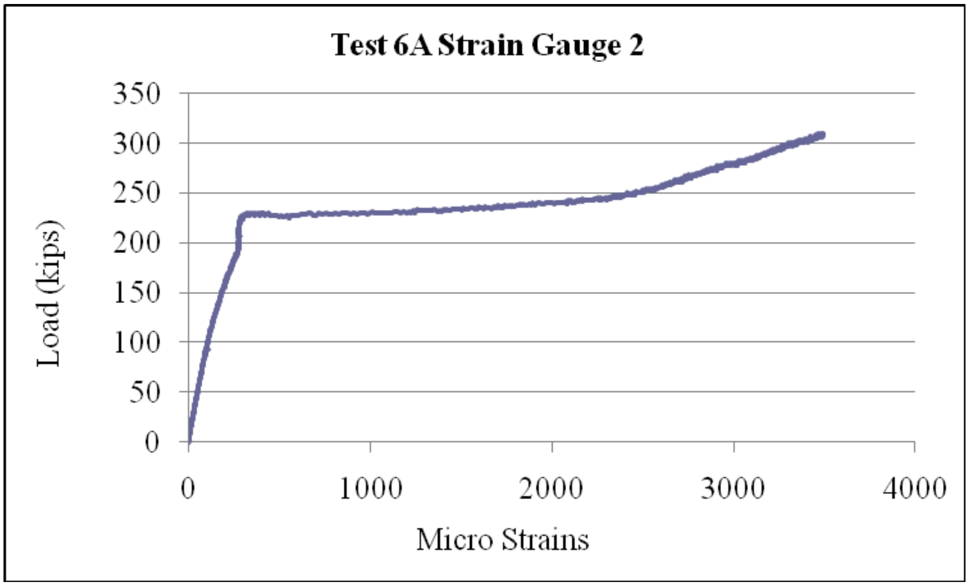

Figure B.92 Test 6A Strain Gauge 2.

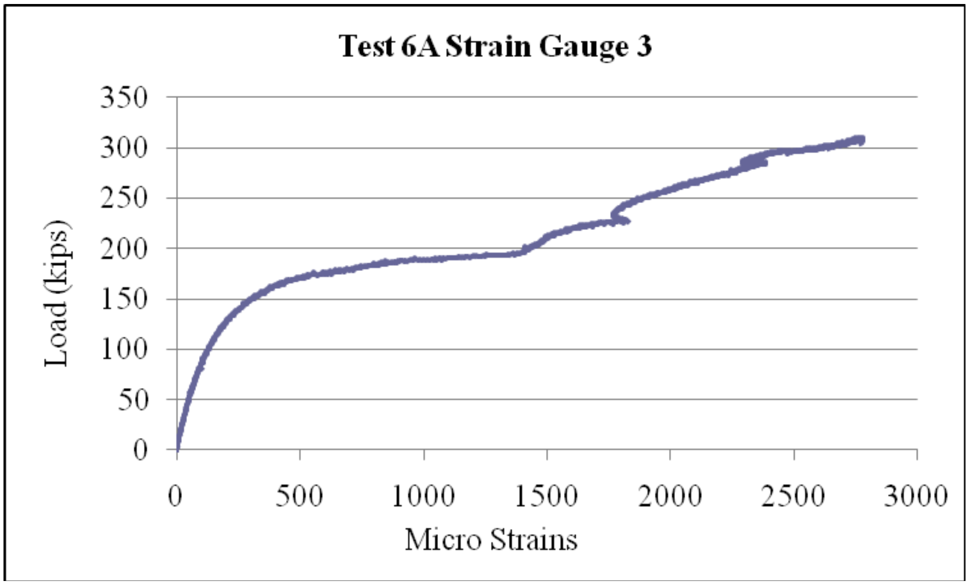

Figure B.93 Test 6A Strain Gauge 3.

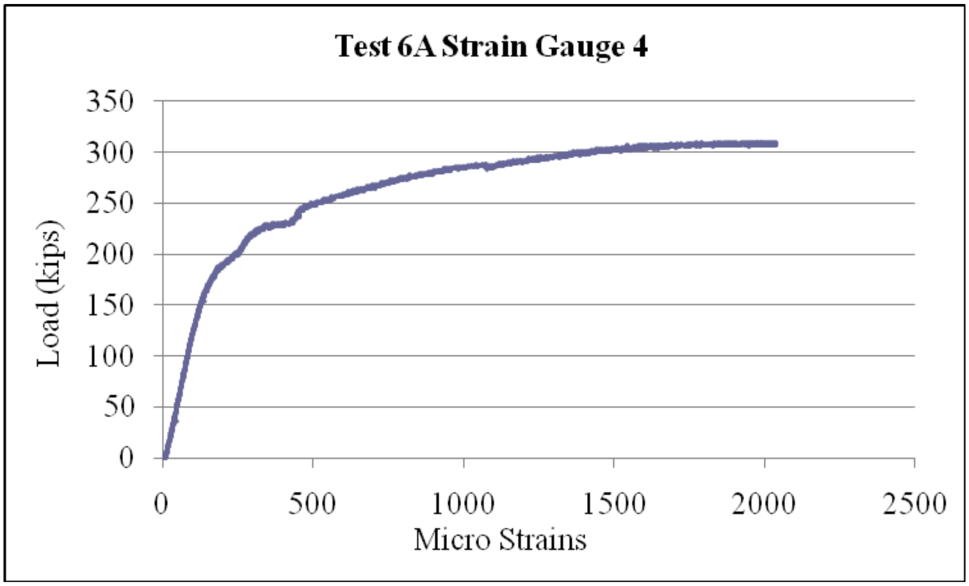

Figure B.94 Test 6A Strain Gauge 4.

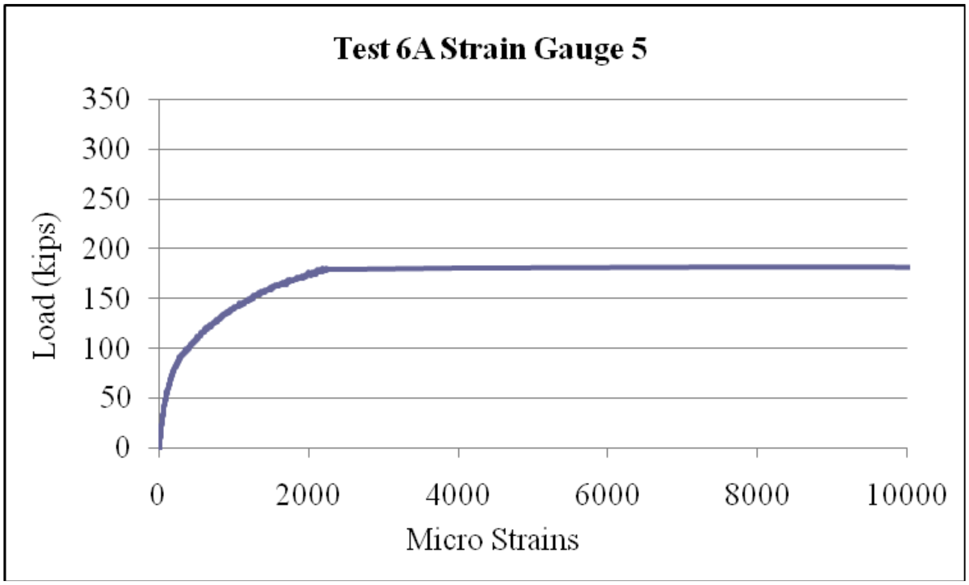

Figure B.95 Test 6A Strain Gauge 5.

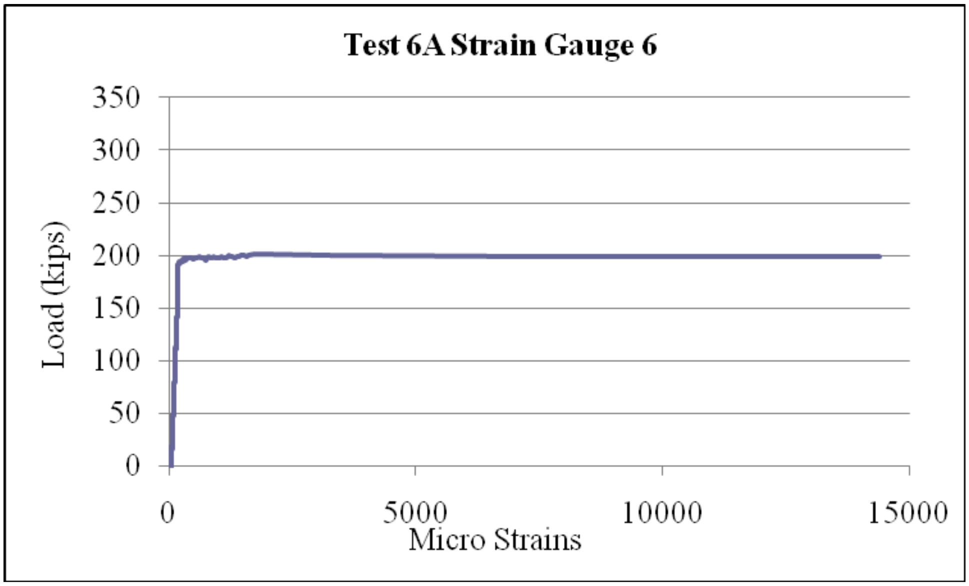

Figure B.96 Test 6A Strain Gauge 6.

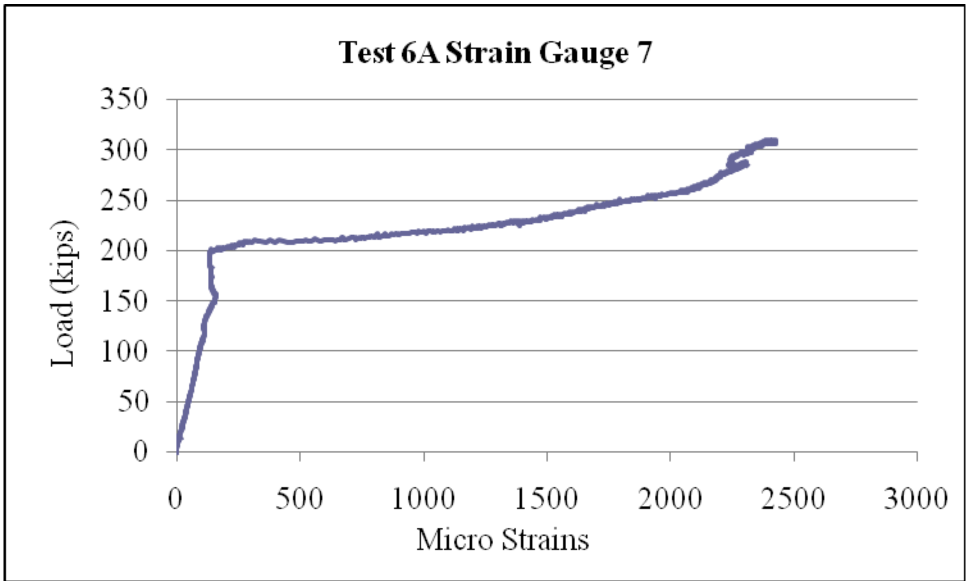

Figure B.97 Test 6A Strain Gauge 7.

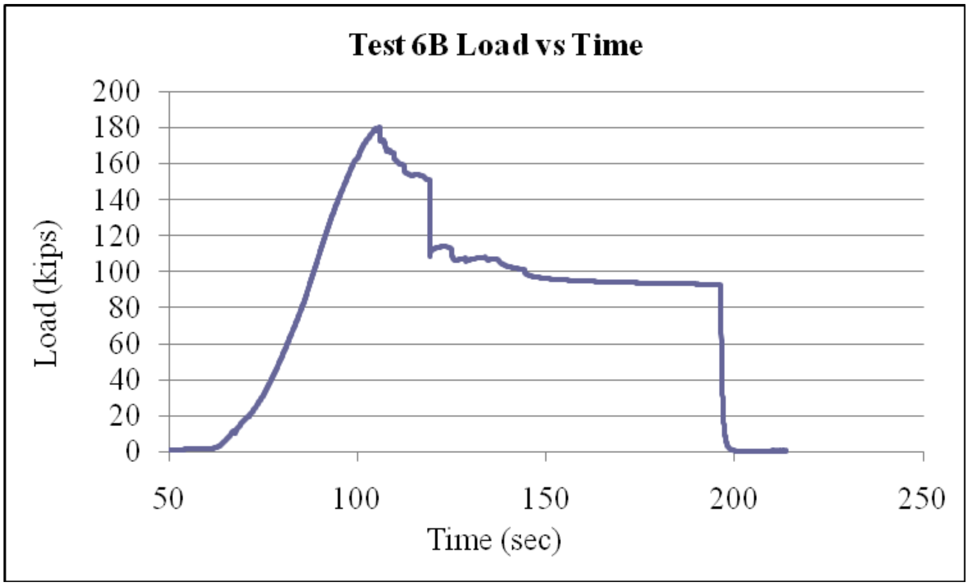

Figure B.98 Test 6B Load vs Time.

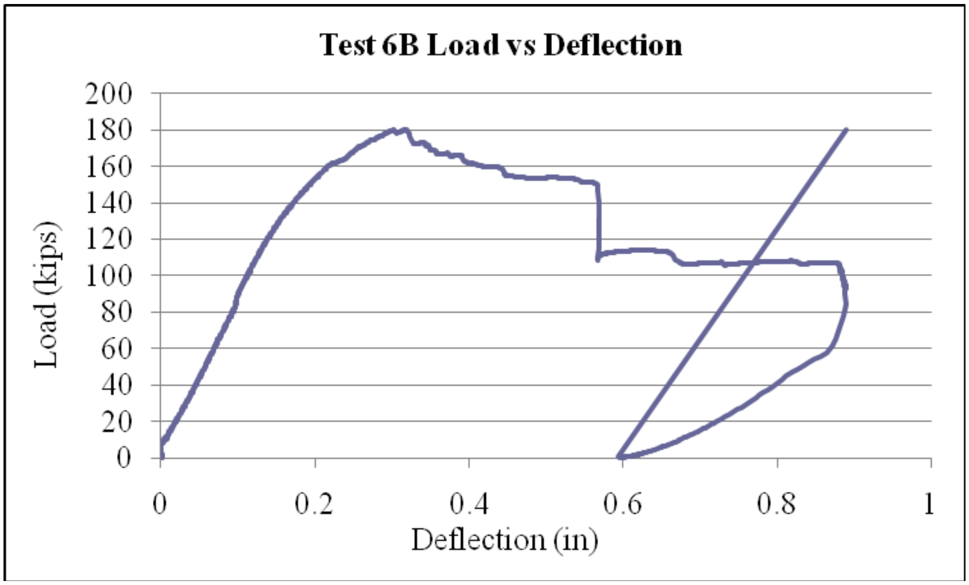

Figure B.99 Test 6B Load vs Deflection.

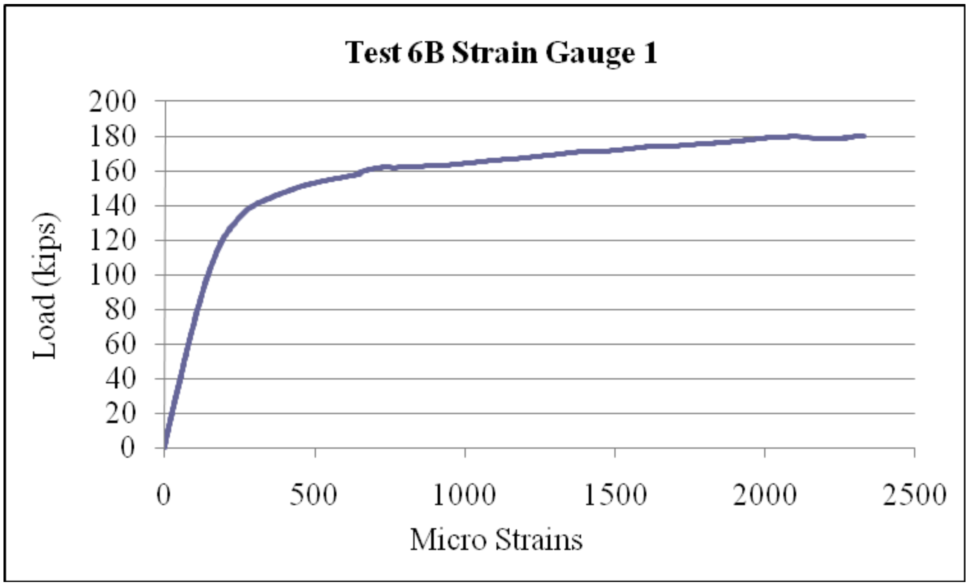

Figure B.100 Test 6B Strain Gauge 1.

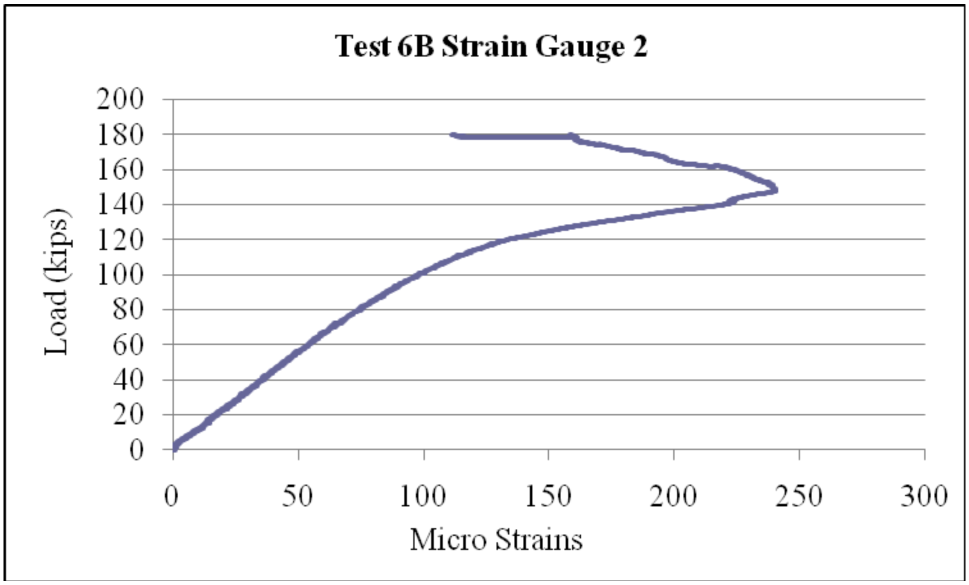

Figure B.101 Test 6B Strain Gauge 2.

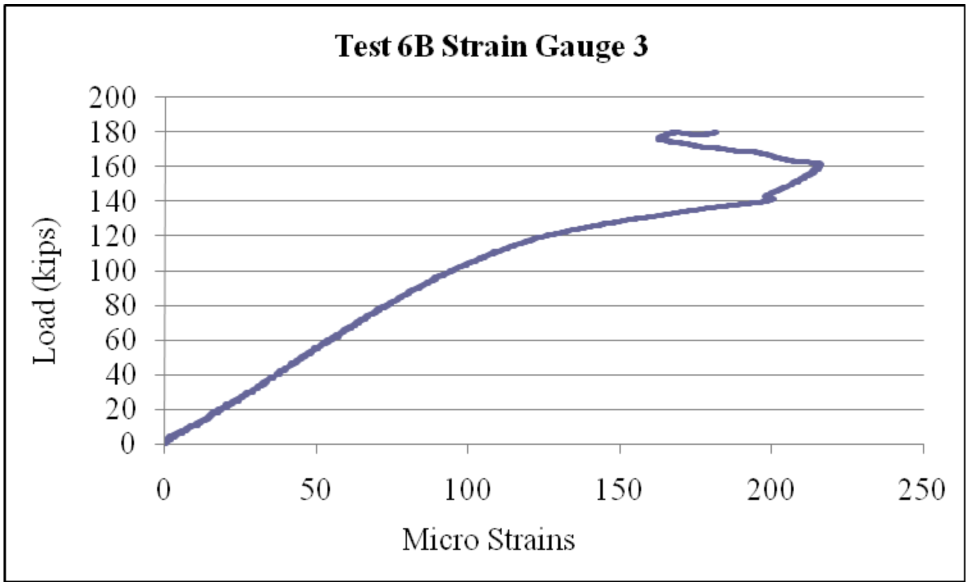

Figure B.102 Test 6B Strain Gauge 3.

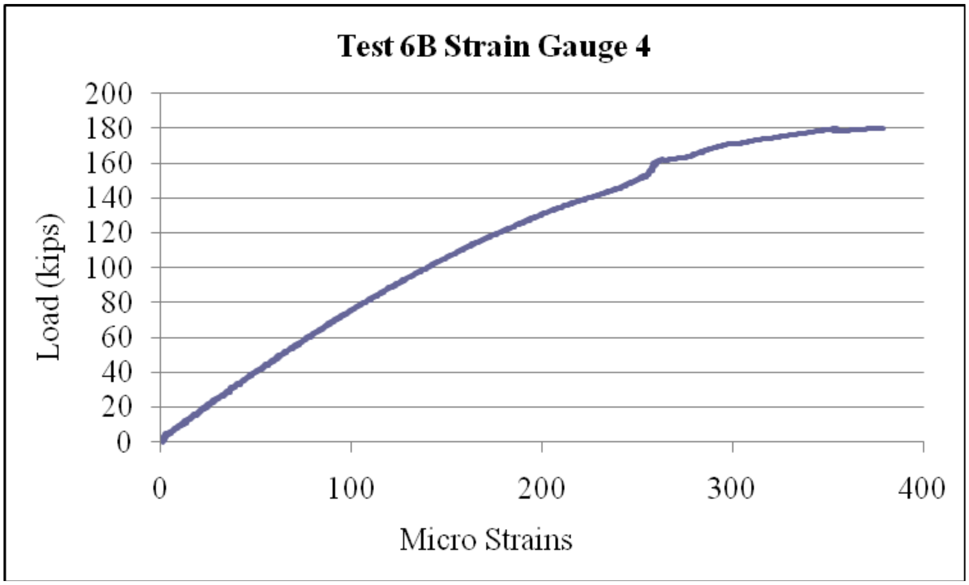

Figure B.103 Test 6B Strain Gauge 4.

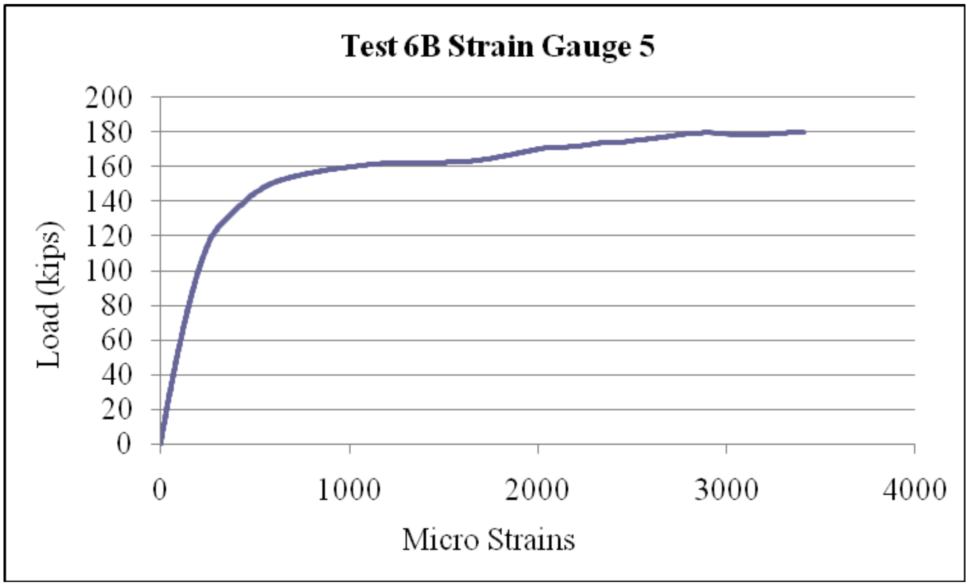

Figure B.104 Test 6B Strain Gauge 5.

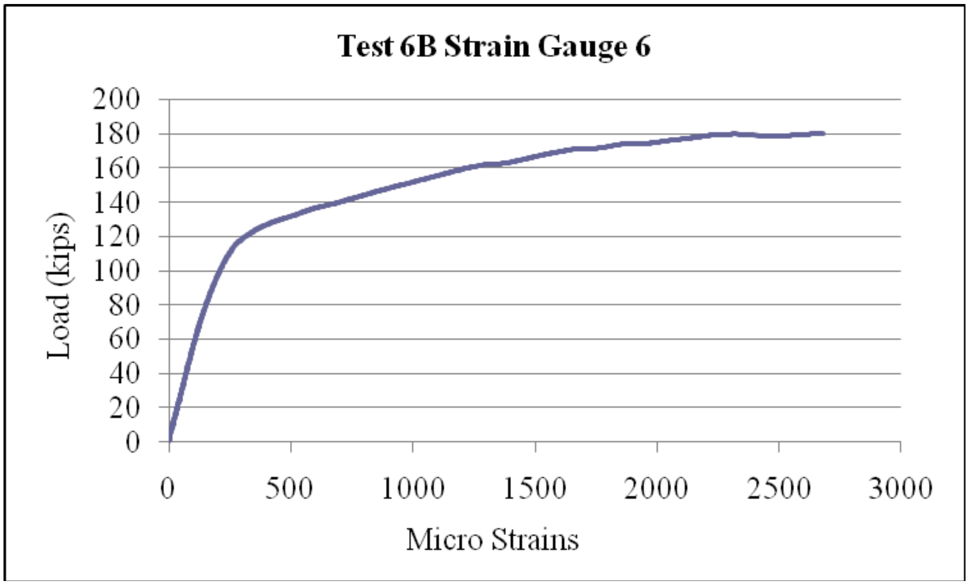

Figure B.105 Test 6B Strain Gauge 6.

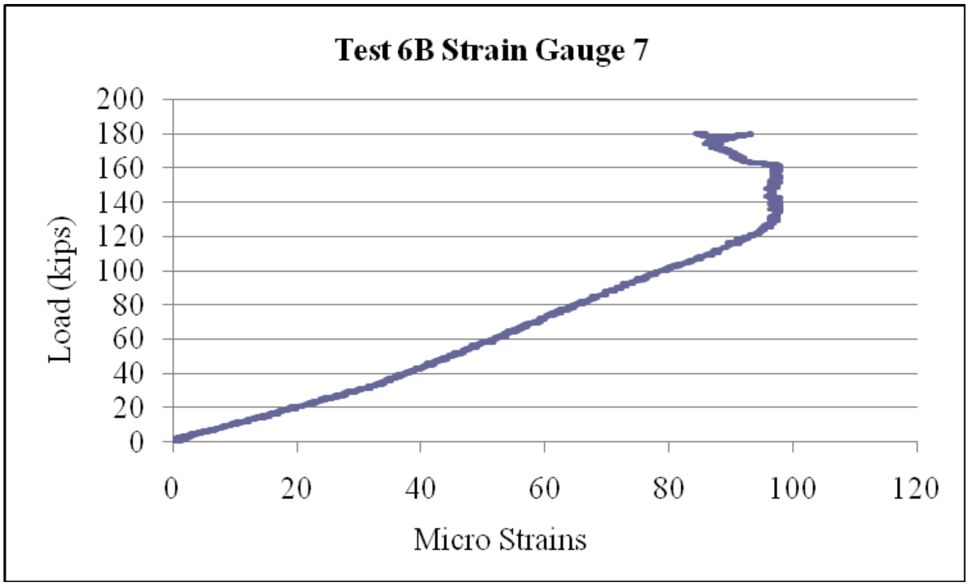

Figure B.106 Test 6B Strain Gauge 7.

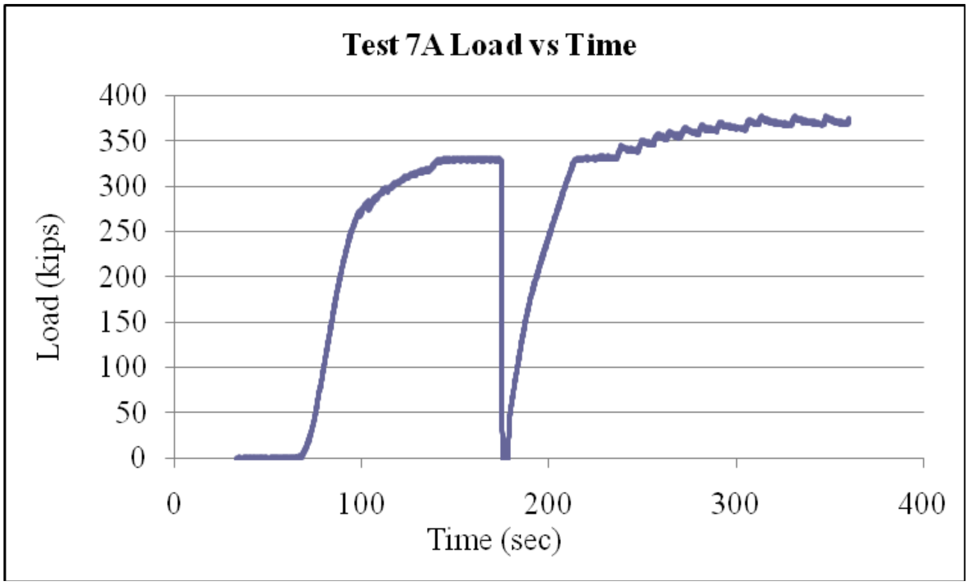

Figure B.107 Test 7A Load vs Time.

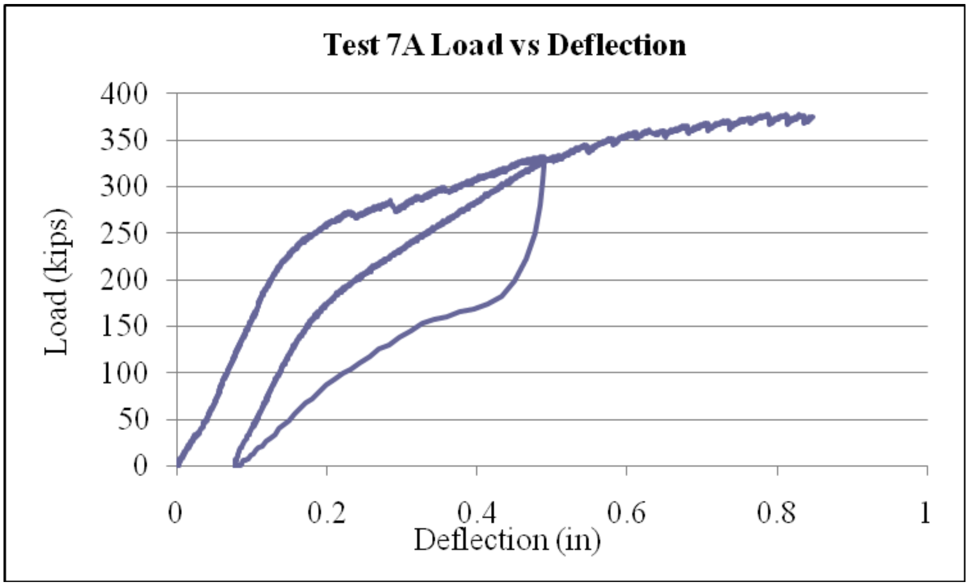

Figure B.108 Test 7A Load vs Deflection.

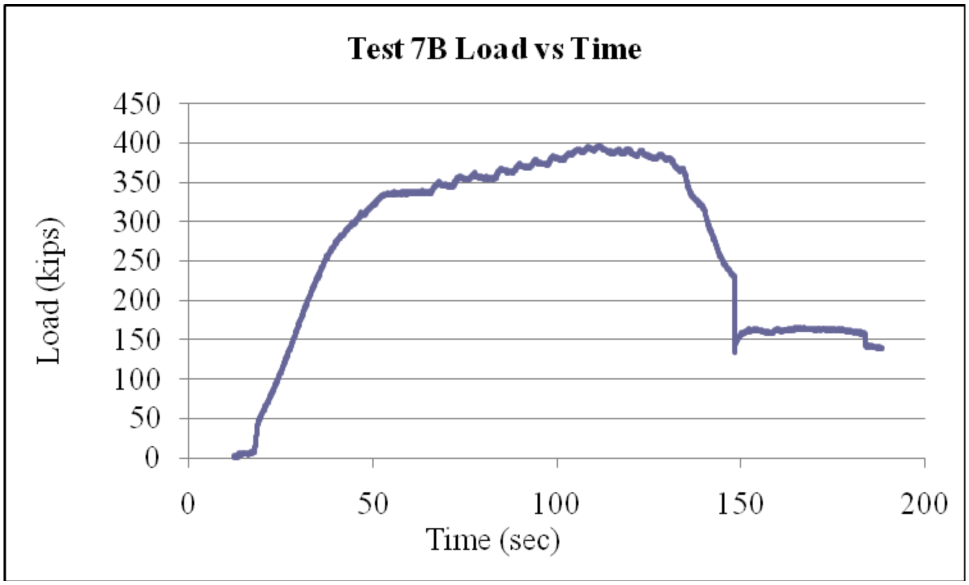

Figure B.109 Test 7B Load vs Time.

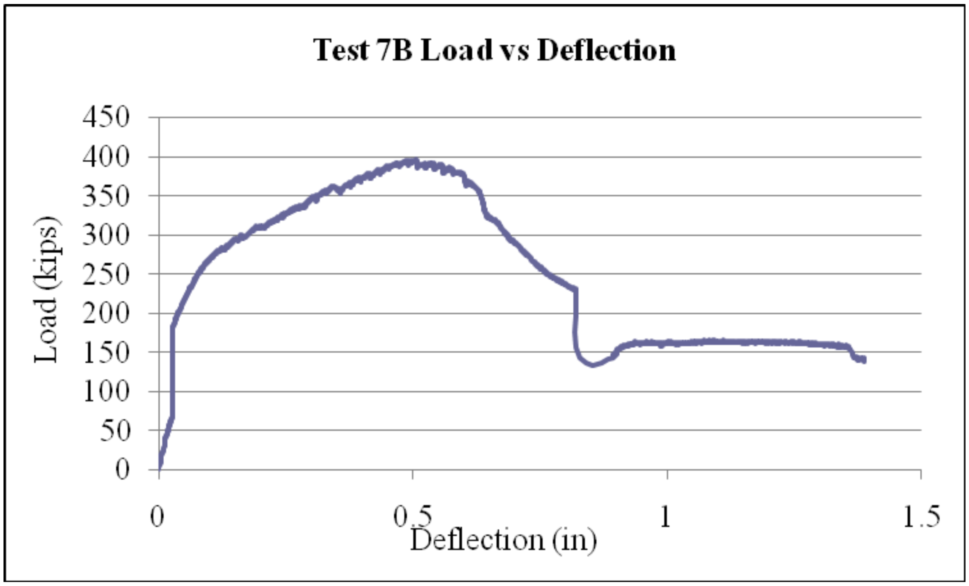

Figure B.110 Test 7B Load vs Deflection.

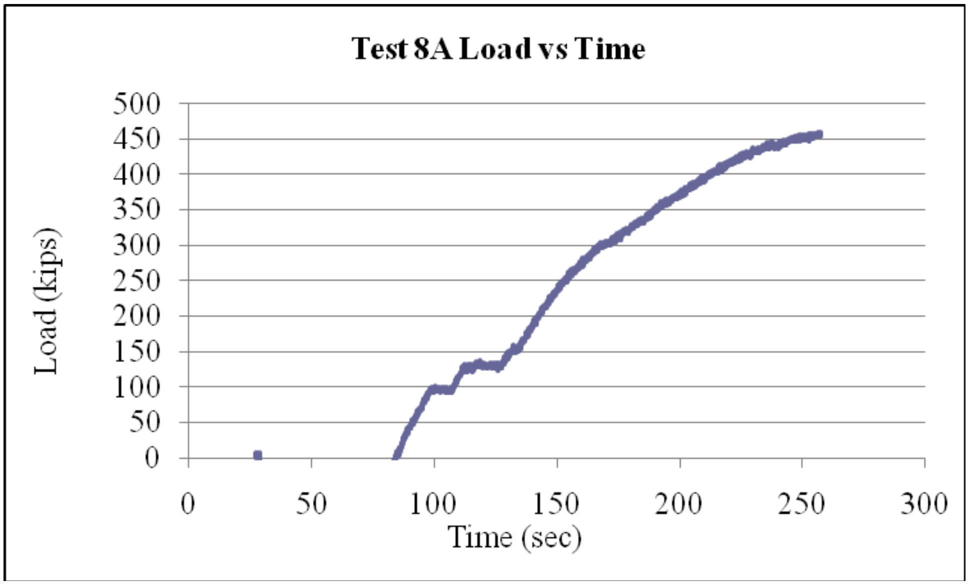

Figure B.111 Test 8A Load vs Time.

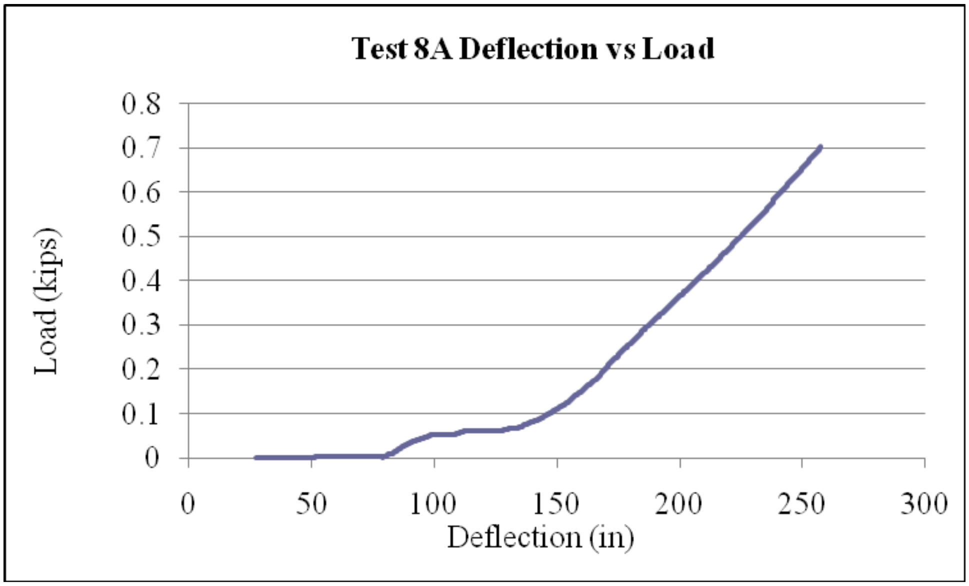

Figure B.112 Test 8A Load vs Deflection.

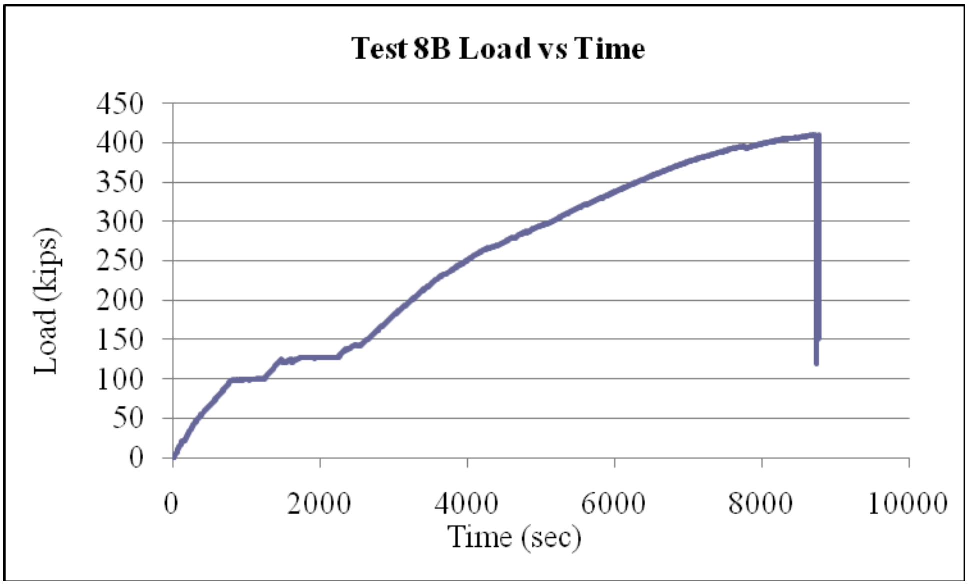

Figure B.113 Test 8B Load vs Time.

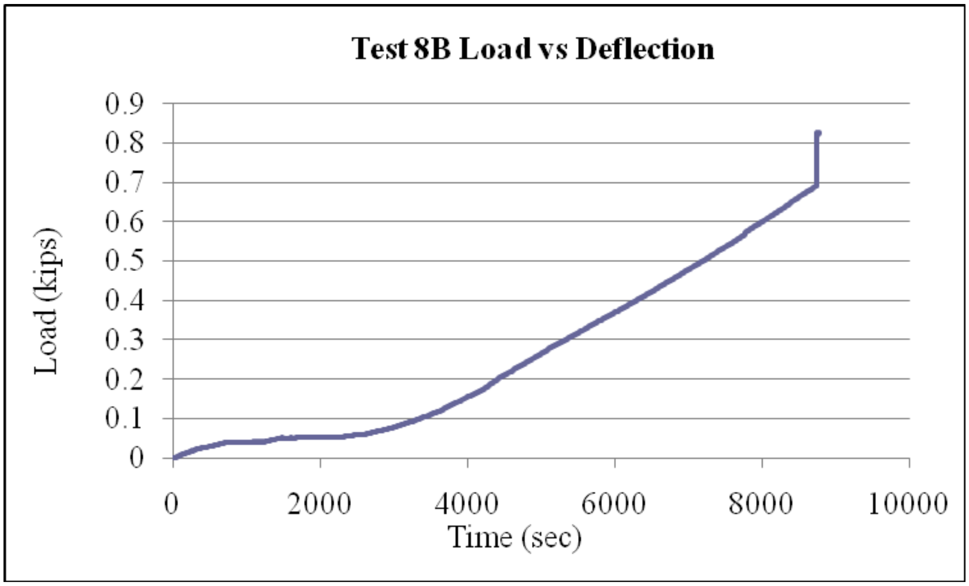

Figure B.114 Test 8B Load vs Deflection.